A peptidomic investigation into enteroendocrine cells and islets of humans and mice

Sam George Galvin

Churchill College, University of Cambridge

This dissertation is submitted for the degree of Doctor of Philosophy

March 2021

Declaration

This dissertation is the result of my own work and includes nothing which is the outcome of work done in collaboration except as specified here and in the main body of the text. Human tissue work in chapter 3 was performed by Pierre Larraufie as well as Geoffrey Roberts. Elise Bernard of AstraZeneca synthesis the novel peptides tested *in vivo* and *in vitro* in chapter 4 and John Hood, also of AstraZeneca, performed the modelling to calculate mass infusion rates of the three top priority novel peptides required for the osmotic pump studies. The work presented here is not substantially the same as any that I have submitted, or, is being concurrently submitted for a degree or diploma or other qualification at the University of Cambridge or any other University or similar institution. I further state that no substantial part of my dissertation has already been submitted, or, is being concurrently submitted for any such degree, diploma, or other qualification at the University of Cambridge or any other University of similar institution. This dissertation does not exceed 60,000 words.

Sam Galvin

A peptidomic investigation into enteroendocrine cells and islets of humans and mice

Sam Galvin

Abstract

Enteroendocrine cells (EECs) of the gastrointestinal (GI) tract and islets of Langerhans (islets) of the pancreas are endocrine cells capable of sensing nutrient intake or the nutrient content of the blood and responding by secreting peptide hormones to control various physiological functions. This thesis focuses on characterising the peptidome of EECs and islets by utilising liquid-chromatography coupled to mass spectrometry (LC-MS).

Due to their ability to control food intake and glucose tolerance, hormones from EECs and islets are of great therapeutic interest for the treatment of type 2 diabetes (T2D) and obesity. I hypothesised that there may be undiscovered peptide hormones derived from EECs or islets that could also be of therapeutic interest for the treatment of T2D. In order to identify potentially novel hormone candidates, peptidomic analyses of mouse EECs, mouse islets and human GI tissue were carried out utilising LC-MS. 13 interesting peptide candidates identified in the peptidomic analyses were picked out to be synthesised for *in vivo* and/or *in vitro* characterisation.

All 13 peptides were screened for activity at Gs or Gi signalling pathways in various cell lines although unfortunately no peptide seemed to exhibit activity through these signalling mechanisms in the cell lines tested. Despite this, studies were carried out to assess the ability of the 2 top peptide candidates to control food intake and glucose tolerance *in vivo.* 1 of these peptides, a peptide derived from progastrin, seemed to mildly improve glucose tolerance in lean mice, an effect that was seen in across several studies. I hypothesised that this progastrin derived peptide may be altering peptide secretions from islets to modulate glucose tolerance but no effect of this novel peptide was seen on insulin, somatostatin-14 or glucagon secretion from islets. The progastrin derived peptide was then administered to diet-induced obese mice to assess its therapeutic potential but unfortunately no effect was seen on glucose tolerance. More work needs to be performed to verifying my findings and investigating a possible mechanism of action before this novel progastrin derived peptide may be considered a gut hormone.

In regard to the peptidome of islets, there are some gaps in the literature that our initial peptidomic analysis did not answer. Questions such as do islets produce GLP1 (glucagon-like

peptide 1) receptor agonists and how is the islet peptidome altered in response to metabolic stress. I therefore carried out an investigation to address these questions. Targeted LC-MS methodology was used to search for intra-islet GLP1 receptor agonists. No peptides derived from glucose-dependent insulinotropic polypeptide (GIP) were found in mouse islets but active GLP-1 was found in both human and mouse islets. Comparisons were made between the abundance of active GLP-1 and glucagon to assess which of these peptides might be responsible for the intra-islet "incretin" effect. My peptidomic analysis of islets from T2D humans and obese mice may not have revealed new major findings but it has provided some clarity over how metabolic stress alters the peptidome of islets in T2D an obesity.

In summary; a comprehensive analysis of the peptidome of EECs and islets was carried out, a number of novel peptide hormone candidates were synthesised and one of which exhibited a mild improvement in the glucose tolerance of lean mice, and clarity was provided on how metabolic stress alters the islet peptidome in mice and humans. I hope that the data produced in this thesis can contribute to a better understanding of the peptidome of the EECs and islets and may contribute to advances in therapeutic options for patients suffering from obesity or T2D.

Contents

Declaration ..... **I**

Abstract ..... **II**

Contents ..... **IV**

Acknowledgments ..... **X**

Abbreviations ..... **XI**

Chapter 1: Introduction ***1***

1.1 The GI tract **1**

1.1.1 Structure of GI tract wall 2

1.1.2 Enteric nervous system 2

1.1.3 Cell types of the GI epithelium 3

1.1.3.1 Stem cells 4

1.1.3.2 Parietal and chief cells 8

1.1.3.3 Enterocytes 9

1.1.3.4 Tuft cells 9

1.1.3.5 Paneth cells 10

1.1.3.6 Goblet cells, mucous neck & surface cells 10

1.1.4 Enteroendocrine cells 11

1.1.4.1 EEC classification 12

1.1.4.2 Gut hormones 13

1.1.4.3 Post-translation processing 13

1.1.4.4 Gut hormones and food intake 14

1.1.4.5 Pancreatic effects of gut hormones 15

1.1.4.6 GI tract actions of gut hormones 16

1.1.4.7 Therapeutic potential of gut hormones in obesity and diabetes 16

1.2 The Pancreas **18**

1.2.1 Innervations of the pancreas 18

1.2.2 Cell types of the pancreas 19

1.2.2.1 Acinar cells 19

1.2.2.2 Ductal cells 19

1.2.3 Islets of Langerhans 20

1.2.3.1 Islet cell differentiation 20

1.2.3.2 Islet peptide hormones 20

1.2.3.3 Distinctions between human and mouse islets 21

1.3 Mass spectrometry **23**

1.3.1 Overview 23

1.3.2 Ionisation processes 23

1.3.3 Mass filters and analysers 24

1.3.3.1 Quadrupole 25

1.3.3.2 Orbitrap 25

1.3.4 Tandem-MS 26

1.3.4.1 De novo peptide sequencing and database searching 30

1.3.5 Mass spectrometry in peptidomics 31
1.4 Thesis aims 32
Chapter 2: General Methods 34
2.1 Chemicals and reagents 34
2.2 Buffers for secretion assays 35
2.2.1 KRB 35
2.3 Animals 35
2.4 Mouse islets isolation 35
2.5 Sample preparation for MS analysis 36
2.5.1 ACN protein crash 36
2.5.2 Solid phase extraction 36
2.5.3 Reduction and alkylation 36
2.6 Mass spectrometry 36
2.6.1 Nano flow rate analysis on Orbitrap mass spectrometer 37
2.6.2 High flow rate analysis on Triple Quadrupole MS 37
2.6.3 LC-MS data processing 37
2.6.4 PEAKS database searching 38
Chapter 3: Selection of novel peptide hormone candidates through peptidomic characterisation of EECs and islets 39
3.1 Introduction 39
3.1.1 Granin proteins 39
3.1.2 Multiple active peptides from prohormones 41
3.1.3 Novel peptide discovery approaches 42
3.2 Aims 45
3.3 Methods 45
3.3.1 Mouse EEC peptidomics 45
3.3.1.1 GI tissue preparation 45
3.3.1.2 FACS of EECs 45
3.3.1.3 Primary mouse GI crypt cultures 48
3.3.2 Islet peptidomics 49
3.3.3 Human GI peptidomics 49
3.3.3.1 Ethics 49
3.3.3.2 Tissue homogenisation and sample preparation 49
3.3.4 Sample preparation 50
3.3.5 LC-MS data analysis and database searching 50
3.4 Results 50
3.4.1 Rationale for novel peptide candidate selection 50
3.4.2 Novel peptide panel for synthesis 52
3.4.3 Priority 1 peptides 53
3.4.3.1 ChgA 435-462a 55
3.4.3.2 Gast p59-79 58
3.4.3.3 Sst 25-36 60

3.4.4 Priority 2 peptide candidates 65
3.4.4.1 Cck derived peptides 65
3.4.4.2 ChgA 358-371 67
3.4.4.3 Ghrl 52-85 71
3.4.4.4 Nec1 90-108 73
3.4.4.5 Pcsk1n 42-59 75
3.4.4.6 Pyy 68-98 77
3.4.4.7 Scg2 184-216 and Scg2 569-610 79
3.4.4.8 Tac1 72-95 83
3.4.5 Other prohormones, processing enzymes and granin proteins 86

3.5 Discussion 91
3.5.1 Summary 91
3.5.2 Granin-derived peptides as hormones 91
3.5.3 Comparison with non-peptidomic approaches 92
3.5.4 Comparison with other peptidomic approaches 95
3.5.5 Shortfalls in my peptidomic methodology 96
3.5.6 Relative quantification of peptides by peak area 97
3.5.7 Conclusion 97

Chapter 4: Characterisation of novel peptide candidates in vivo and in vitro 99

4.1 Introduction 99
4.1.1 Peptide characterisation *in vivo* 99
4.1.2 Similar peptides to priority 1 novel peptide candidates 101
4.1.3 Aims 102

4.2 Methods 103
4.2.1 Peptide synthesis 103
4.2.1.1 Materials 103
4.2.1.2 General procedure for chemical synthesis of peptides 103
4.2.1.3 Cleavage and purification of peptides 103
4.2.1.4 Peptide analysis and characterisation post-synthesis 104
4.2.2 cAMP accumulation assay 104
4.2.2.1 Materials 104
4.2.2.2 Protocol 105
4.2.2.3 Analysis 105
4.2.3 Peptide stability in Plasma 106
4.2.3.1 24-hour stability protocol 106
4.2.3.2 Citrate buffer stabilisation 106
4.2.3.3 Peptide quantification by LC-MS 106
4.2.3.4 Optimising multiple reaction monitoring assays for priority 1 peptide quantification 107
4.2.4 Pharmacokinetics studies 107
4.2.4.1 s.c. PK study for Sst 25-36 & Gast p59-79 108
4.2.4.2 s.c. PK study for ChgA 435-462a 108
4.2.4.3 i.v. PK study for Sst 25-36 & Gast p59-79 108
4.2.4.4 i.v. PK study for ChgA 435-462a 108
4.2.4.5 Peptide extraction from plasma and quantification by LC-MS 108
4.2.5 Modelling of Peptide PK for constant infusion 108
4.2.6 *in vitro* osmotic pump study 111
4.2.6.1 Siliconising 111

4.2.6.2 Pump filling ... 111
4.2.6.3 Controls ... 111
4.2.6.4 Protocol ... 111
4.2.6.5 Peptide extraction ... 112
4.2.6.6 Peptide quantification by LC-MS ... 112
4.2.7 in vivo osmotic pump study 1 ... 112
4.2.7.1 Mice ... 112
4.2.7.2 Pump preparation ... 113
4.2.7.3 Study protocol ... 113
4.2.7.4 Peptide extraction from plasma ... 114
4.2.7.5 Peptide quantification by micro-flow rate analysis on Triple Quadrupole MS ... 114
4.2.8 *in vivo* osmotic pump study 2 ... 114
4.2.8.1 Mice ... 114
4.2.8.2 Pump preparation ... 115
4.2.8.3 Study protocol ... 115
4.2.8.4 Peptide extraction and quantification ... 115
4.2.9 in vivo osmotic pump study 3 ... 115
4.2.9.1 Mice ... 115
4.2.9.2 Pump preparation ... 115
4.2.9.3 Study overview ... 116
4.2.9.4 Tissue preparation ... 116
4.2.9.5 Bicinchoninic acid (BCA) assay ... 116
4.2.9.6 AKT quantification ... 117
4.2.10 Islet experiments ... 117
4.2.10.1 Secretions ... 117
4.2.10.2 Lysates ... 118
4.2.10.3 Sample preparation ... 118
4.2.10.4 Peptide quantification by LC-MS ... 118
4.2.11 LC-MS data analysis ... 119

4.3 Results ... 119
4.3.1 Peptide synthesis ... 119
4.3.2 Peptide activity at Gs or Gi signalling pathways ... 119
4.3.3 Plasma peptide stability ... 122
4.3.4 PK analysis ... 124
4.3.5 *in vitro* osmotic pump assessment ... 126
4.3.6 *in vivo* osmotic pump study 1 ... 128
4.3.7 Priority 1 peptide effect on islet secretions ... 136
4.3.8 *in vivo* osmotic pump study 2 ... 138
4.3.9 *in vivo* osmotic pump study 3 ... 139
4.3.10 ChgA 435-462a and islet peptide content ... 142

4.4 Discussion ... 144
4.4.1 cAMP accumulation screens ... 144
4.4.2 Priority 1 peptide stability and pharmacokinetics ... 144
4.4.3 *In vivo* osmotic pump studies ... 145
4.4.3.1 *In vivo* effects of Gast p59-79 on glucose and insulin tolerance ... 146
4.4.3.2 Food intake and body weight ... 149
4.4.4 Sst 25-36 and neuronostatin ... 149
4.4.5 ChgA 435-462a and serpinin ... 150

4.4.6 Conclusions 151

Chapter 5: Characterisation of the islet peptidome 152

5.1 Introduction 152

5.1.1 Intra-islet GLP1 R agonists 152
5.1.2 Islet peptidome and metabolic disease 153
5.1.3 LC-MS based studies of the islet peptidome 154
5.1.4 Aims 155

5.2 Methods 155

5.2.1 Islet lysate peptidomics 155
5.2.2 Islet secretion peptidomics 155
5.2.3 Assessing the role of the GLP1 R in GSIS 156
5.2.4 Peptidomics of sorted β, α and δ cells 156
5.2.4.1 Mice 156
5.2.4.2 Single cell digestion 156
5.2.4.3 FACS 157
5.2.5 DIO islet peptidomics study 157
5.2.5.1 Mice 157
5.2.5.2 Tissue collection and islet isolation 157
5.2.5.3 Islet lysis 157
5.2.6 T2D vs healthy human islet comparison 157
5.2.7 Sample preparation 158
5.2.8 Standard curve preparation 158
5.2.9 Nano flow rate analysis on Orbitrap mass spectrometer 159
5.2.10 High flow rate analysis on triple quadrupole mass spectrometer 159
5.2.11 Data analysis 159

5.3 Results 160

5.3.1 Mouse islet peptidomics 160
5.3.1.1 Peptidomics of whole lysed mouse islets 160
5.3.1.2 Detection and quantification of GLP-1 (7-36 amide) 162
5.3.1.3 Searching for proGIP-derived peptides 166
5.3.1.4 Peptidomics of FACS purified α, β and δ cells 173
5.3.1.5 Islet secretion peptidomics 176
5.3.1.6 Peptidomics of DIO vs lean mouse islets 179
5.3.2 Human islet peptidomics 182
5.3.2.1 Peptidomics of lysed whole human islets 182
5.3.2.2 Detection and quantification of GLP-1 (7-36 amide) in human islets 184
5.3.2.3 Peptidomics of T2D vs non-diabetic human islets 186

5.4 Discussion 189

5.4.1 Comparison of human and mouse islet peptidomics 189
5.4.2 Intra-islet GLP1 receptor agonists 190
5.4.3 Peptidomics of mouse α, β and δ cells 192
5.4.4 Peptidomic assessment of metabolically stressed islets 195
5.4.5 Normalising data to islet number 196
5.4.6 Conclusions 197

Chapter 6: General discussion 198

6.1 Thesis summary 198
6.2 Searching for novel peptides 198
6.3 Characterising activity of novel hormones 200
6.4 Is Gast p59-79 a gut hormone? 200
6.5 Therapeutic use of Gast p59-79 201
6.6 Intra-islet incretins and implications 202
6.7 Lessons from peptidomics of metabolically stressed islets 203
6.8 Mass spectrometry in peptidomics 204
6.9 Concluding remarks 204
References 206
Appendix 1 223
Appendix 2 225

Acknowledgments

I would like to firstly thank my supervisors at the University of Cambridge, Fiona Gribble and Frank Reimann for providing much guidance and support over the 4 years or my PhD. I would also like to thank everyone within the Gribble/Reimann laboratory for being extremely generous, offering much support both inside and out of the lab with special mention to Richard Kay and Pierre Larraufie.

I am also extremely grateful to have worked and learnt from scientists at AstraZeneca and would like to extend my thanks to staff working in the Cardiovascular, Renal and Metabolism department as well as the *in vivo* sciences team. I am particularly grateful to Jacqui Naylor, Haidee Pitt and Elise Bernard for their support when working at AstraZeneca.

I thank all my friends for keeping me going through the last 4 years especially to Filip, Tom, Hiran, Joy, Vicky, those at Cambridge University Korfball Club and at the Ireland Korfball Association. Their presence during my PhD has made this time some of the most memorable of my life and I'm indebted to them all. Finally, I would like to thank my parents, sister and brother. Their unwavering support has undoubtedly been crucial to me undertaking a PhD and submitting this thesis.

This PhD was funded by the Biotechnology and Biological Sciences Research Council and AstraZeneca

Abbreviations

ACN	Acetonitrile
AgRP	Agouti-related peptide
AKT	Protein kinase B
ANN	Artificial neural networks
ATCC	American Tissue Culture Collection
AUC	Area under the curve
BAT	Brown adipose tissue
BMP	Bone morphogenic protein
BOAT1	Neutral amino acid transporter 1
Boc	t-butyloxycarbonyl
BSA	Bovine serum albumin
cAMP	Cyclic adenosine monophosphate
CASR	Calcium sensing receptor
CBC	Crypt base columnar cells
CCK	Cholecystokinin
CGRP	Calcitonin-gene related peptide
Chg	Chromogranin
CID	Collision-induced dissociation
Cl	Clearance
Css	Steady state plasma concentration
DDA	Data-dependent acquisition
DIO	Diet-induced obese
DIPEA	Diisopropylethylamine
DMEM	Dulbecco's modified eagle media
DMF	Dimethylformamide,
DNA	Deoxyribose nucleic acid
DPP IV	Dipeptidyl peptidase IV
DREADD	Designer receptors exclusively activated by designer drugs
DTT	Dithiothreitol
ECL	Enterochromaffin-like cells
ED_{50}	Half maximal effective dose
EDTA	Ethylenediaminetetraacetic acid
EEC	Enteroendocrine cell
EGF	Epidermal growth factor
ENS	Enteric nervous system
ESI	Electrospray ionisation
EYFP	Enhanced yellow fluorescent protein
F	Bioavailability
FA	Formic acid
FACS	Fluorescence-activated cell sorting

FBS	Foetal bovine serum
FFA	Free-fatty acids
FFAR	Free fatty acid receptor
FSC	Forward scatter
GHSR	Growth hormone secretagogue receptor
GI	Gastrointestinal
GIP	Glucose-dependent insulinotropic polypeptide
GLP-1	Glucagon-like peptide 1
GLP-2	Glucagon-like peptide 2
GPCR	G protein-coupled receptor
GRP	Gastrin-releasing peptide
GRPP	Glicentin-related polypeptide
GSIS	Glucose stimulated insulin secretion
GTT	Glucose tolerance test
GuHCl	Guanidine hydrochloride
HbA1c	Haemoglobin A1c
HBSS	Hank's balanced salt solution
HCTU	2-(6-Chloro-1-H-benzotriazol-1-yl)-1,1,3,3-tetramethylaminium hexafluorophosphate
HFD	High fat diet
HPLC	High performance liquid chromatography
HTRF	Homogeneous time-resolved resonance fluorescence
i.v.	Intravenous
IAPP	Islet amyloid polypeptide
IBMX	3-isobutyl-1-methylxanthine
IP	Intraperitoneal
ITT	Insulin tolerance test
KRB	Krebb's ringer buffer
LC-MS	Liquid-chromatography coupled to mass spectrometry
LI	Large intestines
LPV	Longest peptide varient
MALDI	Matrix assisted laser desorption ionisation
MPC	Multipotent pancreatic progenitor cells
MS	Mass spectrometry
MS/MS	Tandem mass spectrometry
Muc-2	Mucin-2
m/z	Mass to charge ratio
NeuroD1	Neuronal Differentiation 1
NMP	N-Methyl-2-pyrrolidone
NPY	Neuropeptide Y
OGTT	Oral glucose tolerance test
PAM	Peptidylglycine α-amidating monooxygenase
Pbf	2,4,6,7-pentamethyldihydrobenzofuran-5-sulfonyl

PBS	Phosphate buffered saline
PC/Nec	Prohormone convertase/Neuroendocrine convertase
Pcsk1n	ProSAAS
PEG	Polyethylene glycol
PEPT1	Proton-dependent epithelial peptide transporter
PK	Pharmacokinetics
PN-1	Protease nexin-1
PPY	Pancreatic polypeptide
PTM	Post-translational modification
PYY	Peptide YY
RNA	Ribose nucleic acid
RP	Reversed phase
RPMI	Roswell park memorial institute
RT-qPCR	Reverse transcriptase quantitative qPCR
s.c.	Subcutaneous
Scg	Secretogranin
SGLT1	Sodium-coupled glucose transporter 1
SHH	Sonic hedgehog
SI	Small intestines
SRM	Selective reaction monitoring
SSC	Side scatter
SST-14	Somatostain-14
SST-28	Somatostatin-28
T2D	Type-2 diabetes mellitus
tBu	*tert*-butyl
TFA	Trifluoroacetic acid
TIPS	Triisopropylsilane
TOF	Time of flight
Vc	Volume of the central compartment
VIP	Vasoactive intestinal peptide
Vp	Volume of the peripheral compartment
WAT	White adipose tissue

Chapter 1: Introduction

1.1 The GI tract

The gastrointestinal (GI) tract encompasses a variety of organs, sphincters and glands involved in digestion, absorption and excretion. The GI tract also serves numerous other functions. It acts as a barrier to the external environment to help exclude pathogens from the body. It harbours the microbiome, a diverse population of bacteria, viruses, yeast and archaea crucial for the breakdown of indigestible foods such as non-digestible fibre into absorbable forms. Lastly, the GI tract is the largest endocrine organ of the body producing over 20 known hormones involved in the regulation of GI motility, GI secretions, food intake and glucose homeostasis.

The GI tract can be divided into the main organs which are in direct contact with food and accessory organs whose secretions aid in the digestion process. The main organs form a continuous passage from the mouth to the anus and include the oesophagus, stomach, the small and large intestines. The stomach, small and large intestines are not homogeneous entities and exhibit regional differences at the tissue and cellular level leading to each organ being divided into distinct regions (Figure 1.1). Accessory organs include the salivary glands, liver, pancreas and gall bladder.

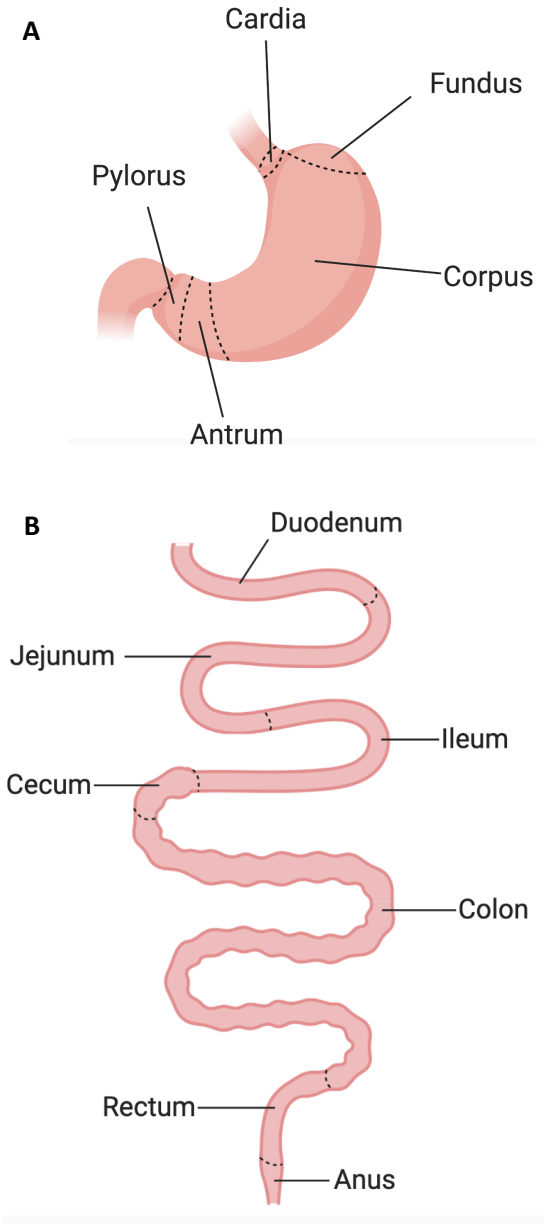

Figure 1.1: Overview of the main organs of the GI tract. *(**A**) Regions of the stomach. (**B**) Regions of the intestines. Duodenum, jejunum and ileum make up small intestines. Cecum, colon, rectum and anus make up large intestines.*

1.1.1 Structure of GI tract wall

The GI tract has various endocrine and exocrine roles as well as being a motile set of organs [1]. In order to carry out these functions the walls of the GI tract can be divided into layers containing different cell types.

The inner most layer is the mucosa and consists of all the tissue from the epithelium down to a smooth muscle layer known as muscularis mucosa. The epithelium forms 3D structures know as villi (small intestines), crypts (intestines) and glands (stomach). These 3D structures serve to increase the surface area of the GI tract for increased absorption or shield specialised epithelial and stem cells from the harsh luminal environment. Different specialised epithelial cells are found within the mucosa of the stomach and intestines to help these organs carry out their primary functions (see section 1.2.3). Beyond the mucosa is the submucosa which is highly perfused and innervated by the vagus and enteric nervous system to control mucosal secretions. Additionally, hormones secreted from enteroendocrine cells (EECs) act on receptors on the neurons to exert wider physiological effects. Several muscle layers surround the submucosa giving the GI tract its motile element. The stomach and intestines possess longitudinal and circular muscle layers allowing peristaltic movements however, the stomach also has an oblique muscle layer permitting churning of stomach contents to aid in mechanical digestion and mixing with gastric secretions. Within the muscle layers are plexuses allowing for autonomous control of GI motility. The outermost layer is the serosa and defines the boundary of the organ. Blood vessels are found in this layer to perfuse the muscle layers in addition to nerves allowing for communication with the central nervous system via the vagal nerve.

1.1.2 Enteric nervous system

The enteric nervous system (ENS) is a subset of the autonomic nervous system responsible for the motility of the small and large intestines as well as controlling secretions from various cell types and is connected to the CNS by the vagus nerve [2]. The ENS receives sensory information from the intestines and can co-ordinate appropriate responses, thus enabling these organs to function-theoretically-independently from the central nervous system. Microcircuits (consisting of interneurons and intrinsic primary afferent fibres) within the ENS allow this semi-autonomous function as these microcircuits can initiate reflexes. The majority of the vagal fibres between the CNS and ENS are afferent fibres and indicating that the brain acts as a receiver of information rather than a transmitter in regard to gut-brain communication. It should be noted however that the ENS rarely functions completely independently as it regularly receives input on enteric function from the CNS. The ENS forms clusters of nerves between the circular and longitudinal muscle layers known as the

myenteric plexus. The submucosal plexus forms in the submucosal region just beneath the mucosa. Between myenteric and submucosal plexi, the ENS can control the muscle layers of the intestines as well as communicate with the mucosa to receive sensory information on luminal contents and influence secretions from epithelial cells [3].

As mentioned, the ENS is crucial in the relaying of intestinal nutrient content the CNS. One of the mechanisms by which nutritional information is transduced into electrical information is through gut hormones. Enteroendocrine cells (EECs) of the GI epithelium sense intestinal content and release gut hormones such as cholecystokinin, peptide YY and glucagon-like peptide-1 which can act directly on vagal sensory neurones via their receptors [4]. This communication between EECs and the ENS is bidirectionsal as vagal stimulation can induce gut hormones release [5, 6]. EECs and gut hormones will be discussed in more detail later on in this chapter.

Many of the main neurotransmitters of the CNS are also found within the ENS with noradrenaline and acetylcholine being the predominant ones [7]. Noradrenergic neurons serve to supplement the actions of the sympathetic nervous system and have broad inhibitory actions across the GI tract. Blood flow to the GI tract is reduced and so too are secretions and GI motility. Somatostatin and neuropeptide Y may also act as secondary neurotransmitters of these noradrenergic neurones. Cholinergic neurons on the induce the opposite effects and induce effects that supplement the 'rest and digest' effects which are induced by the parasympathetic nervous system. GI motility, secretions and blood flow is enhanced allowing the digestion and uptake of nutrients in the circulation.

1.1.3 Cell types of the GI epithelium

Epithelial cells of the GI tract are responsible for the endocrine, protective and absorptive functions of the system and include a variety of specialised cell types to carry out these duties. In the stomach, the cell types are geared towards the digestive function of the organ producing hydrochloric acid and digestive enzyme precursors. Pit-like structures known as gastric glands dominate the epithelial layer of the stomach and harbour stem cells, providing this cell type with a refuge from the acidic environment to differentiate and replenish the epithelium. In the intestines, the dominant cell type is the enterocyte which is highly specialised to perform both its absorptive and protective functions. Projections known as villi increase the surface area of the epithelium and so maximise the exposure of enterocytes to nutrients aiding absorption. Invaginations, known as crypts are also found in the intestinal epithelium and play a role similar to gastric glands in the stomach in that crypts also provide shelter to stem cells from the intestinal lumen. Villi are predominantly found in the jejunum and ileum

as this is where most of the absorption takes place whereas crypts are found throughout the intestines.

The GI epithelium is remarkable. No other epithelial layer of any other organ must perform the multiple functions that the GI epithelial layer performs simultaneously [8]. The lungs are also highly specialised for absorption but would not be able to endure the mechanical strain the GI tract must endure. Similarly, the skin is too specialised at excluding the environment and therefore would not be able to carry out the absorptive role the GI tract must perform. This section will cover the array of cell types found in the different regions of the GI tract and how they are equipped to help the GI tract to carry out its many different functions simultaneously.

1.1.3.1 Stem cells

All cell types of the GI epithelium originate from a pool of stem cells that reside within the gastric glands of the stomach or intestinal crypts. In intestinal crypts, stem cells dwell at the trough migrating up the crypt as they differentiate [8] (figure 1.2) whereas in the stomach these stem cells are found throughout the gastric glands but not in the neck region [9] (figure 1.3). Their location in these evaginations in the GI epithelium provides an ideal environment for the proliferating cell, protecting it from the harsh conditions of the lumen.

1.1.3.1.1 Intestinal Stem cells

Intestinal stem cells (also known as crypt base columnar cells (CBC)) are defined by their position at the base of the crypt and their expression of *LGR5* [10]. +1, +2 and +3 describe their distance away from the trough of the crypt with +1 being at the trough crest. Paneth cells sandwich the CBCs and secrete signalling factors to help maintain the CBC population (figure 1.2). Once CBCs migrate beyond the Paneth cells at the barrier between the stem cell zone and progenitor zone of the crypt, they are referred to as progenitor cells and rapidly divide whilst migrating vertically to become specialised epithelial cells.

Signalling pathways such as Wnt, Notch, EGF and bone morphogenic protein (BMP) dictate which lineage a stem cell will differentiate down whilst maintaining the CBC population. These signalling pathways are induced by secretion of a variety of factors from various cell types of the epithelium and mesenchyme. Wnt signalling is critical for maintenance of the CBC population and [11] and it is for this reason that Wnt signalling inducers (such as R-spondin and WNT) are found at their highest concentration at the trough of the crypt and gradually decrease towards the top. This is due

to the sources of these signalling molecules (Paneth cells as well as $GLI1^+$ [12] and $CD34^+$ [13] mesenchymal cells) being located at the crypt trough.

Notch signalling induces an absorptive phenotype whilst simultaneously inhibiting secretory cell differentiation [14]. For Notch signalling activation there must be physical contact between cells expressing the Notch ligands (DLL1 or DLL4) and cells expressing the Notch receptor (NOTCH1). For this reason, Paneth cells-a major source of DLL1 and DLL4 [15] in the epithelium-are adjacent to CBCs at the base of the crypts.

EGF signalling is not necessarily linked to one phenotypic cell. Instead, it is associated with increased CBC proliferation and therefore this pathway needs to be tightly regulated to avoid over proliferation and formation of tumours. For this reason, CBCs often co-express the EGF receptor (ERBB1) with the negative regulator of this receptor LRIG1 [16]. Wong et al. knocked out *Lrig1* in mice and observed enlarged intestines in these mice attributed to expansion of the stem cell population. EGF signalling is mediated through a variety of receptor tyrosine kinases to control gene expression when activated [17].

BMPs are largely responsible for promoting differentiation of progenitor cells and counteracting their proliferation. BMP signalling therefore must be kept to a minimum in the stem cell zone of the crypt but gradually increase up the crypt to allow differentiation. BMP inhibitors such as Gremlin 1 and Noggin are secreted by smooth muscle cells and myofibroblasts underneath the crypt to dampen down BMP signalling and allow maintenance of the CBC population [13, 18, 19]. BMP2 and BMP4 are the main agonists of BMP receptors of the intestines and are secreted by mesenchymal cells residing in between the crypts and underneath the villi [20, 21]. Secretion of BMP2 & 4 here coupled with the lack of BMP antagonists boosts BMP signalling in the mid-region (transit amplifying zone) of the crypt to allow for CBC differentiation. From here most cell types progress out the crypt into the villi where they undergo apoptosis after up to 5 days. A short life span of differentiated cells allows for constant renewal of the GI epithelium and therefore any damaged cells can be quickly replaced. Due to the harsh conditions of the GI lumen, damage is likely and so constant renewal is vital for the GI epithelium to maintain its function.

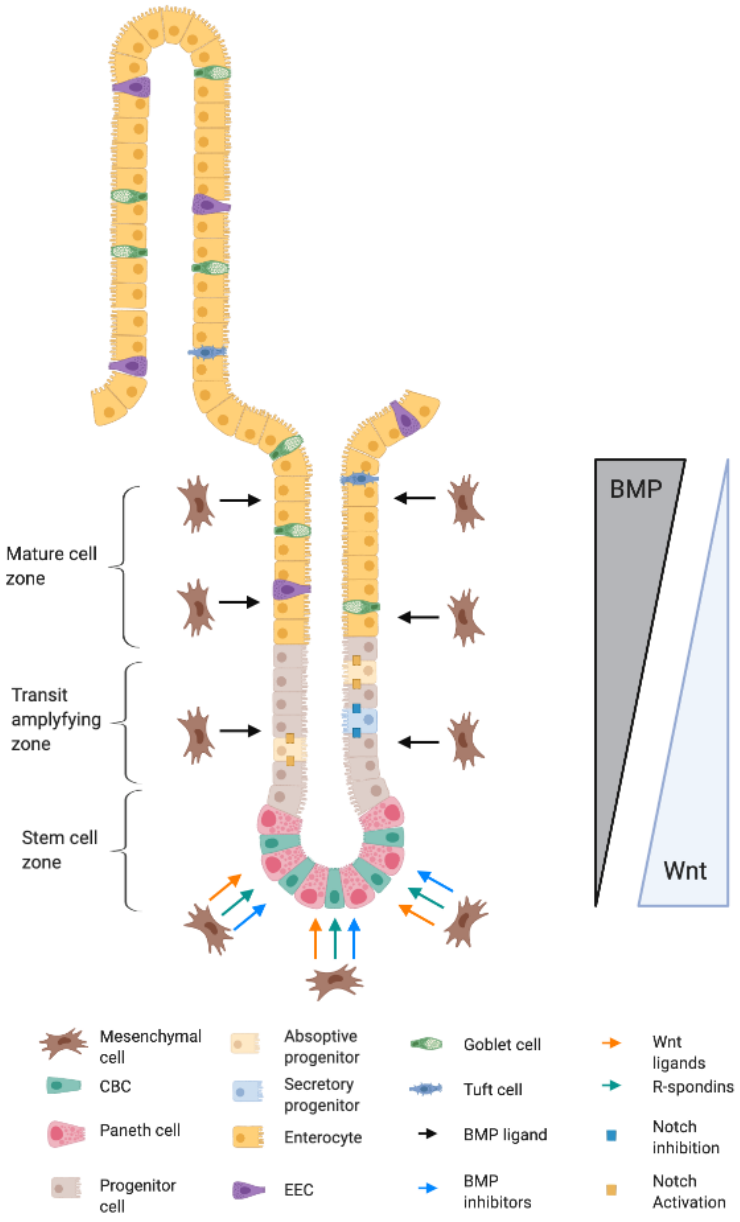

Figure 1.2: Overview of a crypt. *Adapted from Gehart & Clevers (2018) [8].*

1.1.3.1.2 Gastric stem cells

Like their intestinal counterparts, gastric stem cells can be identified as the *Lgr5*$^{+}$ cells in gastric pits [22]. Unlike intestinal stem cells, gastric stem cells are not just found at the bottom of the gastric glands. Instead, there are thought to be several gastric stem cell populations spread throughout the gastric gland with some expressing; *Vil1* (present at the base, neck and isthmus), *Sox2* (neck and isthmus) and *Cckbr* (neck) as well as a population present in the isthmus of the gastric glands [23, 24] (figure 1.3). Strange et al. have even described a population which express *Lgr5* as well as *Bhlha15* and

Mist1 which are chief cell markers [25]. These chief/stem cells can act as 'reserve stem cells' to replace all gastric epithelial cell types in *in vitro* culture. Clearly gastric stem cells are much more diverse than their intestinal counterparts.

Differentiation signalling pathways in the intestines such as BMP and NOTCH are also present in the stomach although the sources and effects of some factors are different [23]. With a lack of absorptive cells in the stomach, Notch doesn't serve as a molecular determinant of cell fate. Instead, Notch seems to act on stem cells to maintain their stem cell phenotype and encourage their proliferation [26]. Activation of antral *Lgr5*$^{+}$ cells leads to their widespread proliferation, expansion of gastric gland formation and a decrease in differentiated cells. BMP4 is also a key signalling molecule but its expression differs from the intestines in that it is only present in the parietal cell-rich areas of the neck (figure 1.3). This is due to the fact that sonic hedgehog is released from parietal cells and activation of sonic hedgehog signalling is required for BMP4 production [27]. Therefore, no BMP4 gradient exists in gastric glands as it does in intestinal crypts. Instead, a BMP4 rich zone shrouds the parietal cell region in the neck, inhibiting the formation of stem cells in this zone. This may be a reason why stem cells are scattered across different regions of the gastric gland as there is only one region where BMP signalling is high enough to inhibit their formation [28]. Other factors such as FGF10 [29, 30], EGF [31], gastrin [24] and WNT [32] are also able to regulate the gastric stem cell population.

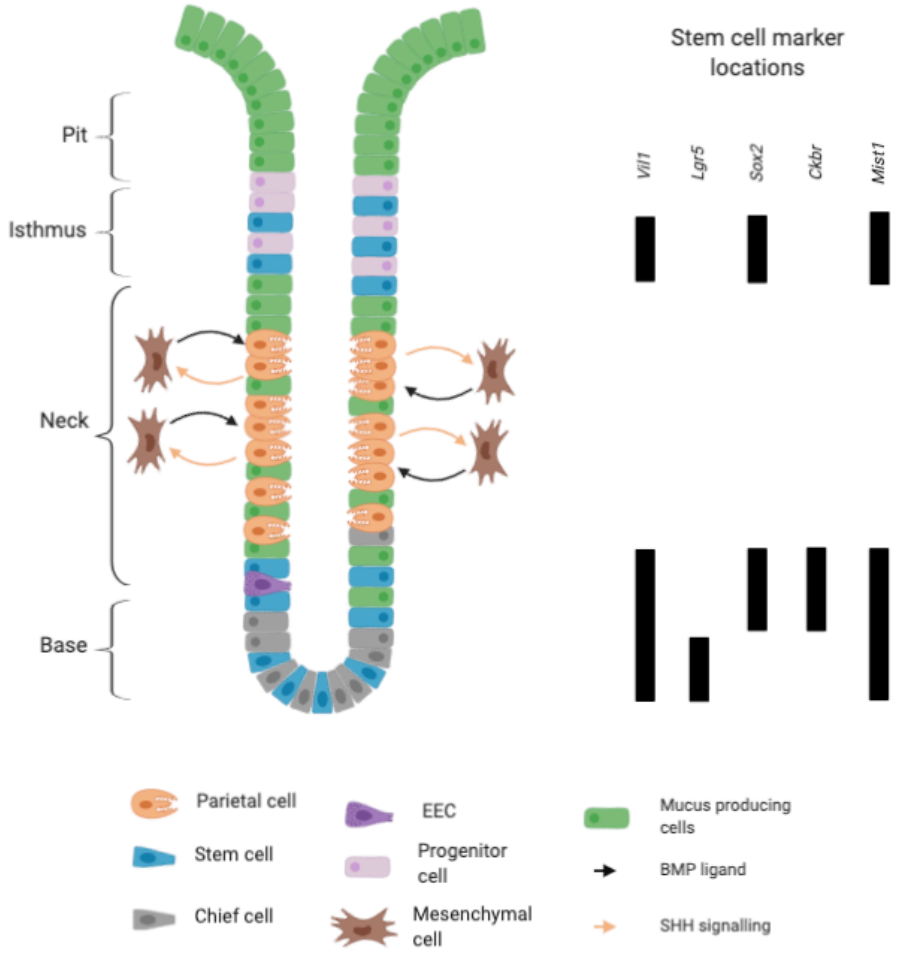

Figure 1.3: Overview of a gastric gland. *Information collated from Bartfeld & Koo (2017) [23] as well as Kim & Shivdasani (2016) [9]. SHH: sonic hedgehog.*

1.1.3.2 Parietal and chief cells

The acidic conditions of the stomach are created by secretions from parietal cells [9]. This cell type is found predominantly in the neck region of corpal gastric glands (figure 1.3). Also located in corpal gastric glands are chief cells which release inactive zymogens such as pepsinogen into the acidic stomach where they unfold, allowing autocleavage of a 44 amino acid region to form the active enzyme pepsin. As the zymogens from chief cells are reliant on the acidic environment created by parietal cells it makes sense that secretions from two cell types should be induced by the same stimuli. Vagal afferents directly activate M3 cholinergic receptors on parietal and chief cells triggering activation of the H^+/K^+ ATPase moving H^+ ions into the stomach [33, 34]. Indirect regulation of parietal cells is also possible through vagal regulation of stomach endocrine cell activity. Somatostatin, gastrin and histamine are released by D-cells, G-cells and enterochromaffin-like (ECL) cells respectively and receptors for these three hormones can act on both parietal and chief cells [35-40]. Histamine and gastrin are released from their respective cells upon vagal stimulation to increase parietal cell output.

Somatostatin on the other hand exerts a basal level of inhibition on parietal cells through activation of Gi coupled somatostatin receptors. Therefore, inhibition of somatostatin release by acetylcholine released from vagal afferents can boost gastric acid secretions. Somatostatin also exerts its inhibitory effects on G-cells and ECL cells and therefore vagal activation boosts gastrin and histamine levels to further boost acid and zymogen secretion.

1.1.3.3 Enterocytes

Enterocytes absorb nutrients and water passing through the intestinal lumen and are the most abundant cell type of the small intestinal epithelial layer. To carry out this absorptive function, enterocytes possess numerous transporters for ions, sugars, peptides, vitamins and fatty acids along their apical membranes [41]. Ion channels are also abundant in their basolateral membranes to create ion gradients to aid the process of nutrient uptake. Although, water can move through gaps between cells in a process known as paracellular transport, water channels (aquaporins) are highly expressed in enterocytes for transcellular uptake of water [42]. Some nutrients such as fatty acids require specialised intracellular transport due to their hydrophobic properties. After uptake, fatty acids are packaged into particles rich in phospholipids (chylomicrons) for transport to the basolateral membrane and exocytosis into the circulation or lymph system [43]. Enterocytes are locked together by tight junctions and adherens junctions to prevent crossing of unwanted substances which may disrupt ion gradients or allow passage of pathogens [44]. As well as forming a barrier against unwanted substances, tight and adherens junctions help maintain polarity of enterocytes, ensuring that channels and transporters are located on correct sides of the cell to create ion gradients in the right direction. For example, a concentration gradient for sodium between the enterocyte cytosol and the intestinal lumen in favour of the cytosol is crucial to the transcellular uptake of glucose by SGLT1 [41].

1.1.3.4 Tuft cells

The function of tuft cells long remained a mystery despite knowledge of their existence, until their role in initiation of type 2 immune responses was described, an immune response initiated by protozoal or helminth parasite invasion of the intestines [45]. Here, Gerbe et al. showed that infections caused an expansion of the tuft cell population in mice and knockout of a gene critical for tuft cell differentiation (*Pou2f3*) caused the disappearance of tuft cells and greatly delayed the onset of the type 2 immune response to expel the parasites. Parasite sensing by tuft cells seems to be possible due to their expression of chemoreceptors such as *Trpm5* [46].

1.1.3.5 Paneth cells

At the base of small intestinal crypts, Paneth cells can be found which play rolls in innate immunity and maintaining stem cell populations. This cell type is the only mature cell type to migrate down the intestinal crypt towards the base [47]. They secrete a wide variety of antimicrobial molecules such as α- and β-defensins, lysozyme and secretory phosphatase A2 [48]. To aid this secretory role, Paneth cells have developed a vast endoplasmic reticulum and Golgi network to maximise production of antimicrobial peptides and their storage in secretory vesicles [49, 50].

Aside from their anti-microbial function, Paneth cells are also critical to the maintenance of the CBC cell population, secreting signalling molecules such as Notch, WNT and essential epidermal growth factor (EGF) [15, 51, 52]. At the trough of the crypt, Paneth cells are interspersed between CBCs so that each CBC is in contact with a Paneth cell (figure 1.2). This is vital for Notch signalling as discussed previously [53].

1.1.3.6 Goblet cells, mucous neck & surface cells

Goblet cells are the most abundant secretory cell type of the intestinal epithelium [54]. They secrete trefoil factors and mucin-2 (Muc-2) to form a thick, protective layer of mucous between the intestinal epithelium and the lumen [55-57]. This acts a barrier to pathogens and the microbiota whilst also a lubricant to ease passing of waste material [58]. It is for this reason that goblet cells become more abundant as you move distally in the intestines as waste material becomes more compact and solid [59]. The mucous layers of the small and large intestines are slightly different with the former consisting of a single loose layer and the latter of 1 firm inner layer and 1 loose outer layer [60]. The inner mucous layer of the large intestine is firm and provides an impermeable barrier to microbes. It is thought that several hundred micrometres above the epithelial layer proteolytic cleavage of mucin proteins occurs to allow the proteins to expand to 3-4 times their size resulting in 2nd layer of mucous which is much looser than the inner layer [61]. This loose layer is where the microbiota of the large intestine resides. The single mucous layer of the small intestine is much like the outer loose layer of larger intestine expect that it does not harbour any microbes. The mucous layers of the small and large intestines are turned over every few hours to allow efficient clearing of waste material and microbes [62]. For this reason, goblet cells are the most abundant secretory cell in the intestinal epithelium as they must produce vast quantities of mucous to keep up with such a high turnover.

Two types of mucous cell are present in the stomach [63]. Mucous neck cells reside within the gastric crypts and produce acidic mucous secretions whereas the mucous surface cells are present on the lumen surface of the gastric epithelium. They produce alkaline mucous secretions whilst also

repairing surface lesions. There is also evidence to suggest these mucous surface cells can respond to infection by Helicobacter pylori by presenting antigens on their surface ready for recognition by immune cells [64].

1.1.4 Enteroendocrine cells

Enteroendocrine cells (EECs) are the hormone secreting cell type of the GI tract. Numerous subsets of these cells have been described which are traditionally classified by the hormone they predominately produce. Despite the numerous subtypes present in the epithelium, EECs are a rare population comprising only around 1% of the GI epithelium [65].

Inhibition of Notch signalling and expression of transcription factors such as *Math1* and *Dil1* force cells towards a secretory cell phenotype. Expression of Neurogenin 3 is then indicative that a cell has committed towards an EEC fate rather than the other secretory cells such as Paneth or goblet cells [66]. A plethora of other transcription factors such as NeuroD1, Pax4, Pax6, and Pdx1 are also crucial for EEC differentiation. In fact, there is a network of transcription factors which interact with differentiating cells to determine the subtype of EEC that is formed [67]. By the time EECs reach the top of the crypt and make contact with the GI lumen, the cells are fully differentiated and survive for around another 3-10 days [68, 69].

Like the other GI epithelial cell types, EECs are highly polar with a luminal facing side abundant in membrane projections known as microvilli to increase the exposure of the apical membrane to the GI lumen. On the basolateral side of the cell, there exists a large pool of secretory vesicles containing gut hormones. Many G-protein coupled receptors (GPCRs), transporters and ion channels are present in EECs enabling this cell type to detect and respond to the luminal contents and nutrient absorption. EECs are able to sense free-fatty acids (FFAs) through activation of FFAR 1-4, bile acids through GPBAR1, sugars through sodium-coupled glucose transporter 1 (SGLT1) and amino acids/polypeptides through neutral amino acid transporter 1 (BOAT1), proton-dependent epithelial peptide transporter (PEPT1) and the calcium sensing receptor (CASR) [70]. It is worth noting that GPCRs such as FFA1, FFA4, CASR, GPBAR1 and GPR119 in EECs are found basolaterally and it is likely that ligands required for the activation of these GPCRs are moved into the basolateral space by transporters [71-74]. Binding of ligands to their GPCR or intake of substances through transporters or channels induces intracellular signalling cascades that ultimately causes a rise in cytosolic cAMP and/or Ca^{2+}. Rises in these intracellular signalling molecules recruit secretory vesicles to the basolateral membrane whereby t-SNARE proteins on the membrane and v-SNARE proteins on the vesicle bind to initiate fusion of the vesicle with the membrane [75]. The contents of the vesicle are released into the

basolateral space whereby they can exert their physiological effects by acting locally or diffuse into the bloodstream to target other organs. 3D modelling shows that some EECs possess basolateral membrane extensions projecting towards other cell types in the mucosa such as neurones of the ENS, myofibroblasts and glia which may allow for direct communication between EECs and these cell types [76-79].

1.1.4.1 EEC classification

EECs are traditionally classified by their predominant hormone. These classes and their predominant hormones are summarised in table 1.1. However, there is a substantial amount of evidence to suggest this classification system needs revising [81-84]. Habib et al. have demonstrated using RT-qPCR and flow cytometry that L-cells purified by fluorescence-activated cell sorting (FACS) from the proximal small intestine possess hormones such as glucose-dependent insulinotropic polypeptide (GIP), secretin and cholecystokinin (CCK) [83]. Further evidence of overlap between EEC lineages comes from Egerod et al. who used liquid-chromatography coupled to mass spectrometry (LC-MS) to show that FACS purified I-cells also seemingly produce peptides from *Gcg*, *Cck*, *Pyy*, *Nts* and *Gip* genes [82]. Haber et al. performed single-cell RNA-seq on 53193 small intestinal epithelial cells from mouse organoids

Cell type	**Secretory products**	**Location**
P/D1 (X/A in mice)	Ghrelin	Stomach
Enterochromaffin-like	Histamine	Stomach
G	Gastrin	Stomach
D	Somatostatin (SST)	Whole GI tract
Enterocromaffin	Serotonin	Stomach, SI and LI
I	CCK	Proximal SI
K	GIP	Proximal SI
L	GLP-1, GLP-2, oxyntomodulin, Glicentin, PYY, Insl5,	Distal SI and LI
M	Motilin	Proximal SI
N	Neurotensin	Distal SI and LI
S	Secretin	Proximal SI

***Table 1.1**: **Summary of major EEC types, their primary secretory products as well as their location in the GI tract**. SI=Small intestine, LI=large intestine. As stated in the text, this classification is outdated and may be changed in the coming years. This classification is included in this thesis as a reference for future referrals to the classical EEC subtypes. Adapted from Furness et al. (2013) [80].*

and discovered cells which co-express *Sct*, *Cck*, *Gcg* and *Ghrl* [85]. All this evidence clearly undermines the canonical '1 hormone, 1 cell' nomenclature of EECs.

1.1.4.2 Gut hormones

There are many known gut-derived peptide hormones produced by EECs and table 1.2 summarises most of these hormones as well as their main physiological actions. All peptide hormones undergo complex processing post-translation to cleave the active hormone from a larger protein known as a prepropeptide as well as modification of certain residues to improve potency for their endogenous receptor.

Hormone	**Primary actions**
CCK	↓ appetite, ↑ pancreatic exocrine secretions, ↓ gastric acid secretion, ↑ gall bladder contraction
Gastrin	↑ gastric acid secretion
Ghrelin	↑ appetite
GIP	Incretin, ↑ fat build up
GLP-1	Incretin, ↓ appetite
GLP-2	↑ intestinal growth, ↓ intestinal motility
Insl5	↑ appetite
Motilin	↑ gastric emptying
Neurotensin	Regulate GI motility, regulate GI secretions
Oxyntomodulin	↓ appetite
PYY	↓ appetite
Secretin	↑ pancreatic exocrine secretions
SST	↓ gastric acid secretion, ↓ gut hormone release

Table 1.2: Major gut hormones and summary of their primary biological actions. *↑=increase, ↓=decrease. Information collated from Gunawardene et al. (2011) [65] as well as Murphy and Bloom (2006) [86].* CCK: Cholecystokinin, GIP: Glucose-dependent insulinotrophic peptide, GLP: Glucagon-like peptide, Insl5: Insulin-like peptide 5, PYY: Peptide YY, SST: Somatostatin, GI: Gastrointestinal.

1.1.4.3 Post-translation processing

Genes coding for the gut hormones are translated to produce prepropeptides. The prepeptide (signal peptide) is required for transportation of the peptide to the lumen of the endoplasmic reticulum [87]. Once inside the endoplasmic reticulum, endopeptidases cleave off the signal peptide to form the prohormone. Generally, these prohormones are thought to be inactive, although there is evidence to

suggest that some, such as progastrin, are biologically active [88]. Further processing occurs through cleavage by endopeptidases such as prohormone convertases or exopeptidases such as carboxypeptidase E. Prohormone convertases (PC) encompasses numerous proteins of which PC1/3, PC2 and furin are present in EECs [89]. These enzymes recognise dibasic and monobasic cleavage sites (RR, KK, RK, KR, R, K) to cleave bioactive gut hormones from their prohormones. Exopeptidases such as carboxypeptidases B and E are able to cleave monobasic residues from the C-terminus of newly formed peptide hormones. Once the peptide is fully cleaved from its prohormone, post-translational modifications (PTM) can be made. C-terminal amidation by peptidylglycine α-amidating monooxygenase (PAM) can significantly improve the potency of a gut hormones by increasing the half-life and enhancing affinity for the hormone receptor [90, 91]. N-terminal pyroglutamate formation is another common PTM and involves the formation of a cyclic residue from glutamine or glutamate [92]. Disulphide bonds can also be formed in the endoplasmic reticulum. Such bonds can be within a peptide or can form between two individual peptide chains. A class of enzymes known as thiol-disulphide oxidoreductases catalyse the formation of peptide disulphide bonds [93]. Formation of pyroglutamate residues is catalysed by the enzyme glutaminyl cyclase [94]. A rarer PTM found on gut hormones is serine or threonine octanoylation [95].

Further processing can occur outside of the cell once peptides have been secreted. Active GLP-1 and PYY (1-36) can be degraded by dipeptidyl peptidase-IV (DPP-IV) into shorter forms with altered pharmacology. Active GLP-1 is degraded into GLP-1 (9-36 amide) which is an antagonist at the GLP1 receptor (GLP1 R) [96]. PYY (1-36) is cleaved to form PYY (3-36) which has different affinities for the subtypes of Y receptors. PYY (3-36) has a high affinity at the Y2 receptor whereas PYY (1-36) has equal affinities for the Y1, Y2 and Y5 receptors [97-99].

1.1.4.4 Gut hormones and food intake

The ability of gut hormones to modulate food intake has attracted a lot of attention given the implications this has for diabetes and obesity treatment. Hormones such as cholecystokinin (CCK), glucagon-like peptide 1 (GLP-1), peptide YY (PYY) and oxyntomodulin are released postprandially to induce satiety [70]. The exact mechanism by which these peptides control food intake is unclear and often multifaceted. Taking GLP-1 as the example, it is known to exert its satiating-inducing effects directly on the hypothalamus when administered centrally [100, 101]. GLP1 R are expressed on neurones of the brainstem and hypothalamus and so it could be that circulating GLP-1 can reach these central receptors through areas lacking a blood brain barrier such as the subfornical organ [102] which is in close proximity to the hypothalamus and area postrema in the brainstem [102, 103]. GLP-1 can

also control food intake indirectly through delaying of gastric emptying [104-106]. Delaying of gastric emptying ensures the stomach is distended for longer after a meal which means gastric mechano-receptors are relaying the signal of satiation to the brain stem via the vagus for longer. Additionally, GLP1 R are present on the vagus and so GLP-1 could be acting on neurons within the GI tract which then signal to the hypothalamus [107]. PYY is also known to regulate food intake through multiple mechanisms. Firstly PYY can inhibit gastric and intestinal motility to prolong satiation and therefore inhibit food intake [108]. Y receptors on enteric neurons mediate this inhibitory action on GI motility when activated by the shorter, DPP-IV cleaved version of PYY (PYY (3-36)) [109, 110]. PYY can also exert its effects on food intake centrally as areas such as the arcuate nucleus are permeable to PYY [111]. PYY can then act on Y receptors expressed on hypothalamic neurons to inhibit secretion of orexigenic neuropeptides such agouti-related peptide (AgRP) and neuropeptide Y (NPY) whilst increasing release of anorexigenic signals such as α-MSH [112, 113].

Hormones with orexigenic effects include ghrelin and insulin-like peptide 5. Again, the physiological mechanisms by which these hormones act are incompletely elucidated. Peripheral or central administration of ghrelin has been shown to induce activation of NPY and AgRP neurones, which in turn, stimulates appetite [114-116]. Ghrelin could also act through the growth hormone secretagogue receptor (GHSR) on the vagus to inhibit signals from mechanosensory afferents in the upper intestines [117]. Although, any inhibitory action is likely to be through activation of intermediary inhibitory neurones as GHSR is Gq coupled [118]. Additionally, central administration of ghrelin promoted motivation to obtain sucrose rewards, implying it has direct central actions [119].

1.1.4.5 Pancreatic effects of gut hormones

Expression of GLP-1 and GIP receptors on pancreatic β-cells is well documented and binding of these peptides to their receptors under high glucose conditions potentiates insulin release. This enhancement of glucose-stimulated insulin secretion (GSIS) gives GIP and GLP-1 their classification of incretin hormones. Additionally, GLP-1 can increase β-cell mass by inhibiting their apoptosis [120] and increasing their proliferation [121], at least in rodents. Expression of GIP and GLP-1 receptors on δ-cells also enables these hormones to enhance SST secretion [107]. However, their effects on the α-cell population of the pancreas differ. GLP-1 inhibits glucagon secretion and therefore regulates glucose homeostasis via 2 complementary pathways. This may not solely be a direct effect on α cells as only a subset of α-cells express GLP1 R [107] but also an indirect effect through inducing SST secretion. SST is a known inhibitor of islet secretions [122]. Seemingly contrary to its incretin action, GIP can increase glucagon secretion [123]. Due to this paradoxical effect on glucagon secretion and

loss of the glucose lowering effect of GIP in type 2 diabetic (T2D) patients GIP analogues have not had as much success in clinical trials in treating T2D or obesity [123]. GLP-1 analogues, conversely, have had much more success and analogues such as liraglutide and exenatide are available as treatments for T2D and obesity.

Other than GLP-1 and GIP, INSL5 may have a role in glucose homeostasis as presented by Burnicka-Turek et al. [124]. However, the mechanism by which INSL5 may be acting is unknown and studies profiling the islet transcriptome have failed to find expression of the receptor for INSL5 (Rxfp4) in pancreatic islets [125, 126].

1.1.4.6 GI tract actions of gut hormones

Numerous gut hormones act within the GI tract to control the flow of luminal contents and secretions which aid in the digestion of said contents. In the stomach, SST, gastrin and histamine are released to control gastric secretions of zymogens, hydrochloric acid and peptide hormones themselves (see section on Chief and parietal cells). In the intestines, GLP-1, PYY, CCK, secretin and GLP-2 are secreted in response to nutrients interacting with EECs. CCK and secretin promote the release of bile acids, digestive enzymes and bicarbonate into the intestines by inducing contraction of the gall bladder and opening of sphincter of Oddi [127]. GLP-1 and PYY slow gastric emptying and intestinal motility to ensure intestinal contents can be properly digested an absorbed before the stomach releases additional contents for the intestines to digest and absorb. This effect is referred to as the ileal brake and is important in efficient digestion and absorption of food. Aside from controlling luminal flow of contents, gut hormones such as glucagon-like peptide 2 (GLP-2) are important for the maintenance of the epithelial layer. GLP-2 can induce crypt cell proliferation and inhibit epithelial cell apoptosis thus helping to maintain the epithelial barrier that guards against unwanted pathogen or nutrient uptake into the blood [128].

1.1.4.7 Therapeutic potential of gut hormones in obesity and diabetes

As we have seen, gut hormones exert numerous physiological actions on the body and so are attractive candidates as pharmaceuticals to treat various diseases. Administering these peptides in their native forms is not feasible due to the short half-lives of gut hormones, and so long-acting versions have been developed for medicinal use. Perhaps the most successful examples of gut hormones analogues are GLP-1 analogues such as liraglutide and exendin-4. These molecules are highly attractive in treating obesity due to their dual efficacy of reducing food intake and improving glucose tolerance. PYY has shown some promise as an anti-obesity drug as the dipeptidyl DPP-IV

cleaved version (PYY 3-36) reduced appetite in both lean [129] and obese individuals [130] when intravenously infused. Additionally, elevated postprandial levels of PYY in subjects who have undergone gastric bypass surgery are thought to be partly responsible for the weight loss seen in this form of surgery [131-133]. This has driven pharmaceutical companies to develop PYY analogues for the treatment of obesity. Oxyntomodulin is a dual agonist at both the GLP-1 and glucagon receptors and holds great therapeutic potential as it induces the beneficial effects of activation of both these receptors [134]. Oxyntomodulin induces weight loss and enhances insulin secretion through GLP-1 R activation as well as boosting energy expenditure through glucagon receptor activation [135]. As a result, several oxyntomodulin analogues or dual GLP-1/glucagon receptor agonists have been developed for diabetes or obesity treatment [136-138].

Dual agonists such as GLP1/glucagon receptor agonists are gaining much attention from pharmaceutical companies as they combine the therapeutic effect of receptor activation of both the glucagon and GLP1 receptor thus enabling them to treat both diabetes and obesity. GLP1 receptor agonism induces improvements in glycemia thereby treating hyperglycaemia in diabetic individuals whereas glucagon receptor agonism can increase energy expenditure to reduce body weight [139]. Seeing as obesity and diabetes are common comorbidities, these dual GLP1/glucagon receptor agonists have huge potential in these diseases. MEDI0382 (AstraZeneca) and SAR425899 (Sanofi) are dual GLP1/glucagon receptor agonists in clinical trials and have been shown to reduce body weight and HbA1c levels (a measure of diabetes progression) in obese/diabetic patients [140, 141]. Dual GIP/GLP1 receptor agonists may also be of therapeutic use in diabetic patients. GIP analogues have been developed [142] but don't possess the same therapeutic benefits that GLP-1 analogues do due to the impairment of GIP signalling in T2D and the lack of effect on food intake. However, when GIP and GLP-1 receptor activation are combined into dual agonists the weight loss seen in diet-induced obese (DIO) mice is greater than with GLP-1 analogues alone and so dual GLP-1/GIP receptor agonists such as LY3298176 (Eli Lily) have been developed and have shown efficacy in clinical trials for T2D treatment [143-145]. Therefore, it can be seen that these dual agonists can provide greater therapeutic effect than from GLP-1, glucagon or GIP analogues alone and it will be interesting to see whether tipple agonists at GLP1/GIP/glucagon receptors induce further beneficial therapeutic effects beyond that seen for dual agonists.

1.2 The Pancreas

The pancreas resides beneath the stomach in between the proximal duodenum and spleen, however only the duodenum receives the pancreatic juice it produces [146]. Similar to the stomach, small and large intestines, the pancreas can be split into several different regions; the tail which is the distal region sitting next to the spleen, the body resides in the centre and the head which is where the main pancreatic duct joins the bile duct to enter the duodenum. There are no definite anatomical or histological differences that define the boundaries between these regions, more differential densities of specialised cells. The majority of the endocrine tissue is found at the tail which gradually becomes sparser moving towards the head where exocrine tissue takes over as the dominant specialised structure. Running throughout the pancreas are a network of ducts forming a 'drainage system' from the exocrine cells into the main pancreatic duct and then into the duodenum. Unlike the major organs of the GI tract, this accessory organ does not possess a muscle layer and therefore is incapable of the peristaltic movements seen in the intestines. Secretions from the exocrine tissue rely on ion and pressure gradients to reach the duodenum. Despite the lack of musculature, the pancreas is highly innervated by the vagal nerve of the parasympathetic nervous system enabling neuronal control of endocrine and exocrine secretions.

1.2.1 Innervations of the pancreas

The pancreas receives autonomic input to influence its exocrine and endocrine functions. Neuronal regulation of exocrine secretions is largely indirect as parasympathetic neurones rarely form synapses with exocrine cells (acinar cells) and sympathetic nerves don't innervate these cells [147]. Instead, the vasculature perfusing the acinar tissue is highly innervated and thereby activation of these neurones controls blood flow to the acinar tissue and in turn controls production of the pancreatic juices. Sympathetic activation results in constriction of these blood vessels and a decrease in exocrine output whereas the opposite occurs with parasympathetic activation. A few parasympathetic fibres do innervate acinar and ductal cells and so firing of these neurones can directly increase exocrine secretions [147, 148]

Similar to innervation of exocrine tissue, neuronal control of pancreatic endocrine cell (islets) function is mainly indirect by controlling blood flow to the islets. However human islets may have some direct connections with parasympathetic fibres and both β and δ cells respond to the major neurotransmitter released by the parasympathetic nerves, acetylcholine [149]. Acetylcholine may also act in a paracrine fashion to modulate insulin and SST secretion as it seems the major source of acetylcholine in islets is α cells [150].

1.2.2 Cell types of the pancreas

1.2.2.1 Acinar cells

Acinar cells are the specialised cells constituting the exocrine tissue which makes up around 96-99% of the total pancreatic volume in humans [151]. Acinar cells cluster together to form grape-like structures at the end of ducts, known as acini. These cells have a distinct ultrastructure due to a vast endoplasmic reticulum required for synthesis of enzymes and a high density of secretory vesicles at the apical side. These granules (zymogen granules) store the enzymes until release into the lumen of the acini. Embedded in the basolateral membrane are GPCRs for numerous ligands including neurotransmitters such as acetylcholine or hormones such as CCK, substance P, gastrin-releasing peptide (GRP) and vasoactive intestinal peptide (VIP) [152]. Binding of these ligands to their GPCRs induces exocytosis of the zymogen granules through Ca^{2+}-/cAMP-dependent mechanisms. Receptor tyrosine kinases are also found on the basolateral membrane of acinar cells such as the insulin receptor and activation of this receptor tyrosine kinase can modulate synthesis of proteins by acinar cells [153-155].

1.2.2.2 Ductal cells

Ductal cells line the luminal side of the ductal system which transports exocrine secretions from the acini to the duodenum [156]. Ducts in the immediate vicinity of acini are usually very thin consisting of just a single layer of ductal cells. These are referred to as intralobular ducts. These merge with larger interlobular ducts which have the single layer of ductal cells reinforced with a layer of collagen. Interlobular ducts merge into the main pancreatic duct which has an extremely thick layer of collagen supporting the ductal cells lining the lumen. The role of the ductal cells is to secrete large volumes of water along with bicarbonate ions to help neutralise the acidic chyme entering the duodenum. Basolateral GPCR activation by agonists such as secretin and acetylcholine induces intracellular cAMP and Ca^{2+} accumulation within these cells to activate apical transporters and channels such as the cystic fibrosis transmembrane conductance regulator to release HCO_3^- ions and Cl^- into the lumen of the duct. The movement of ions into the lumen creates a high osmotic pressure driving water to follow through the paracellular route.

1.2.3 Islets of Langerhans

Islets of Langerhans (islets) constitute the endocrine tissue of the pancreas which makes up between 1-4% of total pancreatic volume [151]. Islets are spherical structures of predominantly specialised endocrine cells defined by the hormones they produce. Insulin and islet amyloid polypeptide (IAPP) producing β cells dominate islets comprising around 50-70% of human islets. α cells are the next most prevalent cell type of islets making up 20-40% of human islets. Other proglucagon derived peptides are produced by α cells such as glicentin-related poly peptide (GRPP), oxyntomodulin and GLP-1. The production of the latter peptide is controversial and will be investigated later on in this thesis. The last endocrine 3 cell types are PP cells, δ cells and ε cells which secrete pancreatic polypeptide (PPY), SST-14 and ghrelin respectively and only constitute about 6% of human islets. Islets also contain vascular endothelial cells which line the capillaries responsible for perfusing the islet.

1.2.3.1 Islet cell differentiation

Unlike EECs which are replenished from a pool of stem cells, islet cells are self-maintaining. Therefore, differentiation of islet cells from multipotent pancreatic progenitor cells (MPC, the cell population from which all pancreatic cell types differentiate) occurs during gestation when the pancreas is forming. Activation of Notch signalling in these cells forces MPCs towards an acinar cell fate [157] where as Neurogenin 3 signalling forces MPCs to an endocrine precursor state [158]. *Pax4* is essential for the formation of a β/δ cell precursor from these endocrine progenitors as *Pax4* null mice lack δ-cells and have a severely reduced number of β-cells [159]. *Arx* performs a similar role for the formation of α/PP cell precursors [160, 161]. From these two precursor types, a network of transcription factors such as *NeuroD1*,*Nkx2.2*, *Rfx6* and *Isl1* control the differentiation into specific islet cell types [162].

1.2.3.2 Islet peptide hormones

Islets secrete a plethora of hormones affecting numerous physiological functions including glucose homeostasis and food intake. Table 1.3 summarises the main hormones produced by islet cells as well as their cells of origin and physiological effects. In addition to these hormones, it has been postulated that GLP-1 [163], truncated forms of GIP [164] and CCK [165] are produced by islets. The production of GLP-1 in islets is not unexpected due to the high levels of proglucagon in α cells. However, the paracrine role of intra-islet GLP-1 [84] and the predominant form of GLP-1 produced by islets is unclear. Production of GIP and CCK by islets is not widely accepted, with studies analysing the transcriptome of human and mouse islets failing to find evidence of *GIP* or *CCK* expression in islets

[125, 126]. A LC-MS based study by Taylor et al. failed to find any peptides from proGIP or proCCK in supernatants from human and mouse islets further shedding doubt on the presence of these hormones in the endocrine pancreas [166]. It should be noted though that Taylor et al. did not use much starting material to analyse islet secreted peptides and so low abundance peptides may be below their lower limit of detection.

Hormone	**Islet cell type of origin**	**Actions**
Insulin	β	↓ glucose production in various tissue, ↑ glucose uptake in various tissues, ↑ glycogen synthesis in hepatocytes, ↓ blood glucose [167]
IAPP	β	↓ gastric emptying, ↓ glucagon secretion, ↓ appetite [168]
Glucagon	α	↑ glucose production by hepatocytes , ↑ blood glucose [167]
PPY	PP	↓ pancreatic exocrine secretions, ↓ appetite [169]
SST-14	δ	↓ GI and pancreatic secretions
Ghrelin	ε	↑ appetite
PYY	α, δ	↓ appetite

Table 1.3: Main hormones produced by islet cells. *↑=increase, ↓=decrease*

1.2.3.2.1 Therapeutic potential of islet hormones in T2D and obesity

We have already seen the potential of glucagon receptor agonists to treat T2D and obesity when combined with GLP-1 receptor agonism but are there other islet hormones with therapeutic potential in these disease states? An IAPP analogue called pramlintide has been approved for the treatment of T2D due to its ability to control glycemia through reduced glucagon secretion and gastric emptying [170]. This effect of delaying of gastric emptying enables pramlintide to reduce food intake and in phase 2 clinical trials for obesity treatment pramlintide has shown beneficial effects on weight gain [171]. PPY shares structural homology with PYY and so also acts on the NPY receptors responsible for mediating the anorectic effects of PYY [172]. Indeed, PPY has been shown to reduce food intake in lean humans [173], obese mice [174] and obese humans [175]. With this knowledge, PPY analogues have been developed for the treatment of obesity [176, 177]

1.2.3.3 Distinctions between human and mouse islets

At this point it is worth mentioning that there are certain differences between the islets of human and mice. Firstly, there is considerable difference in the cytoarchitecture of human and mouse islets. In murine islets, there is a distinct mantle and a core to the islet with non-β cells mainly residing in the mantle and β cells dominating the core of the islet [178]. Human islets don't have this clearly defined

mantle and core as with a more varied distribution of endocrine cells. This difference in cytoarchitecture is important to note as common methods to liberate islets from pancreatic tissue involve digesting the tissue with an enzyme. Non-β cells around the mantle of murine islets are therefore more exposed and could be lost if the digestion of the tissue is carried out for too long. This could bias any studies on murine islets towards β cells as this cell type is more protected within the core of the islet. However, as human islets have a more varied distribution of endocrine cells, non-β cells may be more protected within the core of the islet. This contrast in cytoarchitecture also leads to dissimilarities in paracrine signalling and the pattern of microcirculation of the islet endocrine cells. Afferent arterioles reach the islet periphery and enter through the mantle where they divide into smaller vessels to perfuse the core and then converge into venules and exit the islet [179]. In murine islets where non-β cells reside in the mantle and β cell in the core, non-β cells are perfused first and β cells second. Secretory products from non-β cells are brought to the β cells but not vice-versa thereby non-β cell secretory products such as glucagon, somatostatin may act on β cells to alter the activity of β cells. In human islets where endocrine cells are more randomly scattered across the islet, there is no order in endocrine cell perfusion so secretory products from all cell types enter the arterioles and can act on other endocrine cell types which boarder these arterioles. In human islets it appears that all endocrine cell types have connections with vessels [178]. Therefore, it seems that the is more bi-directional crosstalk between non-β cells and β cells in human islets but in mouse islets it is more one way from non-β cells to β cells.

Further differences between human and mouse islets are that in mice β cells dominate the islets even more so than in humans accounting for 60-80% of all islet cells meaning the proportions of all other islet cell types are decreased [151]. Additionally, *Pyy*, a gene predominantly expressed in the intestines and encoding the anorectic hormone PYY, is expressed in α, δ and PP cells of mouse islets whereas it is absent in human islets. There are numerous other distinctions in islets between the two species such as their innervations by the autonomic nervous system but those mentioned above are of more relevance for this thesis. Whilst these differences do not substantially affect the function of the islets, they are important to consider when studying mouse pancreata in lieu of human.

1.3 Mass spectrometry

1.3.1 Overview

Mass spectrometry is a technique used to detect the mass to charge ratio (*m/z*) of analytes within a sample. When coupled to high performance liquid chromatography (HPLC) it becomes a very powerful tool to detect and quantify multiple analytes in complex samples. Samples are injected onto a chromatography column which separates analytes based on their physico-chemical properties for example separating according to charge, size or hydrophobicity depending on the column chemistry. In this thesis a reversed-phase (RP) HPLC column was used which separates analytes based on their hydrophobicity with hydrophilic molecules eluting first and hydrophobic molecules eluting last. Once eluted from the column a technique such as electrospray ionisation (ESI) is used to convert analytes to a gaseous and charged state [180]. The gaseous charged analytes are then introduced into the mass spectrometer where a series of charged plates (ion guides) are used to remove any uncharged species and carry the analytes to a mass analyser and then the detector where their *m/z* is calculated.

1.3.2 Ionisation processes

ESI is a common method used for adding a charge to analytes and converting them to gas [180]. It involves applying a high temperature to the ion source and high voltages to the end of the capillary through which the mobile phase is flowing to achieve gaseous, charged ions. The strong electric field funnels the mobile phase into a cone like structure know as a Taylor Cone. The polarity of the charge applied to the capillary determines the charge given to the analytes. Mobile phase modifiers such as formic acid can be added to the mobile phase to facilitate the addition of a charge to analytes as they pass through the capillary. At the tip of the cone, droplets form where multiple like-charged analytes share the same droplet. High temperatures and a drying gas aid the evaporation of liquid from the droplet, concentrating the like-charge ions in the droplet. Eventually the repulsive electrostatic forces overcome the surface tension of the droplet and it explodes forming many smaller droplets. This process continues till very little mobile phase is left and analytes are almost all gaseous and charged (figure 1.4).

MALDI is another method by which analytes can be introduced into the mass spectrometer [181]. It involves embedding analytes in a solid matrix containing acid which is then vaporised by exposure to a high energy laser. A plume of gaseous matrix with the embedded analytes is generated and taken up into the mass spectrometer. The acid present in the matrix allows for ionisation of the analyte.

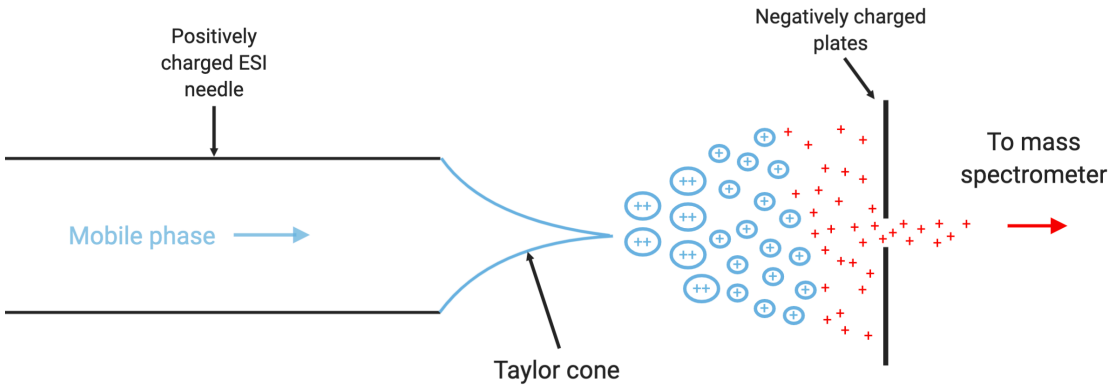

Figure 1.4: Summary of ESI in positive mode. *Analytes flow through a positively charged ESI needle. As the analytes pass out of the needle a Taylor cone is formed due to the presence of a strong electric field. Analytes containing droplets form at the cone tip which reduce in size until eventually all analytes are in gaseous form. Negatively charged plates attract the positively charged ions towards it and into the mass spectrometer.*

The advantage of using ESI is that it can be more easily coupled to a HPLC system to separate analytes prior to introduction to the mass spectrometer. This boosts the sensitivity of the instrument as not all analytes will be introduced at once. Instead, a steady stream of analytes, separated based on a certain physico-chemical property, will proceed to the mass analyser over a period of time. MALDI can be coupled to an LC system but this approach is complicated by the heterogeneity of the matrix [182]. Additionally, ESI produces multiply charged ions whereas MALDI predominantly produces singly charged ions. Theoretically, the mass range for analysers using ESI as the input source is endless as no matter how large a protein is, given enough charges, its *m/z* will fall within the detection limit of the mass analyser. Proteins could be analysed intact without enzymatic digestion giving greater information on the structure. Producing many multiply charged ions does have its drawbacks as the signal for an analyte is 'diluted' over several charge states, meaning the signal for a particular ion may not accurately reflect its concentration in the sample and sensitivity may be compromised. Preparing calibration curves, introducing isotopically labelled standards to the samples or optimising chromatographic conditions are all methods of mitigating the issue of ion signal not accurately reflecting concentration but do not aid the issue of reduced sensitivity.

1.3.3 Mass filters and analysers

A quadrupole mass filter and an Orbitrap mass analyser are used in this thesis and so will be briefly described in this section.

1.3.3.1 Quadrupole

A quadrupole mass filter/analyser consists of 4 electrically charged rods arranged in parallel as shown in figure 1.5. A fixed direct current and alternating radio frequency is applied to these rods to generate an electric field with opposite rods possessing identical potentials [183]. Ions are focused from the source and through the centre of the quadrupole rods. Changing the radio frequency applied to the rods will stabilise the flight of ions with a certain *m/z* and so only these ions will be able to pass through the quadrupole and to the detector. All other ions will have unstable flights and so will not pass through to the detector. Single quadrupole mass spectrometers have low resolving powers and therefore are mainly used in mass spectrometers as an initial mass filter where only ions of a specific *m/z* are selected to pass through the quadrupole to then reach a secondary mass analyser via a fragmentation chamber. The main secondary mass analysers in hybrid systems are the Orbitrap, Time of Flight or another quadrupole system. The addition of a quadrupole mass filter further improves the selectivity of mass spectrometry where a precursor – product ion transition can significantly increase signal to noise values for quantitative /qualitative purposes.

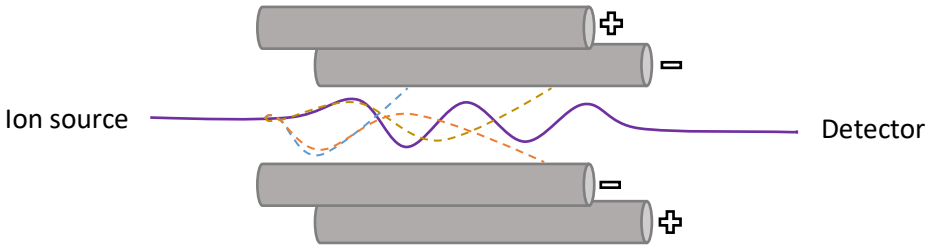

Figure 1.5: A quadrupole mass filter. *Dotted lines represent ions whose flight is not stabilised by the direct current and radio frequency through the quadrupole and therefore are filtered out. Only ions with a stable flight (solid purple line) make it to the detector.*

1.3.3.2 Orbitrap

The Orbitrap mass analyser is an ion trap mass analyser consisting of a central electrode encapsulated by two end-cap electrodes [184]. Gaseous analytes are injected into the space in between the central and encapsulating electrodes. By applying a voltage between the central and encapsulating electrodes, a radial electric field is created which causes the ions to orbit around the central electrode. As orbiting ions pass either of the encapsulating electrodes, an electric current is generated and the strength of this current is determined by the *m/z* of the analyte. See figure 1.6 [185] for a simplified schematic of an Orbitrap mass analyser. A Fourier transformation is then used to convert this electric current into the mass spectrum. Orbitrap mass spectrometers are extremely accurate, high resolution

mass analysers. Coupling an Orbitrap mass analyser to a quadrupole as an initial mass filter combines the benefits of both these systems into an instrument capable of high; selectivity, mass accuracy and resolving power. This is the case with the Thermo Q-Exactive ™ Hybrid Quadrupole-Orbitrap mass spectrometer (ThermoFisherScientific) used later on in this thesis.

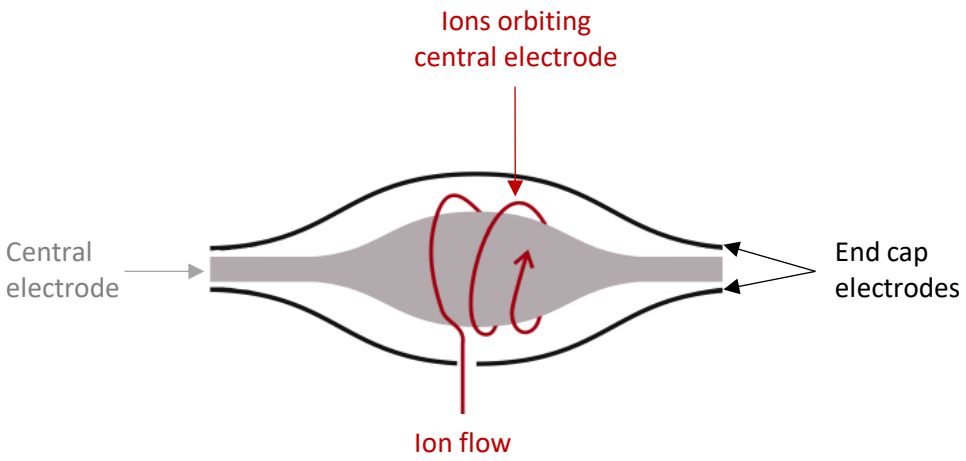

Figure 1.6: Diagram of an Orbitrap mass analyser. *Adapted from Demartini et al. (2013) [185]. Ions enter the mass analyser and start orbiting the central electrode.*

1.3.4 Tandem-MS

An analyte can be selected for further analysis where it is bombarded with atoms of an inert gas such as helium or nitrogen to fragment the analyte in a collision cell in a process known as collision induced dissociation (CID). The fragments are transferred into the mass analyser where their *m/z* values are calculated. This process is known as tandem-MS or MS/MS and gives users information as to what the analyte is composed of. With peptide analysis MS/MS can tell the user what amino acids make up the peptide.

Collision cells can be added to Orbitrap and quadrupole mass analysers to give them the ability to perform MS/MS analysis. In an Orbitrap mass analyser (such as the Q-Exactive Hybrid Quadrupole-Orbitrap mass spectrometer used in this thesis) ions undergo an initial scan in the Orbitrap analyser before certain ions are fragmented in the collision cell and reintroduced to the Orbitrap for *m/z* determination. The ions fragmented can be determined by which are most abundant in the initial scan (data-dependent acquisition or DDA) or predetermined by the user (product ion scanning). For a quadrupole analyser a common configuration to incorporate a collision cell is in a triple quadrupole mass spectrometer. This system consists of 3 quadrupole mass filters in a linear arrangement (figure 1.7). The first quadrupole (Q1) is where the flights of desired precursor ions are stabilised allowing them to pass into the second quadrupole (q2). q2 is the collision cell where CID occurs and product

ions of the desired precursors are formed. In the third quadrupole (Q3) only certain product ions are selected to pass to the detector. This targeted process of selecting specific product ions of certain precursors is known as selective reaction monitoring (SRM) and enables triple quadrupoles to achieve far superior sensitivity for the chosen analytes than Orbitrap analysers. However, increased sensitivity comes at a price of decreased resolving power and mass accuracy.

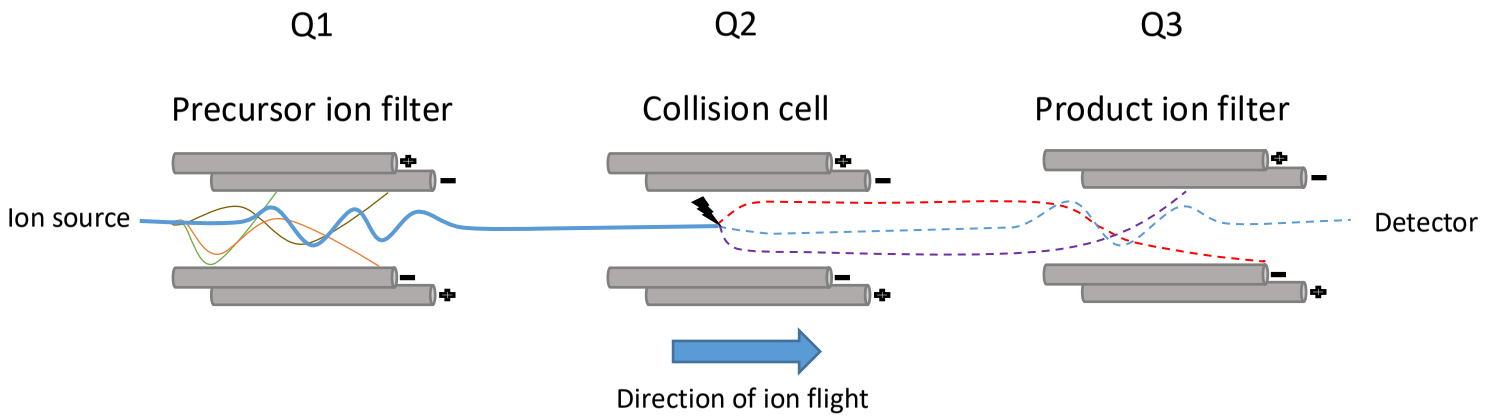

Figure 1.7: Overview of Triple quadrupole mass spectrometer. *Solid lines are precursor ions. Dotted lines are product ions.*

During MS/MS, peptides can fragment at specific points along the peptide backbone (figure 1.8A). To sequence a peptide, fragmentation occurs at the peptide bond between amino acids creating fragments composed of whole polypeptides. The sequence of the precursor peptide can be determined by matching up the fragment masses with the expected masses of amino acids for a known peptide sequence. Fragmentation does not always occur between the peptide bond as shown in figure 1.8A. Each dotted line in figure 1.8A represents the most common fragmentation points and the letters and numbers correspond to the name of the resulting fragments. If the peptide is fragmented within a peptide between the α carbon and the carbon in the carboxyl group, then the N-terminal fragment is called the 'a' ion and the C-terminal fragment is known as the 'x' ion. If fragmentation occurs at the peptide bond then the N-terminal fragment is the 'b' ion and the C-terminal fragment is the 'y' ion. CID can predominantly produce 'b' and 'y' ions which are preferred for sequencing peptides. Fragmentation within a peptide between the α carbon and the nitrogen atom in the amino group generates N-terminal fragments known as 'c' ions and C-terminal fragments known as 'z' ions. Ions also have a number associated with them. N-terminal fragments are numbered by how many amino acids away from the N-terminus they are, and C-terminal fragments are numbered due to how many amino acids they are from the C-terminus (figure 1.8B).

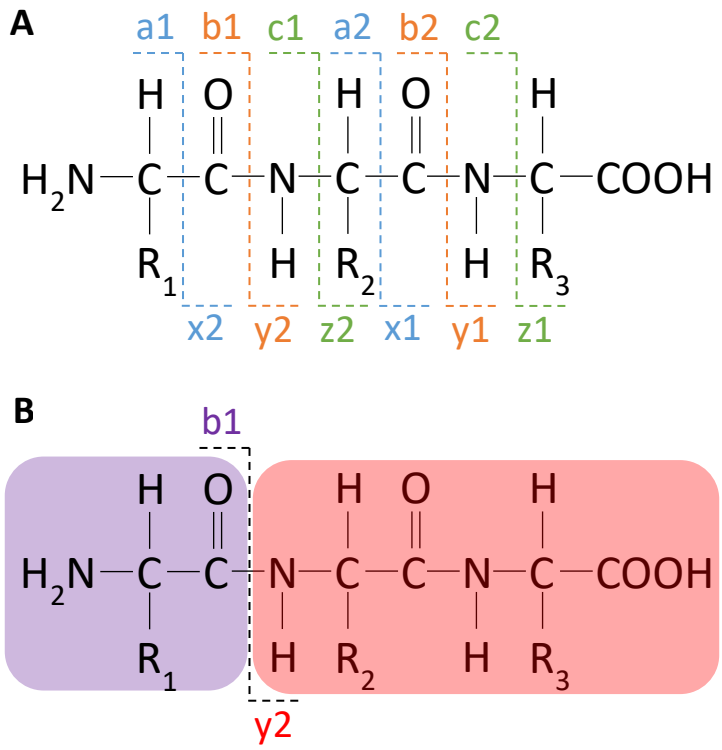

Figure 1.8: The major fragmentation points during MS/MS in a peptide. *(A) A tripeptide with all the different points within each peptide where fragmentation can occur during MS/MS. (B) An example of what the fragments from the tripeptide would be called if fragmentation occurred between the peptide bond of first and 2nd amino acids. The area highlighted in purple is called the b1 ion as it is the N-terminal fragment composed of 1 amino acid. The area highlighted in red is the y2 ion as it is the C-terminus fragment composed of 2 amino acids.*

1.3.4.1 De novo peptide sequencing and database searching

In full scan mode (i.e. without any ion filters set on a quadrupole filter) Orbitrap mass spectrometers are ideal for analysing all analytes in a sample down to low nanomolar or high picomolar ranges depending on the complexity of the sample matrix. When run with DDA, many MS/MS spectra can be generated for de novo sequencing and database matching using a software such as PEAKS studio (Bioinformatics solutions). This software takes each MS/MS spectrum and builds a picture of which amino acids are present by calculating the difference between ions within each MS/MS spectrum and identifying which amino acids correspond to these differences (figure 1.9). The software can also adjust the expected masses of the amino acids to account for potential PTMs such as amidations, pyro-glutamates and oxidations. Once a sequence has been assigned to each spectrum, the software tries to match each sequence to a known peptide sequence from a protein database such as the Swissprot database or a custom one generated from translated assembled RNA-seq data. This process is extremely important for novel peptide identification as it allows the user to detect previously

undiscovered cleavage products from known prohormones or proteins if using a database such as Swissport. If a custom database is used, then peptides from previously unannotated proteins or prohormones can be identified.

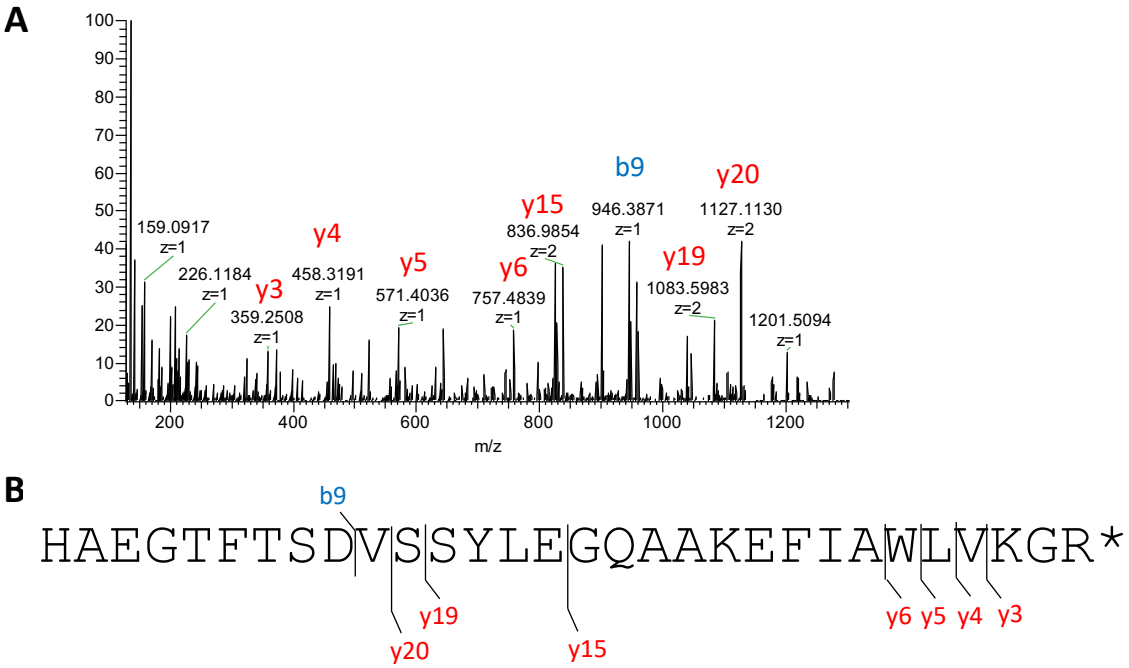

Figure 1.9: *(**A**) MS/MS spectra produced by the fragmentation of GLP-1 (7-36 amide). Several ions corresponding to the b and y ions of GLP-1 (7-36 amide) have been annotated. (**B**) Sequence of GLP-1 (7-36 amide) with ions visible in the MS/MS spectrum annotated. * represents an amidated residue.*

An important step to enable peptide de novo sequencing and database searching is to reduce disulphide bridges enabling peptides to be analysed in their linear form. By linearising peptides, the MS/MS spectra of a peptide is simplified as it will contain fragments of the linear peptide and not fragments of the intact disulphide bonded peptide. Database matching software such as PEAKS cannot match MS/MS spectra with fragments of several peptides joined by disulphide bonds to known peptides. Therefore, if you wish to match peptides using database matching software, it is necessary to reduce samples with dithiothreitol to break apart these disulphide bonds and alkylate the peptides to prevent reforming of the bonds prior to sample analysis.

1.3.5 Mass spectrometry in peptidomics

Historically, assays dependent on antibodies are the method of choice for peptide identification and quantification. LC-MS based methods hold numerous benefits over immune-based assays which

include; ability to detect multiple analytes in each sample, ability to identify subtle differences between peptides such as PTMs without any additional reagents, antibody independent and therefore not subject to off-target binding. As a result, mass spectrometry is an increasingly useful tool in the field of peptidomics. LC-MS based methods are being used for absolute quantification of peptides in human and rodent plasma and are reaching similar detection limits to immune-based methods [186-189]. LC-MS is also being used to identify biomarkers that can lead to faster diagnoses of certain diseases [190]. The physiology of EECs is being probed with LC-MS to better understand how EECs can be classified [82] and how they are stimulated [191]. MS/MS and database searching is being utilised to characterise the peptidome of the various tissue types from human and mouse which may uncover previously unidentified peptide hormones [166, 192, 193]. As well as being able to identify hormones, LC-MS can be used to rule out production of peptides in certain tissue. For example, intra-islet GLP-1 and GIP production is debated and the use of promiscuous antibodies to identify GIP and active GLP-1 in the pancreas has fuelled the debate. Use of LC-MS in this area could help to provide clarity.

1.4 Thesis aims

Peptide hormones derived from EECs or islets collectively have a plethora of physiological actions and as a result have great therapeutic potential. With the knowledge that multiple active peptides can be cleaved from one prohormone or from proteins such as Chromogranin A and Secretogranins, I hypothesised that there may be more bioactive hormones in the gut, yet to be discovered.

To identify potential novel peptides, I characterised the peptidome of FACS purified EECs as well as primary islets utilising LC-MS with MS/MS analysis and a peptide identification software called PEAKS. I then isolated gastric glands, intestinal crypts from each region of the intestines and whole islets and collected supernatants using various secretagogues to analyse the secreted peptidome of EECs. Potential candidates were identified based on various parameters such as abundance in EECs or islets, conservation with the equivalent human sequence and if they were secreted.

A panel of 13 peptides were synthesised for *in vitro* and *in vivo* testing to identify biological activity. All peptides were applied to various cell lines and intracellular cAMP levels were measured to assess activity at Gs or Gi coupled receptors. Additionally, the most promising candidates were analysed *in vivo* to assess their pharmacokinetics and ability to modulate glucose homeostasis or food intake in lean or DIO mice. One peptide was found to affect glucose tolerance and its ability to modulate islet hormone secretions and insulin signalling was assessed.

After completing the novel peptide discovery project, I focused on characterising the islet peptidome to better understand intra-islet paracrine signalling specifically focusing on islet production of active GLP-1. I next assessed how the islet peptidome was altered by obesity in mice and by T2D in humans to investigate how these pathogenic states may affect processing of islet proteins and prohormones.

Chapter 2: General Methods

2.1 Chemicals and reagents

Reagent	**Supplier**	**Identification number**
General		
Phosphate buffered saline (PBS)	Sigma	D8537
Bovine serum albumin (BSA)	Sigma	A6003
Ethylenediaminetetraacetic acid (EDTA)	Sigma	E9884
Dithiothreitol (DTT)	Sigma	D0632
Secretion experiments		
Forskolin	Sigma	F6886
3-Isobutyl-1-methylxanthine (IBMX)	Sigma	I7018
Adrenaline	Fisher	10434253
D-(+)-Glucose	Sigma	G7021
Cell culture		
Dulbecco's Modified Eagle Media (DMEM) (4.5g glucose)	Sigma	D6546
Roswell Park Memorial Institute (RPMI)	Sigma	R8758
Hank's Balanced Salt Solution (HBSS)	Sigma	H9269
RPMI without $CaCl_2$ or $MgCl_2$	Sigma	R8758
Penicillin/Streptomycin	Sigma	P0781
L-glutamine	Sigma	G7513
Matrigel	Corning	354234
ROCK inhibitor Y27632	Tocris	1254/10
Foetal bovine serum (FBS)	Gibco	10270-106
Mass spectrometry		
Acetonitrile (ACN)	Sigma	1.00029
LC-MS grade H_2O	Fisher	M/0112/17
Formic acid (FA)	Fisher	A117-50
Methanol	Fisher	M/4058/17
Acetic acid	Fisher	0714
Iodoacetamide	Sigma	I5161
Ammonium bicarbonate	Sigma	09830
Tissue digestion or homogenisation		
Collagenase V	Sigma	C9263
Collagenase XI	Sigma	C9407
Guanidine hydrochloride (GuHCl)	Sigma	G3272
Trypsin-EDTA in Ca^{2+} free HBSS (10×)	Sigma	T4674

2.2 Buffers for secretion assays

2.2.1 KRB

- For primary mouse islet secretions.
- LC-MS grade H_2O with 129mM NaCl, 2 mM $NaHCO_3$, 4.8 mM KCl, 1.2 mM KH_2PO_4, 2.5 mM $CaCl_2$, 1.2 mM $MgSO_4$, 10 mM HEPES.
- Adjusted to pH 7.4 with 1M NaOH.

2.3 Animals

All procedures were carried out with prior approval of the University of Cambridge Animal Welfare and Ethical Review Board and followed the regulations set out in the Animals (Scientific Procedures) Act 1987. Animal work was performed under either project licence 70/7824 or PEE50F6065. Mice used were from a C57BL/6N/J background and were sacrificed by a schedule 1 method.

2.4 Mouse islets isolation

Mice were sacrificed by a schedule 1 method and dissected to expose the intestines and pancreas. Using a 30g bent needle, the pancreas was inflated with ice cold 0.75 mg/mL solution of Collagenase V in HBSS. The pancreas was then removed and placed in 1 mL of the same Collagenase V solution. The pancreas was then incubated at 37^{o}C for 12 mins after which the pancreas was shaken vigorously for 1 minute to dislodge islets from the digested tissue. Exocrine tissue was removed by adding ice cold HBSS to the preparation, allowing digested tissue and islets to settle to the bottom and then removing the supernatant. This wash process was repeated 5 times. On the last wash, ice cold HBSS with 0.1 % BSA was added to the preparation and poured out into a petri dish. Addition of BSA to the HBSS preventing islets from sticking to the dish. Using a light microscope and a P10 pipette, islets were picked from the preparation and placed in fresh, ice cold HBSS with 0.1% BSA. This process of picking islets into fresh HBSS (0.1% BSA) was repeated until only islets were present in the dish and no exocrine tissue remained.

2.5 Sample preparation for MS analysis

The following techniques were used repeatedly to extract peptides from samples for LC-MS analysis. All samples analysed by LC-MS were subjected to an acetonitrile protein crash, solid phase extraction, reduction and alkylation unless otherwise specified.

2.5.1 ACN protein crash

80% ACN was added to samples in the ratio of 3:1 in favour of ACN. Samples were vortexed thoroughly and centrifuged at 4^{o}C for 5 min at 12000 rpm to pellet proteins and cellular debris. The supernatant was removed and dried down overnight at RT using a centrifugal evaporator. If the sample contained a very high concentration of salt such as 6M GuHCl solution, two phases would form after centrifugation. In this case, the top phase was discarded and the bottom taken for drying down overnight in a centrifugal evaporator.

2.5.2 Solid phase extraction

Solid phase extraction (SPE) was used to purify peptides in samples. Samples that had been dried down were reconstituted in 200 µL 0.1% formic acid (FA) in water. An Oasis HLB PRIME µElution plate (Waters) was used to extract the peptides. Samples were loaded onto the sorbents then washed with 0.1% FA in water then 200 µL of 5% methanol and 1% acetic acid in water. Two separate additions of 25 µL of 60% methanol and 10% acetic acid in water were used to elute the peptides.

2.5.3 Reduction and alkylation

Linear peptides were obtained by reducing disulphide bonds between cysteines and alkylating to prevent reforming of these disulphide bonds. Samples were dried down after SPE and the pellet suspended in 10 mM DTT in 50 mM ammonium bicarbonate solution. After a 1 hour incubation at 60^{o}C, iodoacetamide in 50 mM ammonium bicarbonate solution was added to the samples to reach a final concentration of 15 mM iodoacetamide and incubated in the dark at RT for 30 minutes. 0.1% FA in water (v/v) was added to acidify samples before LC-MS analysis

2.6 Mass spectrometry

Two LC/MS systems were used. A Thermo Fisher Ultimate 3000 nano LC system (Thermo Fisher Scientific) coupled to a Q Exactive Plus Orbitrap mass spectrometer (Thermo Fisher Scientific) and a Xevo TQ-XS triple quadrupole LC-MS (Waters) coupled to a either a H-class Aquity UPLC system

(Waters) or a M-Class UPLC system (Waters). The method settings for the Orbitrap mass spectrometer were the same throughout this thesis and so will be described in the section below. However, the method settings for the TQ-XS triple quadrupole mass spectrometer changed depending on the peptides being analysed and so will be detailed in the methods section for each chapter.

2.6.1 Nano flow rate analysis on Orbitrap mass spectrometer

Peptides were analysed using a nano fluidics system to achieve the greatest sensitivity for detection. The total run time for each sample was 130 minutes during which both the 0.3 × 5 mm peptide trap column and 0.075 × 250 mm nanoEase™ column (Thermo Fisher Scientific) were kept at 45°C. Chromatography buffers used were 0.1% FA in water (v/v) (buffer A) and 0.1% FA in ACN (v/v) (buffer B). The starting chromatography condition was 2.5% of B which was maintained for 15 minutes to load the peptides onto the trap column at a flow rate of 30 µL/minute. The trap column was then set in-line with the nano column at a flow rate of 300 nL/minute where the gradient increased linearly to 50% of B over 145 minutes, after which the conditions were stepped up to 90% of B to wash/clean the column for 20 minutes. Positive ESI was used with the spray voltage set to 1.8 kV. The S-lens voltage was set to 70 V to improve the transmission of analytes with higher *m/z* values. The scan range for the run was between *m/z* values of 400-1600 at a resolution of 75000. Data dependent acquisition was used where the ten most abundant ions from each scan cycle were selected for MS/MS analysis.

2.6.2 High flow rate analysis on Triple Quadrupole MS

A Xevo TQ-XS triple quadrupole mass spectrometer coupled to H-class Aquity UPLC system enabled high throughput and targeted sample analysis. Therefore, when a balance needed to be struck between sensitivity and throughput, this method was used. The column used was a Waters HSS T3 2.1×50 mm column at 60 °C and flowing at 350 µL/minute. LC-MS/MS analysis was performed using positive ESI with a spray voltage of 3 kV, desolvation temperature 600°C, gas flow rate 1000 L/hour and cone voltage of 40 V. Gradient specifications as well as precursor, product and collision energies differed depending on the peptides being analysed. These will be specified in methods sections for each chapter. However, in all cases, buffer A was 0.1% FA in water (v/v) and buffer B was 0.1% FA in ACN (v/v).

2.6.3 LC-MS data processing

Raw files from the Orbitrap MS were processed using Xcalibur v4.3.73.11 (Thermo Fisher Scientific). Peak areas from these raw files were obtained by selecting 3 ions in the ^{13}C distribution pattern of a

peptide in the highest abundance charge state and integrating the area under the curve (AUC) on the chromatogram for these three ions.

Raw files from the Triple Quadrupole MS were analysed using Mass lynx v4.2 (Waters). Peak areas were obtained by integrating the AUC on the chromatogram created by product ions specific to precursor ions from certain peptides.

2.6.4 PEAKS database searching

Raw files containing MS/MS spectra were loaded into the software package, PEAKS (v8.5) (Bioinformatics Solutions), to be searched against the mouse or human Swissprot databases to identify peptides up to 65 amino acids in length. Precursor and product ion tolerances were set to 10 ppm and 0.05 Da respectively meaning the software would still match an analyte sequence even if the mass of product ions were out by 0.05 Da and the ppm of the precursor was off by 10 ppm. Post-translation modifications were included in the database search (fixed carbamidomethylation modifications at cysteine residues (a consequence of the reduction and alkylation process), and variable modifications included oxidation at methionine residues, C-terminal amidation, N-terminal-acetylation and N-terminal pyro-glutamate formation). A false discovery rate of 1% was applied to reduce false positive matches.

Chapter 3: Selection of novel peptide hormone candidates through peptidomic characterisation of EECs and islets

3.1 Introduction

As we have seen, enteroendocrine cells (EECs) and islet cells are established peptide hormone producing cell populations of gastrointestinal (GI) tract and pancreas and so any search for novel peptide hormones should at least encompass these cells. In addition to the established hormones, such as insulin, glucagon, glucagon-like peptide-1 (GLP-1) and cholecystokinin (CCK), EECs and islets produce a plethora of proteins of which, established prohormones, granins and processing enzymes are of high relevance for this chapter. In this section, I will discuss the rationale for searching for novel gut peptides from these proteins and the approaches previous studies have taken to identify them.

3.1.1 Granin proteins

Granin proteins are a large family of acidic, soluble proteins found in vesicles of secretory cells [194]. Chromogranin A (ChgA) was the first granin protein to be discovered in the 1950s [195] and the family has since expanded to include; secretogranin (Scg) 1, Scg2 (or ChgB), Scg3, Scg4, Scg5 (or 7B2), Scg6, Scg7 (or VGF) and Pcsk1n (proSAAS). These proteins bind solutes inside the vesicle such as catecholamines and Ca^{2+} to reduce the osmotic stress exerted on these intracellular structures and thus preventing diffusion of solutes into the cytosol [196]. Multiple cell types are now known to produce granin proteins including Islet of Langerhans cells and EECs. With a high frequency of mono- and dibasic cleavage points in their sequence, these proteins are processed by prohormone convertases PC1/3 and PC2 to produce numerous peptides some of which have been shown to exert physiological actions [197-199] (table 3.1). ChgA, Scg1, Scg2 and proSAAS are the most prevalent in EECs and islets and so only peptides from these proteins are listed in table 3.1.

Protein	Peptide	Location	Effect
ChgA	Vasostatin-1, -2	Parathyroid gland	Vasorelaxant and cardio-suppressive through inhibition of parathyroid hormone release [200, 201]. Antibacterial properties [202] .
ChgA	Chromafungin		Antifungal properties [203]
ChgA	Pancreastatin	Pancreas, adrenal gland	Stimulate glycogenolysis in hepatocytes [204]. Decrease glucose uptake by adipocytes [205]. Inhibits GSIS in rats [206].
ChgA	Catesatin	Adrenomedullary cells	Antihypertensive effects by inhibiting release of catecholamines [207].
ChgA	WE14	Pancreatic β-cells	Auto-antigen for CD8+ T-cells in type 1 diabetes (T1D) [208].
ChgA	Parastatin, GE25	Parathyroid gland	Vasorelaxant and cardio-suppressive through inhibition of parathyroid hormone release [209].
ChgA	Serpinin, (p-Glu)-Serpinin, Serpinin-RRG	AT-20 cells (cortical neuron cell line), heart	Regulates granule biogenesis through upregulation of protease nexin-1 [210]. Positive inotrope [211].
Scg1	CgB-41	Parathyroid gland	Inhibition of parathyroid hormone release [212].
Scg1	BAM	Rat brain [213], adrenomedullary chromaffin cells [214].	None found
Scg1	Secretolytin	Chromaffin cells	Antibacterial properties [215].
Scg2	Secretoneurin	Anterior pituitary	Potentiates release of luteinizing hormone pituitary cells in response to gonadotroph releasing hormone [216].
Scg2	Manserin	Pituitary gland [217], duodenal villi [218], islets [219].	Unknown
proSAAS	bigSAAS, little SAAS, KEP	Rat adrenal medulla [220]	Unknown
proSAAS	'PEN-LEN' derived peptides	Neuroendocrine and endocrine cells	PC1/3 inhibitor [221]

Table 3.1: Physiological actions of peptides derived from ChgA, Scg1, Scg2 and proSAAS*. These peptides are annotated on their protein of origin in figure 3.1.*

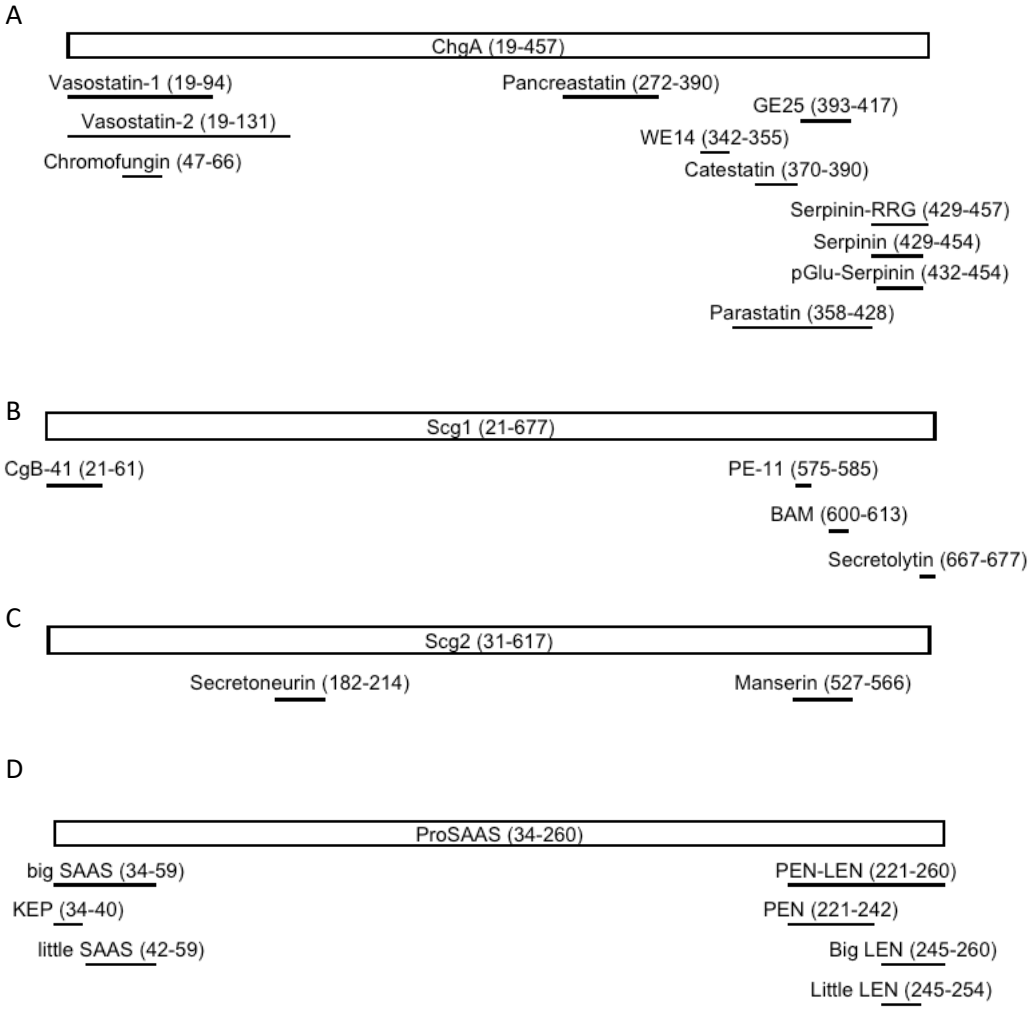

Figure 3.1: Peptides derived from ChgA (A), Scg1 (B), Scg2 (C) and ProSAAS (D). *Numbers in brackets represent the position on the prepropeptide.*

3.1.2 Multiple active peptides from prohormones

Proglucagon is perhaps the most obvious example of a gut-derived prohormone which produces multiple active peptides (figure 3.3). Glucagon, GLP-1 and GLP-2 all primarily bind to different specific G-protein coupled receptors (GPCRs) to induce different, sometimes conflicting, physiological effects. Pro-opiomelanocortin (POMC) is also cleaved to form multiple peptides acting on different receptors [222]. MSH, ACTH and γ-lipotropin bind to melanocortin receptors whereas β-endorphin binds to opioid receptors. However, it should be noted that *Pomc* is predominantly expressed in the CNS. Aside from proglucagon, other prohormones found in either EECs or islets are known to be processed into multiple active peptides. However, the multiple peptides derived from the likes of prosomatostatin, procholecystokinin and proPYY are merely different versions of each other acting primarily on the

same family of receptor. For example, PYY (3-36) is a DPP IV cleaved version of PYY (1-36) and both act on the NPY family of receptors although they have different affinities for the NPY receptor subtypes [223].

Prohormone	Length in amino acids	% of amino acids exactly conserved between humans and mice	No. of monobasic residues	No. of dibasic sites
Proglucagon	160	91	9	7
Prosomatostatin	116	97	10	1
Procholecystokinin	95	80	10	3
ProPYY	69	70	10	1
Proghrelin	94	89	8	3
Progastrin	100	79	3	3
Proneurotensin	147	82	15	3
ProGIP	132	69	12	3
ProPOMC	267	72	18	8

Table 3.2: Certain characteristics of known prohormones

This begs the question; does proglucagon have special characteristics enabling production of multiple hormones whereas other prohormones are only known to produce one or two? In terms of expression, *Gcg* (the gene coding for proglucagon) is no more highly expressed in its cell of origin than other the other gut derived prohormones. High expression is an important trait for peptide hormones if they are to reach high enough levels in the surrounding tissue and circulation to exert their biological effects [85, 224]. Proglucagon does possess numerous dibasic cleavage points however it is no better conserved than other prohormones such as prosomatostatin (table 3.2). Furthermore, proglucagon doesn't contain many monobasic cleavage sites compared to other prohormones (table 3.2). These are all important factors to consider seeing as all known gut derived peptide hormones; are flanked by mono- or dibasic cleavage sites, highly conserved between humans and mice and highly expressed in specific populations of endocrine cells. Therefore, when searching for novel peptides, it is logical to search for peptides which share these characteristics of high homology, flanked by mono- or dibasic residues and high expression. A good place to start would be the prohormones know to produce at least one active peptide which are rich in cleavage sites, highly conserved and highly expressed in EECs and islets.

3.1.3 Novel peptide discovery approaches

As has been shown, granin proteins and prohormones are sources of bioactive peptide hormones and many more peptides could yet be discovered. Many approaches have been taken to identify novel

peptides. Corbière et al. provide a review outlining 5 strategies which have been used over the last 70 years to identify neuropeptides [225]. Table 3.3 summarises these approaches, detailing their drawbacks as well as some examples of peptides discovered by each approach.

A peptidomic-based approach to identifying novel peptides has not been extensively used until recently potentially due to the expense of the specialist instruments required. Several studies do analyse the peptidome of various cell and tissue types such as islets [166, 226] and the hypothalamus [192, 227], however, an in-depth picture of the cleavage products from prohormones, granins and processing enzymes is not given and none of the peptides identified are synthesised for characterisation of biological activity. Egerod et al. analysed extracts of purified CCK-expressing cells of the small intestines but only reported the top 11 most abundant proteins found with the number of peptides from these proteins [82]. No information on the peptides found were given. This leaves scope for a study to characterise the peptidome of all EECs and islets in greater detail and select a panel of interesting peptides for characterisation of potential biological activity.

Approach	Description	Drawbacks	Examples
Identification based on biological activity	Applying homogenised tissue extracts to cell lines or tissue preparations and observing a biological response	Low throughput, often need input from another method to know which tissue extract to apply to which cell line. If biological activity found need subsequent purification and retesting of extracts to isolate bioactive peptide.	Somatostatin [228], Serpinin [210]
Receptor-based identification	Screening of synthetic peptide libraries or tissue extracts for activity at orphan GPCRs (radioligand binding assays or measurement of intracellular signalling activation)	Radioligand binding assays require radiolabelled ligand for receptor. Assessment of specific intracellular signalling pathways	Orexin [229]
Identification by peptide characteristics	Purification of peptides based on a certain characteristic such as C-terminal amidation. Searching for sequences flanked by dibasic residues	Not all peptides share same characteristics. E.g. only 50% of active peptides are amidated. Therefore, could exclude potential candidates	Cholecystokinin, [230] Neuropeptide Y [231]
Identification using genomics	Sequencing genome of multiple species and predicting the amino acid sequences coded by certain genes. Identification of conserved sequences between species	Doesn't give information on the final processed form of peptide. Information on PTMs or additional cleavage by prohormone convertases will still need to be obtained	Urotensin II [232], GLP-1 [233], Neuronostatin [234]
Peptidomic-based approach	Peptide extraction from tissue or cell homogenates, analysis by LC-MS, de novo peptide sequencing from tandem-MS spectra. Can identify known peptides by matching against protein databases	Need to preserve peptide sequence during sample processing and extraction and avoid degradation. Huge numbers of peptides can be identified making it difficult to ascertain which are bioactive and which are break down products.	

Table 3.3: Approaches to novel peptide discovery as outlined in Corbière et al. [225].

3.2 Aims

1. Characterise the peptidome of mouse EECs, mouse islets and human GI tissue.
2. From this peptidomics data, identify a panel of peptide candidates to be synthesised for characterisation of potential biological activity.

3.3 Methods

Figure 3.2 summarises the workflow used to characterise the peptidomics of mouse EECs, mouse islets and human GI tissue.

3.3.1 Mouse EEC peptidomics

3.3.1.1 GI tissue preparation

After schedule 1 the GI tract was removed, separated into different regions (stomach, proximal small intestines (SI), mid-SI, distal SI and large intestines (LI)). The proximal SI, mid-SI and distal SI represented 10 cm segments along the SI. Tissue was flushed with cold PBS to remove content, stripped of the muscle layer and diced into 1 mm^2 pieces.

3.3.1.2 FACS of EECs

Mice

NeuroD1-Cre/Rosa26^{YFP} mice (referred to as NeuroD1 mice) [235] were used to isolate the enteroendocrine cell population from the GI tract. NeuroD1 mice are a transgenic mouse line in which Cre-recombinase, under the control of the NeuroD1 promoter, is used to trigger expression of YFP in NeuroD1 expressing cells. NeuroD1 is a transcription factor important for the differentiation of GI stem cells into EECs and therefore, in the context of the intestinal epithelium, the NeuroD1 promoter will be exclusively active in EECs.

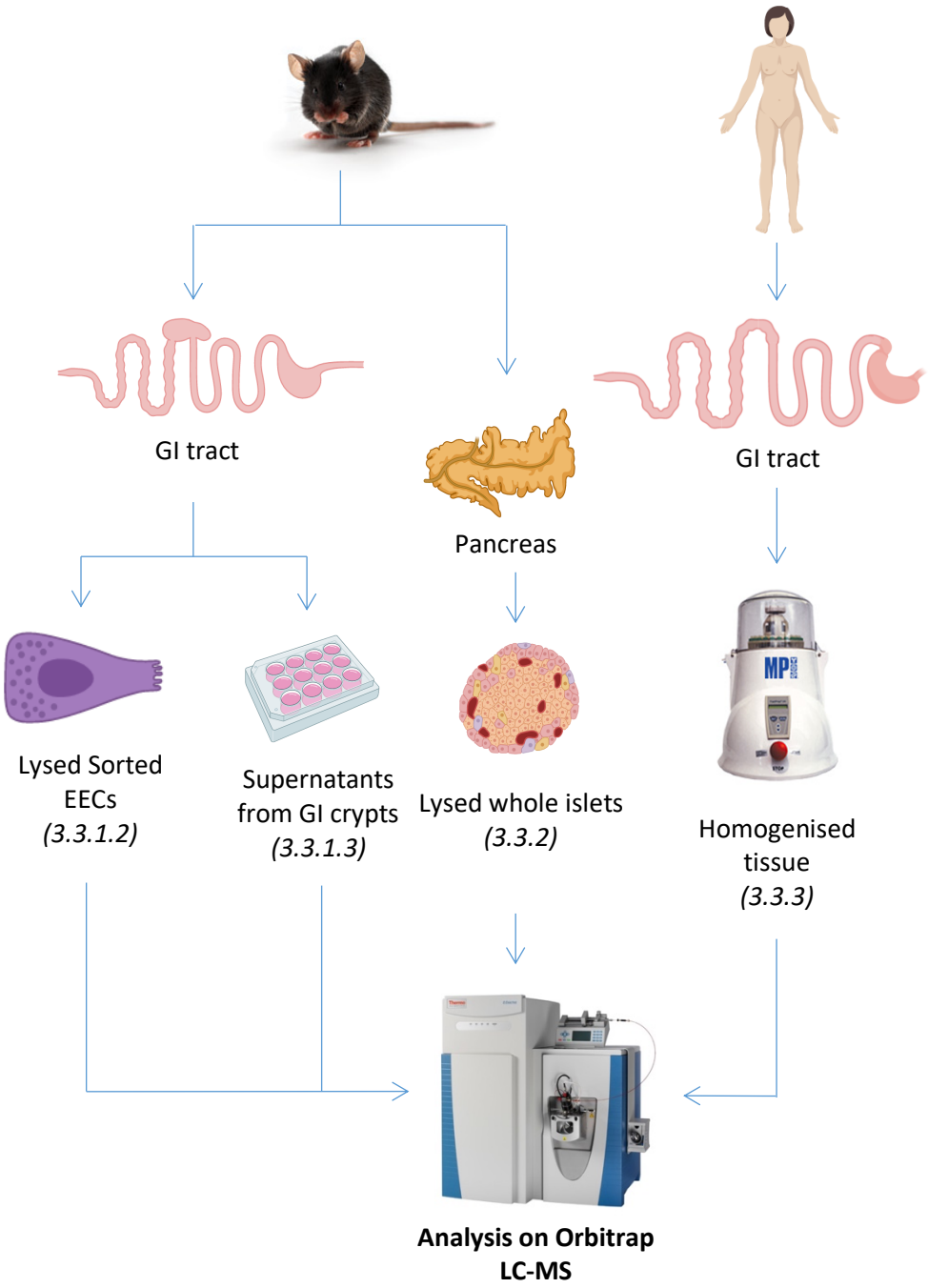

Figure 3.2: Schematic of workflow to characterise peptidome of mouse EECs, mouse islets and human GI tissue*. Mouse GI tract dissected from mice for isolation of EECs by cell sorting as well as collection of stimulated and basal supernatants from cultured crypts. Mouse pancreas also dissected for isolation of whole islets. Different regions of human GI tract collected for homogenisation. Peptidomics analysed of all samples analyse by on an Orbitrap LC-MS. Numbers in brackets relate to the section describing the methods used.*

Digestion of GI tissue for FACS

Intestines: Tissue prepared as described in section 3.3.1.1 but kept intact after removal of the muscle layer. The tissue was transferred to PBS containing 1 mM DTT and EDTA (5mM EDTA for small intestinal tissue, 15mM for large intestinal tissue) for 50 minutes. Every 10 minutes during this time tissue was transferred into PBS (with 10 µM Y-27632) and shaken to remove villi and crypts. Villi and crypts were pelleted by centrifuging at 300 g for 5 minutes at 4^{o}C. Villi and crypts were resuspended in HBSS (with 0.25 µg/mL trypsin and EDTA) and incubated at 37^{o}C for 5 minutes to obtain single cells. HBSS (with 10% FBS and 10 µM Y-27632) was added at the end of the 5 minutes to inactivate trypsin. Single cells were centrifuged (500 g, 5 minutes, 4^{o}C), re-suspended in HBSS (with 0.1 % BSA and 10 µM Y-27632) then filtered twice, first with a 100 µm filter then with a 50 µm filter to remove aggregates.

Stomach:

Solution A

- PBS with 1.3 mg/mL Pronase E (Fisher Scientific)

Solution B

- dd$H_2$0 containing NaH_2PO_4 (0.5 mM), Na_2HPO_4 (1 mM), NaCl (70mM), KCl (5 mM), $NaHCO_3$ (20 mM), Glucose (11 mM), HEPES (50 mM), EDTA (1 mM), BSA (1 mg/mL).

Solution C

- dd$H_2$0 containing NaH_2PO_4 (0.5 mM), Na_2HPO_4 (1 mM), NaCl (70mM), KCl (5 mM), $NaHCO_3$ (20 mM), Glucose (11 mM), HEPES (50 mM), $CaCl_2$ (1 mM), $MgCl_2$ (1.5 mM), BSA (1 mg/mL).

Solution D

- dd$H_2$0 containing NaCl (140 mM), $MgSO_4$ (1.2 mM), $CaCl_2$ (1 mM), HEPES (50 mM), glucose (11 mM), BSA (1 mg/mL), DTT (0.5 mM).

The stomach was dissected out from the GI tract, inverted and incubated in solution A for 10 minutes at room temperature. The stomach was then incubated alternately in solution B at 37^{o}C for 30 minutes and then solution C at 37^{o}C for 7 minutes. The supernatants from each incubation were centrifuged at 300 g for 5 minutes at 4^{o}C. Pellets were washed in solution D, centrifuged (300 g, 5 minutes, 4^{o}C) and pellets re-suspended in HBSS with 1 mg/mL BSA and 10 µM Y-27632. A 50 µm filter was used to remove any cell clusters

Cell Staining: The cell suspensions for the intestines and stomach were stained with 1 in 1000 anti-CD45-PE (Fisher Scientific) to identify immune cells as well as 1 in 1000 DAPI (Sigma) and 1 in 1000 Draq5 (Invitrogen) to identify live cells when performing fluorescence-activated single cell sorting (FACS).

FACS

FACS was carried out on single cell suspensions using a BD FACSJazz. Single cells were gated using forward scatter (FSC) and side scatter (SSC). Live cells were gated by gating around the DAPI negative and Draq5 positive cells. Cells were then sorted based on their fluorescence in the YFP channel. YFP positive cells (EECs) were sorted into Protein LoBind Eppendorf tubes with 800 µL 80 % ACN and subjected to a protein crash (see section 2.5.1).

3.3.1.3 Primary mouse GI crypt cultures

Stomach

The stomach was dissected out from the GI tract and inverted. DMEM containing 0.35 mg/mL of collagenase XI (Sigma) was added to the stomach, shaken and left to incubate at 37^{o}C for 50 minutes. Every 10-15 minutes the supernatant was removed, centrifuged at 300g for 5 minutes at 4^{o}C and the pellet re-suspended in DMEM (with 10 % FBS, 1% penicillin & streptomycin and 1% L-glutamine). Each fraction had a 20 µL aliquot removed to assess the quality and number of crypts under a light microscope. Fresh DMEM media with collagenase XI was added to the tissue after removal of the supernatant and the tissue shaken. Fractions with numerous crypts were pooled, filtered using a 70 µm filter and washed with DMEM media (with 10 % FBS, 1% penicillin & streptomycin & 1% L-glutamine and 10 µM Y-27632). The crypt preparation was distributed evenly between 4 wells of a 12-well plate-which had been pre-coated with Matrigel (Corning)-and placed in a humidified incubator at 37^{o}C.

Small intestines

Identical to stomach except 0.3 mg/mL collagenase XI was used in the digestion media and the tissue was incubated in digestion media 2 times for 5 minutes and 3 times for 10 minutes.

Large intestines

Identical to stomach except 0.4 mg/mL collagenase XI was used in the digestion media. Additionally crypt preparations were evenly distributed between 6 wells of a 12-well plate.

Buffer 138

- For primary GI crypt cell secretion assays
- LC-MS grade H_2O with 138 mM NaCl, 4.2 mM $NaHCO_3$, 4.5 mM KCl, 1.2 mM NaH_2PO_4, 2.6 mM $CaCl_2$, 1.2 $MgCl_2$, 10 mM HEPES.
- Adjusted to pH 7.4 with 1M NaOH.

GI crypt cell secretion peptidomics

16-24 hours after culturing, cells were washed twice with buffer 138 and incubated at 37^{o}C with buffer 138 for 1 hour. The basal supernatant from each well of each tissue type was pooled into a Protein LoBind tube and cellular debris was pelleted by centrifuging at 200g for 5 mins at 4^{o}C. The supernatant was then removed and snap frozen. Immediately after removal of the basal supernatant, fresh buffer 138 was added to each well with forskolin (10 μM), IBMX (10 μM) and glucose (10 mM). Forskolin, IBMX and glucose (FIG) increase intracellular cAMP to stimulate peptide secretion. After a 1 hour incubation at 37^{o}C, the stimulated supernatants from each well of each tissue type was removed, pooled and treated in the same way to the basal supernatant.

3.3.2 Islet peptidomics

See section 2.4 for detail on mouse islet isolation. After resting, islets were washed in KRB with 5.5 mM glucose before transferring into a Protein LoBind tube (Ependorff) with 250 μL 6M guanidine hydrochloride (GuHCl). Lysates were freeze-thawed three times to aid cell lysis before a protein crash (see section 2.5.1).

3.3.3 Human GI peptidomics

Performed by Pierre Larraufie and Geoffrey Roberts

3.3.3.1 Ethics

A local ethics review committee (09/H0308/24) approved human studies where tissue was collected from patients undergoing surgical resection by the Human Research Tissue Bank at Addenbrooke's Hospital, Cambridge, UK. All human tissue samples were utilised on the day of collection.

3.3.3.2 Tissue homogenisation and sample preparation

~30 mg pieces of human GI mucosa were homogenised in 250 μL 6 M GuHCl with Lyzing MatrixD (MPbio) beads using a FastPrep-24 homogeniser. 4 cycles of 40 seconds shaking at 6 m/s were used

to homogenise tissue. Samples were prepared for LC-MS/MS analysis with a protein crash (section 2.5.1).

3.3.4 Sample preparation

All supernatants, protein crashed cell lysates and protein crashed homogenates were extracted using SPE (see section 2.5.2), reduced and alkylated (see section 2.5.3).

3.3.5 LC-MS data analysis and database searching

See section 2.6.1 for details on sample running using Orbitrap mass spectrometer and section 2.6.3 for details on data analysis with Xcalibur software. MS/MS spectra from raw data files were sequenced and matched against the mouse or human Swissport database using PEAKS software package (section 2.6.4).

3.4 Results

3.4.1 Rationale for novel peptide candidate selection

Peptide hormone candidates for synthesis were identified in the peptidomic data of human and mouse EECs and islets. I employed a set of criteria to aid in the selection of novel peptide candidates for synthesis. No algorithm was used to select peptides based on these criteria as was done in the papers by Zhang et al., Samson et al. or Yosten et al [234, 236, 237]. Instead, I focused on peptides derived from known prohormones or granin proteins in NeuroD1 sorted cells and then applied the criteria to manually narrow down the list of potential candidates making final selection decision based on similar peptides poorly annotated in the literature.

These criteria were based on physical characteristics that most peptide hormones share. Some of these characteristics have been mentioned already such as a peptide being flanked by mono- or dibasic residues and conservation between species. Others haven't been discussed such as a peptide exhibiting regulated secretion. By this I mean that a peptide's secretion can be induced by secretagogues. This is a trait of all peptide hormones as it enables EECs to respond to nutrients binding to GPCRs by secreting their hormones.

Some characteristics of known peptides were noticed once looking at the peptidomic data. Clear cleavage points on the preprohormones seem to be indicative of some bioactive hormones. Take GLP-1 as an example (figure 3.3). There is a clear cleavage point in preproglucagon at position 97 and 129-130 as no peptides detected in NeuroD1 sorted cells span over these residues. The same can be

seen for ghrelin (figure 3.13) and PYY (figure 3.16A). Clear cleavage points are not always seen such as for CCK (figure 3.10) but in some cases do seem to indicate an active hormone.

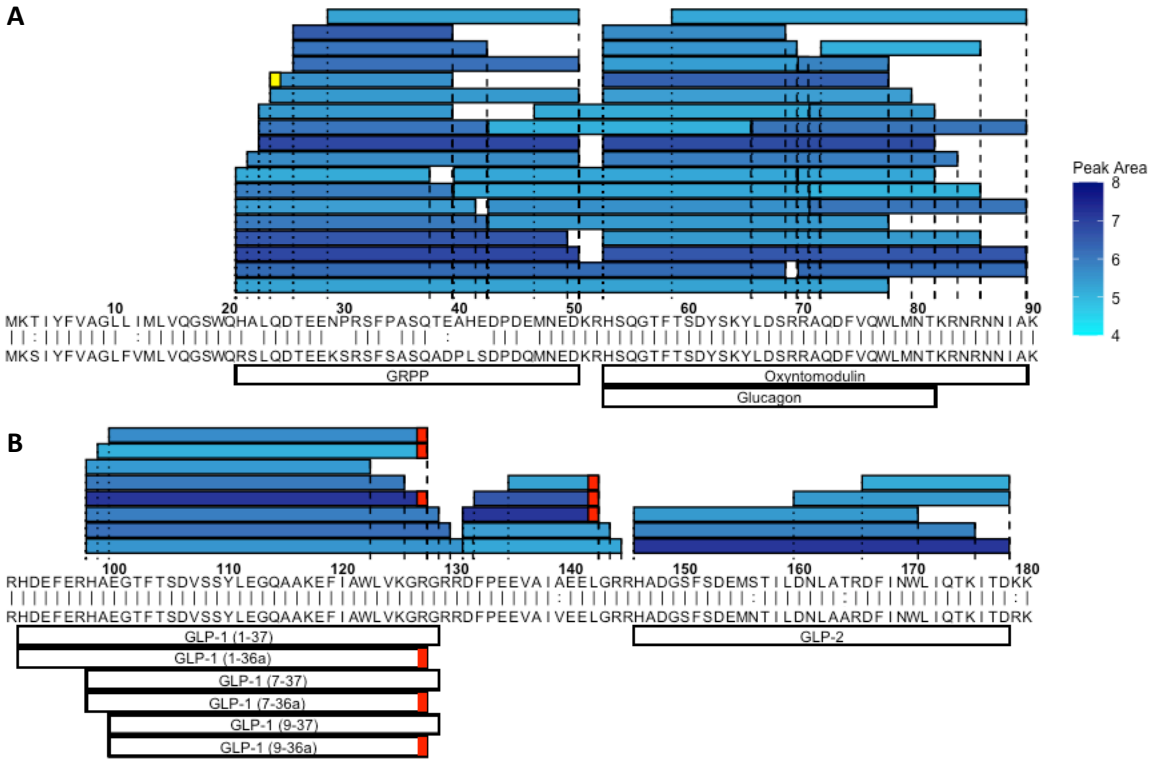

Figure 3.3: Peptides derived from preproglucagon in NeuroD1 sorted cells from all regions of mouse the GI tract*. (**A**) Peptides from positions 1-90. (**B**) Peptides from positions 90-180. Murine prepropeptide is aligned to the human prepropeptide where '|' represent identical residues and ':' represent chemically similar amino acids. Shading in blue is a measure of the peptide's peak area (log scale). Peptides described in literature are annotated on the bottom. Red boxes indicate C-terminal amidations.*

Furthermore, a literature search was performed to find peptides that have not been annotated as extensively as the classical gut hormones of table 1.2 and this was used to help guide candidate selection. For example, neuronostatin is a computer-predicted prosomatostatin derived peptide shown to regulate food intake as well as numerous other physiological functions although it is not certain it is endogenously produced [234, 238-240]. I therefore searched the peptidomic data for neuronostatin or for a similar peptide that could be the endogenous version responsible for the actions of neuronostatin *in vivo*.

The following criteria were used to identify novel peptide candidates for synthesis.

1. Flanked by mono- or dibasic residues

2. Present in NeuroD1 sorted cells
3. Present in homogenised human GI tissue
4. >50% conservation with human sequence
5. Exhibits regulated secretion from mouse GI epithelial cells
6. Clear cleavage points in preprohormones
7. Presence in lysed islets

To be selected, a peptide had to satisfy points 1-4. Peptides did not have to satisfy each of points 5-7 as these were only used to choose between candidates which had already satisfied points 1-4.

3.4.2 Novel peptide panel for synthesis

Table 3.4 displays all the novel peptides selected for synthesis. Each peptide will be referred to by the protein from which it originates, the amino acids it spans on the prepropeptide and any modifications to the amino acids. For example, the peptide in row 1 of table 3.4 will be called ChgA 435-462a as it originates from ChgA, spans amino acids 435 to 462 on the prepropeptide and is amidated at the C-terminus. Pyroglutamate residue are denoted by a 'p' prior to the amino acids which the peptide spans. For example, Gast p59-79 has a pyroglutamate residue on the N-terminus. Human peptides will be referred to in the same way but the gene name will be in capitals.

Table 3.4 also summarises; any PTMs on each peptide, the human and mouse tissues in which the peptides are found, the mouse tissues in which the peptides are secreted from, the species of plasma the peptides are found in and any similar peptides which have previously been described in the literature. Similar peptides are defined as peptides which span over the same regions on the prepropeptide. All these data will be displayed in greater detail in this chapter.

Table 3.5 shows the sequence alignment for each peptide in table 3.4 against the equivalent human sequence. All peptides showed greater than 65% conservation with their equivalent human sequences apart from Pyy 68-98.

Based on the peptidomic data as well as similar peptides described in the literature, novel peptide candidates were assigned to either priority 1 or priority 2. Priority 1 peptides (highlighted in blue in table 3.4 and 3.5) were to be synthesised for *in vitro* and *in vivo* characterisation but priority 2 peptides (highlighted in green in table 3.4 and 3.5) were synthesised for *in vitro* testing only.

Gene	Position	PTM	Human tissue	Mouse tissue	Mouse tissues secreted from	Similar annotated peptides
ChgA	435-462a	Amidation	S, P, M	Is, S, P, M	S, M, C	Serpinin, Serpinin-RRG, p-Glu Serpinin
Gast	p59-79	Pyroglutamte	S, P	S, P	S, P	Big gastrin, Gastrin
Sst	25-36		S, P, M, D, C	Is, S, P, M	S	Antrin, Neuronostatin
Cck	p21-44	Pyroglutamte	S, P, M, D	S, P, M, D, C	S, P, M, D, C	
Cck	46-63		S, P, M, D	S, P, M, D, C	M, D	
ChgA	358-371		S, P, M, D, C	Is, S, P, M	S, P, M	WE-14
Ghrl	52-85		S	S	S	Obestatin
Nec1	90-108		S, P, M, D	Is, S, P, M	S, P, M	
Pcsk1n	42-59		S, P, M, D, C	Is, S, P, C		Big SAAS
Pyy	68-98		D, C	S, P, M, D, C	D, C	
Scg2	184-216		S, P, M, D, C	Is, S, P, C		Secretoneurin
Scg2	569-610		S, P, M, D, C	Is, S, P, C		
Tac1	72-95		S, P, M, D, C	P, M, D		Neuropeptide K

Table 3.4: *Novel peptide candidates selected for synthesis. Is=Islets, S=Stomach, P=Proximal SI, M=Mid-SI, D=Distal SI, C=Colon.*

3.4.3 Priority 1 peptides

Figures 3.4 – 3.9 show the alignments of peptides identified to their prepropeptide sequences of origin. These figures relate to the priority 1 peptides and will be used to explain rationale for selecting these peptides for synthesis. Figure 3.20 looks specifically at secretion of peptides from supernatants of cultured GI epithelial cells and will also be used to support the selection of peptide candidates for synthesis.

Peptide name	Sequence alignment	% of aa exactly conserved	% of aa exactly conserved + % chemically similar amino acids
ChgA 435-462a	AEDQELESLSAIEAELEKVAHQLQALRR# |||||||||||||||||||||||| PEDQELESLSAIEAELEKVAHQLQALRR#	96.4	96.4
Gast p59-79	*QLGPQGPQHFIADLSKKQRPR ||||||| |::|| |||| | *QLGPQGPPHLVADPSKKQGPW	71.4	81.0
Sst 25-36	APSDPRLRQFLQ |||||||||||| APSDPRLRQFLQ	100.0	100.0
Cck p21-44	*QPVVPAEATDPVEQRAQEAPRRQL ||| ||: : |||:||||||| *QPVPPADPAGSGLQRAEEAPRRQL	62.5	75.0
Cck 46-63	VLRTDGEPRARLGALLA ||||| ||:|||||| SQRTDGESRAHLGALLA	77.8	83.3
ChgA 358-371	WSRMDQLAKELTAE ||:|||||||||| WSKMDQLAKELTAE	92.9	100.0
Ghrl 52-85	ALEGWLHPEDRGQAEETEEELEIRFNAPFDVGIK || |||:||| |||| |:|||:|||||||||| ALAGWLRPEDGGQAEGAEDELEVRFNAPFDVGIK	79.4	88.2
Nec1 90-108	LSDDDRVTWAEQQYEKERS ||||||| |||||||||| LSDDDRVIWAEQQYEKERS	94.7	94.7
Pcsk1n 42-59	SLSAASAPLVETSTPLRL ||||| || || | |: GLSAASPPLAETGAPRRF	61.1	66.7
Pyy 68-98	DVPAALFSKLLFTDDSDSENLPFRPEGLDQW | | |:|| :| | | : | || | | DGPDTLLSKTFFPDGEDRP-VRSRSEGPDLW	41.9	54.8
Scg2 184-216	TNEIVEEQYTPQSLATLESVFQELGKLTGPSNQ |||||||||||||||||||||||||| || TNEIVEEQYTPQSLATLESVFQELGKLTGPNNQ	97.0	97.0
Scg2 569-610	IPVGSLKNEDTPNRQYLDEDMLLKVLEYLNQEQAEQGREHLA :||| ||:||||||| |||:|:|||||||| || ||||:| FPVGPPKNDDTPNRQYWDEDLLMKVLEYLNQEKAEKGREHIA	76.2	88.1
Tac1 72-95	DADSSVEKQVALLKALYGHGQISH |||||:|||||||||||||| DADSSIEKQVALLKALYGHGQISH	95.8	95.8

Table 3.5: *Sequence alignment of mouse peptide candidates (on top) vs equivalent human peptide. '\|' represent the same amino acid. ':' represent chemically similar amino acids. * represents pyroglutamates. # represents amidated residues. aa = amino acids*

3.4.3.1 ChgA 435-462a

A clear cleavage point is present at position 356-357 of preproChgA and cleavage here yields many C-terminal peptides (figure 3.4). From all these C-terminal peptides, ChgA 435-462a stands out as the most abundant (figure 3.5). ChgA 435-462a is highly conserved in humans (table 3.5), is produced by EECs all along the GI tract (table 3.4), exhibits regulated secretion (figure 3.20) and several similar peptides have been described in the literature as possessing activity in other tissue types. For these reasons, ChgA 435-462a was selected for synthesis and assigned priority 1.

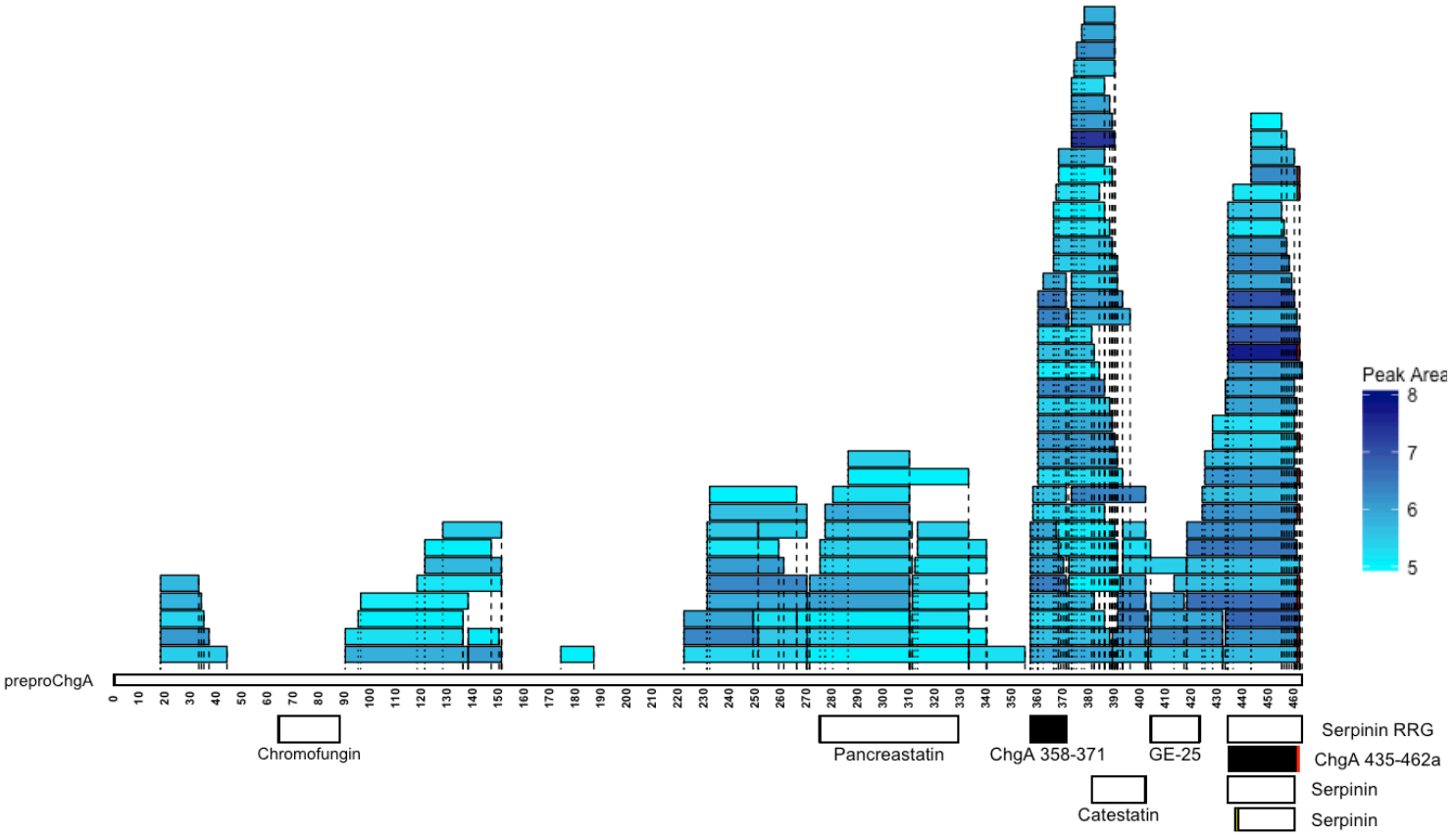

Figure 3.4: Peptides derived from preproChgA in NeuroD1 sorted cells from all regions of the mouse GI tract. *Shading in blue is a measure of the peptide's peak area (log scale). Peptides described in Troger et al. (2017) [241] are annotated at the bottom. Parastatin and vasostatins have been omitted as they are too long to be match by the PEAKS software. Peptides in black were selected for synthesis (ChgA 435-462a and ChgA 358-371).*

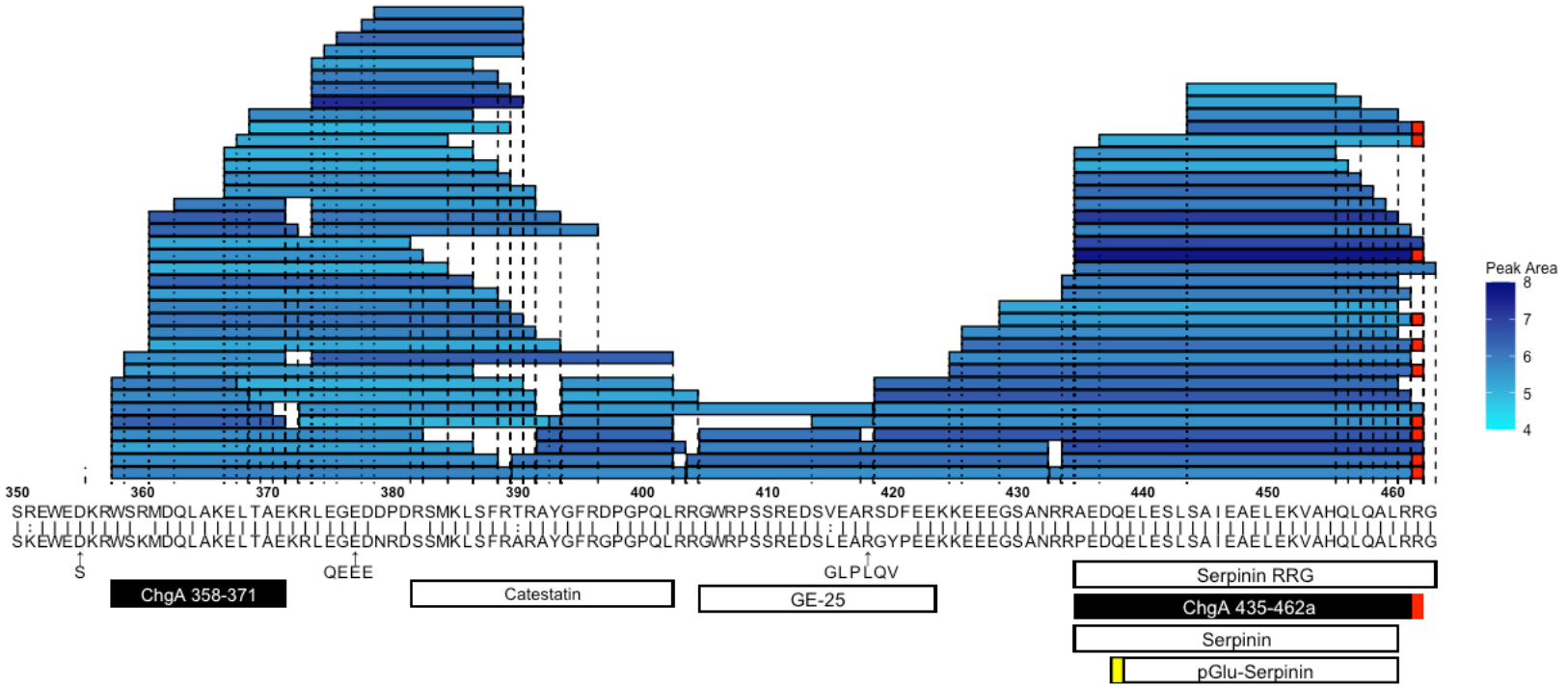

Figure 3.5: Peptides derived from the C-terminus of the ChgA protein in NeuroD1 sorted cells from all regions of the mouse GI tract. *Murine prepropeptide is aligned to the human prepropeptide where '|' represent identical residues and ':' represent chemically similar amino acids. Shading in blue is a measure of each peptide's peak area (log scale). Peptides described in Troger et al. (2017) [241] are annotated on the bottom. Parastatin is not annotated on the bottom as it is too long to be match by the PEAKS software. Peptide selected for synthesis in black (ChgA 435-462a and ChgA 358-371). Red boxes indicate amidations. Yellow box represents a pyroglutamate residue. For other peptides from preproChgA in NeuroD1 sorted cells see figure 3.4.*

3.4.3.2 Gast p59-79

In NeuroD1 sorted cells, a clear cleavage point can be seen in preprogastrin at dibasic residues 57-58 yielding an amidated peptide that also has a N-terminal pyroglutamate residue at position 59 (figure 3.6). This peptide is known as big gastrin and is the precursor to gastrin. Numerous C-terminally truncated fragments of big gastrin were also detected, many of which possessed a pyroglutamate residue on the N-terminus. One of these fragments (Gast p59-79) overlapped with the first 4 amino acids of gastrin and was similar in abundance to big gastrin although not quite as abundant as gastrin. Gast p59-79 is fairly well conserved (table 3.5) and its release from stomach and duodenal epithelial cells is increased upon stimulation with forskolin, IBMX and glucose (FIG) (figure 3.20). For these reasons Gast p59-79 was selected for synthesis and deemed a priority 1 peptide.

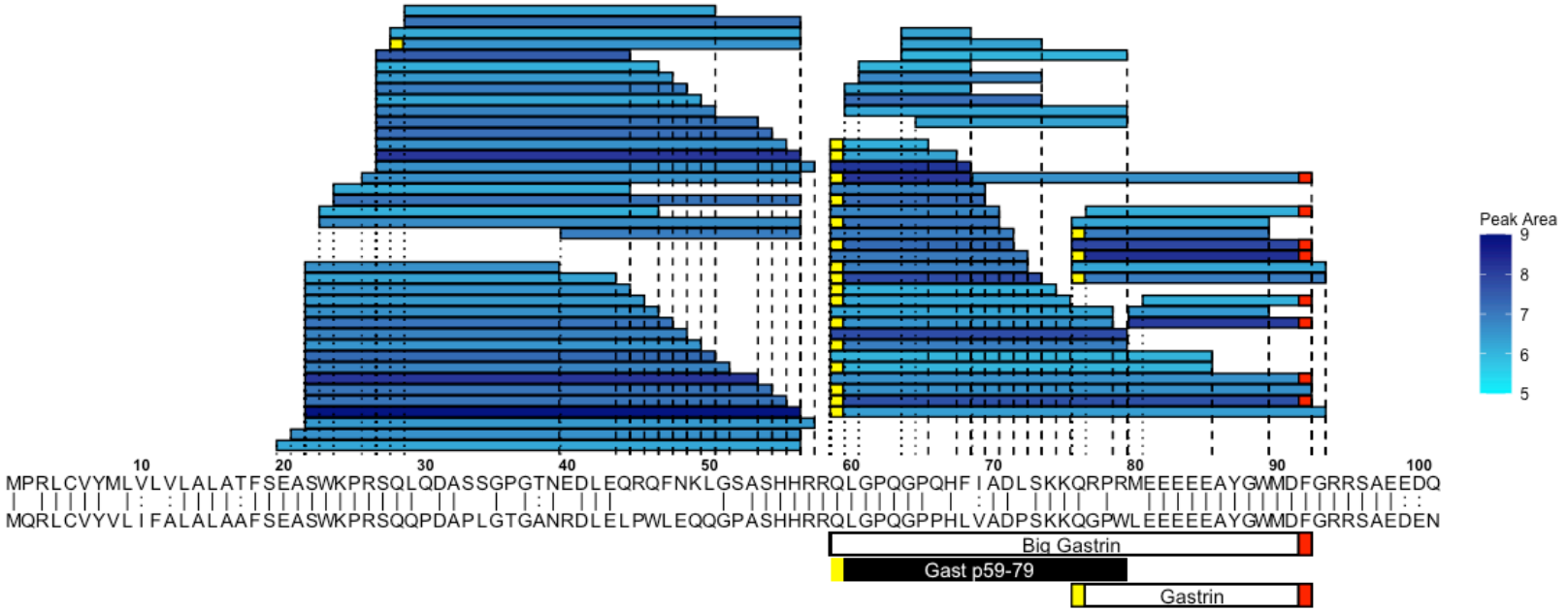

Figure 3.6: Peptides derived from preprogastrin in NeuroD1 sorted cells from all regions of the mouse GI tract. *Murine prepropeptide is aligned to the human prepropeptide where '|' represent identical residues and ':' represent chemically similar amino acids. Shading in blue is a measure of each peptide's peak area (log scale). Peptides described in literature are annotated on the bottom with peptide selected for synthesis in black (Gast p59-79). Red boxes indicate C-terminal amidation. Yellow boxes represent a pyroglutamate.*

3.4.3.3 Sst 25-36

Preprosomatostatin is highly conserved between humans and mice sharing 97% of the same amino acids (table 3.2). With only 2 peptides known to be cleaved from preprosomatostatin I postulated that there could be more due to the high homology. As the C-terminus of preprosomatostatin is known to be cleaved at positions 88 and 102 to form the well annotated peptides SST-28 and SST-14 respectively, I looked to the N-terminus of preprosomatostatin for candidates. No clear cleavage point exists as it did with preprogastrin (figure 3.6) and so to guide my candidate selection I looked at the peptidomics of the cultured GI epithelial cells. Sst 25-36 stood out as an abundant N-terminal fragment of preprosomatostatin in the supernatants (figure 3.8A). Additionally, Sst 25-36 is 100% conserved in humans (table 3.5) and a similar peptide known as neuronostatin has been described in the literature. Neuronostatin was not seen in NeuroD1 sorted cells (figure 3.7), lysed islets (figure 3.8B), supernatants from cultured GI epithelial cells (figure 3.8A) or homogenates of human GI tissue (figure 3.9). As Sst 25-36 overlaps with the N-terminal half of neuronostatin, I hypothesised that Sst 25-36 could exhibit the biological activity that neuronostatin has been described to have. Sst 25-36 was deemed a priority 1 peptide and synthesised.

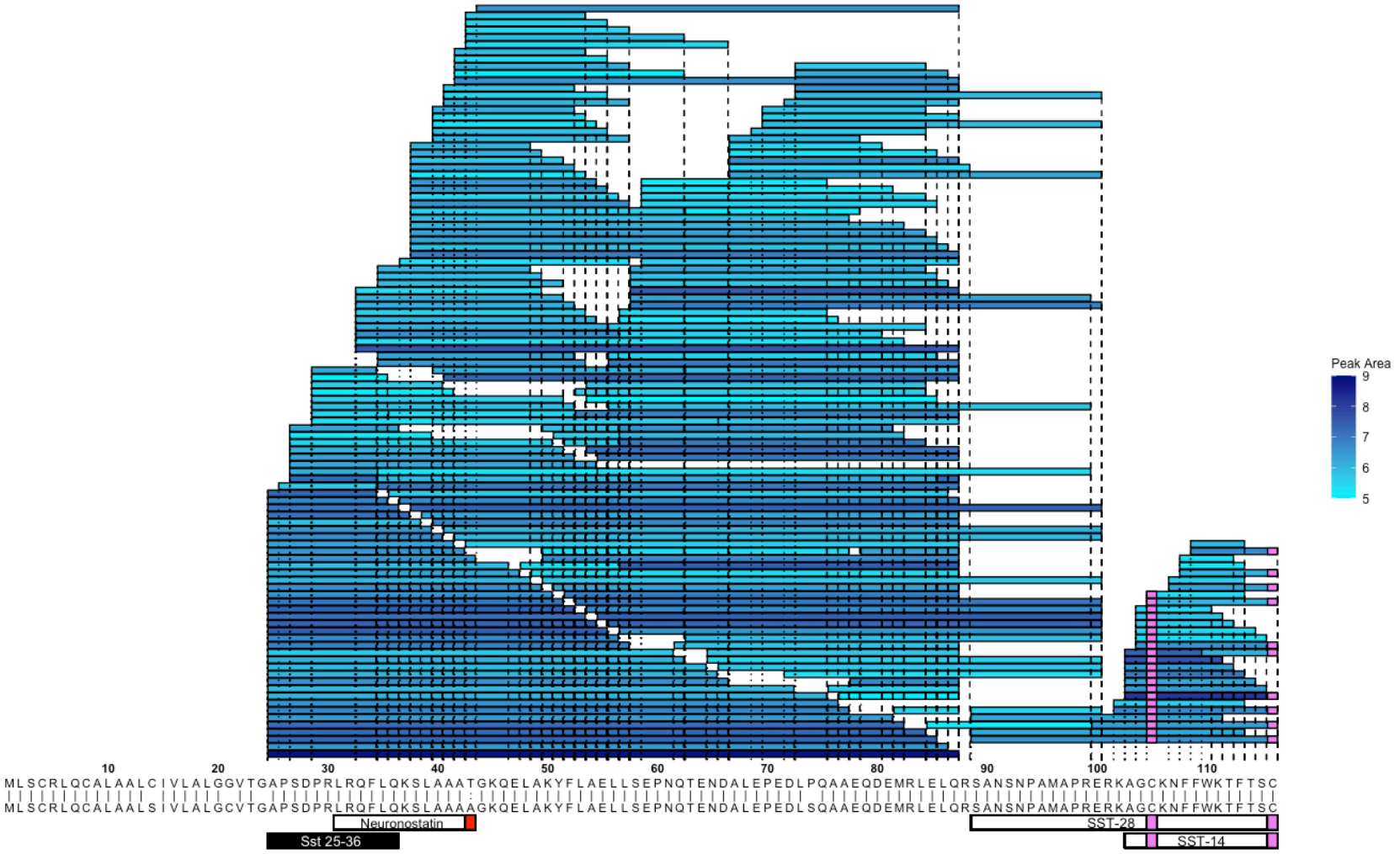
Peak Area
9
8
7
6
5
10
20
30
40
50
60
70
80
90
100
110
MLSCRLQCALAALCIVLALGGVTGAPSDPRLRQFLQKSLAAATGKQELAKYFLAELLSEPNQTENDALEPEDLPQAAEQDEMRLELQRSANSNPAMAPRERKAGCKNFFWKTFTSC
MLSCRLQCALAALSIVLALGCVTGAPSDPRLRQFLQKSLAAAAGKQELAKYFLAELLSEPNQTENDALEPEDLSQAAEQDEMRLELQRSANSNPAMAPRERKAGCKNFFWKTFTSC
Neuronostatin
Sst 25-36
SST-28
SST-14

Figure 3.7: Peptides derived from preprosomatostatin in NeuroD1 sorted cells from all regions of the mouse GI tract. *Murine prepropeptide is aligned to the human prepropeptide where '|' represent identical residues and ':' represent chemically similar amino acids. Shading in blue is a measure of each peptide's peak area (log scale). Peptides described in literature are annotated on the bottom with peptide selected for synthesis in black (Sst 25-36). Red boxes indicate C-terminal amidation. Pink boxes represent carbamidomethylations.*

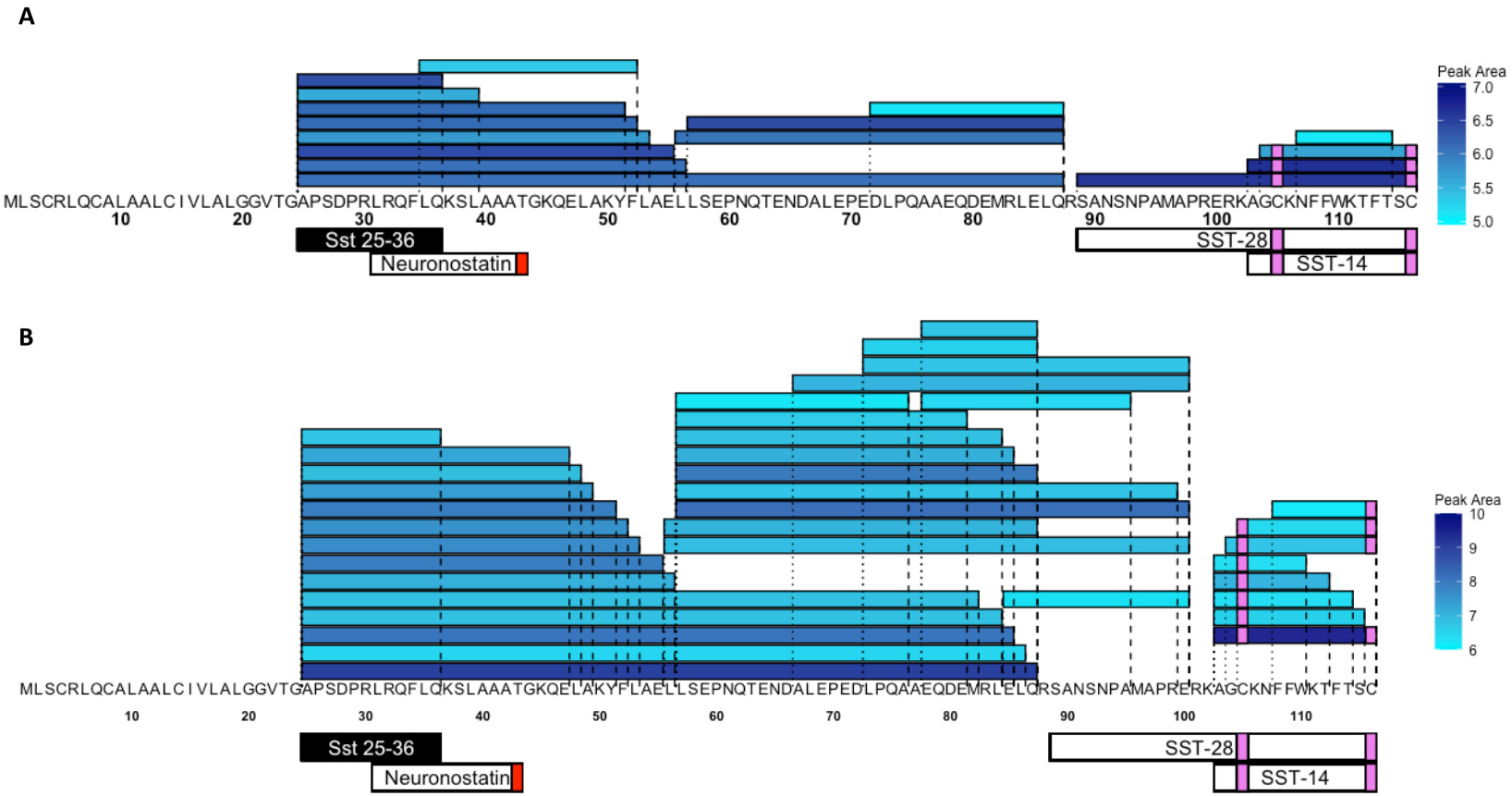

Figure 3.8: Preprosomatostatin derived peptides. *(**A**) Peptides derived from preprosomatostatin found in supernatants from GI epithelial cells across the GI tract. (**B**) Peptides derived from preprosomatostatin found in whole lysed mouse islets. Shading in blue is a measure of the peptide's peak area (log scale). Pink boxes represent carbamidomethylation. Red boxes indicate C-terminal amidation.*

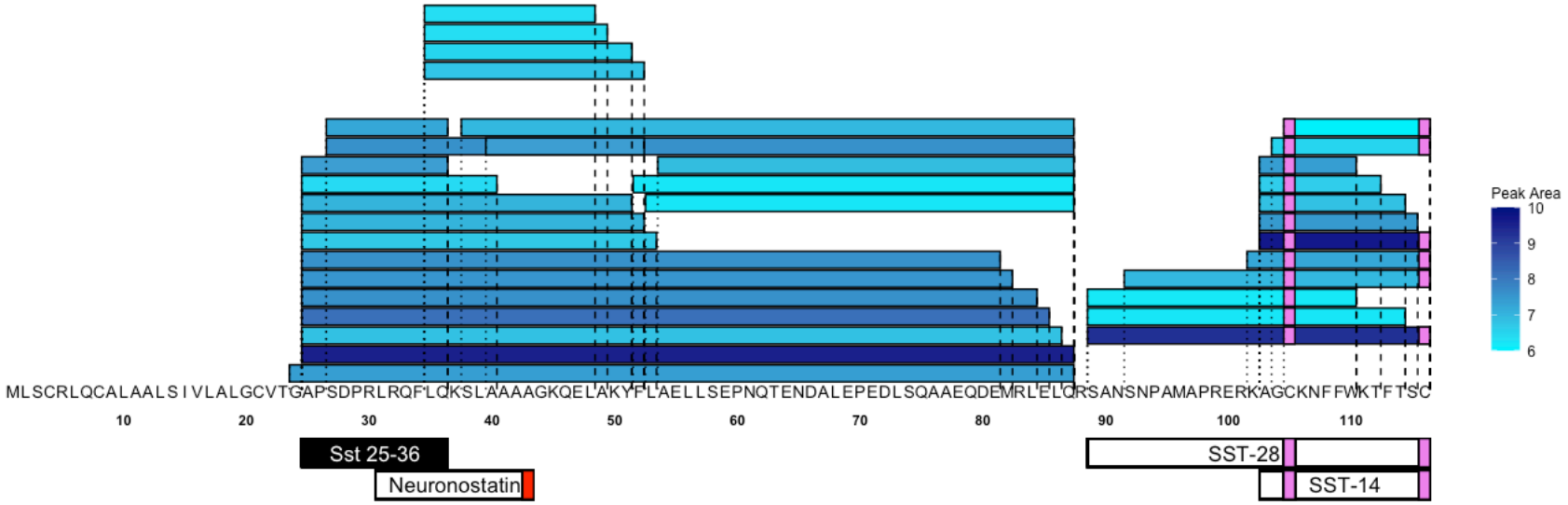

Figure 3.9: Peptides derived from preprosomatostatin found in tissue homogenates from all regions of the human GI tract. *Shading in blue is a measure of the peptide's peak area (log scale). Pink boxes represent carbamidomethylation. Red boxes indicate C-terminal amidation.*

3.4.4 Priority 2 peptide candidates

Figures 3.10 – 3.19 show the alignments of peptides identified to their prepropeptide sequences of origin. These figures relate to the priority 2 peptides and will be used to explain rationale for selecting these peptides for synthesis. Figure 3.20 looks specifically at secretion of peptides from supernatants of cultured GI epithelial cells and will also be used to support the selection of peptide candidates for synthesis.

3.4.4.1 Cck derived peptides

N-terminal fragments of procholecystokinin such as Cck p21-44 and Cck 46-63 attracted my interest due to the fact abundance in NeuroD1 sorted cells (figure 3.10) and are relatively well conserved in humans (table 3.5). Additionally, a clear cleavage point is present at position 45 in procholecystokinin (figure 3.10) and both Cck p21-44 and Cck 46-63 exhibited regulated secretion from cultured epithelial cells all along the GI tract (figure 3.20). For these reasons both peptides were selected for synthesis.

It should be noted that CCK-8 and CCK-12 are sulphated peptides containing mostly hydrophobic and acidic amino acids. CCK-8 possess no basic amino acids whereas CCK-12 possesses only one. Therefore CCK-8 and -12 will not easily pick up positive charges during ESI and so will be difficult to detect as analytes that are not positively charged will be filtered out before reaching the mass analyser.

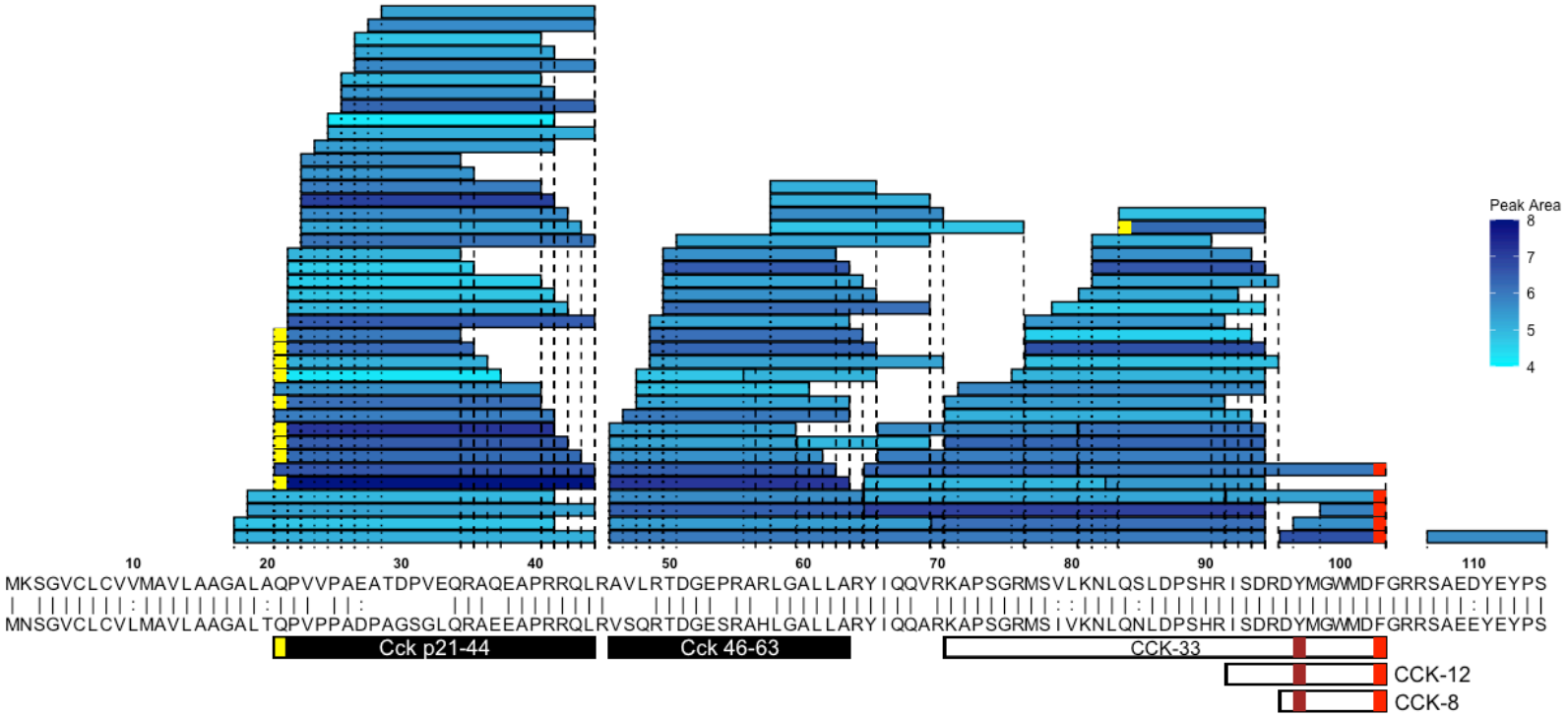

Figure 3.10: Peptides derived from preprocholecystokinin in NeuroD1 sorted cells from all regions of the GI tract. *Murine prepropeptide is aligned to the human prepropeptide where '|' represent identical residues and ':' represent chemically similar amino acids. Shading in blue is a measure of the peptide's peak area (log scale). Peptides described in literature are annotated on the bottom. Peptides selected for synthesis in black (Cck p21-44 and Cck 46-63). Red boxes indicate C-terminal amidations. Yellow box represents a pyroglutamate. Brown boxes represent sulphations.*

3.4.4.2 ChgA 358-371

As discussed in section 3.4.3.1, cleavage of preproChgA at position 356-357 yields many C-terminal peptides (figure 3.5). Aside from ChgA 435-462a there are several other peptides which attracted my attention. ChgA 374-391 is the next most abundant in this C-terminal region after ChgA 435-462 however only 59% of amino acids are conserved between humans and mice with the human peptide possessing 4 extra amino acids (Table 3.6) and therefore not a very attractive candidate. Looking at the peptides produced from preproChgA in cultured mouse GI epithelial (figure 3.11A) or human tissue (figure 3.11B) didn't aid in selection of an additional candidate. However, from looking in lysed islets ChgA 358-371 stands out due to its abundance and the presence of a clear cleavage point at both its N- and C-termini (figure 3.12). Coupled with the fact that ChgA 358-371 is better conserved than ChgA 374-391 (table 3.5) and it is secreted upon stimulation of gastric EECs (figure 3.20), ChgA 358-371 was selected over ChgA 374-391 for synthesis.

Peptide name	Sequence alignment	% of amino acids exactly conserved	% of amino acids exactly conserved + % chemically similar amino acids
ChgA 374-391	LEG----EDDPDRSMKLSFRTR ||| | | |||||| | LEGQEEEEDNRDSSMKLSFRAR	59.1	59.1
Pcsk1n 62-89	AVPRGEAAGAVQELARALAHLLEAERQE |||||||||||||||||||||||| SVPRGEAAGAVQELARALAHLLEAERQE	96.4	96.4
Tac1 111-125	ALNSVAYERSAMQNYE |||||||||||||||| ALNSVAYERSAMQNYE	100.0	100.0

***Table 3.6: Conservation of alternate peptide candidates considered for synthesis**. '\|' represent the same amino acid. ':' represent chemically similar amino acids.*

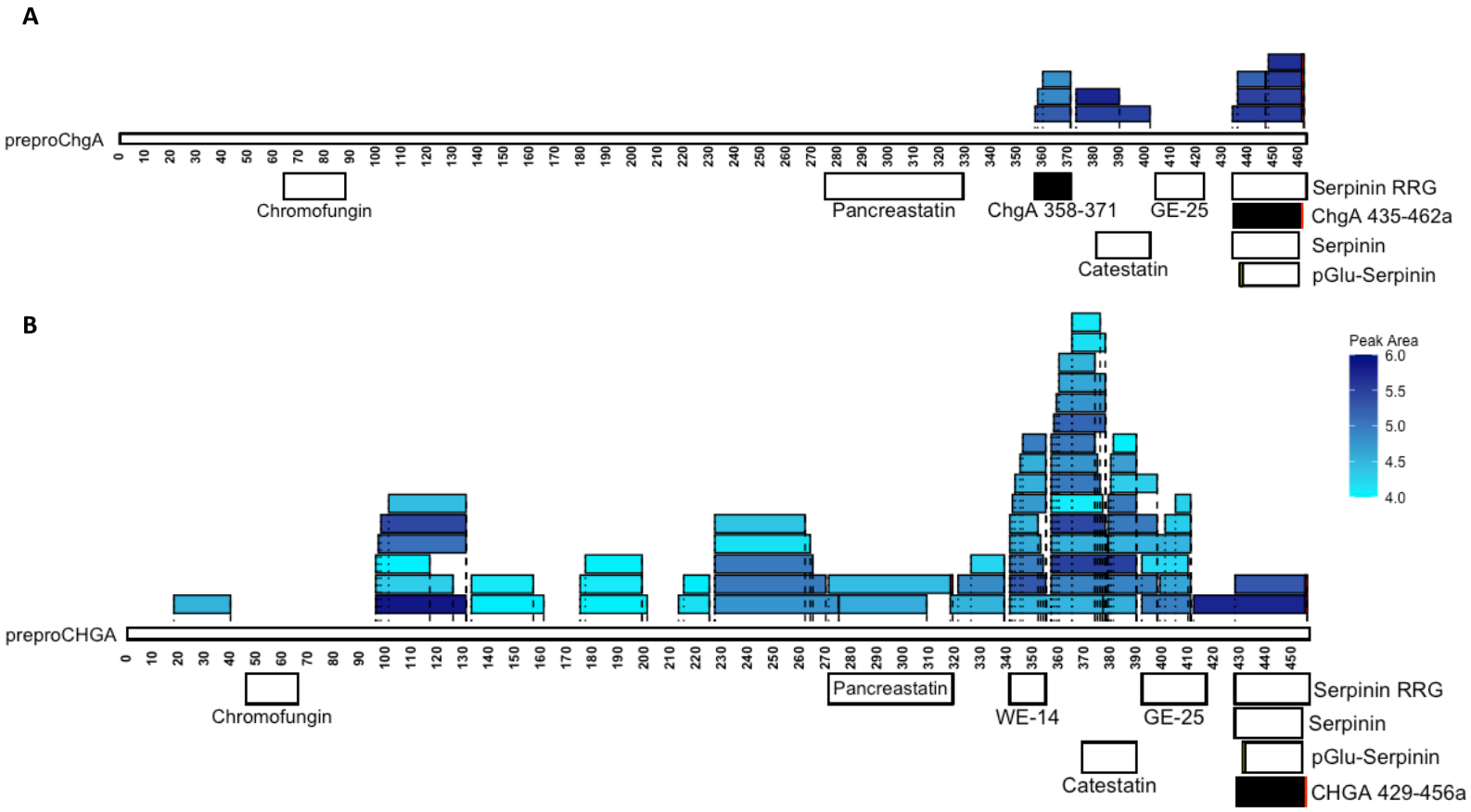
A
preproChgA
Chromofungin
Pancreastatin
ChgA 358-371
GE-25
Catestatin
Serpinin RRG
ChgA 435-462a
Serpinin
pGlu-Serpinin
B
Peak Area
6.0
5.5
5.0
4.5
4.0
preproCHGA
Chromofungin
Pancreastatin
WE-14
GE-25
Catestatin
Serpinin RRG
Serpinin
pGlu-Serpinin
CHGA 429-456a

Figure 3.11: PreproChgA derived peptides. *(**A**) Peptides derived from preproChgA found in supernatants from GI epithelial cells across the GI tract. (**B**) Peptides derived from preproCHGA found in tissue homogenates from all regions of the human GI tract. Peptides described in Troger et al. [241] are annotated on the bottom. In both A and B parastatin and vasostatins have been omitted as they are too long to be match by the PEAKS software. Peptides selected for synthesis in black. WE-14 is the human equivalent to ChgA 358-371 and CHGA 429-456a is the human equivalent of ChgA 435-462a. Shading in blue is a measure of the peptide's peak area (log scale). Red boxes represent C-terminal amidations.*

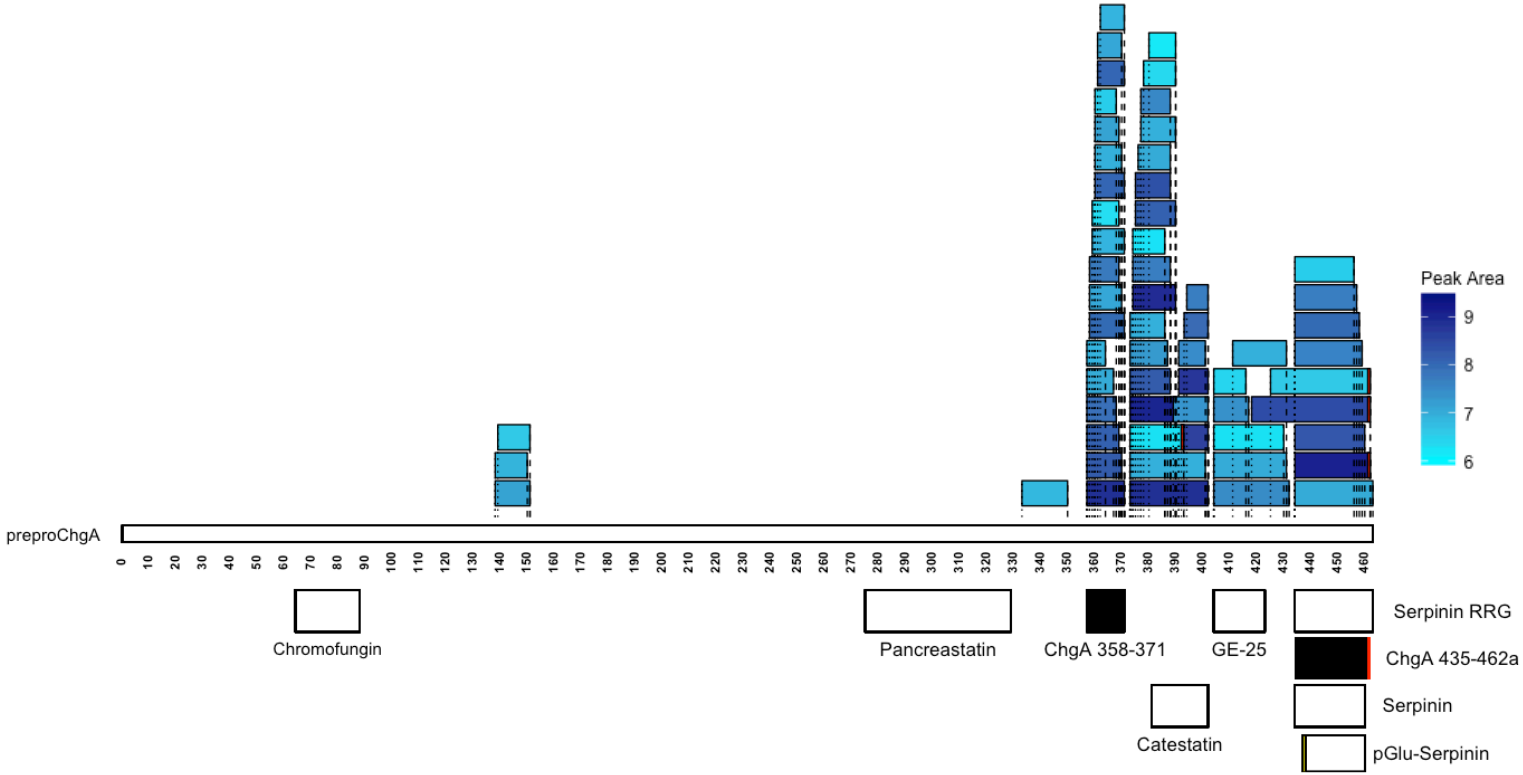

Figure 3.12: Peptides derived from preproChgA found in lysed mouse islets. *Shading in blue is a measure of the peptide's peak area (log scale). Peptides described in Troger et al. (2017) [241] are annotated on the bottom and peptides selected for synthesis are in black (ChgA 435-462a and ChgA 358-371). Parastatin and vasostatins have been omitted as they are too long to be match by the PEAKS software. Red boxes represent C-terminal amidatied residues.*

3.4.4.3 Ghrl 52-85

A clear cleavage point can be seen at position 51 on preproghrelin which yields a N-terminal fragment known as ghrelin (figure 3.13). Ghrelin is a well annotated biological active hormone and so novel peptide candidates from proghrelin were identified from the C-terminal side of this clear cleavage point. Ghrl 52-85 is an abundant peptide derived by cleavage at position 51 and shares 79.4% of the same amino acids with the equivalent human sequence (table 3.5). Found in NeuroD1 sorted cells of the stomach (table 3.4), it also exhibits regulated secretion from cultured stomach epithelial cells (figure 3.20). Ghrl 52-85 overlaps with the first 12 amino acids of the annotated peptide obestatin but obestatin was not detected in NeuroD1 sorted cells. Therefore, I hypothesised that Ghrl 52-85 may possess the same biological activity as obestatin and selected it for synthesis.

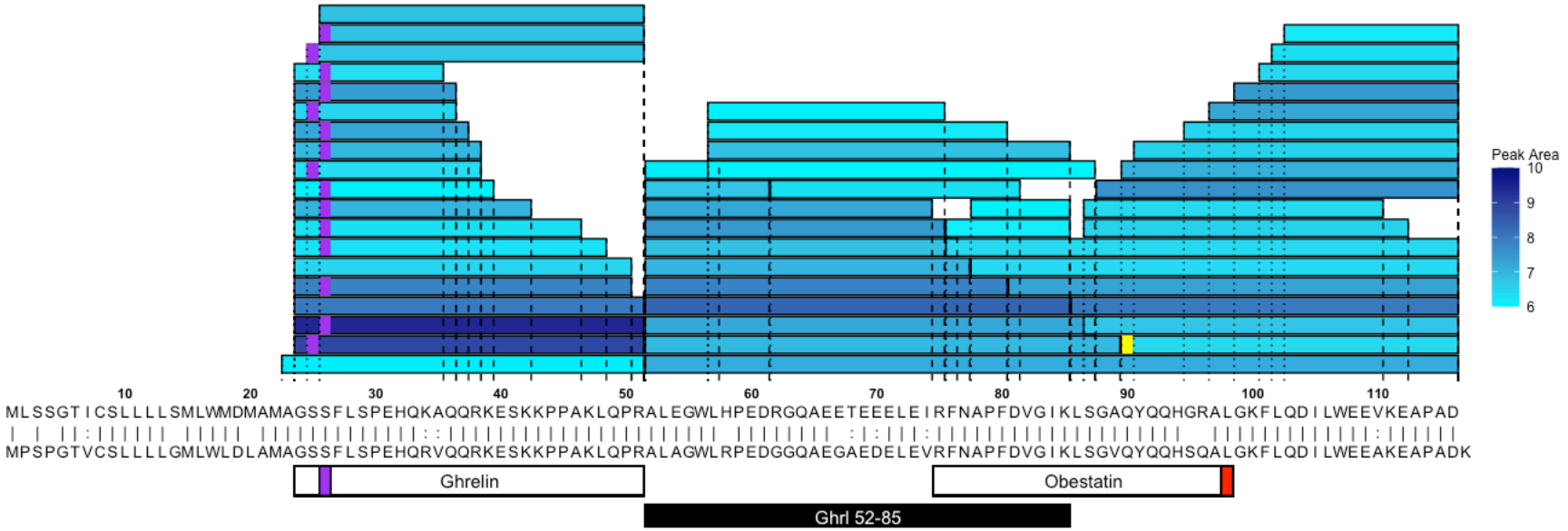

Figure 3.13: Peptides derived from preproghrelin in NeuroD1 sorted cells from all regions of the GI tract. *Shading in blue is a measure of the peptide's peak area (log scale). Murine prepropeptide is aligned to the human prepropeptide where '|' represent identical residues and ':' represent chemically similar amino acids. Peptides described in literature are annotated on the bottom. Peptide selected for synthesis in black (Ghrl 52-85). Red box indicates C-terminal amidation. Yellow box represents a pyroglutamate. Purple boxes denote octanoylation.*

3.4.4.4 Nec1 90-108

Neuroendocrine convertase 1 (Nec1) also known as Prohormone convertase 1/3 (PC1/3) is a processing enzyme responsible for cleaving prohormones to form active peptides at basic residues and is cleaved from a larger prepropeptide to form the active enzyme as well as a propeptide. Peptides derived from this active enzyme as well as the propeptide were detected in NeuroD1 sorted cells and so I searched these peptides for potential candidates. Nec1 90-108 appeared interesting as it was highly conserved (table 3.5), one of the most abundant peptides detected in murine NeuroD1 cells (figure 3.14C) as well as being one of the 2 peptides detected in secretions from GI epithelial cells (figure 3.14B) As this peptide showed regulated secretion from the stomach and proximal SI (figure 3.20) it an attractive candidate and so it was selected for synthesis.

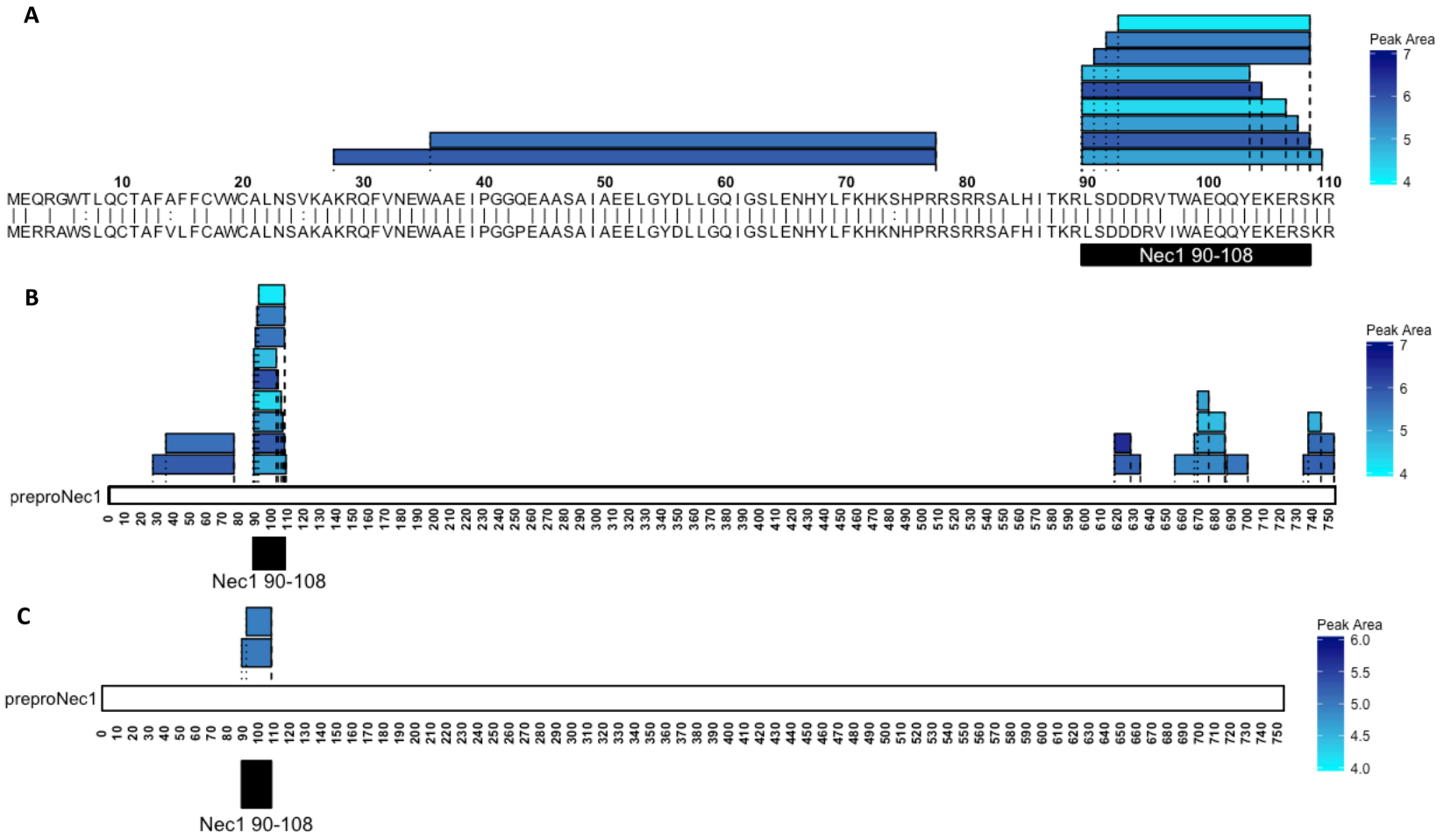
A
Peak Area
7
6
5
4
10 20 30 40 50 60 70 80 90 100 110
MEQRGWTLQCTAFAFFCVWCALNSVKAKRQFVNEWAAEIPGGQEAASAIAEELGYDLLGQIGSLENHYLFKHKSHPRRSRRSALHITKRLSDDDRVTWAEQQYEKERSKR
MERRAWSLQCTAFVLFCAWCALNSAKAKRQFVNEWAAEIPGGPEAASAIAEELGYDLLGQIGSLENHYLFKHKNHPRRSRRSAFHITKRLSDDDRVIWAEQQYEKERSKR
Nec1 90-108
B
Peak Area
7
6
5
4
preproNec1
0 10 20 30 40 50 60 70 80 90 100 110 120 130 140 150 160 170 180 190 200 210 220 230 240 250 260 270 280 290 300 310 320 330 340 350 360 370 380 390 400 410 420 430 440 450 460 470 480 490 500 510 520 530 540 550 560 570 580 590 600 610 620 630 640 650 660 670 680 690 700 710 720 730 740 750
Nec1 90-108
C
Peak Area
6.0
5.5
5.0
4.5
4.0
preproNec1
0 10 20 30 40 50 60 70 80 90 100 110 120 130 140 150 160 170 180 190 200 210 220 230 240 250 260 270 280 290 300 310 320 330 340 350 360 370 380 390 400 410 420 430 440 450 460 470 480 490 500 510 520 530 540 550 560 570 580 590 600 610 620 630 640 650 660 670 680 690 700 710 720 730 740 750
Nec1 90-108

Figure 3.14: Peptides derived from preproNec1. *(**A**) Peptides derived from N-terminus of preproNec1 in NeuroD1 sorted cells from all regions of the mouse GI tract. Murine prepropeptide is aligned to the human prepropeptide where '|' represent identical residues and ':' represent chemically similar amino acids. (**B**) Peptides derived from the whole of preproNec1 in NeuroD1 sorted cells from all regions of the mouse GI tract. (**C**) Peptides derived from preproNec1 found in supernatants from cultures GI epithelial cells from all regions of the mouse GI tract. Shading in blue is a measure of the peptide's peak area (log scale). Peptide selected for synthesis in black (Nec1 90-108).*

3.4.4.5 Pcsk1n 42-59

Peptides detected in NeuroD1 sorted cells from preproPcsk1n originated from either the N- or C-termini and no peptides derived from the middle of the sequence were detected (figure 3.15B). None of the detected peptides stood out due to their abundance. Unfortunately, no peptides from preproPcsk1n were detected in supernatants from GI epithelial cells and so I searched the peptides seen in human GI tissue homogenates to guide peptide selection from preproPcsk1n. Figure 3.15C displays all preproPCSK1N-derived peptides in homogenates of human GI tissue. PCSK1N 42-59 stands out here as the most abundant peptide. This peptide can be seen in all regions of the human and mouse GI tract (table 3.4) and is relatively well conserved between humans and mice (table 3.5). Taking all this into account Pcsk1n 42-59 was selected for synthesis. Pcsk1n 62-89 was also considered as a candidate as it is highly conserved (table 3.6) but was dropped in favour of Pcsk1n 42-59 due to its low abundance in human tissue.

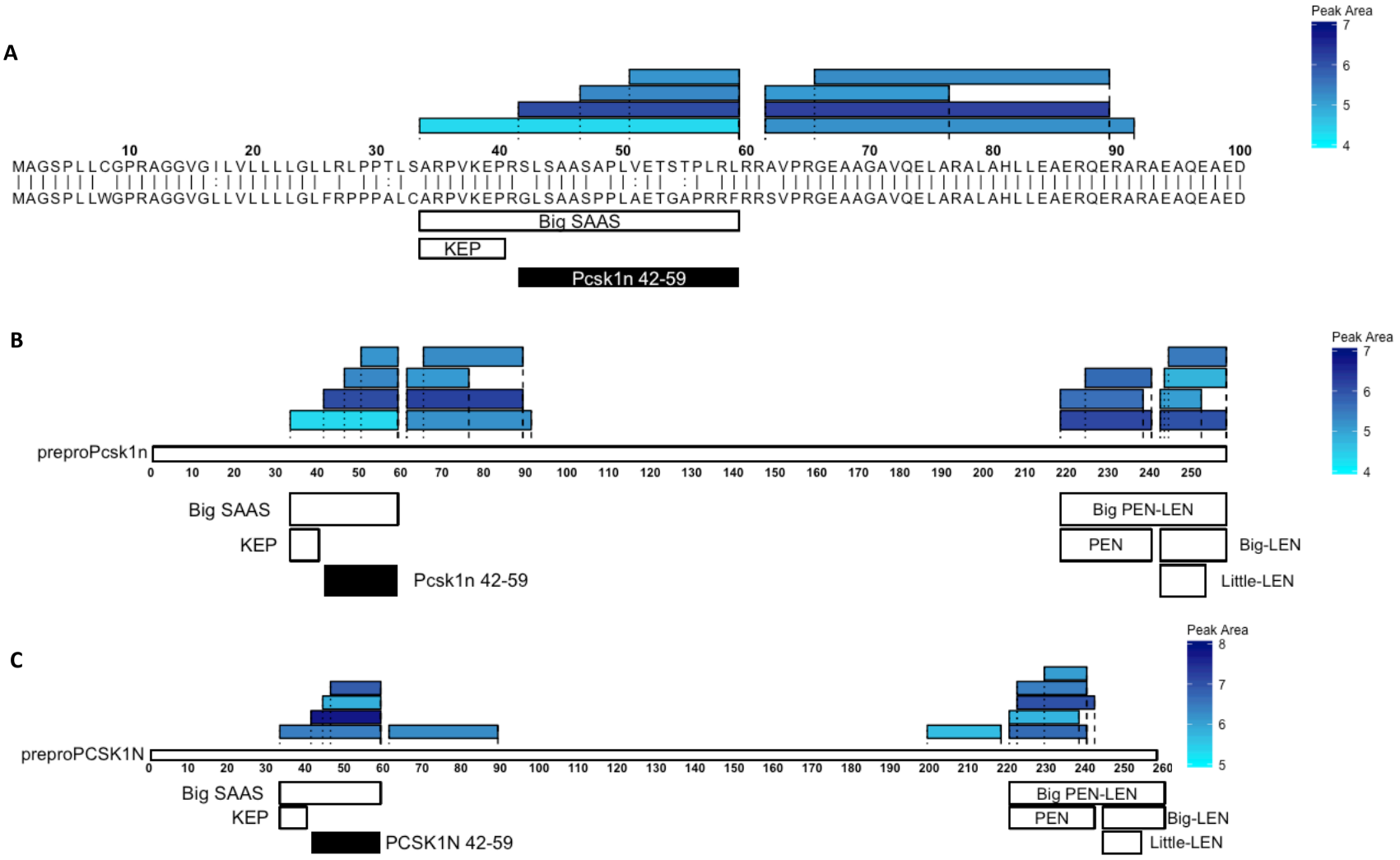
A
Peak Area
7
6
5
4
10 20 30 40 50 60 70 80 90 100
MAGSPLLCGPRAGGVGILVLLLLGLLRLPPTLSARPVKEPRSLSAASAPLVETSTPLRLRRAVPRGEAAGAVQELARALAHLLEAERQERARAEAQEAED
MAGSPLLWGPRAGGVGLLVLLLLGLFRPPPALCARPVKEPRGLSAASPPLAETGAPRRFRRSVPRGEAAGAVQELARALAHLLEAERQERARAEAQEAED
Big SAAS
KEP
Pcsk1n 42-59
B
Peak Area
7
6
5
4
preproPcsk1n
0 10 20 30 40 50 60 70 80 90 100 110 120 130 140 150 160 170 180 190 200 210 220 230 240 250
Big SAAS
KEP
Pcsk1n 42-59
Big PEN-LEN
PEN
Big-LEN
Little-LEN
C
Peak Area
8
7
6
5
preproPCSK1N
0 10 20 30 40 50 60 70 80 90 100 110 120 130 140 150 160 170 180 190 200 210 220 230 240 250 260
Big SAAS
KEP
PCSK1N 42-59
Big PEN-LEN
PEN
Big-LEN
Little-LEN

Figure 3.15: Peptides derive from preproPcsk1n. *(**A**) Peptides derived from the N-terminus of preproPcsk1n. Murine prepropeptide is aligned to the human prepropeptide where '|' represent identical residues and ':' represent chemically similar amino acids. (**B**) Peptides derived from the whole of preproPcsk1n in NeuroD1 sorted cells from all regions of the mouse GI tract. (**C**) Peptides derived from preproPCSK1N tissue homogenates from each region of the human GI tract. Shading in blue is a measure of the peptide's peak area (log scale). Peptides described in the literature are annotated. Peptide selected for synthesis in black (Pcsk1n 42-59).*

3.4.4.6 Pyy 68-98

A clear cleavage point can be seen at the dibasic residues of positions 66-67 on preproPyy yielding PYY (1-36) (figure 3.16A). Pyy 68-98 is the C-terminal fragment produced by cleavage of preproPyy at these amino acids and is similar in abundance to the PYY (1-36) in murine NeuroD1 sorted cells across the GI tract (table 3.4). Secretion of Pyy 68-98 is induced by addition of FIG to ileal and colonic epithelial cells (figure 3.20). Unfortunately, this peptide shows <50% conservation with the equivalent human sequence and so violates one of the criteria I set out for novel peptide selection. An exception was made for this peptide however as when chemically similar amino acids are taken into account, Pyy 68-98 shares 55% homology with the human sequence. Additionally, in mouse islets Pyy 68-98 seems to be far more abundant than the active hormones derived from preproPyy (figure 3.16B).

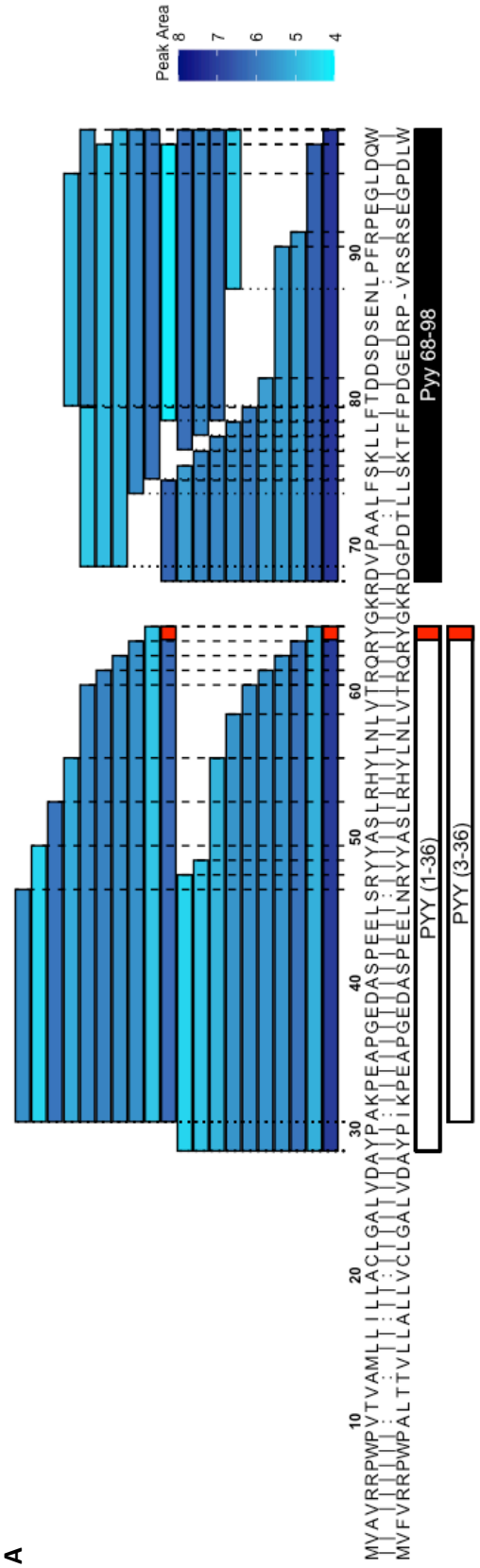

Figure 3.16: Peptides derived from proPYY. *(**A**) Peptides derived from proPYY in NeuroD1 sorted cells from all regions of the GI tract. Murine prepropeptide is aligned to the human prepropeptide where '|' represent identical residues and ':' represent chemically similar amino acids. Shading in blue is a measure of the peptide's peak area (log scale). Peptides described in literature are annotated on the bottom. Peptide selected for synthesis in black (Pyy 68-98). Red boxes indicate C-terminal amidations. (**B**) Quantification of PYY (1-36), PYY (3-36) and Pyy 68-98 in lysed mouse islets from 6 different mice.*

3.4.4.7 Scg2 184-216 and Scg2 569-610

Numerous propreScg2 derived peptides were seen in NeuroD1 sorted cells and so it was difficult to select candidates based on just this data alone (figure 3.17). As no peptides from Scg2 were detected in supernatants of mouse GI epithelial cells I looked at the peptidomics of the human GI tract to help select candidates from preproScg2 (figure 3.18). The 2 most abundant peptides were SCG 182-214 and SCG 569-610. Both these peptides were well conserved with the equivalent mouse sequences (Scg2 184-216 and Scg 569-610 on table 3.5) although the position of Scg2 184-216 on preproScg2 is slightly shifted. Scg2 184-216 has been described in the literature as secretoneurin although its potential as a gut hormone has not been assessed. For these reasons, both Scg2 184-216 and Scg2 569-610 were selected for synthesis.

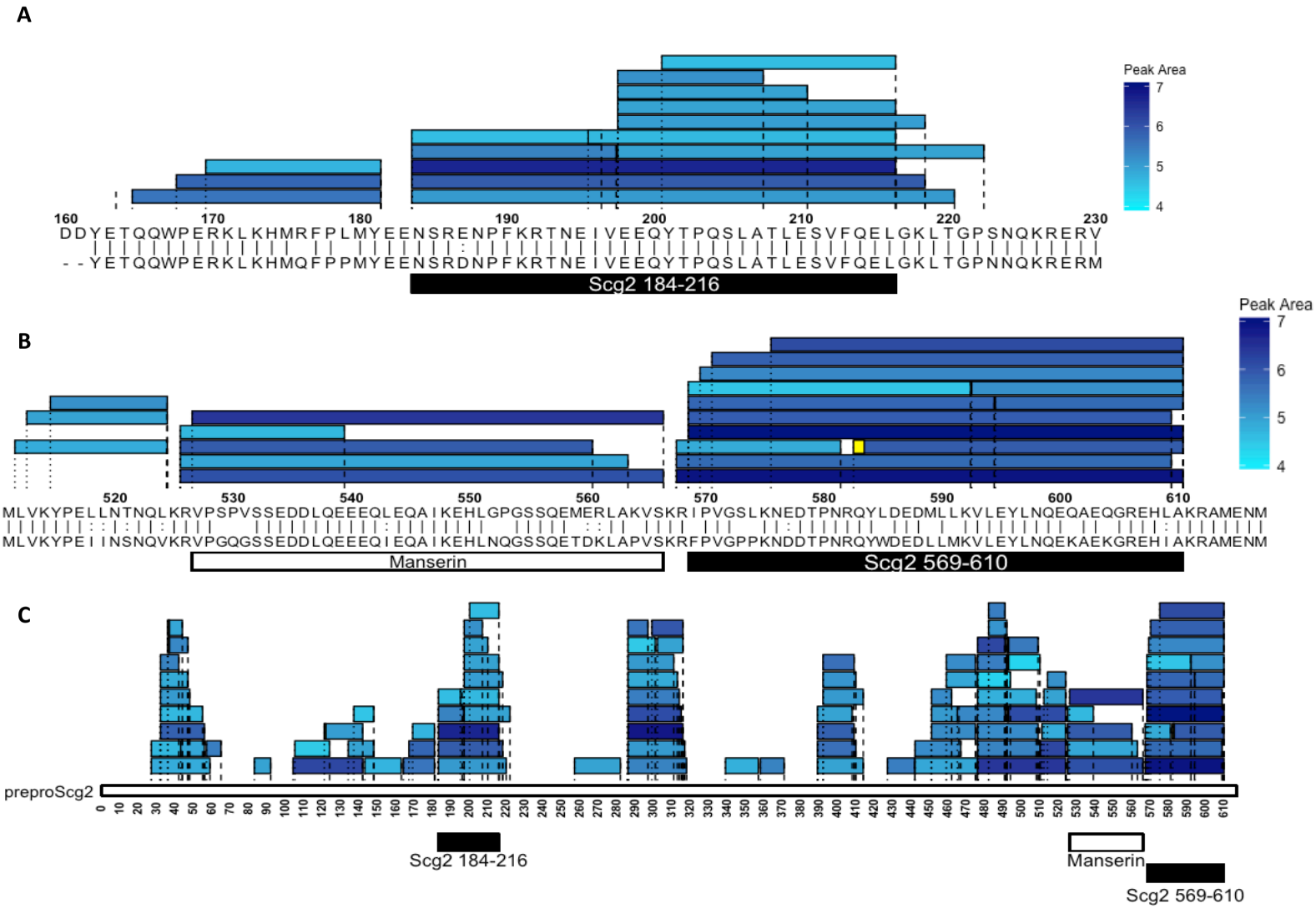
A
Peak Area
7
6
5
4
160
170
180
190
200
210
220
230
DDYETQQWPERKLKHMRFPLMYEENSRENPFKRTNEIVEEQYTPQSLATLESVFQELGKLTGPSNQKRERV
--YETQQWPERKLKHMQFPPMYEENSRDNPFKRTNEIVEEQYTPQSLATLESVFQELGKLTGPNNQKRERM
Scg2 184-216
B
Peak Area
7
6
5
4
520
530
540
550
560
570
580
590
600
610
MLVKYPELLNTNQLKRVPSPVSSEDDLQEEEQLEQAIKEHLGPGSSQEMERLAKVSKRIPVGSLKNEDTPNRQYLDEDMLLKVLEYLNQEQAEQGREHLAKRAMENM
MLVKYPEIINSNQVKRVPGQGSSEDDLQEEEQIEQAIKEHLNQGSSQETDKLAPVSKRFPVGPPKNDDTPNRQYWDEDLLMKVLEYLNQEKAEKGREHIAKRAMENM
Manserin
Scg2 569-610
C
preproScg2
0
10
20
30
40
50
60
70
80
90
100
110
120
130
140
150
160
170
180
190
200
210
220
230
240
250
260
270
280
290
300
310
320
330
340
350
360
370
380
390
400
410
420
430
440
450
460
470
480
490
500
510
520
530
540
550
560
570
580
590
600
610
Scg2 184-216
Manserin
Scg2 569-610

Figure 3.17: Peptides derived from the preproScg2 in NeuroD1 sorted cells from all regions of the mouse GI tract. *Peptides derived specifically from (**A**) positions 160-230 and (**B**) positions 411-617. For **A** and **B** the murine prepropeptide is aligned to the human prepropeptide where '|' represent identical residues and ':' represent chemically similar amino acids. (**C**) Peptides derived from the whole of preproScg2. Shading in blue is a measure of the peptide's peak area (log scale). Peptides described in Troger et al. (2017) [241] are annotated on the bottom. Peptide selected for synthesis in black (Scg2 184-216 and Scg2 569-610). Yellow boxes denote pyroglutamate residues.*

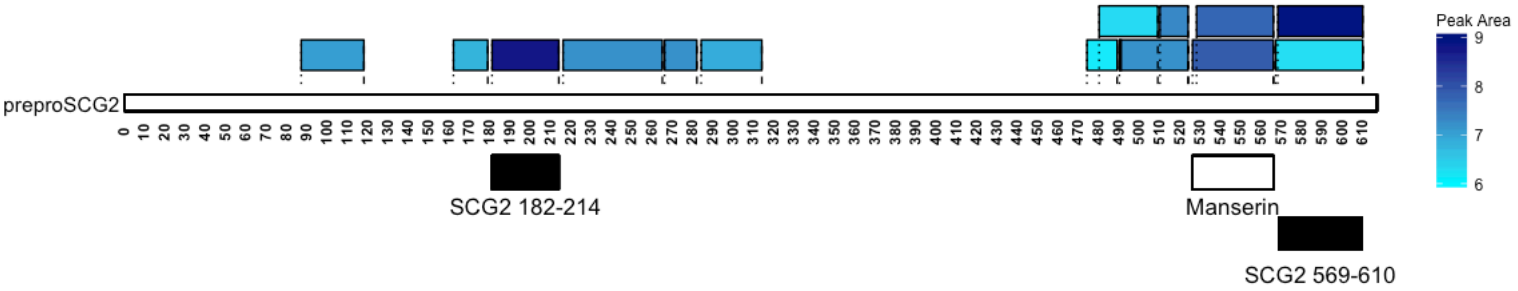

Figure 3.18: Peptides derived from preproSCG2 in tissue homogenates from all regions of the human GI tract. *Shading in blue is a measure of the peptide's peak area (log scale). Peptides described in Troger et al. (2017) [241] are annotated on the bottom. Peptides selected for synthesis in black. SCG2 182-214 is the human equivalent to Scg2 184-216.*

3.4.4.8 Tac1 72-95

Just 7 peptides derived from preprotachykinin-1 were detected in murine NeuroD1 sorted cells and none were seen in supernatants of epithelial cells from any region of the GI tract (figure 3.19A). Nevertheless, I decided to select Tac1 72-95 for synthesis due to the fact it was higher in abundance than annotated peptides also derived from preprotachykinin-1 such as neurokinin A and substance P in addition to its high conservation with the equivalent human sequence (table 3.5). In homogenised human GI tissue, a version of this peptide with one peptide cleaved off the C-terminus (TAC1 92-94) was the most abundant peptide derived from preproTAC1 (figure 3.19B). Tac 111-125 was a potential candidate for selection as it is 100% conserved with the equivalent human (table 3.6) sequence but was not selected for synthesis due to its low abundance compared to other preproTac1 derived peptides in mouse GI tissue. Additionally Tac1 72-95 had the characteristic of being a truncated version of neuropeptide K-an agonist at tachykinin receptors expressed in the central nervous system [221]. Tac1 72-95 could represent a novel gut derived peptide from this preprohormone.

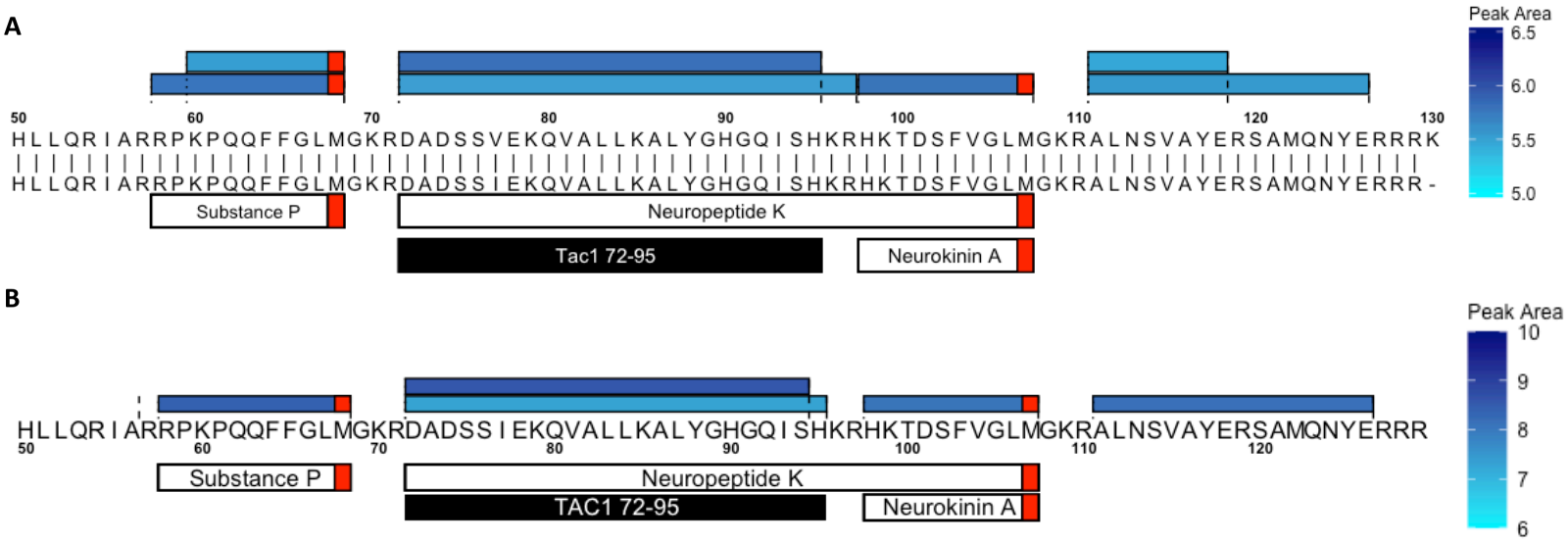

Figure 3.19: Prepprotachykinin derived peptides. *(**A**) Peptides derived from preprotachykinin in NeuroD1 sorted cells from all regions of the mouse GI tract. Murine prepropeptide is aligned to the human prepropeptide where '|' represent identical residues and ':' represent chemically similar amino acids. (**B**) Peptides derived from preproTAC1 in homogenised human tissue from all regions of the GI tract. Shading in blue is a measure of the peptide's peak area (log scale). Peptides described in literature are annotated on the bottom. Peptide selected for synthesis in black (Tac1 72-95). Red boxes indicates C-terminal amidation. No peptides were detected from positions 1-49 on the prepropeptide and so this portion of the peptide is not displayed.*

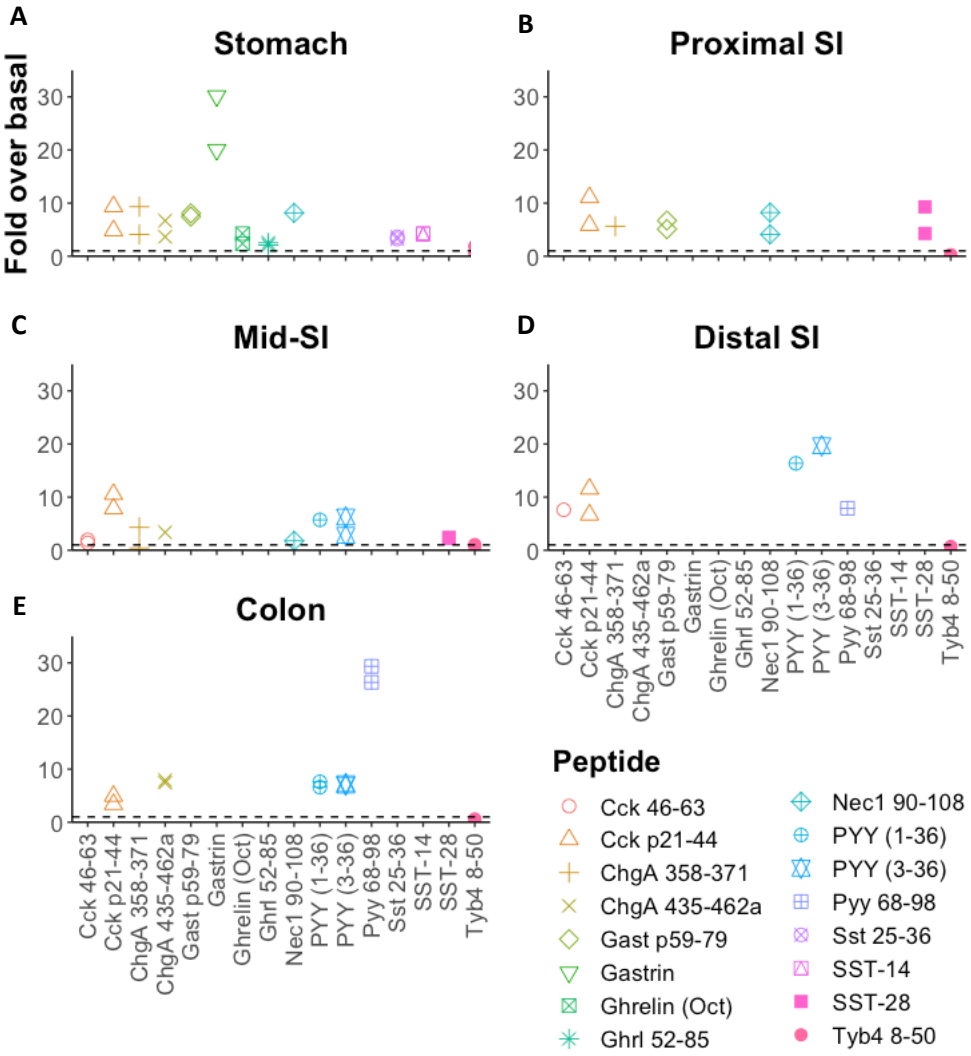

Figure 3.20: Peptide quantification in supernatants from primary mouse GI crypts. *(**A**) Stomach, (**B**) proximal SI, (**C**) mid-SI, (**D**) distal SI, (**E**) colon. Fold over basal is calculated by normalising the peak area of the stimulated supernatant (forskolin, IBMX, glucose) to the peak area of the basal supernatant. Tyb4 8-50 is an actin derived peptide. This peptide is not likely to be present in secretory vesicles of EECs and its release should not be stimulated by addition of forskolin, IBMX and glucose.*

3.4.5 Other prohormones, processing enzymes and granin proteins

Peptides were detected from various other preprohormones such as preproneurotenisn (figure 3.21), preproGIP (figure 3.22), preprosecretin (figure 3.23) and preproScg1 (figure 3.24) in NeuroD1 sorted cells but none of these peptides were selected for synthesis. This was due to the fact that none of the peptides derived from these other prohormones looked as promising as the ones selected based on the criteria set out in section 3.4.1. No peptides from other granin proteins or processing enzymes such as Scg3, Scg5 or Nec2 were detected in sorted NeuroD1 cells.

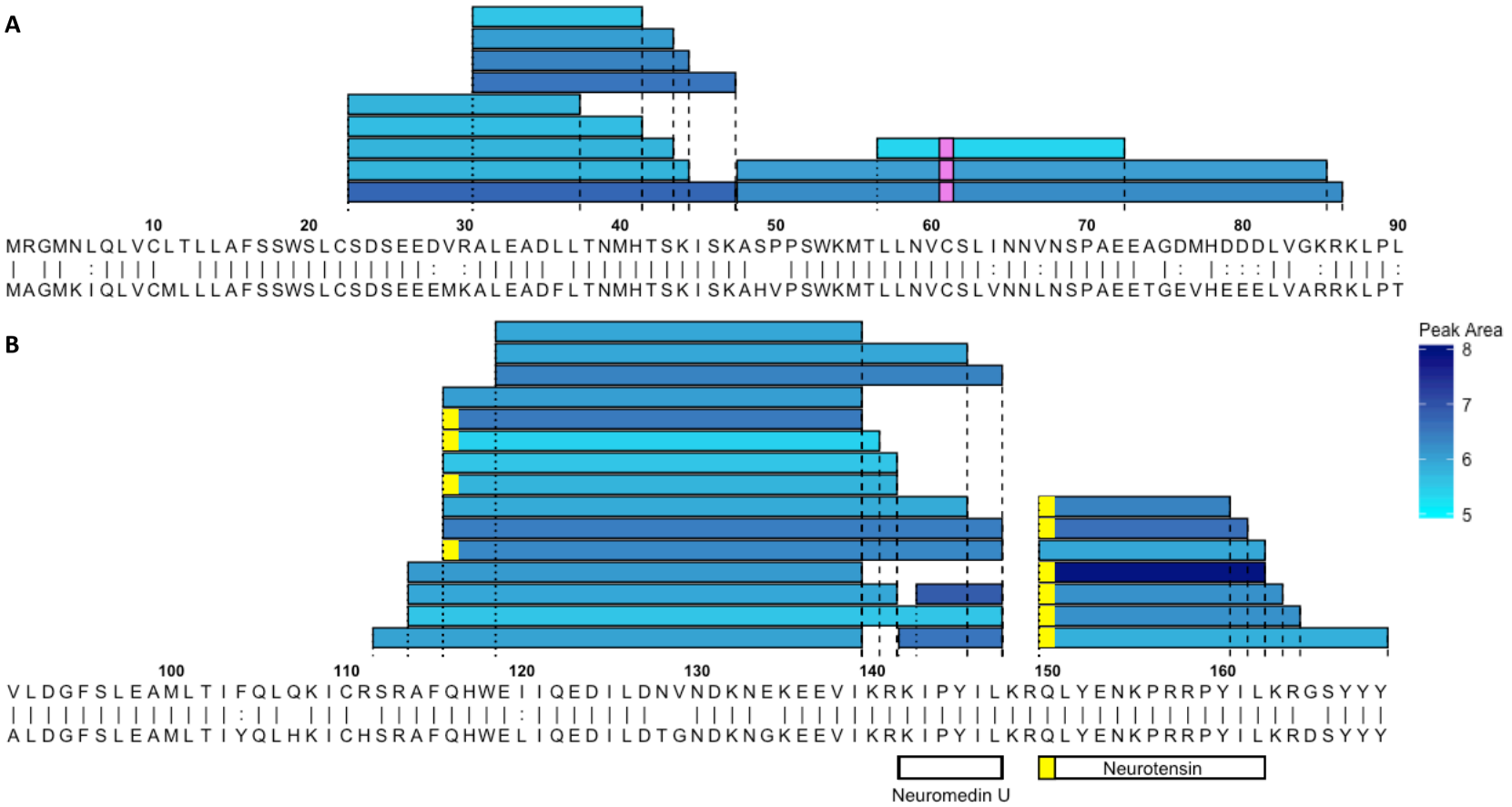

Figure 3.21: Preproneurotensin derived peptides in NeuroD1 sorted cells from all regions of the mouse GI tract. *Peptides from positions 1-90 (**A**) and 90-170 (**B**). Murine prepropeptide is aligned to the human prepropeptide where '|' represent identical residues and ':' represent chemically similar amino acids. Shading in blue is a measure of the peptide's peak area (log scale). Yellow boxes represent proglutamate residues. Pink boxes represent carbamidomethylation. Peptides described in the literature are annotated at the bottom.*

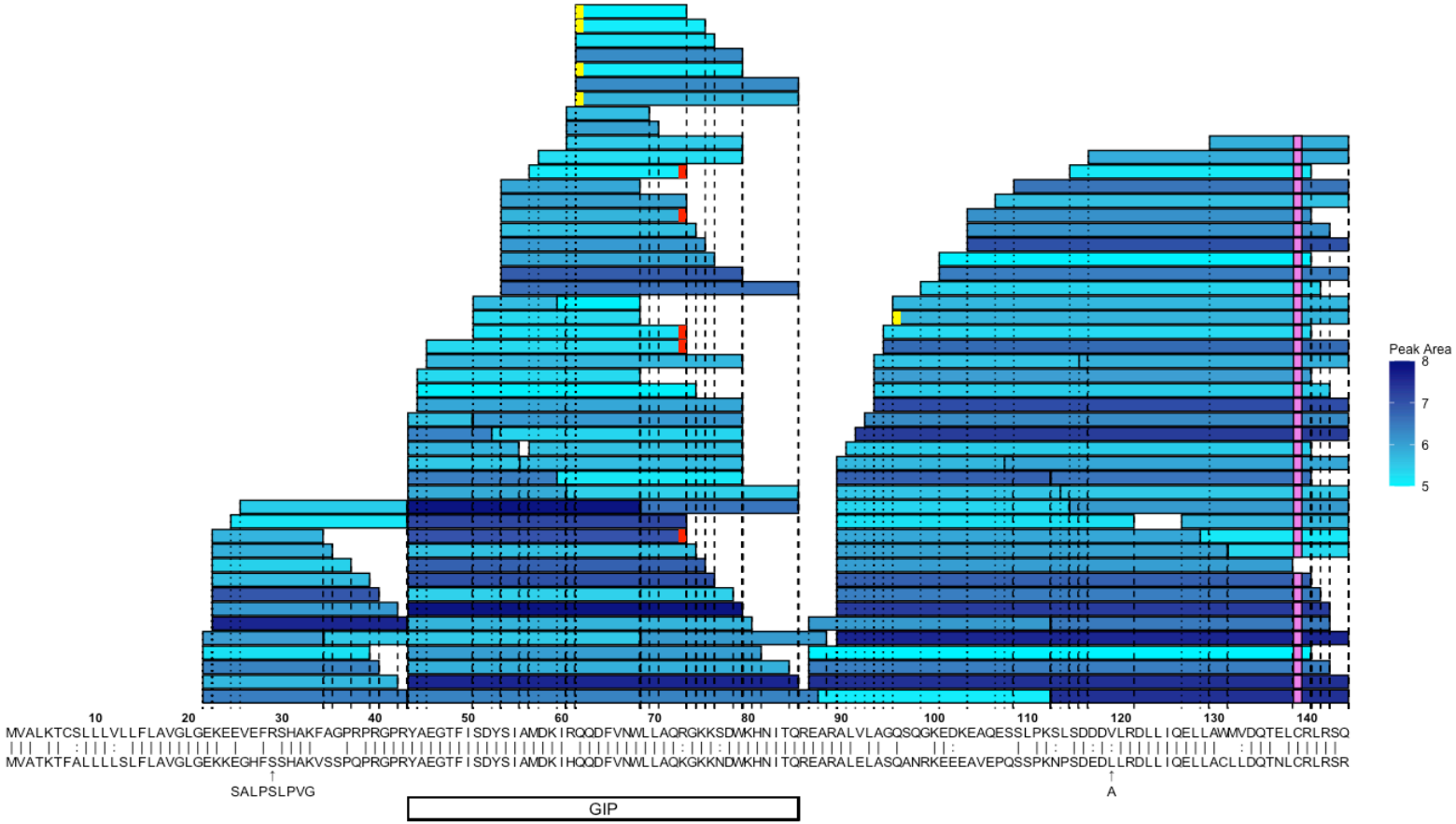

Figure 3.22: Peptides derived from preproGIP in NeuroD1 sorted cells from all regions of the mouse GI tract. Shading in blue is a measure of the peptide's peak area (log scale). Murine prepropeptide is aligned to the human prepropeptide where '|' represent identical residues and ':' represent chemically similar amino acids. Pink boxes represent carbamidomethylation. Red boxes indicate C-terminal amidations. Yellow boxes represent pyroglutamate residues. Peptides described in the literature are annotated at the bottom.

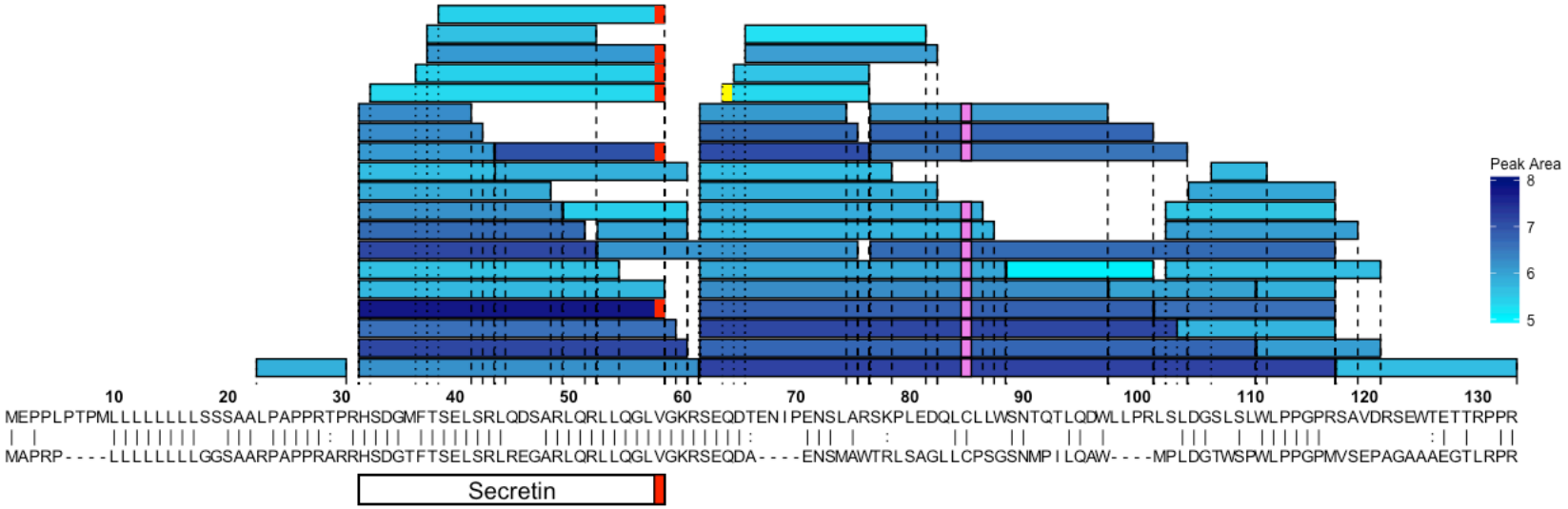

Figure 3.23: Peptides derived from preprosecretin in NeuroD1 sorted cells from all regions of the mouse GI tract. *Shading in blue is a measure of the peptide's peak area (log scale). Murine prepropeptide is aligned to the human prepropeptide where '|' represent identical residues and ':' represent chemically similar amino acids. Pink boxes represent carbamidomethylation. Red boxes indicate C-terminal amidation. Yellow box indicates a pyroglutamate residue. Peptides annotated in the literature are displayed at the bottom.*

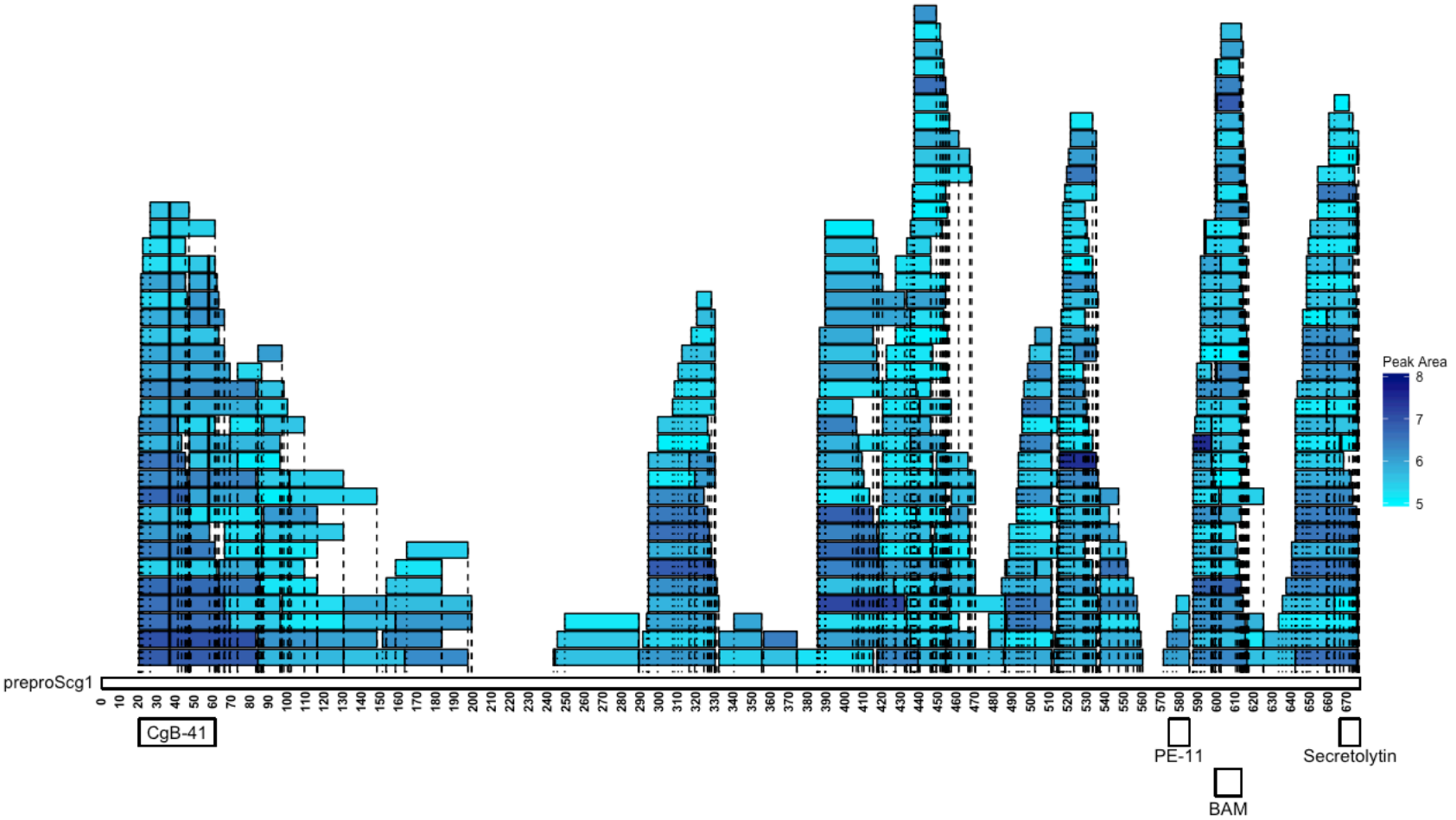

Figure 3.24: Peptides derived from preproScg1 in NeuroD1 sorted cells from all regions of the mouse GI tract. *Shading in blue is a measure of the peptide's peak area (log scale). Peptides described in Troger et al. (2017) [241] are annotated at the bottom.*

3.5 Discussion

3.5.1 Summary

The search for novel peptide hormone candidates centred around characterising the peptidome of lysed murine EECs and was supported by peptidomics data from; stimulated supernatants of mouse GI epithelial cells, lysed whole mouse islets and homogenised human GI tissue. With thousands of peptides detected originating from hundreds of different genes, I employed certain criteria to narrow down the candidates. Using these criteria, 13 peptide candidates were selected for synthesis and characterisation of potential biological activity. 7 of these 13 candidates were products from prohormones, 4 were products from granins proteins and 1 was a product of a processing enzyme.

3.5.2 Granin-derived peptides as hormones

Table 3.1 summarises many granin-derived peptides described in the literature with most possessing biological activity of some kind. Some peptides have complementary actions such as parastatin and vasostatin however some have conflicting actions. Serpinin is well characterised as a positive inotrope and hypothesised to be a positive allosteric modulator of the β1 adrenoceptor [211]. These actions seemingly conflict with the cardio-suppressive effects of vasostatins, parastatin and catestatin through inhibition of parathyroid hormone release [200, 201, 207, 209]. Moreover, pancreastatin is released with catecholamines and its actions mimic them as pancreastatin induces a 'fight or flight' state [241]. Again, seemingly in conflict with vasostatin and parastatin.

With multiple peptides exerting seemingly conflicting physiological actions, can peptides derived from granins act as effective gut hormones? This issue is further complicated by expression of granins in numerous cell types such as the chromaffin cells, EECs, β cells and α cells [241, 242]. Secretions from these tissue types can be induced by different physiological states such as stress releases adrenaline from chromaffin cells, hyperglycaemia releases insulin from β cells, hypoglycaemia induces glucagon release from α cells and GLP-1 is release post-prandially from EECs. If proteins such as ChgA are produced in all these cells types, how can the peptides released aid in alleviating the physiological state if they have conflicting actions?

One explanation is that these peptides only exert their actions in a paracrine or autocrine manner. Parastatin, vasostatin and catestatin all seem to exert their antihypertensive/cardio-suppressive effects indirectly by supressing catecholamine or parathyroid hormone release [200, 201, 207, 209]. Therefore, these peptides act locally but not as hormones. Another explanation is that differential processing of the granin proteins prevents production of peptides with conflicting actions

in the same cell type. In the peptidomic data from mouse EECs it seems as though N-terminal fragments from ChgA are processed to form ChgA 435-462 which is very similar to the positive inotrope Serpinin. The vasorelaxant catestatin wasn't detected. It should be noted that a similar peptide to catestatin was detected (ChgA 374-391) and larger cardio-suppressive peptides such as vasostatin and parastatin would not have been matched by PEAKS identification software as the software only matches peptides up to 65 amino acids in length.

3.5.3 Comparison with non-peptidomic approaches

As mentioned, I used a peptidomic-driven approach to identify novel peptides using known active peptide characteristics to guide my final selection. The approach taken by a collaboration between the laboratories of Willis Samson and that of Aaron Hsueh contrast with mine as their approach is driven by *in silico* predictions of peptide sequences. This collaboration developed an algorithm to search the whole Swissport proteome for peptide sequences that are; conserved between species; flanked by mono- or dibasic cleavage sites, part of a larger prohormone or protein that doesn't contain transmembrane domains and does contain a signal peptide [234, 237, 243]. After predicting a peptide sequence called neuronostatin, Samson et al. extracted porcine pancreas using magnetic beads coupled to antibodies against neuronostatin and analysed these extracts by MALDI-time of flight (TOF) MS after fractionation by high-performance liquid chromatography (HPLC) [234]. An analyte with a similar mass to neuronostatin was found and microsequencing of the fraction containing this analyte confirmed the sequence was that of neuronostatin. The issue with this approach is that peptides are predicted and not necessarily produced *in vivo*. Additionally, by targeting the extraction process to neuronostatin and not performing MS/MS analysis, an incomplete picture of prosomatostatin processing was generated in this paper. Therefore, the authors can't be confident that neuronostatin is not a product of or precursor to some other bioactive peptide. Despite this subsequent studies have found that neuronostatin can affect cardiac contractility [240, 244] food intake [239, 245] and islet secretions [238]. I did not detect neuronostatin or any other prosomatostatin derived peptides cleaved at position 31 in human GI tissue, mouse EECs or mouse islets. I hypothesised that some other N-terminal prosomatostatin peptide may be responsible for the biological activity that neuronostatin has been shown to possess and as a result selected Sst 25-36 as a novel peptide candidate. This highlights the importance of untargeted peptidomic analysis with MS/MS to identify novel peptides and not to base peptide selection almost entirely on computer predicted sequences.

Another approach to drive peptide candidate selection is to look for at changes between a disease state and a corresponding treatment state. Zhang et al., took this approach as they analysed

the transcriptome of EECs in diet-induced obese (DIO) rats which had undergone Roux-en-Y gastric bypass surgery and their sham controls [236]. Gastric bypass, and in particular the Roux-en-Y form of this surgery, is the most successful treatment for diabetes and obesity [246]. This surgical intervention is thought to bring about diabetes remission and weight loss through altered; nutrient absorption [247], EEC secretions [248], bile acid secretions [249] and central neuronal circuits [250]. Although it is well documented that the plasma levels of certain EEC-derived hormones such as CCK, GLP-1 and PYY change after surgery [251-253], Zhang et al. hypothesised there could be additional peptides contributing to this anti-diabetic/obesity effect. In this study Zhang et al. performed bulk RNA-seq on isolated EECs from different regions of the intestines in DIO sham operated rats and DIO rats treated with Roux-en-Y surgery. The authors translated their transcriptomic data to build their own library of the proteomic content of EECs. Peptides were predicted using a similar bioinformatics approach to Samson and Hsueh but with two improvements. The first was they could predict sequences of peptides from previously unknown genes. The second was that their candidate selection could be guided by differential expression in a model of weight loss and diabetes remission improving the chances of discovering a novel peptide hormone. Whilst, this study suffers for the same issue as Samson and Hsueh in that peptides are predicted and may not be found endogenously, the authors present an interesting approach to novel peptide identification.

Zhang et al. synthesised 5 novel peptides for *in vivo* testing. These peptides originated from 3 genes; *Apl, Npw* and *FAM3D*. Surprisingly peptides from none of these genes were detected in the NeuroD1 sorted cells. Perhaps the differences in methods used to isolate the EEC population can explain this discrepancy. I isolated EEC based on YFP expression in the *NeuroD1* positive population of the GI tract whereas Zhang et al. isolated theirs using laser capture microdissection of *ChgA* positive cells. The *ChgA* and *NeuroD1* expressing populations are overlapping but not quite analogous. The *ChgA+* population may exhibit a slight bias to enterochromaffin cells as *Tph1+* cells are the highest expressors of *ChgA* in the mouse intestinal epithelium [85]. Additionally, the laser capture technique may not be able to isolate single cells due to the resolution of the laser thus introducing cells either side of *ChgA+* cells into the analysis [254].

My criterion of >50% homology between human and mice was quite low compared to the cut-offs used by Zhang et al. [236]. Although no minimum homology value was specified in this paper, all 5 of the peptides selected for *in vivo* characterisation were >70% conserved between humans and rodents. My cut-off of 50% seems even lower when considering that most peptide hormones are >80% conserved (table 3.7). However, if cut-off values for homology were too stringent, then active peptides with low homologies will be filtered out and never identified. GRPP is only 67% conserved and so going

by the homology shown by the peptides selected by Zhang et al. their algorithms would have filtered out GRPP as a peptide candidate.

Peptide	% of amino acids exactly conserved	% of amino acids exactly conserved + % chemically similar amino acids
CCK-12	100.0	100.0
CCK-33	90.9	97.0
CCK-8	100.0	100.0
Gastrin	81.3	87.5
Ghrelin	100.0	100.0
GIP	100.0	100.0
GLP-1	100.0	100.0
GLP-2	93.9	93.9
Glucagon	100.0	100.0
GRPP	63.3	66.7
IAPP	83.8	91.9
Insl5 A Chain	71.4	81.0
Insl5 B chain	79.2	95.8
Insulin A Chain	95.2	100.0
Insulin B chain	93.3	93.3
Neurotensin	100.0	100.0
Obestatin	87.0	91.3
Oxyntomodulin	100.0	100.0
PPY	86.1	86.1
PYY (1-36)	91.7	94.4
PYY (3-36)	90.9	93.9
Secretin	85.2	88.9
SST-14	100.0	100.0
SST-28	100.0	100.0

Table 3.7: Conservation of known peptide hormones from EECs and islets between humans and mice.

3.5.4 Comparison with other peptidomic approaches

Other studies have utilised a peptidomic-driven approach to identify novel peptide candidates. Taylor et al. analysed the peptidomics of forskolin- and glucose-induced secretions from isolated human and mouse islets detecting numerous islet derived peptides [166]. Several elution buffers were used during extraction in this study to increase the coverage of peptides detected. Samples loaded onto the SPE sorbent were subject to an initial elution with 25% ACN and 0.1% FA in H_20 to elute hydrophilic peptides. An elution with 60% ACN and 0.1% FA in H_20 followed to elute hydrophobic peptides and the two eluates were analysed separately. My methods only used one elution buffer of 60% organic solution and therefore hydrophobic and hydrophilic peptides would be present in this elution. By separating hydrophobic and hydrophilic peptides for analysis, Taylor et al. may boost their sensitivity for low abundance peptides due to decreased ion suppression during ESI. Interestingly, many peptides I selected for synthesis were also detected by Taylor et al. Peptides such as Pyy 68-98, ChgA 435-462a, Pcsk1n 42-59, Scg2 184-216 and Scg2 569-610 were identified in murine islet supernatants indicating these peptides are not breakdown products generated during sample preparation but endogenously produced.

The issue of preventing *ex vivo* degradation of peptides is a crucial one in peptidomic analysis due to their linear structure and therefore vulnerability to peptidases. Incomplete enzyme inactivation by Samson et al. post tissue collection could have meant N-terminal prosomatostatin peptides were degraded *ex vivo* into neuronostatin leading to the identification of a potentially non-endogenous peptide. In this chapter's methods, peptide degradation *ex vivo* was prevented by lysing EECs in 80% ACN. The high percentage of organic solvent would lyse cells and precipitate high molecular weight proteins thus inactivating peptidases. Whole mouse islets and human tissue was lysed or homogenised in 6M GuHCl as 80% ACN alone did not sufficiently lyse whole tissue or multicellular structures. A subsequent protein crash was performed but I can't guarantee enzyme inactivation immediately after tissue homogenisation or islet cell lysis.

Secher et al. optimised their enzyme inactivation methods when characterising the peptidome of rat hypothalamus [227]. The authors attempted to inactive enzyme activity by; irradiating whole heads in a microwave oven, heating dissected brains to 95°C in an air-evacuated cartridge [255] or perfusing protease inhibitors into anaesthetised mice before decapitation and heat inactivation at 95°C. The last method was deemed to be the most effective at preventing neuropeptide degradation and used in a large-scale peptidomic characterisation of the rat hypothalamus. I experimented with adding protease inhibitors such diprotin (Sigma I9759), phosphoramidon (Sigma, R7385) and a tissue culture protease inhibitor cocktail (Sigma, P1860). As these small molecule or peptide inhibitors were very abundant in the samples, they interfered with peptide identification by preventing fragmentation

of analytes that co-eluted with the inhibitors. As a result, protease inhibitors were not used as peptide identification would be hindered and column life would be shortened by overloading it with these molecules. Nevertheless, Secher et al. were able to detect many neuropeptides and several of the granin-derived peptides detected were identical to those which I selected for synthesis (ChgA 435-462a, Scg2 569-610).

One criticism of the peptide identification process used by Secher et al. was their use of an algorithm to assemble peptides into the longest peptide variant (LPV) [227]. Peptide ladders can be seen in peptidomic analysis where proteases remove one amino acid at a time thus generating multiple peptides derived from one precursor peptide. By merging overlapping sequences into their LPVs the number of peptides detected in their samples was reduced from 14416 to 2835. Although this reduces sample complexity it could mean final peptide forms are missed. Gastrin is an active N-terminally truncated version of big gastrin (figure 3.6). By using the LPV algorithm, gastrin would be merged into big gastrin in the peptide identification process and the final active form of gastrin would be missed.

3.5.5 Shortfalls in my peptidomic methodology

The extraction methodology used to analyse the peptidome of these tissue types should have enabled an untargeted and comprehensive analysis, detecting the vast majority of peptides in the extracts. However, there are certain pitfalls in my methodology meaning some peptides may have slipped by. For example, using electrospray ionisation (ESI) in positive mode would mean that peptides which are not positively charged in highly acidic conditions such as sulphated versions of CCK-8 would not be detected. These peptides would not pick up a positive charge and so would be removed by ion guides inside the mass spectrometer. To negate this issue samples could have been reanalysed but using ESI in negative mode.

Furthermore, peptides longer than 65 amino acids would not be matched by the PEAKS database search. Peptides such as glicentin (originates from proglucagon) and vasostatins (originates from ChgA protein) would not be matched regardless of if they were present in the raw data files and produced good MS/MS spectra. These peptides could be identified by manual identification, but such a task is not feasible due to the huge time investment needed to complete it. Instead, alternate methods of computationally matching MS/MS data to peptide sequences in protein databases could be used. Machine learning and neural networks such as DeepNovo have been developed that enable de novo sequencing of MS/MS spectra and subsequent peptide matching [256, 257]. Such models are trainable and could be programmed to de novo sequence large peptides enabling matching of

peptides larger than 65 amino acids. DeepNovo was able to reconstruct the sequences of proteins considerably longer than 65 amino acids such as the light and heavy chains of antibodies. The downside of such machine learning models for de novo sequencing is that they require a considerable amount of expertise to devise and programme and such expertise was not available for this project.

3.5.6 Relative quantification of peptides by peak area

In this chapter, relative quantification has been used to assess peptide abundance in samples. This involves integrating the signal for a given peptide over time (area under the curve or peak area) and gives a measure of the total number of ions in the sample for that peptide which is then used as a surrogate for peptide abundance. While this is a very common approach to quantification in peptidomic studies where 1000s of peptides are quantified, it is not a good measure of absolute amount of peptide in each sample. [258]. Peptides can ionise with different efficiencies as they undergo ionisation during ESI and therefore the number of ions detected by the mass spectrometer does not necessarily accurately reflect peptide abundance in the sample [259]. This makes it difficult to compare the peak area of different peptides as dissimilarities in ionisation efficiencies may account for disparities in the peak area of peptides rather than differences in peptide levels in the original sample. This is not an issue for studies comparing levels of the same peptide across multiple samples, but it is for studies comparing levels of different peptides as is the case with this chapter where novel peptides were selected partly for their abundance in samples. However, peptide abundance was not the sole reason why novel peptides were selected for synthesis as a range of criteria were also used such as (but not limited to) conservation in humans, exhibiting regulated secretion and being flanked by basic residues. Peptide peak area was used to help guide candidate selection and in fact one of the priority 1 peptide candidates, Sst 25-36, was not highly abundant in FACS purified murine EECs when compared to other peptides derived from the same prohormone (see figure 3.7). By utilising a range of criteria to select novel peptides and not basing peptide selection purely on peptide peak area, I hope to select the most promising candidates as novel peptides and not simply those have avoided which ionised with the highest efficiency during ESI.

3.5.7 Conclusion

The peptidomics of EECs have been characterised in this chapter as well as 13 novel peptides selected for synthesis and characterisation of their biological activity. These peptides are derived from processing enzymes, known prohormones or granin proteins which are highly expressed in EECs and known to produce other bioactive hormones. By using a peptidomics driven approach to select these

13 candidates, peptides that are endogenously produced have been identified that may have been overlooked if a transcriptomic or *in silico*-based approach was used as has been done in previous studies. Chapter 4 will focus on the *in vitro* and *in vivo* characterisation of these peptides.

Chapter 4: Characterisation of novel peptide candidates in vivo and in vitro

4.1 Introduction

In chapter 3, the peptidomics of murine enteroendocrine cells (EECs), murine islets and human gastrointestinal (GI) tissue were characterised to search for novel peptide candidates that may be biologically active and a panel of 13 peptides were selected for synthesis. In this chapter, these peptides are tested *in vivo* and *in vitro* to search for any potential biological activity. Specifically, I look at the potential of the novel peptide candidates to modulate food intake and glucose tolerance, as peptides exhibiting these actions are of therapeutic interest for the treatment of diabetes and obesity. Before presenting my findings, I will first look at how other studies have sought to characterise the activity of peptides *in vivo* and how peptides similar to the priority 1 peptide candidates have been characterised *in vivo* and *in vitro.*

4.1.1 Peptide characterisation *in vivo*

Appetite and glucose tolerance are complex physiological mechanisms affected by numerous factors and assessing the role of a peptide in glucose tolerance or appetite should be primarily performed *in vivo.* Due to the rapid clearance of most endogenous gut hormones, the method of administration and dosing frequency can be crucial to ensuring maximal exposure of the animal to the peptide and therefore accurate assessment of a peptide's *in vivo* efficacy. Acute studies can be performed where peptides are administered at high doses and food intake or glucose tolerance monitored immediately when circulating levels of peptide are at their highest. This approach was taken by Zhang et al. who acutely injected 5 novel peptides into diet-induced obese (DIO) rodents before oral glucose tolerance or food intake was immediately assessed [236]. Additionally, a study by Taylor et al. focused on acutely characterising the anti-diabetic and anorexic effects of Xenin, a peptide postulated to be co-secreted with GIP by EECs [260, 261]. The authors administered Xenin to mice before food intake was monitored or a glucose tolerance test (GTT) performed [261]. Xenin was found to reduce food intake for 2 hours after subcutaneous (s.c.) administration and improve glucose tolerance when simultaneously injected with the glucose challenge.

Chronic studies can also be performed where daily injections of a peptide are administered in the hope of achieving a steady state plasma concentration of the peptide. With a consistent exposure

of the animal to the peptide, food intake and glucose tolerance measurements can be made throughout the study. Such an approach has been employed to further characterise the effects of xenin where DIO mice were given twice daily intraperitoneal (IP) injections of the peptide for 21 days with glucose tolerance and food intake monitored throughout [262]. Issues with chronic studies giving bolus injections of peptides are with the clearance of the peptide. Even with twice daily injection, peptide levels are almost certainly not going to reach a steady state in the circulation and the exposure of the animal to the peptide will be highly variable.

Peptides can be modified by altering the sequence [262] or addition of molecules such as polyethylene glycol (PEG) to improve circulating half-life [263]. The issue with this approach is that peptide activity can be compromised through sequence or structural changes. Alterations should only be made once an activity of the peptide has been discovered so modified peptides can be tested to see if the activity is maintained.

Another method of mitigating the issue of rapid peptide clearance is to administer the peptide centrally, an approach taken by Samson et al. to characterise the effects of neuronostatin on food intake [234]. The issue with this approach is that if the peptide acts peripherally, then no effect will be seen as the peptide will not be exposed to its site of action.

Administering peptides to animals by bolus injections is a common method used when assessing peptides *in vivo*. An alternative method of administration is through an osmotic pump [264] (figure 4.1). Osmotic pumps are filled with an agent and implanted into animals in a one-off surgical procedure. Over an extended period of time the agent is released at a constant rate allowing for consistent exposure of the animal to the drug and minimal handling of the animal. Osmotic pumps have been used to infuse numerous peptides to rodents including secretin [265], PYY (3-36) [266], insulin [267], obestatin [268] and exendin-4 [269, 270]. With only a one-off surgery required, osmotic pumps are particularly useful for *in vivo* studies monitoring food intake as frequent bolus injections of the peptide are not required and so stress caused by handling is minimised [269, 271]. One drawback of using osmotic pumps is that peptides need to be stable at 37^{o}C for long periods of time and not prone to aggregating or degrading.

To choose the optimal route of delivery, pharmacokinetics (PK) studies can be performed [272]. PK studies provide information on the bioavailability, absorption from peripheral compartments and clearance and so can help when choosing optimal delivery routes, dosing regimens and dosages for a peptide.

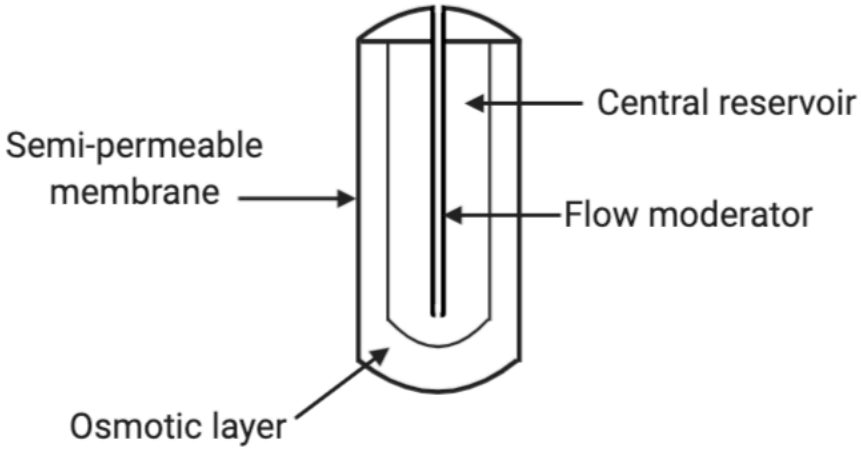

Figure 4.1 Schematic of an osmotic pump. *The central reservoir is filled with an agent to be delivered. Water can be drawn from the interstitial fluid through the semi-permeable outer membrane of the pump into the osmotic layer. This influx of water causes the osmotic layer to swell compressing the central reservoir and the agent is 'squeezed' out of the flow moderator and into the animal.*

4.1.2 Similar peptides to priority 1 novel peptide candidates

Only 3 of the 13 peptides selected for synthesis in chapter 3 were tested *in vivo*. In this section I will summarise how peptides similar to the priority 1 peptides have been characterised previously.

Neuronostatin is derived from prosomatostatin and overlaps with 6 amino acids of Sst 25-36 which is one of my priority 1 peptides. Neuronostatin has been infused into rodents to characterise its ability to control food intake and glucose tolerance. Samson et al. acutely administered neuronostatin intracerebroventricularly to rats and observed reduced food intake compared to vehicle treated controls [234]. Additionally, an intra-arterial infusion of neuronostatin resulted in decreased insulin release and impaired glucose tolerance during an intraperitoneal (IP) glucose tolerance test (GTT). The effects of neuronostatin are thought to be induced by direct action on islets. Salvatori et al. applied 100 nM neuronostatin to isolated rat islets for 3 hours and found *Gcg* mRNA was increased [238]. It was also found that 1000 nM of neuronostatin could enhance glucagon secretion at 2 and 20 mM glucose and impair glucose stimulated insulin secretion (GSIS). GPR107 is thought to mediate the effects on islets of neuronostatin as knockdown of this receptor with siRNA reduced the ability of neuronostatin to modulate *Gcg* mRNA [273].

Serpinin is a peptide derived from the C-terminus of the ChgA protein and almost identical to one of the priority 1 peptides selected for synthesis in this thesis (ChgA 435-462a). Serpinin has been

shown to increase granule biogenesis in a murine pituitary cell line through enhancing mRNA levels of protease nexin-1 (PN-1) [210]. PN-1 is a serine protease inhibitor and prevents degradation of granin proteins in vesicles thus helping to stabilise the vesicle [274]. The effects of serpinin may extend beyond neuroendocrine cells as Thomsen et al. report that amidation of ChgA is crucial for insulin granule biogenesis in a β cell line [275]. Serpinin represents a C-terminally truncated version of the amidated ChgA 435-462a which was selected for synthesis in chapter 3. Perhaps ChgA 435-462a plays a similar role to Serpinin in β cells. Serpinin has also been shown to act as a positive inotrope on rat Langendorff isolated heart preparations with a smaller version of serpinin, pGlu-serpinin, showing enhanced potency in this *ex vivo* preparation [211]. However, no studies have been published which infuse serpinin into animals to monitor food intake or glucose tolerance.

Big gastrin (or gastrin-34) is a 34 amino acid long peptide cleaved from progastrin by PC1/3 [276]. This 34 amino acid peptide is then cleaved by PC2 to produce the peptide hormone gastrin which controls gastric acid secretions and regulates the gastric stem cell population [24, 36]. Big gastrin may also act as the precursor to one of my priority 1 peptide candidates, Gast p59-79, which overlaps with the first 4 amino acids of gastrin. The sequence of amino acids responsible for activity of gastrin at its target receptors (cholecystokinin (CCK) family of receptors) represents the last 5 amino acids of gastrin at the C-terminus and is referred to as pentagastrin [277]. Big gastrin also possesses the pentagastrin sequence and therefore is considered to possess the same biological activity as gastrin [278]. The effects of big-gastrin derived peptides on food intake are poorly annotated, however, potential effects on glucose tolerance are better researched. One study has shown that islets from humans with haemoglobin A1c (HbA1c) levels higher than 42 mmol/mol show an increase in their expression of *INS*, *GCG*, *SST* when treated with 100 nM gastrin and that these effects are mediated through the CCKB receptor [279]. Gastrin has also been shown to affect β cell regeneration and β-cell mass in murine models exhibiting hyperglycaemia [280-285]. Gastrin did not induce these effects in mice exhibiting normoglycemia, however. Therefore, gastrin may possess some glucose lowering effects in pathophysiological states such as diabetes. Although, in all of these studies gastrin was co-infused to mice with GLP-1 receptor agonists, EGF or transforming growth factor-α so it is not clear if gastrin alone can induce these positive effects on β cells.

4.1.3 Aims

1. Synthesise novel peptide candidate panel.
2. Assess activity of all peptide candidates at Gs and Gi signalling pathways in various relevant cell types.
3. Assess the pharmacokinetics of the priority 1 peptide candidates.

4. Validate the release of the priority 1 peptides from osmotic pumps.
5. Assess the effect of the priority 1 peptide candidates on food intake and glucose tolerance during chronic *in vivo* studies.

4.2 Methods

4.2.1 Peptide synthesis

Performed by Elise Bernard (AstraZeneca, UK)

4.2.1.1 Materials

N-α-Fmoc-L-amino acids were obtained from Bachem. NOVASYN® TGR (TentaGel Rink) and NOVASYN® TGA (TentaGel Wang) synthesis resins were obtained from Novabiochem, Merck Biosciences. Arginine was incorporated as the sidechain 2,2,4,6,7-pentamethyldihydrobenzofuran-5-sulfonyl (Pbf) derivative. Asparagine and glutamine were incorporated as their sidechain trityl derivatives. Lysine was incorporated as the sidechain t-butyloxycarbonyl (Boc) derivative. Serine, threonine and tyrosine were incorporated as sidechain *tert*-butyl (tBu) ethers, and aspartate and glutamate as their sidechain *tert*-butyl (*Ot*Bu) esters. 1-Boc-L-pyroglutamic acid, N-α-Fmoc-L-Leu-OH-$^{13}C_6$,^{15}N and synthesis reagents were obtained from Sigma-Aldrich. N-Methyl-2-pyrrolidone (NMP), Dimethylformamide (DMF), Triisopropylsilane (TIPS), Diisopropylethylamine (DIPEA), Trifluoroacetic acid (TFA) and HCTU (2-(6-Chloro-1-H-benzotriazol-1-yl)-1,1,3,3-tetramethylaminium hexafluorophosphate), pyridine, acetic anhydride and piperidine were all purchased from Sigma.

4.2.1.2 General procedure for chemical synthesis of peptides

All peptides were prepared by automated synthesis (PTI Prelude) using the Fmoc/*t*Bu protocol. Peptides ChgA 435-462a and its isotopically labelled version were prepared as C-terminal carboxamides on NOVASYN® TGR resin and all other peptides were prepared as C-terminal carboxylic acids on NOVASYN® TGA resin. All amino acids (both natural and unnatural) were coupled at room temperature using HCTU/DIPEA in NMP, capping residual functionality with a solution of acetic anhydride and pyridine. Fmoc group was deblocked using piperidine in 20% DMF in water (v/v) at room temperature.

4.2.1.3 Cleavage and purification of peptides

Crude peptides were cleaved from the resin support with a cocktail of 95% TFA (v/v), 2.5% TIPS (v/v), 2.5% water (v/v) for 3 hours at room temperature with agitation. Cleaved peptides were concentrated

by rotary evaporation and precipitated by addition of cold diethyl ether. Crude peptides were dried under a flow of nitrogen for 1 h, reconstituted in 10% ACN in water (v/v) and filtered prior to purification by RP-HPLC. Crude peptides were loaded onto an Agilent Polaris C8, 21.2×250 mm, 5 µm column. Analytes were eluted at 20 mL/min with a linear gradient where solvent B (ACN with 0.1% TFA v/v) was increased from 5-50% whilst solvent A (water with 0.1% TFA v/v) was decreased from 95-50% over 30 minutes using a Varian SD-1 Prep Star binary pump system, monitoring for UV absorption at 210 nm. The desired peptide-containing fractions were pooled, frozen and lyophilized.

4.2.1.4 Peptide analysis and characterisation post-synthesis

To verify molecular masses against calculated theoretical values, purified peptides were characterized by single quadrupolar LC-MS using a Waters Mass Lynx 3100 platform. Positive ESI was used as the source. Analytes were loaded onto a Waters X-Bridge C18, 4.6×100 mm, 3 µm column and eluted using a linear gradient where solvent B (ACN with 0.1% TFA v/v) was increased from 10-90% whilst solvent A (water with 0.1% TFA v/v) was decreased from 90-10% over 10 minutes at 1.5 mL/min at room temperature. Analytes were detected by both UV absorption at 210 nm and ionization using a Waters 3100 mass detector.

4.2.2 cAMP accumulation assay

4.2.2.1 Materials

Cell types

Cell type	Origin	Screened in Gs?	Screened in Gi?
MIN6	Mouse β cell line	Yes	Yes
Rat hepatocyte	Primary	Yes	No
SK-N-MC	Human neuronal cell line	Yes	Yes
αTC1	Mouse α cell line	Yes	No
STC-1	Mouse small intestinal EEC line	Yes	No

Table 4.1: Cell types in which cAMP accumulation assay was performed, either in Gs or Gi. *Rat hepatocytes, αTC1 and STC-1 were not screened in Gi mode as no working positive control peptide could be found. I attempted a Gi screen with SST-28 as the positive control for αTC1 and STC-1 but SST-28 did not induce a consistent inhibitory effect.*

All cell types were acquired from the American Tissue Culture Collection (ATCC). Table 4.1 shows the cell types used as well as their origin and if they were screened in Gs or Gi mode.

cAMP- Gs dynamic kit

The cAMP-Gs dynamic kit operates on the principle of homogenous time-resolved resonance fluorescence (HTRF) and was purchased from Cisbio. It consisted of lysis buffer, an anti-cAMP-Cryptate labelled antibody (donor) and cAMP labelled with d2 (acceptor). The antibody and labelled cAMP were made up according to the manufacturer's instructions.

Control peptides

α-Calcitonin-gene related peptide (CGRP), β-CGRP, GLP-1 (7-36), Glucagon, PYY (1-36), PYY (3-36), SST-28 and IAPP were purchased from Bachem and were made up in PBS with 0.1% BSA.

4.2.2.2 Protocol

An 11-point 1 in 3 dilution curve of each test & control compound was made up in a 96-well U-bottom plate (Greiner) and transferred into a black shallow well U-bottom 384-well plate (Corning) in duplicate. All dilutions were made in assay buffer which was composed of HBSS supplemented with; 25 mM HEPES, 0.1 % BSA and 0.5 mM IBMX. The appropriate cell line was added to all wells of the 384-well plate and incubated at room temperature for 30 minutes. The d2 labelled cAMP was then added to all wells except A23, B23, C23, D23, A24, B24, C24 and D24. These wells would act as a background control where no FRET signal should be detected due to the absence of any acceptor. The anti-cAMP cryptate-labelled antibody was added to all wells immediately after the addition of the labelled cAMP. The plate was left to incubate for 1 hr and the emission of light at wavelengths 665 and 620 nm was measured on an Envision plate reader (ThermoScientific).

To screen peptides for Gi signalling the same protocol was used except 15 μM forskolin was added to all wells just after test peptides and before cells were added to the wells.

4.2.2.3 Analysis

The ratio of light at wavelengths 665:620 was calculated and multiplied by 10000 to obtain what will be referred to as the HTRF reading. The HTRF reading was then converted into % activation by the following equation:

$$\% \ activation = ((SR\text{-}BR)/(CR\text{-}BR))*100$$

SR (sample HTRF reading) = HTRF reading obtained from test peptides along with cells

BR (background HTRF reading) = HTRF reading obtained from wells with only cells present

CR (control HTRF reading) = HTRF reading obtained from wells with cells and highest concentration of positive control.

% inhibition was calculated by the following equations:

$$\% \text{ inhibition} = ((FR-SR)/(FR-CR))*100$$

FR (forskolin HTRF reading) = HTRF reading obtained from wells with cells and forskolin only.

These equations enabled the data to be normalised to a positive control and removed the background signal.

4.2.3 Peptide stability in Plasma

4.2.3.1 24-hour stability protocol

The three priority one peptides were spiked into plasma, incubated at 37^{o}C and 40 µL aliquots were taken at various time points over 24 hours. These time points were as follows; 0, 5 ,10, 15, 30, 60 minutes and 2, 4, 7 and 24 hours. The aliquots were subjected to a protein crash (section 2.5.1) and SPE (section 2.5.2).

4.2.3.2 Citrate buffer stabilisation

Citrate buffer consisted of 0.1 M sodium citrate (Sigma) dissolved in water (w/v) and adjusted to pH 3 with citric acid powder (Sigma).

Priority 1 peptides were spiked into 2 aliquots of plasma. One aliquot was stabilised with 1 in 10 (1 part citrate buffer to 9 parts plasma) (v/v) dilution of citrate buffer and the other aliquot not stabilised as a control. Three 40 µL samples were taken from each plasma type immediately after spiking peptides (0 min) as well as 15 min post-spiking. The aliquots were subjected to a protein crash (see section 2.5.1) and SPE (see section 2.5.2).

4.2.3.3 Peptide quantification by LC-MS

See section 2.6.2 for details on the system used, column and MS instrument settings. Start and end conditions as well as collision energies, precursor and product ions were specific to the peptide being analysed and are listed in table 4.2. 20 µL of sample was injected onto the column and starting conditions held for 30 seconds to allow peptide binding to the column. The % buffer B was increased

to the end conditions over the course of 3.5 minutes. The column was flushed with 90% buffer B for 1.5 minutes before starting conditions restored. Total run time per sample was 5.5 min.

Peptide	**Sst 25-36**	**Sst 25-36 IS**	**Gast p59-79**	**Gast p59-79 IS**	**ChgA 435-462a**	**ChgA 435-462a IS**
% B (start)	12.5	12.5	12.5	12.5	20	20
% B (end)	50	50	50	50	60	60
Collision energy	18	18	18	18	18	18
Precursor *(m/z)*	476.6	478.9	596.8	479.2	635.9	638.9
Product *(m/z)*	529.3	532.73	626.6	471.9	721.4	725.8

Table 4.2: Specifications used to quantify the 3 priority 1 peptides using the Xevo TQ-XS mass spectrometer when coupled to high flow LC system.

4.2.3.4 Optimising multiple reaction monitoring assays for priority 1 peptide quantification

To quantify the priority 1 peptides using the Xevo TQ-XS triple quadrupole mass spectrometer, tandem mass spectrometry (MS/MS) assays had to be first optimised. This involved; analysing the peptides in full scan mode to identify the most abundant precursor ion of the peptide, optimising the collision energy used to fragment the peptide ions and then selecting product ions which were highly abundant in the resulting MS/MS spectra and had a larger *m/z* value than the precursor ion so as to improve the selectivity of the assay for the peptide. Table 4.2 displays the precursor ions, collision energies and product ions selected to quantify each of the priority 1 peptides and their internal standards after this optimisation process. Precursor ions and product ions selected were checked against data from the Orbitrap mass spectrometer and the theoretical masses of the peptides and their fragments to ensure did correspond to ions and fragments of the peptides.

4.2.4 Pharmacokinetics studies

Male mice aged between 8-10 weeks were used. The study design for each peptide's PK study varied depending on data from the *in vitro* plasma stability experiment and also depended on the route of administration. In all studies, citrate buffer (pH3, 0.1 M) was added to plasma at a dilution of 1 in 10 to prevent enzyme degradation of peptides. The specifics of each protocol are summarised below.

4.2.4.1 s.c. PK study for Sst 25-36 & Gast p59-79

10 mg/kg of peptide were injected s.c. into 6 mice for each peptide. Blood was taken from 3 mice at 2, 10 and 30 minutes post-injection and from the other 3 mice at the following time points; 6, 15 and 45 minutes. 80 µL blood was taken from the tail vein and collected into EDTA coated microvette tubes (STARSEDT). Blood was centrifuged at 2000g for 10 mins at 4^{o}C and the plasma separated.

4.2.4.2 s.c. PK study for ChgA 435-462a

1 or 3 mg/kg of peptide were injected s.c. into 6 mice. Blood was taken from 3 mice at 2.5, 15, 60 and 120 minutes post-injection and at the following time points from the other 3 mice; 7.5, 30 and 90 minutes. 40 µL blood was collected from the tail vein into EDTA coated microvette tubes. Blood was centrifuged at 2000g for 10 mins at 4^{o}C to separate plasma.

4.2.4.3 i.v. PK study for Sst 25-36 & Gast p59-79

1 mg/kg of peptide was injected via the tail vein into 8 mice for each peptide. 40 µL blood was taken from the tail vein and collected into EDTA coated microvette tubes. Blood was taken from 4 mice at 1, 6 and 12 minutes post-injection and the following time points from the other 4 mice; 3, 9 and 30 minutes. Blood was centrifuged at 2000g for 10 mins at 4^{o}C and the plasma separated.

4.2.4.4 i.v. PK study for ChgA 435-462a

1 mg/kg of peptide was injected via the tail vein into 8 mice. Blood was taken from 4 mice at each of the following time points: 3, 15, 60, 120 and from the other 4 mice at the following time points: 8, 30, and 90 minutes post-injection. 40 µL blood was taken from the tail vein and collected into EDTA coated microvette tubes. Blood was centrifuged at 2000g for 10 mins at 4^{o}C to obtain the plasma.

4.2.4.5 Peptide extraction from plasma and quantification by LC-MS

Plasma samples were subjected to a protein crash using 80% ACN (see section 2.5.1) with 0.1% FA and 10 ng/mL of the appropriate internal standard was added and extracted by SPE (see section 2.5.2). See section 4.2.3.3 for details on LC-MS analysis.

4.2.5 Modelling of Peptide PK for constant infusion

Performed by John Hood

Modelling was performed using SAAM II v2.2.1 (The Epsilon Group) with a Rosenbrock integrator and no maximum number of iterations. Starting with data from i.v. PK studies, a model was built for each

peptide to estimate the following parameters; clearance (Cl), volume of the central compartment (Vc), volume of the peripheral compartment (Vp), intercompartmental clearance (Q).

After these 4 parameters were fixed, data from the s.c. PK studies were added to each peptide's model and 2 more parameters could be estimated; bioavailability (F) and absorption from a s.c. deposit (Ka). Bioavailability (F) could be calculated using the following equation;

$$F = (dose\ normalised\ s.c.\ AUC / dose\ normalised\ i.v.\ AUC) * 100$$

Figure 4.2 displays a diagrammatic view of the models built using the PK data and the parameters calculated. Using the parameters of Vc, Vp, Q, Ka and F, the mass infusion rate required to cancel out the Cl of the peptide was calculated, aiming to achieve a steady state plasma concentration (Css) of 1 nM. This was an iterative process and the software repeated the calculation until the desired Css had been achieved. With the mass infusion rate, the concentration of peptide in an osmotic pump required to reach a Css of 1 nM could be calculated using the following equation;

$$Pump\ concentration\ of\ peptide\ (\mu g/mL) = \left(\frac{Mass\ infusion\ rate\ (mg/g/day)}{Volume\ delivery\ (\mu L/day)}\right) * mouse\ weight\ (g)$$

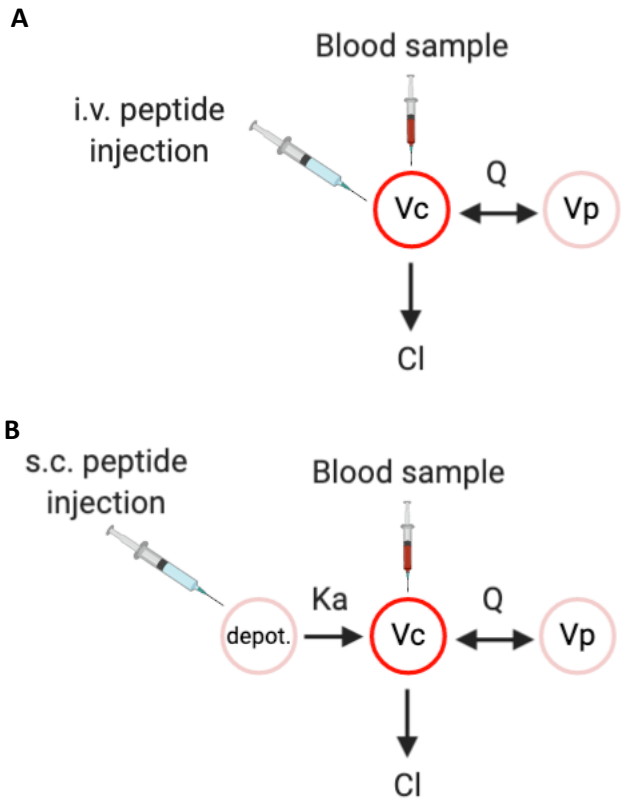

Figure 4.2: Diagrammatic view of PK parameters calculated from i.v. and s.c. PK studies. *(**A**) Peptide injected intravenously into the central compartment. Distribution rate to peripheral compartments is determined by Q. Clearance from the central compartment is determined by Cl. Blood samples taken from central compartment to quantify peptide levels. (**B**) Peptide injected subcutaneously. Absorption into the central compartment is determined by Ka. Q determines distribution to peripheral compartments and Cl determines clearance from the body. Blood samples taken from central compartment for peptide quantification.*

4.2.6 *in vitro* osmotic pump study

This experiment assessed the release of 3 different peptides by osmotic pump. Additionally, pumps were siliconized or BSA was added to the peptide vehicle to investigate if these measures could prevent peptide binding and improve release of peptides.

4.2.6.1 Siliconising

AquaSil (Thermo Scientific) was diluted from a 20% stock to 0.5% in water. 2004 model Alzet pumps were filled with this 0.5% AquaSil solution for 20 seconds. AquaSil was removed and replaced with methanol to wash off any residual siliconizing fluid and siliconized pumps were left in a fume hood at room temperature from 24 hours to allow any residual fluid to dry.

4.2.6.2 Pump filling

Gast p59-79, ChgA 435-462a and Exenatide were made up in either PBS or PBS with 0.1% BSA. The concentrations of peptide used were identical to the concentrations necessary for the *in vivo* studies (Gast p59-79: 4mg/mL, ChgA 435-462a: 1.5 mg/mL, Exenatide: 0.15 mg/mL). Each peptide was filled into one of three pumps; a siliconized pump, a pump where 0.1% BSA was added to the peptide vehicle and a pump which had not been siliconized or had BSA added to the vehicle (now referred to as 'normal'). Pumps and their flow moderators were weighed before and after filling to ensure the pumps were filled correctly. Each pump was placed in 1 mL PBS in a 2 mL Protein LoBind Eppendorf and incubated at 37^{o}C.

4.2.6.3 Controls

To assess the recovery of peptide from the osmotic pumps, six aliquots each containing all three peptides at different concentrations were made up according to the mass delivery rate of peptides from the osmotic pumps. These concentrations were; 96 µg/mL for Gast p59-79, 36 µg/mL for ChgA 435-462a, 3.6 µg/mL for Exenatide (Bachem). These were the estimated concentrations of peptide that would be present in the Protein LoBind Eppendorfs tube containing the pumps after four days at 37^{o}C. One of the control aliquots was immediately stored at -80^{o}C whereas the other five were stored at 37^{o}C along with the tubes containing the pumps. To control for peptide binding to the outside of the osmotic pump, an osmotic pump was added to the control samples.

4.2.6.4 Protocol

Every four days the osmotic pumps were transferred to a fresh Protein LoBind Eppendorf tube containing 1 mL PBS and placed back at 37^{o}C. The tube from which the pump had been transferred

was stored at -80^{o}C. Additionally, one of the control samples was removed, had the osmotic pump it contained transferred to another control sample and stored at -80^{o}C. To estimate the peptide concentrations in the samples, a calibration line of each peptide was made up PBS. The calibration points for all peptides were: 10, 25, 50, 100, 250, 500, 750 ng/mL.

4.2.6.5 Peptide extraction

All samples and calibration points were then acidified with 50 uL of 1 % FA (v/v) and spiked with internal standards to reach a final concentration of 20 ng/mL of internal standard. GLP-1 (7-36 amide) was used as an internal standard for exenatide instead of an isotopically labelled version of exenatide due to availability. All samples and calibrants were extracted by SPE (see section 2.5.2).

4.2.6.6 Peptide quantification by LC-MS

Peptides were quantified using an almost identical method to that described in section 4.2.3.3 but exenatide and GLP-1 (7-36 amide) were quantified instead of Sst 25-36 an its IS using the specifications listed in table 4.3. For specifications use to quantify Gast p59-79, ChgA 435-462a and their internal standards see table 4.2.

	Exenatide	***GLP-1 (7-36 amide)***
% B (start)	20	20
% B (end)	60	60
Collision energy	28	30
Precursor (*m/z*)	1047.5	825.4
Product (*m/z*)	1264.3	1126.8

Table 4.3: Specifications used to quantify exenatide using the Xevo TQ-XS mass spectrometer when coupled to high flow LC system.

4.2.7 in vivo osmotic pump study 1

4.2.7.1 Mice

20 male mice, aged between 6-8 weeks, were housed individually in BioDAQ automated food intake cages (Research diets) and fed a standard chow diet. Mice were randomly assigned to one of 4 treatment groups; Gast p59-79, ChgA 435-462a, exenatide, vehicle.

4.2.7.2 Pump preparation

2004 model Alzet osmotic pumps were filled two days prior to surgery under sterile conditions to allow priming of the pumps. Osmotic pumps and their flow regulator were weighed before and after filling to ensure correct filling. Gast p59-79 and exantide were dissolved in sterile PBS with 0.1 % BSA prior to filling and ChgA 435-462a was dissolved in PBS without BSA. Vehicle infusing pumps were filled with PBS (0.1% BSA). The mass delivery rate of each peptide were as follows; ChgA 435-462a = 0.3 mg/kg/day, Gast p59-79 = 0.8 mg/kg/day, exenatide = 0.03 mg/kg/day.

4.2.7.3 Study protocol

Figure 4.3 shows a diagrammatic overview of the whole study. Food intake was monitored from day -7 to the end of the study (day 28) using BioDAQ cages. On day 0, 2004 model osmotic pumps were surgically implanted subcutaneously in the intrascapular region of mice anaesthetised with isoflurane. Intraperitoneal glucose tolerance tests (IP GTT) were performed at 7, 14, 21 and 28 days post-surgery. These procedures consisted of a 6 hour fast prior to a 2 g/kg IP glucose challenge and blood glucose levels were measured using AlphaTrak glucose strips (Zoetis) at -5, 15, 30, 45, 60 and 90 minutes. During the IP GTT performed on day 14, an additional 40 μL of blood was collected at -5 and 15 minutes into EDTA coated glass capillary tubes and plasma separated by centrifuging at 2000g for 5 minutes at 4^{o}C. Plasma insulin levels were quantified by the Core Biochemical Assay Laboratory (Cambridge biomedical Campus, Cambridge) using a mouse insulin assay (Meso Scale Discovery). After the IP GTT on day 28 mice were terminally anaesthetised and blood collected via cardiac puncture into EDTA coated vacutainer (BD). Plasma was separated by centrifuging at 2000 g for 5 min at 4^{o}C. Citrate buffer (pH3, 0.1 M) was added to the plasma collected from Gast p59-79 infused mice at a dilution of 1 in 10.

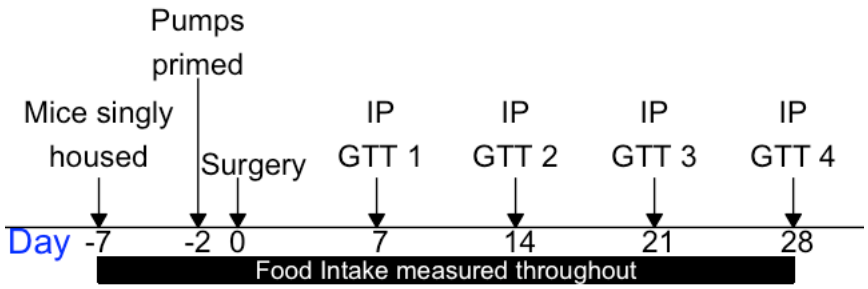

Figure 4.3: Overview of osmotic pump study 1. *Mice singly housed from day -7. Osmotic pumps primed to help achieve maximal release rate on day -2. Pumps implanted during surgery on day 0 and intraperitoneal (IP) IP GTT performed every 7 days after surgery until day 28 when mice were culled Baseline readings taken 3 days prior to surgery*

4.2.7.4 Peptide extraction from plasma

100 µL plasma was crashed with 80% ACN with 0.1% FA (section 2.5.1) and 10 ng/mL of the appropriate internal standard. After evaporation samples were re-suspended in 500 µL 0.1% FA (v/v) before SPE (section 2.5.2).

4.2.7.5 Peptide quantification by micro-flow rate analysis on Triple Quadrupole MS

When quantifying only a few low abundance peptides in a complex matrix, the Waters Triple Quadrupole LC-MS coupled to a Waters M-Class UPLC system provided the greater sensitivity over the H-class UPLC system. Therefore, the M-Class UPLC system coupled to a triple quadrupole MS was used to quantify Gast p59-79, ChgA 435-462a and exenatide in terminal bleed samples from osmotic pump study 1. The total run time for each sample was 30 minutes during which both the 0.18 × 20 mm nanoEase™ trap column (Waters) and 0.15 × 100 mm nanoEase™ column (Waters) were kept at 35°C. Chromatography buffers used were 0.1% FA in water (v/v) (buffer A) and 0.1% FA in ACN (v/v) (buffer B). Analytes were loaded onto the trap at a flow rate of 10 µL/min with at 10% buffer B. The trap column was then set in-line with the 0.15 × 100 mm nano column at a flow rate of 1 µL/min where the gradient increased linearly to 52.5% of B over 15 minutes, after which the conditions were stepped up to 85% of B to wash/clean the column for 7.5 minutes. Positive ESI was used with the spray voltage set to 3.5 kV. The S-lens voltage was set to 30 V to remove smaller peptides. Specific precursor ions were selected for fragmentation and certain product ions were monitored. These precursor and product ions are listed in table 4.4 along with their collision energies.

Peptide	***Exenatide***	***GLP-1 (7-36a)***	***Gast p59-79***	***Gast p59-79 IS***	***ChgA 435-462a***	***ChgA 435-462a IS***
Collision energy	28	30	18	18	18	18
Precursor (m/z)	1047.5	825.4	477.7	479.2	635.9	638.9
Product (m/z)	1264.3	1126.8	470.5	471.9	721.4	725.8

Table 4.4: Specifications used to quantify peptides using the Xevo TQ-XS mass spectrometer when coupled to micro-flow LC system

4.2.8 *in vivo* osmotic pump study 2

4.2.8.1 Mice

16 male mice, aged between 6-8 weeks, were housed individually and fed a standard chow diet. Fasting blood glucose levels were measured 1 day prior to surgery and mice were divided into two

treatment groups of matching fasting blood glucose levels. One group received Gast p59-79 and the other vehicle (PBS with 0.1% BSA).

4.2.8.2 Pump preparation

Pumps were filled as in section 4.2.7.2 but with a few differences: pump model 1007D was used to deliver either PBS or Gast p59-79 and pumps were prepared on the day of surgery as the priming time for this pump model was very short. The mass infusion rate of Gast p59-79 was 0.8 mg/kg/day.

4.2.8.3 Study protocol

On day 0, 1007D model Alzet pumps were surgically implanted in the intrascapular region of mice anaesthetised with isoflurane. Mice were acclimatised to handling by receiving s.c. injection of PBS at days 4, 5 and 6 post-surgery. An IP GTT was performed 7 days after surgery as in the previous osmotic pump study (section 4.2.7.3). After the IP GTT on day 7, mice were terminally anaesthetised and blood collected via cardiac puncture into EDTA coated microvette tubes. Plasma was separated by centrifuging at 2000 g for 5 min at 4^{o}C and stabilised with 1 in 10 dilution of citrate buffer (pH3, 0.1 M).

4.2.8.4 Peptide extraction and quantification

Peptides were extracted from plasma as in section 4.2.7.4 and quantified by LC-MS as in section 4.2.7.5

4.2.9 in vivo osmotic pump study 3

4.2.9.1 Mice

16 male mice, aged between 6-8 weeks, were singly housed. 8 were fed a high fat diet (HFD) (60% fat, Research Diets) for 16 weeks and the other 8 were fed a standard chow diet. 3 days prior to surgery, an IP GTT was performed so that mice could be randomised according to fasting blood glucose, AUC during the IP GTT and body weight.

4.2.9.2 Pump preparation

Pumps were filled as in section 4.2.7.2 but with a few differences: pump model 1004 was used to deliver either saline or Gast p59-79 and no BSA was added to the vehicle as the pump concentration of peptide was thought to be high enough so that any binding that did occur would be negligible. The mass infusion rate of Gast p59-79 was 0.8 mg/kg/day.

4.2.9.3 Study overview

Figure 4.4 shows a diagrammatic overview of the study. On day 0, mice were anesthetised with isofluroane and 1004 model osmotic pumps were surgically implanted in the intrascapular region. 2 mice were culled after surgery due to excessive weight loss (mouse #5 and #12). An IP GTT was performed 7 days after surgery as in the previous 2 osmotic pump studies (section 4.2.7.3). 14 days post-surgery, an oral GTT (OGTT) was performed. The OGTT was identical to the IP GTT but glucose was administered orally. 21 days post-surgery an insulin tolerance test (ITT) was performed. The ITT was identical to the IP GTT however, 0.75 U/kg of humulin (Fisher Scientific), instead of glucose, was administered IP. 28 days post-surgery mice were fasted for 6 hours and administered with 0.75 U/kg humulin IP. 15 minutes post-challenge mice were culled by cervical dislocation. Liver, white adipose tissue (WAT) and skeletal muscle were excised, and a small piece of each was snap frozen in liquid nitrogen for quantification of phosphorylated-AKT (protein kinase B) as a measure of insulin signalling.

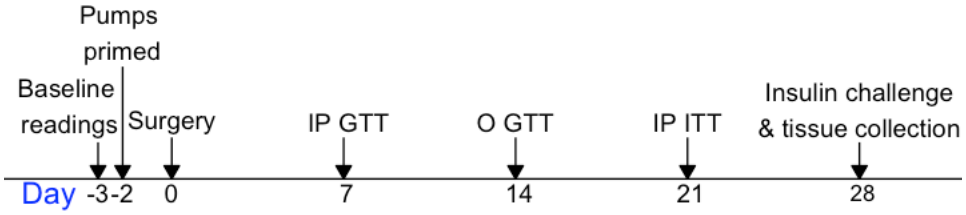

Figure 4.4: Osmotic pump study 3. Osmotic pumps primed 2 days prior to surgery to help achieve maximal release rate. Pumps implanted during surgery on day 0. IP GTT performed on day 7, oral GTT performed on day 14 and an insulin tolerance test (ITT) performed on day 21. On day 28 mice given insulin challenge and culled 15 minutes later for tissue collection.

4.2.9.4 Tissue preparation

50-100 mg pieces of WAT, liver and skeletal muscle were homogenised in MSD lysis buffer with phosphatase inhibitor cocktail I (serine/threonine protein phosphatase inhibitors, MSD), phosphatase inhibitor cocktail II (tyrosine protein phosphatase inhibitors, MSD), protease inhibitor solution (MSD) and 1 Qiagen metal bead. Homogenised tissue was allowed to rest at 4^{o}C for 2 hours to allow protein solubilisation and then spun at 10000 g for 10 minutes at 4^{o}C. Supernatants were aspirated and stored at -80^{o}C.

4.2.9.5 Bicinchoninic acid (BCA) assay

Protein content of all homogenised tissue samples was assessed using a Pierce BCA protein assay kit (ThermoScientific) according to the manufacturer's instructions. Briefly, a 7-point standard curve of

albumin (25-2000 µg/mL) was prepared in MSD lysis buffer and 25 µL of standard or sample was transferred to a 96-well plate in duplicate. 200 µL of working reagent (50 parts reagent A: 1 part reagent B) was added to each well and the plate was incubated at 37^{o}C for 30 min. Absorbance at 562 nm was measured on an envision plate reader (Thermo Fisher Scientific). The absorbance at 562 nm of unknown samples was compared against the standard curve to calculate concentration values.

4.2.9.6 AKT quantification

Kits

Total and phosphorylated-AKT (pAKT) were quantified using respective kits from MSD (total-AKT kit catalogue number K150MOD-1, pAKT (Ser473) kit catalogue number: K151CAD-1)

Sample dilution

Tissue homogenates were diluted in MSD lysis buffer to achieve the same protein concentration in all samples of the same tissue type.

Protocol

1. 150 µL of 3% BSA (w/v) solution was added to all wells of 2 separate MULTI-SPOT 96-well 4-spot AKT plates and plates were incubated at RT for 1 hour on a plate shaker.
2. Plates were washed 3 times with 1× Tris buffer.
3. 25 µL of sample of AKT calibrant was added to each well of both plates in duplicate and incubated for 1hr on a plate shaker.
4. Plates were washed 3 times with 1× Tris buffer.
5. 25 µL of 1× anti-total AKT antibody or 1× anti-pAKT antibody in 1 % BSA solution was added to all wells of 1 plate. Plates were incubated at RT on a plate shaker for 1 hr.
6. Plates were washed 3 times with 1× Tris buffer.
7. 150 uL of 1× read buffer was added to all wells of both plates and read on an MSD instrument

4.2.10 Islet experiments

4.2.10.1 Secretions

Islets were isolated as in section 2.4. Islets were rested for 1 hour by incubating at 37^{o}C in KRB with 0.1% BSA and 5.5 mM glucose to recover after the isolation process. 10 islets were then transferred to each 2 mL protein LoBind Eppendorf tube for 45 min at 37^{o}C with 300 µL of KRB (section 2.2.1) + 0.001% BSA + one of the following:

1. 1 mM glucose

2. 16.7 mM glucose
3. 1 mM glucose + 100 nM Sst 25-36
4. 16.7 mM glucose + 100 nM Sst 25-36
5. 1 mM glucose + 100 nM Gast p59-79
6. 16.7 mM glucose + 100 nM Gast p59-79
7. 1 mM glucose + 100 nM ChgA 435-462a
8. 16.7 mM glucose + 100 nM ChgA 435-462a

At the end of the incubation 270 µL of supernatant was removed and snap frozen. Care was taken not to remove any islets when removing the supernatant.

4.2.10.2 Lysates

Islets were isolated as in section 2.4 and cultured overnight in RMPI media + 10% FBS + 5% Penicillin/Streptomycin + increasing concentrations of ChgA 435-462a. After 24 hours, islets were washed in HBSS (5.5mM glucose), lysed in 200 µL of GuHCl and a protein crash performed as in 2.5.1.

4.2.10.3 Sample preparation

On the day of analysis supernatants were defrosted and acidified with 30 µL of 1% FA (aq) (v/v) whereas dried down islet lysates were reconstituted in 0.1% FA (v/v). All samples were then subjected to SPE (section 2.5.2).

4.2.10.4 Peptide quantification by LC-MS

See section 2.6.2 for details on the system used, column and MS instrument settings. 40 µL of sample was injected onto the column for 30 seconds with starting conditions set at 90% A and 10% B before the % B was increased to 50% over the course of 7.5 minutes. The column was flushed with 90% B for 2 minutes before initial conditions were restored. Total run time per sample was 10 min. Table 4.5 details the peptides quantified as well as their product ions, precursor ions, collision energies and dwell times.

Peptide	***Precursor (m/z)***	***Product (m/z)***	***Collision Energy***	***Dwell time (s)***
Insulin-1	967.8	331.2	40	0.025
SST-14	546.6	726.3	15	0.025
Glucagon	871.5	1040.2	27	0.025

Table 4.5: Specifications used to measure islet peptides using the Xevo TQ-XS mass spectrometer when coupled to high flow LC system.

4.2.11 LC-MS data analysis

Raw files from Xevo TQ-XS mass spectrometer were analysed using MassLynx (section 2.6.3)

4.3 Results

4.3.1 Peptide synthesis

16 peptides were synthesised by Elise Bernard at Astrazeneca, UK (table 4.6). 13 of these were the novel peptides described in chapter 3 and 3 were stable isotope labelled versions needed for quantification by mass spectrometry.

Peptide	**Sequence**
ChgA 435-462a	AEDQELESLSAIEAELEKVAHQLQALRR#
Gast p59-79	*QLGPQGPQHFIADLSKKQRPR
Sst-25-36	APSDPRLRQFLQ
Cck p21-44	*QPVVPAEATDPVEQRAQEAPRRQL
Cck 46-63	VLRTDGEPRARLGALLA
ChgA 358-271	WSRMDQLAKELTAE
Ghrl 52-85	ALEGWLHPEDRGQAEETEEELEIRFNAPFDVGIK
Nec1 90-108	LSDDDRVTWAEQQYEKERS
Pcsk1n 42-59	SLSAASAPLVETSTPLRL
Pyy 68-98	DVPAALFSKLLFTDDSDSENLPFRPEGLDQW
Scg1 184-216	TNEIVEEQYTPQSLATLESVFQELGKLTGPSNQ
Scg2 569-610	IPVGSLKNEDTPNRQYLDEDMLLKVLEYLNQEQAEQGREHLA
Tac1 72-95	DADSSVEKQVALLKALYGHGQISH
ChgA 435-462a IS	AEDQELESLSAIEAELEKVAHQL†QAL†RR#
Gast p59-79 IS	*QLGPQGPQHFIADL†SKKQRPR
Sst-25-36 IS	APSDPRLRQFL†Q

Table 4.6: Peptides synthesised by Elise Bernard at Astrazeneca, UK. *† represents ^{13}C and ^{15}N labelled leucine residues. * represents pyroglutamate residues. # represents amidation. IS=Internal standard.*

4.3.2 Peptide activity at Gs or Gi signalling pathways

All novel peptide candidates were applied to various cell lines and intracellular cAMP quantified to assess activity at Gs or Gi signalling pathways. All cell lines used were considered as potentially relevant for maintaining glucose homeostasis (MIN6, αTC1, hepatocytes, STC-1) or possibly involved in regulating food intake (SK-N-MC). Additionally, cell lines used express receptors for known peptide hormones and therefore likely also a variety of potential targets for any novel peptide hormones. Unfortunately, none of the 13 peptides synthesised seemed to induce cAMP accumulation in

hepatocytes, SK-N-MC, STC-1 or αTC1 cells (figure 4.5). Peptides known to activate Gs signalling in each cell line were used as positive control to ensure the assay was working correctly. The ability of the novel peptide candidates to activate Gi signalling was also assessed in each of these cell lines by adding forskolin at the same time as adding the novel peptides. Only the SK-N-MC cell line provided repeatable and trustworthy results when screening for Gi signalling but no novel peptide candidate was seen to show Gi activity (figure 4.6). Supplementary figures 1 and 2 (see appendix 1) show data obtained from MIN6 cells when screening for Gs and Gi activity. The data from the novel peptide candidates are highly variable and difficult to form conclusions from and so this data is displayed in appendix 1.

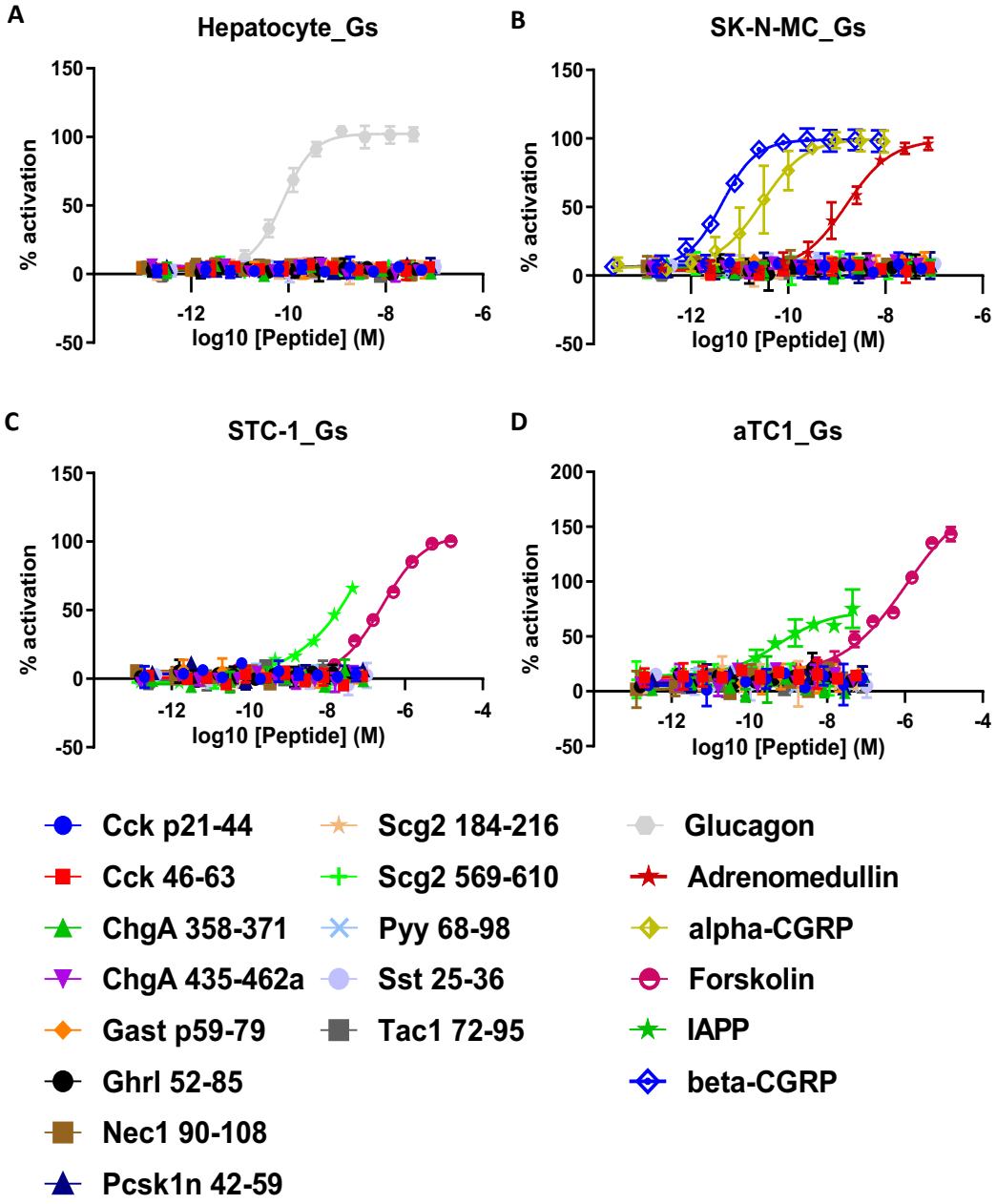

Figure 4.5: cAMP accumulation assays. *Gs signalling in hepatocytes (**A**), SK-N-MC (**B**), STC-1 (**C**) and αTC1 (**D**) cells. Each data point represents n=3-4 with standard deviation.*

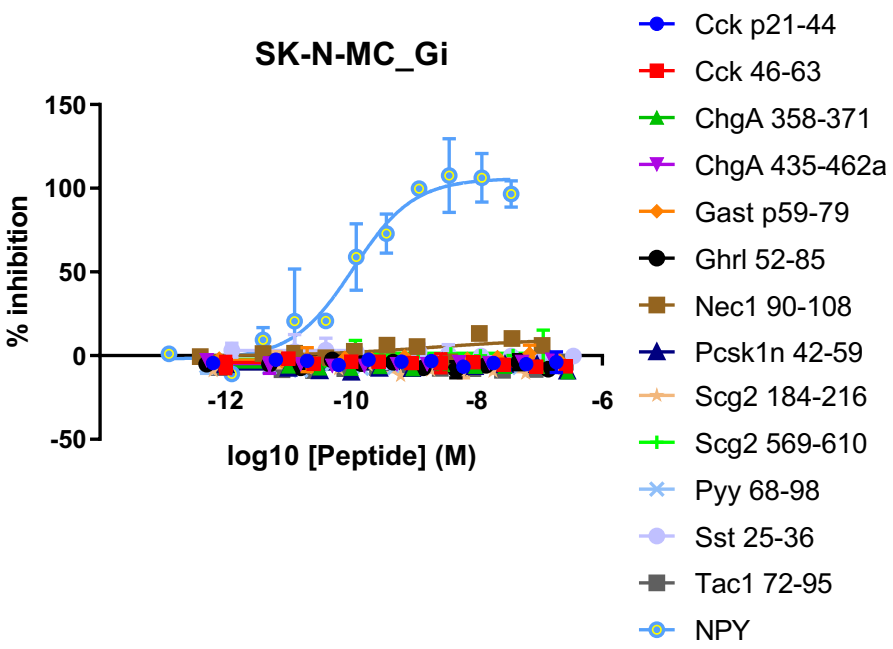

Figure 4.6: Screening for Gi activity in SK-N-MC cell line. *NPY used as positive control.*

4.3.3 Plasma peptide stability

Before characterising the peptides *in vivo*, I wanted to get an idea of how quickly these peptides might be degraded. To do this I spiked each of the priority 1 peptides into mouse plasma and incubated the plasma at 37^{o}C, taking samples at various time points over 24 hours and then quantifying peptide levels by LC-MS (figure 4.7A). ChgA 435-462a seemed to be quite stable in plasma as the levels of this peptide didn't drop below 90% of the 0 min time point until after 180 minutes post-addition. However, Gast p59-79 was degraded much quicker with levels dropping to 9.78% of baseline after 60 minutes. Sst 25-36 appeared to be degraded the quickest with levels dropping to just 0.7% of baseline after 30 minutes.

With 2 of the 3 priority 1 peptides being very quickly degraded in plasma, a method of inactivating enzymes in the plasma was needed. This was crucial for PK studies as degradation of peptides post-sample collection can lead to incorrect calculation of PK parameters. Addition of citrate buffer to plasma could prevent degradation of Gast p59-79 (figure 4.7C) and Sst 25-36 (figure 4.7D) as levels of these peptides were significantly higher 15 minutes after peptide addition to plasma compared to the non-stabilised 'normal' plasma controls ($p<0.0001$ for Sst 25-36, $p<0.0001$ for Gast p59-79). Furthermore, the citrate buffer seemed to improve the recovery of Gast p59-79 and Sst 25-36 as levels of these peptides were significantly higher at 0 minutes in the citrate plasma compared

to the normal plasma (p<0.0001 for Sst 25-36, p=0.001 for Gast p59-79). 0.1 M citrate buffer also seemed to improve the stability of ChgA 435-462a in plasma (figure 4.7B, p=0.001) and improve recovery (p=0.0036). Therefore, when performing the PK studies, citrate buffer was added to the plasma using a 1 in 10 dilution to avoid peptide degradation post-sample collection for all 3 priority 1 peptides.

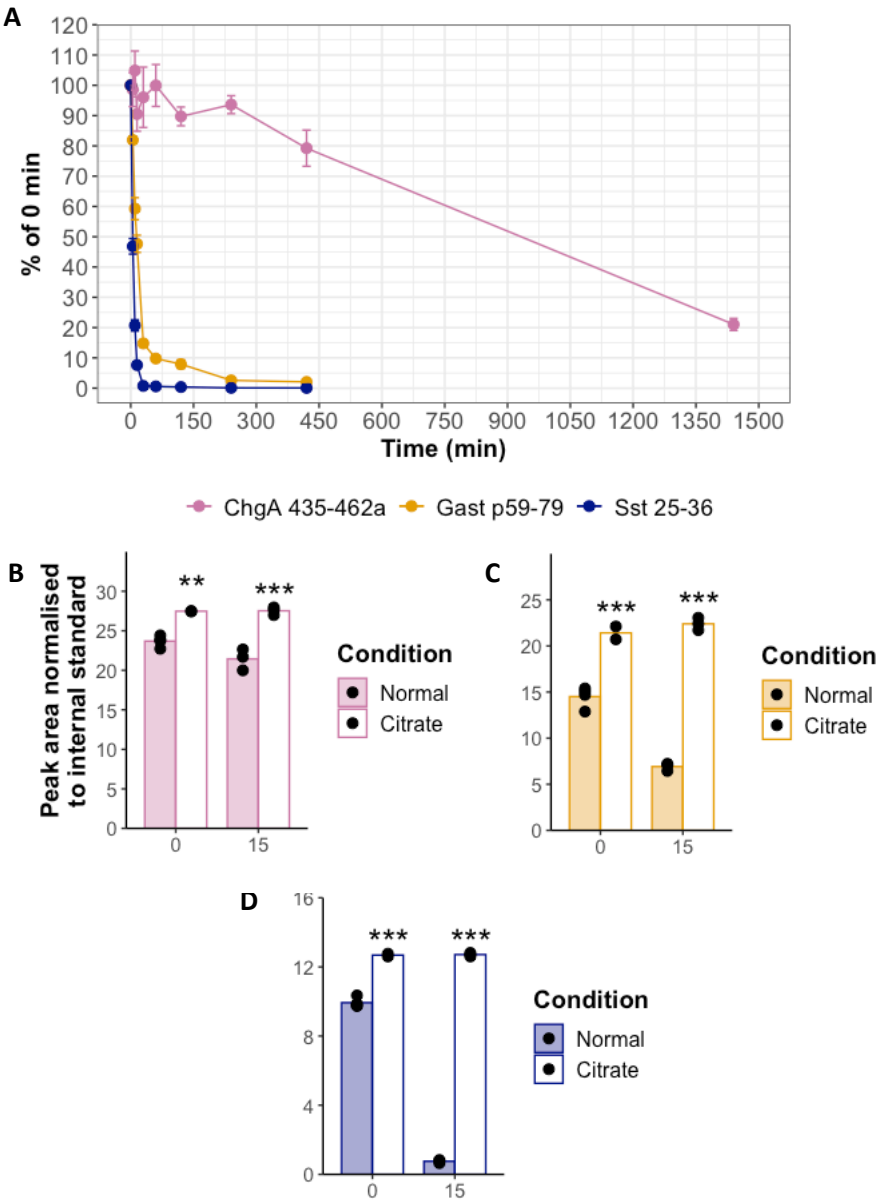

Figure 4.7: Plasma stability of priority 1 peptides. *(**A**) Stability of priority 1 peptides in mouse plasma at 37°C over 24 hours. Data expressed as a peak area normalised to the peptide's corresponding internal standard and expressed as a % of the 0 min time point. Stability of ChgA 435-462a (**B**), Gast p59-79 (**C**) and Sst 25-36 (**D**) in plasma at both 0 and 15 minutes after spiking. Plasma stabilised with 1 in 10 (1 part citrate buffer : 9 parts plasma) vs non-stabilised plasma as a control (Normal). Data represents n=3. Statistical tests carried out 2-way ANOVA with Dunn post-hoc copmarisons. **: p<0.01, ***: p<0.005 vs corresponding time point in non-stabalised 'normal' plasma.*

4.3.4 PK analysis

The PK studies were customised depending on how quickly the peptide was shown to be degraded in plasma (figure 4.7A). For Gast p59-79 and Sst 25-36 - which were degraded rapidly - peptides were only administered s.c. at one very high dose of 10 mg/kg as it was thought any lower doses would result in plasma peptide levels that were too low to detect. Additionally, all blood samples were taken up to 45 minutes post-administration. For ChgA 435-462a two doses for s.c. administration were given to improve the reliability of the bioavailability value calculated and blood samples taken were spread out over a 2 hour period. Data from the PK studies are shown in figure 4.8.

Peptide	Route	Dose (mg/kg)	Bioavailability (%)	AUC (µg*hr/mL)
ChgA 435-462a	i.v.	1	NA	0.362
ChgA 435-462a	s.c.	1	46.7	0.169
ChgA 435-462a	s.c.	3	50.4	0.547
Gast p59-79	i.v.	1	NA	0.503
Gast p59-79	s.c.	10	110	0.558
Sst 25-36	s.c.	10	-	0.0033

Table 4.7: Bioavailability and AUC of the 3 peptides for each dose and route of administration. *i.v.= intravenous, s.c.=subcutaneous*

The bioavailability of ChgA 435-462a was calculated to be between 46.7-50.4% whereas the bioavailability of Gast p59-79 was much higher at over 100% (table 4.7). As this >100% value is impossible it is likely that the error margins in the data account for it. Unfortunately, the bioavailability of Sst 25-36 could not be calculated as no i.v. PK data could be collected for this peptide. Half-lives based on the data from s.c. administration for each peptide are displayed in table 4.8.

Using the PK data for each priority 1 peptide, models were built using SAAM II software to estimate the mass delivery rate required to reach a steady state concentration (Css) of 1 nM. Table 4.8 displays the mass infusion rates estimated as well as the required pump concentrations to achieve these mass infusion rate for a 20 g mouse at a release volume of 6 µL/day. The pump concentration of 412 mg/mL for Sst 25-36 is not feasible so, based on this and the poor PK data for this peptide, I decided to not progress with Sst 25-36. The pump concentrations of the other 2 priority 1 peptides were much more feasible and so I progressed with these two peptides into *in vivo* osmotic pump studies.

	T ½ (min)	Mass infusion rate to reach Css of 1 nM (mg/kg/day)	Pump concentration (mg/mL)
ChgA 435-462a	36.0	0.290	1.00
Gast p59-79	18.1	0.770	2.66
Sst 25-36	7.40	82.3	412

Table 4.8: *Half-lives (T ½) of each peptide estimated from peak plasma concentration during s.c. administration. Mass infusion rates required to reach a Css of 1 nM along with pump concentrations of each peptide required to achieve mass infusion rate for a 20 g mouse infused with 6 μL/day from osmotic pump. Modelling to estimate mass infusion performed by John Hood at Astrazeneca, UK.*

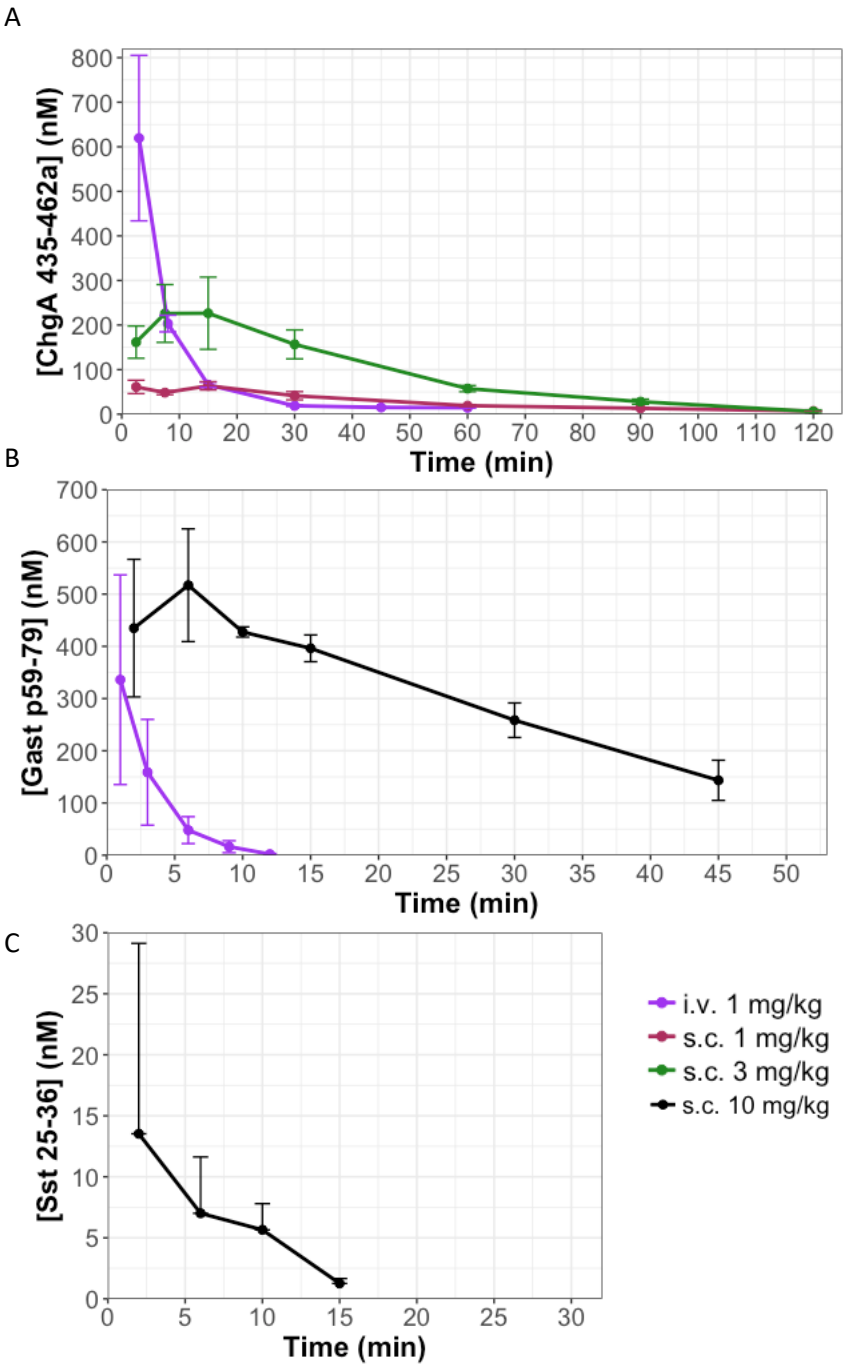

Figure 4.8: PK analysis analysis of priority 1 peptides. *ChgA 435-462a (**A**), Gast p59-79 (**B**) and Sst 25-36 (**C**) at various doses and routes of administration. Each data point is n=3-4 with standard deviation. When Sst 25-36 was administered i.v., the peptide was not detectable at any time point after administration.*

4.3.5 *in vitro* osmotic pump assessment

Peptide stability at 37^{o}C was verified by spiking Gast p59-79 and ChgA 435-462a into multiple aliquots of PBS and placing them in incubator at 37^{o}C. Over 30 days, aliquots were taken out and frozen for LC-MS analysis. Figure 4.9A displays these data and shows that both Gast p59-79 and ChgA 435-462a are stable at 37^{o}C for up to 30 days as peptide levels did not change meaningfully over this time.

Next peptide release from osmotic pumps was verified at the pump concentrations required to achieve the mass infusion rates detailed in table 4.8. The methodology for this experiment is described in section 4.2.7 and results displayed in figures 4.8A-C. Exenatide was selected as a positive control for the *in vivo* osmotic pump study and a mass infusion rate of 0.03 mg/kg/day was selected. This infusion rate has been previously shown to be an effective dose for reducing food intake and improving glucose tolerance [269, 270]. Maximal release of ChgA 435-462a and Gast p59-79 from normal osmotic pumps wasn't achieved until after day 4 but after this time, release seemed to be consistent for the remaining 16 days (figure 4.9B and C). Siliconising pumps prevented loss of these peptides through binding, and levels of peptide released from the siliconized pumps were almost identical to the control samples once max release had been achieved. Adding 0.1% BSA to the peptide vehicle also reduced loss through binding of Gast p59-79 and levels from these pumps containing BSA were similar to control samples. However, 0.1% BSA seemed to interfere with release of ChgA 435-462a as levels of this peptide released from pumps containing BSA were much lower than the control samples. Exenatide did not seem to be very stable at 37^{o}C as almost a 5-fold reduction in peptide levels was seen in the control sample between day 0 and 4. Even though adding 0.1% BSA to the vehicle for exenatide seemed to prevent peptide binding compared to normal pumps, levels of exenatide released from BSA-containing pumps ranged between just 12.5-23.8% of the control samples. Clearly release of exenatide from osmotic pumps was not as efficient as Gast p59-79 or ChgA 435-462a.

In summary, no method of binding prevention worked for all 3 peptides and there were issues with stability of exenatide at 37^{o}C as well as release from the osmotic pumps. Nevertheless, I decided to continue to the *in vivo* osmotic pump study using BSA as the method of preventing binding for exenatide and Gast p59-79 but no method of binding prevention for ChgA 435-462a.

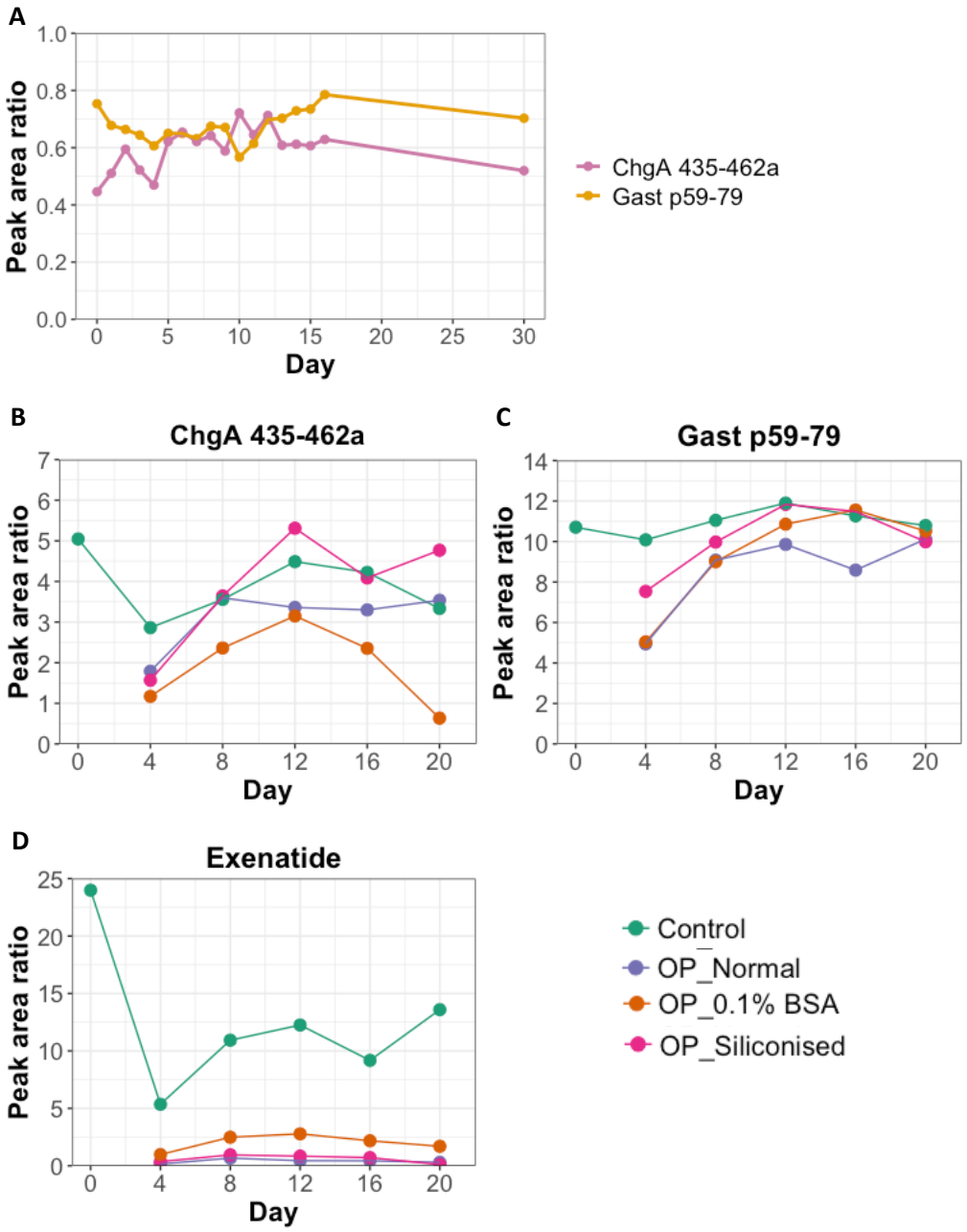

Figure 4.9: *(**A**) Stability of Gast p59-79 and ChgA 435-462a at 37°C in PBS over 30 days. Release from 2004 model Alzet osmotic pumps of ChgA 435-462a (**B**), Gast p59-79 (**C**) and exenatide (**D**) over 20 days. All data are n=1 and expressed as peak area ratio where the peak area of the peptide is normalised to its internal standard.*

4.3.6 *in vivo* osmotic pump study 1

ChgA 435-462a and Gast p59-79 were infused into mice for 28 days using osmotic pumps and body weight, food intake and glucose tolerance of these mice monitored. PBS (vehicle) and exenatide were infused into separate groups of mice as negative and positive controls respectively. Average body weights of each group on certain days are displayed in figure 4.10B. No significant difference was seen between the vehicle treated group and either of the priority 1 peptides on any of the days displayed. ChgA 435-462a and Gast p59-79 also did not affect food intake as no significant difference was seen between either of these peptides and the vehicle treated mice on any week (figure 4.10A). Similarly, no effect of exenatide was seen on food intake or body weight despite its well annotated ability to do so. Although, on day 0 it seems as though the exenatide group were slightly lighter than the vehicle group. At this point, osmotic pumps had not been implanted and so any difference in weight was not as a result of exenatide. Likely by chance, mice that were going to be infused with exenatide did not gain as much weight as the other mice in the study during the pre-surgery week (figure 4.10C). However, once pumps were implanted, the mice infused with exenatide caught up with the mice in the other groups in terms of body weight.

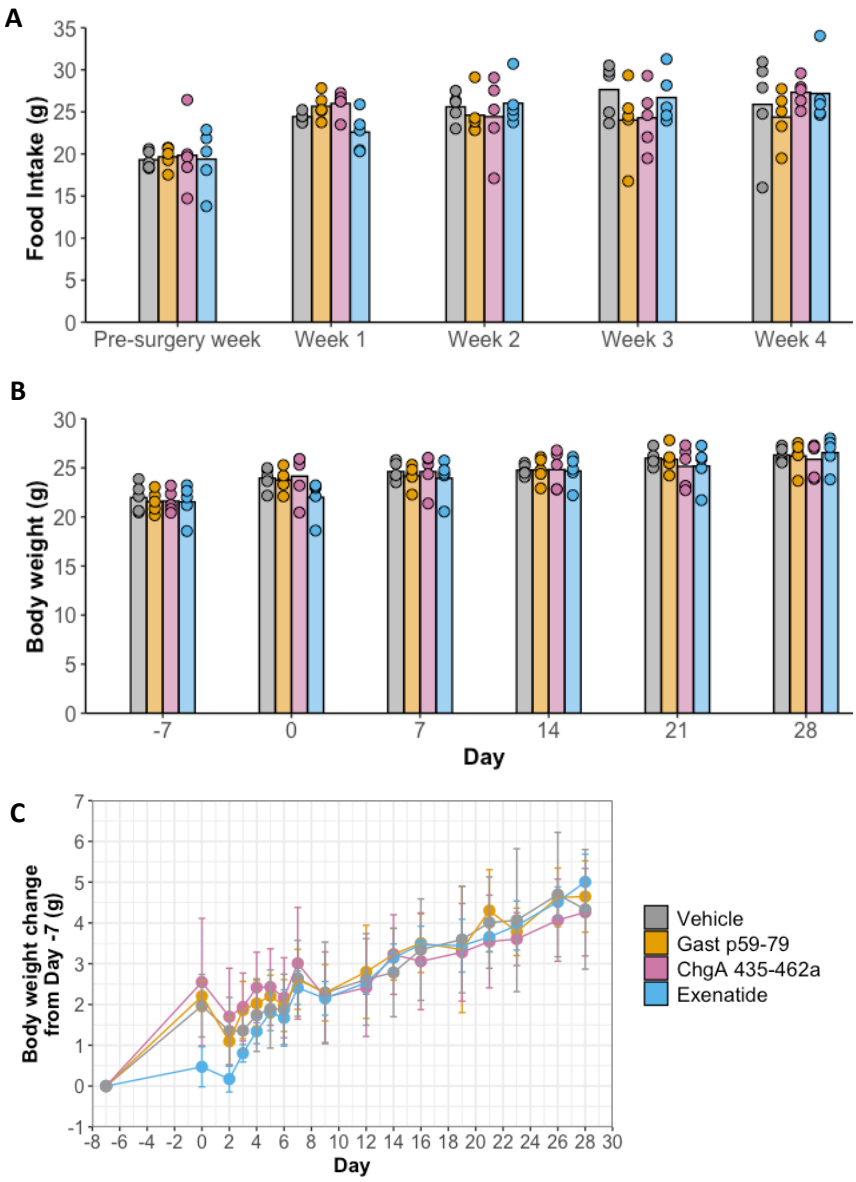

Figure 4.10: Food intake and body weights from osmotic pump study 1. *(**A**) Average weekly food intake. The pre-surgery week constituted 12pm on day -7 to 8am on day 0 before surgery. Week 1 started at 12pm on day 0 after surgery and ended on day 7 before IP GTT 1. Each subsequent week followed the same pattern of starting at 12 pm after a procedure and ending at 8am 1 week later at the beginning of the fasting period for the next procedure. Food intake was measured continuously using BioDAQ food intake cages. (**B**) Average body weights from when mice were singly housed (day -7) to the end of the study (day 28). Data represent n=5 with standard deviation. Statistical analysis was performed using a Kruskal-Wallis test to compare each of the 3 peptide treatment groups with the vehicle on each week (**A**) or day (**B**). (**C**) Average change in body weights for each treatment group from day -7. Data represents point is n=5 for each group with error bars in C represent standard deviation.*

Gast p59-79 seemed to slightly improve glucose tolerance as significant reductions in blood glucose levels were seen at 15 and 30 min during the IP GTT on day 7 and at 30 min during the IP GTT on day 7 (figure 4.11A) and at 30 min on day 28 (figure 4.11G). Although, the AUCs of Gast p59-79 treated mice were not significantly lower than those of the vehicle treated mice in any of the 4 IP GTTs (figure 4.11B, D, F, H). Quantification of plasma insulin levels pre- and post-glucose challenge during the IP GTT on day 14 revealed no significant difference between the Gast p59-79 or the vehicle treated mice at either time point (figure 4.11I). No significant effect of ChgA 435-426a was seen at any time point compared to the vehicle or in the AUC over the 4 IP GTTs (figure 4.11). As expected, exenatide dramatically improved glucose tolerance in all 4 IP GTTs (figure 4.11).

Terminal bleeds were taken after the IP GTT on day 28 to quantify plasma levels of the treatment peptides (table 4.9). Only ChgA 435-462a was detectable in terminal bleeds and levels varied from 0.93-6.58 nM (see figure 4.12 for calibration line). Both Gast p59-79 and exenatide were undetectable in all terminal bleeds from mice infused with those peptides. An analyte with a similar precursor, product ion *m/z* and retention time to Gast p59-79 masked detection of this peptide at levels below 5 ng/mL (figure 4.13). This interfering peptide can be seen in blank plasma (figure 4.13B) as well as plasma from all mice in osmotic pump study 1 including mice that were not infused with

Mouse	Treatment group	[Peptide] (nM)
1	Vehicle	NA
2	ChgA 435-462a	BLLQ
3	Vehicle	NA
4	Gast p59-79	ND
5	Gast p59-79	ND
6	ChgA 435-462a	6.58*
7	ChgA 435-462a	2.95
8	Exenatide	ND
9	ChgA 435-462a	1.79
10	Vehicle	NA
11	Vehicle	NA
12	ChgA 435-462a	0.93
13	Exenatide	ND
14	Exenatide	ND
15	Gast p59-79	ND
16	Exenatide	ND
17	Exenatide	ND
18	Gast p59-79	ND
19	Vehicle	NA
20	Gast p59-79	ND

Table 4.9: Treatment peptide quantification in terminal bleeds from osmotic pump study 1*. ND=None detected. BLLQ=Below lower limit of quantification. * = above upper limit of quantification so calibration line extrapolated to estimate peptide concentration. Upper and lower limits of quantification defined as minimum and maximum concentrations on calibration line (see figure 4.12)*

Gast p59-79 (figure 4.14A and B) and therefore it is likely to be endogenous to mouse plasma. The interfering peptide is unlikely to be endogenous Gast p59-79 in blood as performing a full scan analysis with MS/MS on the Orbitrap mass spectrometer failed to detect Gast p59-79 (figure 4.14E and F).

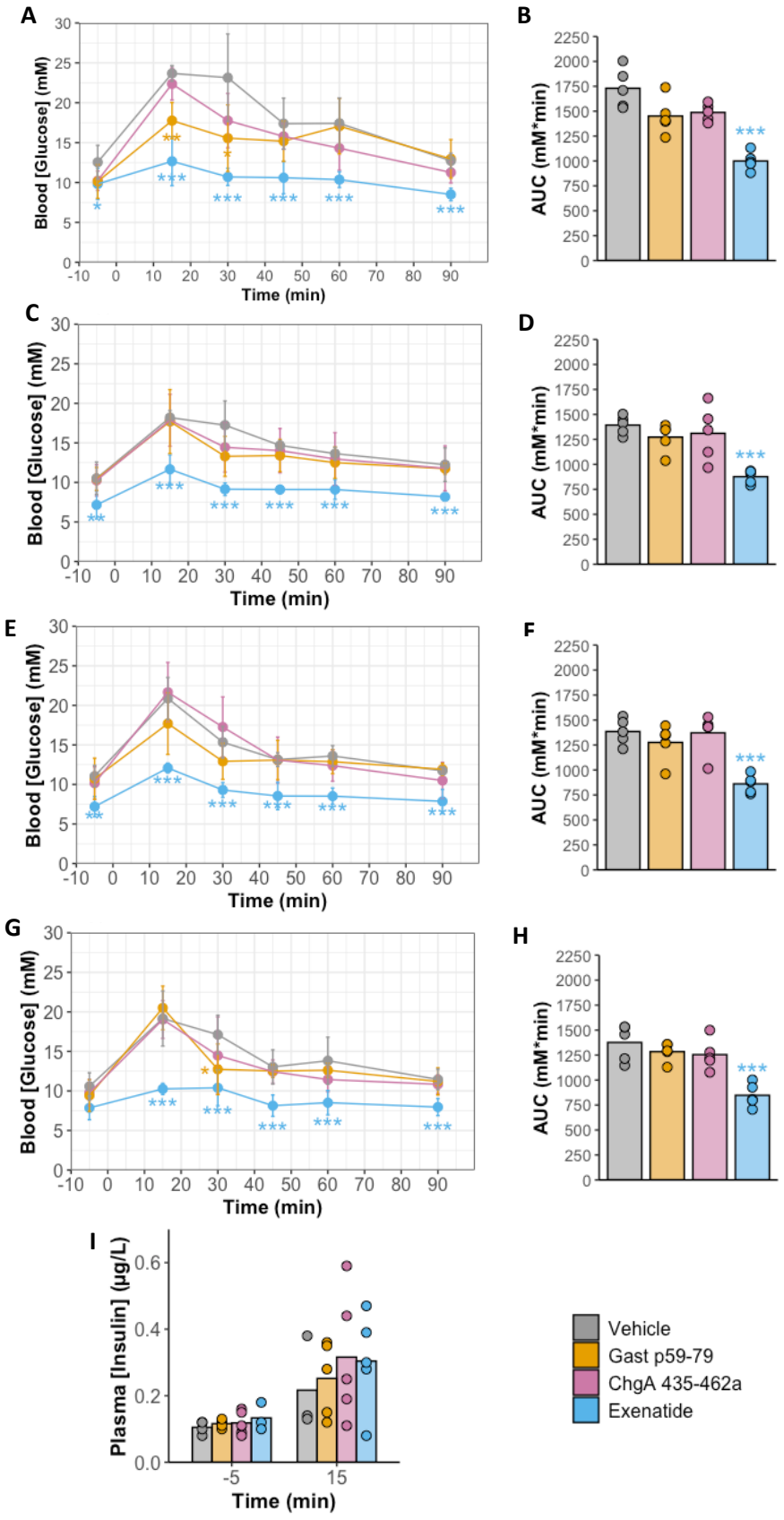
A
Blood [Glucose] (mM)
Time (min)
B
AUC (mM*min)
C
Blood [Glucose] (mM)
Time (min)
D
AUC (mM*min)
E
Blood [Glucose] (mM)
Time (min)
F
AUC (mM*min)
G
Blood [Glucose] (mM)
Time (min)
H
AUC (mM*min)
I
Plasma [Insulin] (µg/L)
Time (min)
Vehicle
Gast p59-79
ChgA 435-462a
Exenatide

Figure 4.11: IP GTTs from osmotic pump study 1*. Glucose excursions from week 1 (**A**), week 2 (**C**), week 3 (**E**) and week 4 (**G**) after 2 g/kg IP glucose challenge along with corresponding AUC for each week (**B**, **D**, **F**, **H**). (**I**) Plasma insulin quantification at 5 min pre- and 15 min post- 2g/kg IP glucose challenge on day 14. Data represents n=5 for each group with error bars showing standard deviation. Data analysed with a Kruskal-Wallis test with post-hoc Dunn comparisons. *: p<0.05, **: p<0.01, ***:p<0.005. Plasma insulin quantification performed by Core Biochemical Assay Laboratory (Cambridge Biomedical campus, Cambridge UK).*

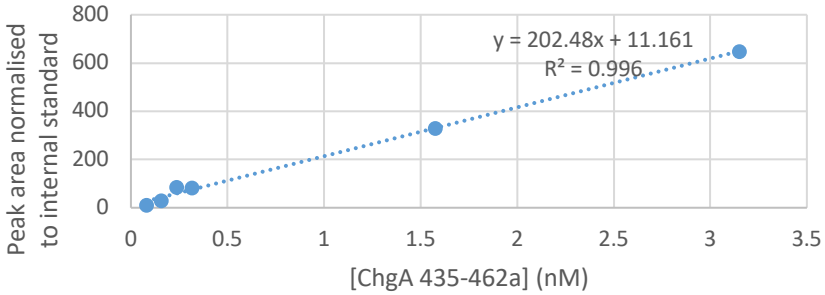

Figure 4.12: Calibration line for ChgA 435-462a to quantify the peptide in terminal bleeds from osmotic pump study 1.

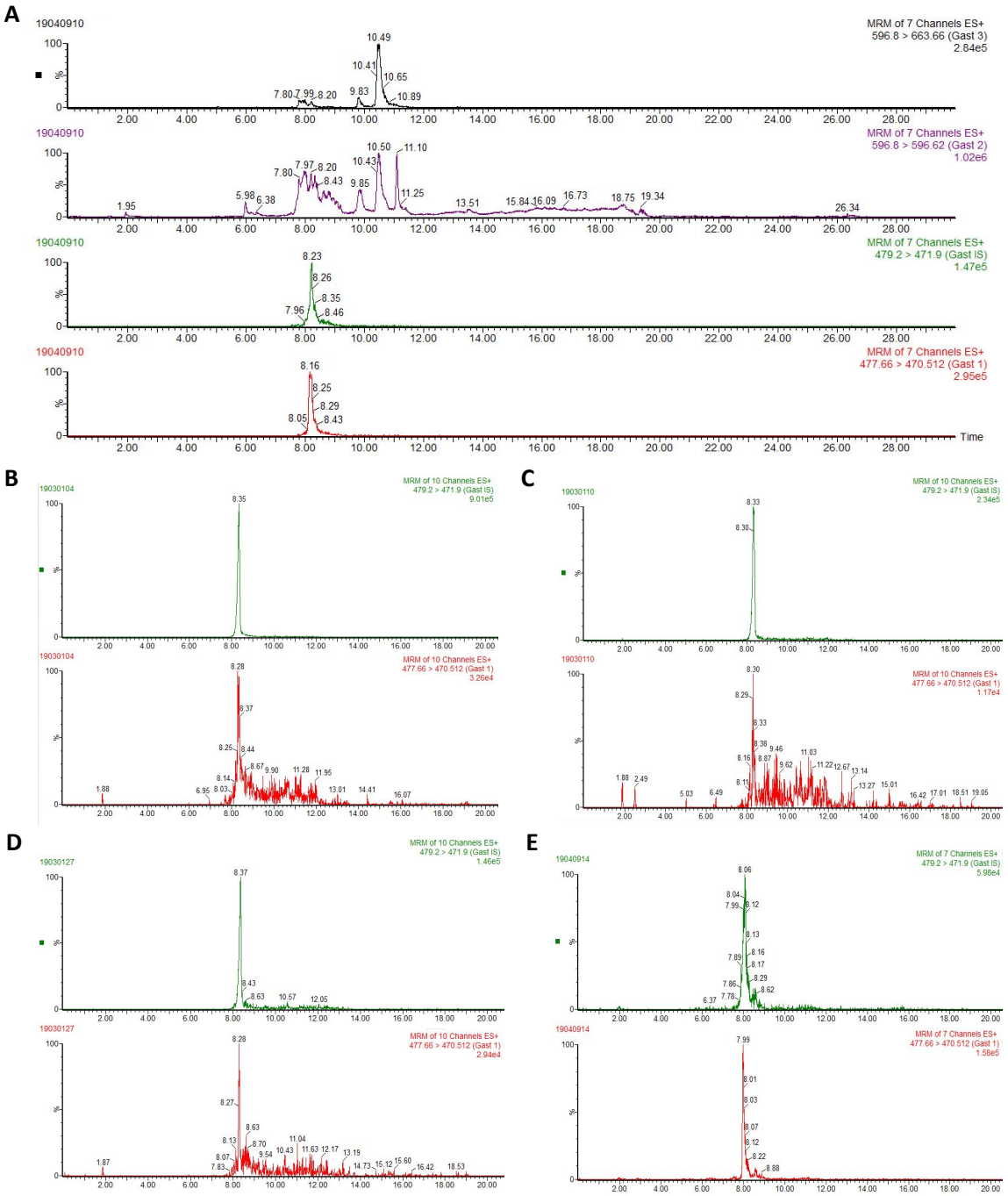

Figure 4.13: Chromatograms monitoring for product ions of Gast p59-79 and Gast p59-79 internal standard (IS) in terminal bleeds from osmotic pump study 1. *(**A**) 50 ng/mL Gast p59-79 spiked into blank plasma, monitoring for 3 different product ions of Gast p59-79 (black, purple and red traces) and Gast p59-79 IS (green trace). (**B**) Blank plasma with no Gast p59-79 spiked, (**C**) plasma spiked with 5 ng/mL Gast p59-79, (**D**) plasma from mouse #15 (infused with Gast p59-79) in osmotic pump study 1, (**E**) plasma from mouse #2 in osmotic pump study 2 (not infused with Gast p59-79). (**B-E**) Green trace is Gast p59-79 IS and red trace is Gast p59-79. Gast p59-79 can be seen at 50 ng/mL in plasma but the presence of an interfering peptide endogenous to plasma, prevents detection at levels ≤5 ng/mL and in the plasma of mice infused with Gast p59-79 during osmotic pump studies 1 and 2.*

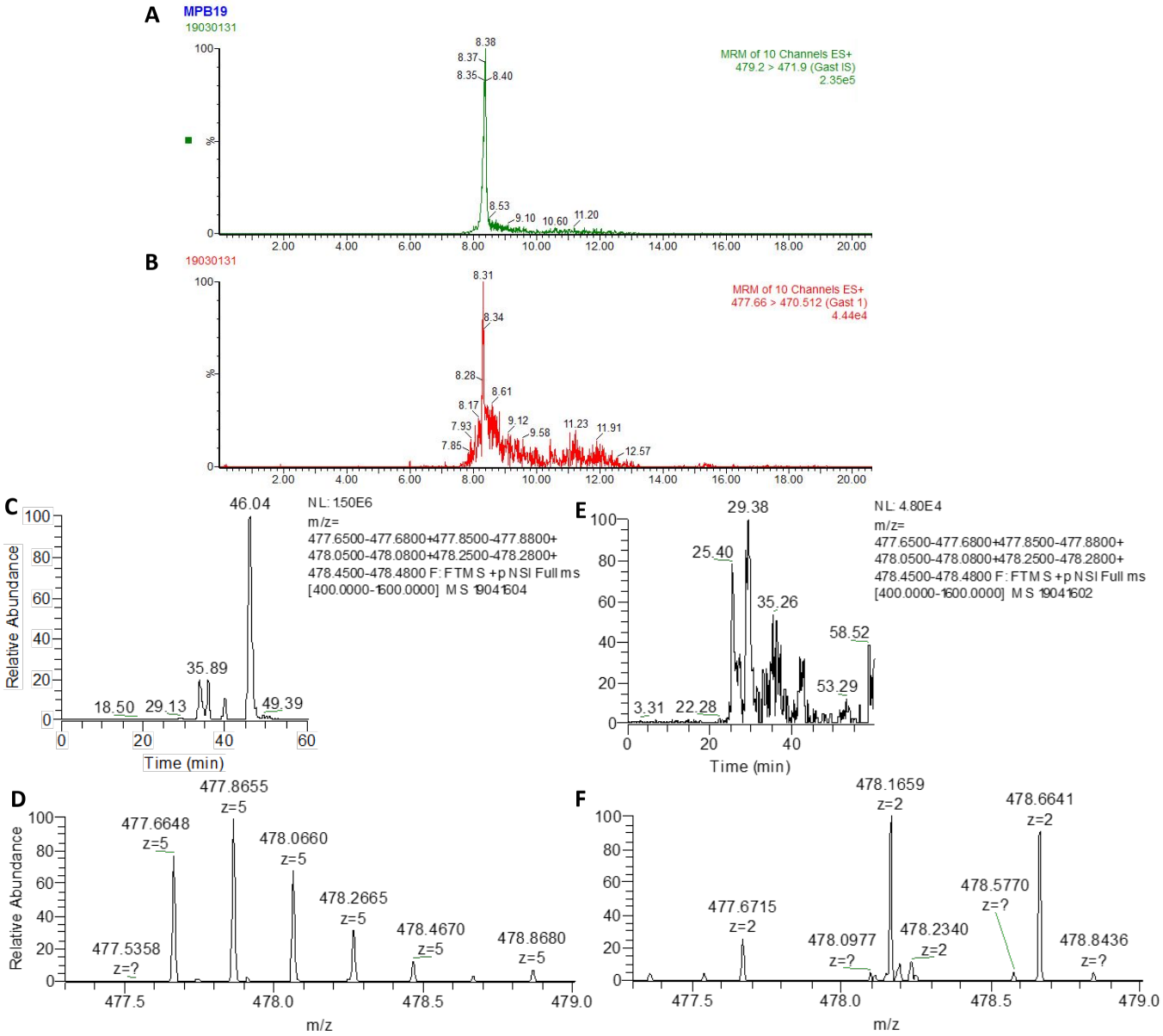
A
MPB19
19030131
MRM of 10 Channels ES+
479.2 > 471.9 (Gast IS)
2.35e5
B
19030131
MRM of 10 Channels ES+
477.66 > 470.512 (Gast 1)
4.44e4
C
NL: 150E6
m/z=
477.6500-477.6800+477.8500-477.8800+
478.0500-478.0800+478.2500-478.2800+
478.4500-478.4800 F: FTMS +p NSI Full ms
[400.0000-1600.0000] MS 19041604
Relative Abundance
Time (min)
E
NL: 4.80E4
m/z=
477.6500-477.6800+477.8500-477.8800+
478.0500-478.0800+478.2500-478.2800+
478.4500-478.4800 F: FTMS +p NSI Full ms
[400.0000-1600.0000] MS 19041602
Time (min)
D
Relative Abundance
m/z
F
m/z

Figure 4.14: Searching for identity of interfering peptide. *(**A** and **B**) Data from terminal bleed sample of mouse #19 from osmotic pump study 1 analysed on the Xevo TQ MS. X axis displays time (min) and y axis displays relative abundance. Mouse # 19 was infused with vehicle during osmotic pump stud 1. Chromatograms from monitoring for product ions of (**A**) Gast p59-79 IS and (**B**) Gast p59-79. Gast p59-79 IS elutes at 8.38 min in (**A**) however an analyte with a similar precursor and product m/z and retention time is generating a signal at 8.31 min in (**B**). Seeing as mouse #19 was not infused with Gast p59-79 this interfering analyte could be endogenous Gast p59-79 or some other analyte endogenous to plasma. To identify this interfering analyte, plasma samples were analysed on an Orbitrap MS and data shown in (**C**-**F**). (**C** and **D**) Data from plasma sample spiked with Gast p59-79. In (**C**) a peak at 46.04 min can be seen on the extracted ion chromatogram and which corresponds to Gast p59-79. The product ion spectrum in (**D**) displays the expected 13C distribution pattern for Gast p59-79 in the $[M+5H]^{5+}$ state. (**E** and **F**) Data from terminal bleed sample of mouse #19. Some signal can be seen at 46.04 min on the extracted ion chromatogram (**E**). An analyte with a m/z of 477.6715 can be seen in the product ion spectrum of (**F**). As this analyte has a similar m/z to Gast p59-79 in the $[M+5H]^{5+}$ state it is likely to be the interfering analyte seen in (**B**).*

4.3.7 Priority 1 peptide effect on islet secretions

Gast p59-79 exhibited a small but significant effect on glucose tolerance during 2 of the 4 IP GTTs in osmotic pump study 1. Gast p59-79, along with the other priority 1 peptides, were applied to isolated mouse islets and insulin, glucagon and SST-14 were quantified in supernatants. This was to assess if any of the priority 1 peptide candidates directly modulated islet hormone secretion. No significant effect was seen on glucagon, insulin-1 or SST-14 secretion from islets at 1 or 16.7 mM glucose of any of the 3 priority 1 peptide candidates (figure 4.15). Therefore, it is unlikely that the potential glucose normalising effects of Gast p59-79 are mediated through direct modulation of islet hormone secretion.

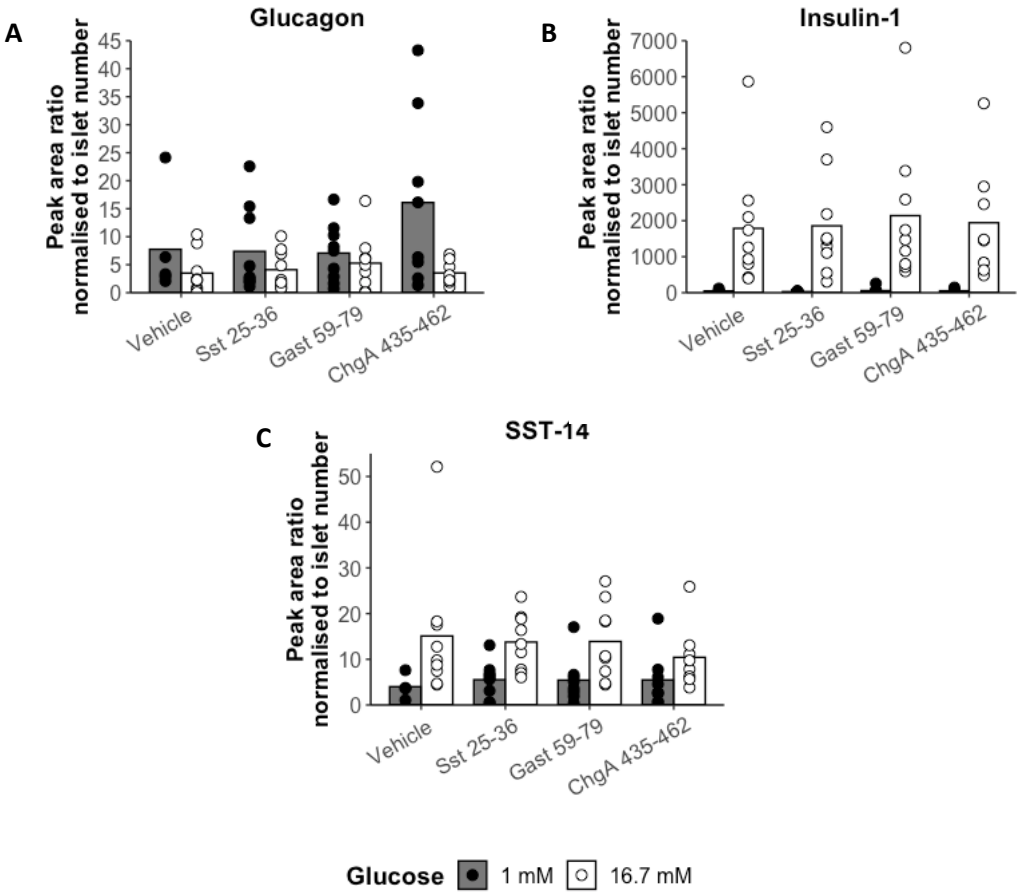

Figure 4.15: Priority 1 peptides have no direct effect on secretion of insulin, glucagon or SST-14 from mouse islets. *Effect of 100 nM priority 1 peptides on secretion of glucagon (**A**), insulin-1 (**B**) and SST-14 (**C**) from primary mouse islets at two concentrations of glucose (1 mM, 16.7 mM). Individual data points are overlain on group means with n=9 in each condition. Statistical comaprisons were made using a Kruskal-Wallis test to compare the 3 peptide treatment groups vs the vehicle at both concentrations of glucose.*

4.3.8 *in vivo* osmotic pump study 2

A follow up *in vivo* osmotic pump study was performed to try and replicate the glucose normalising effect of Gast p59-79 seen in osmotic pump study 1. A study was set up in which 16 mice were randomised into 2 groups of 8 mice according to fasting blood glucose (figure 4.16C). One group received Gast p59-79 and the other vehicle. A week after implanting the osmotic pumps, an IP GTT was performed and terminal bleeds taken to assess Gast p59-79 levels in plasma. Figure 4.16 summarises the results of this 2nd osmotic pump study. An effect of Gast p59-79 on glucose tolerance similar to that found in study 1 was seen during the IP GTT as blood glucose levels were significantly lower at 30 minutes post-challenge compared to vehicle (figure 4.16A). Additionally, the peak in glucose levels seemed to be lower in the Gast p59-79 treated mice but not significantly. The AUC was not significantly lower than vehicle treated mice (figure 4.16B). In line with osmotic pump study 1, Gast p59-79 did not affect body weight (figure 4.16C). No statistical comparison was made between baseline and post-surgery fasting blood glucose as mice were naïve to handling when baseline measurements were taken.

When quantifying Gast p59-79 in terminal bleeds, the same issue arose as with osmotic pump study 1. An analyte similar to Gast p59-79 masked detection of this peptide and so the concentration of Gast p59-79 in the plasma is unknown (figure 4.13).

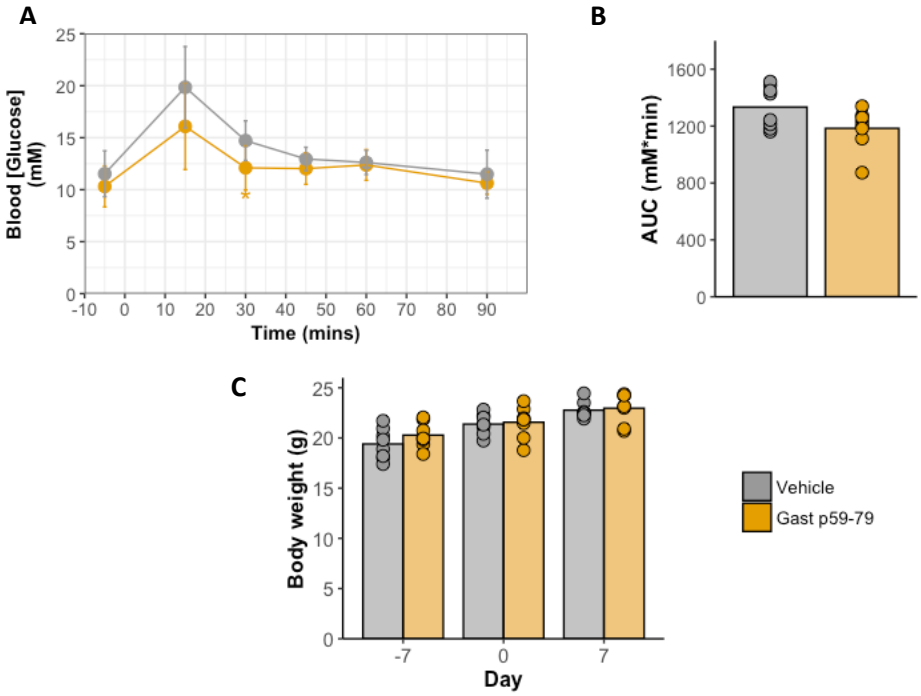

Figure 4.16: Data from osmotic pump study 2. *GTT 7 days after surgery with 2 g/kg IP glucose challenge (**A**) and corresponding AUC (**B**). (**C**) Body weights at the start of study (day -7), the day of surgery (day 0) and the day of the IP GTT (day 7). Data represent n=8 per group with error bars showing standard deviation. Statistical analysis was performed using a Mann-Whitney U test. *p<0.05.*

4.3.9 *in vivo* osmotic pump study 3

A 3rd osmotic pump study was performed to investigate the effect of Gast p59-79 on insulin tolerance, oral glucose tolerance as well as insulin signalling in various tissue types. As the effect on IP glucose tolerance seen in osmotic pump studies 1 and 2 was quite small, DIO mice were used in the hope that a larger effect on glucose tolerance may be seen in this obese and potentially diabetic mouse model. Also, it was hoped that the therapeutic potential of Gast p59-79 could be assessed by using DIO mice. 16 mice were fattened for a period of 16 weeks and an IP GTT was performed on the mice 3 days prior to surgery to randomise the mice into 1 of 2 groups of matched AUC during this IP GTT (figure 4.17B).

Although no effect of Gast p59-79 was seen on body weight (figure 4.17A), all mice lost an average of 3 g in the week after surgery and mice #5 and #12 lost 5.36 and 7.66 g respectively. These 2 mice were culled 4 days after surgery due to excess weight loss and worsening of the wound over where the osmotic pump was implanted. The remaining mice did regain the lost weight throughout the rest of the study. This ubiquitous weight loss in the week after surgery was not seen in either of the prior 2 osmotic pump studies (figure 4.10B and figure 4.16B).

7 days after pump implantation an IP GTT was performed but no effect of Gast p59-79 was observed. There was no significant difference at any time point in blood glucose levels between the two treatment groups (figure 4.17C) and the AUC were similar (figure 4.17D). The mice did seem to be glucose intolerant and perhaps diabetic as the peak in blood glucose levels didn't occur until 30 minutes post-challenge whereas in the previous two osmotic pump studies the peak in blood glucose occurred at 15 minutes (figures 4.10 and 4.16A). During the OGTT on day 14, Gast p59-79 seemed to worsen glucose tolerance, however no significant difference was seen between the two treatment groups in the AUC (figure 4.17F) or in blood glucose levels at any time point (figure 4.17E). An unexpected effect of Gast p59-79 was seen in the ITT. The blood glucose levels of the two treatment groups diverged 45 minutes post-insulin challenge after being similar for the first 30 minutes of the ITT (figure 4.17G). A significant difference between treatment groups was seen in blood glucose levels 90 and 120 minutes post-insulin challenge and in the AUC (figure 4.17H).

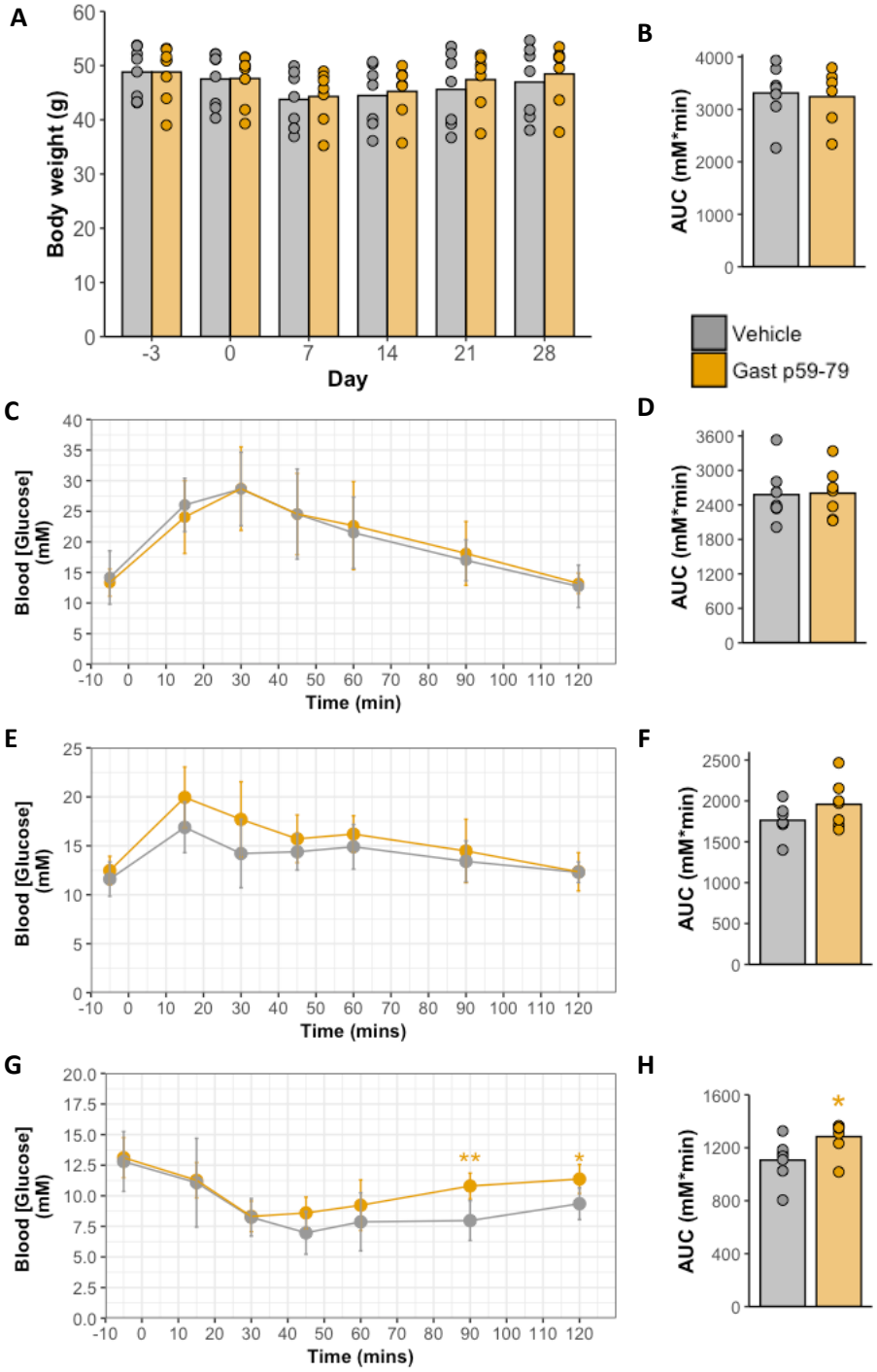

Figure 4.17: Data from osmotic pump study 3. *(**A**) Body weights on procedure days from day of baseline measurements (day -3) to the end of the study (day 28). (**B**) Baseline AUC during IP GTT performed on day -3 to randomise mice into treatment groups. Glucose excursions during an IP GTT 1 week after surgery (**C**), OGTT 2 weeks after surgery (**E**) and ITT 3 weeks after surgery (**G**) along with corresponding AUCs for each procedure (**D**, **F**, **H**). All GTTs performed with 2 g/kg glucose challenge and ITT performed with 0.75 U/kg insulin challenge. Data represents n=7/group with standard deviation. Statistical analysis was performed using a Mann-Whitney U test versus the vehicle treated group for each time point (**C**, **E**, **G**) or day (**A**). *p<0.05, **p<0.01.*

28 days after surgery, mice received an IP injection of humulin and were culled 15 minutes later to collect liver, skeletal muscle and white adipose tissue (WAT) for quantification of phosphorylated-AKT (pAKT) and total-AKT. AKT (also known as protein kinase B) is phosphorylated downstream of insulin receptor activation and comparison of total-AKT to pAKT in tissue or cells is used as a measure of insulin signalling [286]. The greater the proportion of pAKT : total-AKT, the stronger the insulin signalling. No significant difference in the percentage of pAKT was seen between the treatment groups in any of the tissue types tested (figure 4.18A). However, there is a great deal of variability in the data with mice #1, 2, 14 and 15 exhibiting greater percentages of pAKT than the other mice. These mice were the lightest mice of the cohort (figure 4.18D) and so this leaner phenotype could be responsible for their apparent increased insulin signalling.

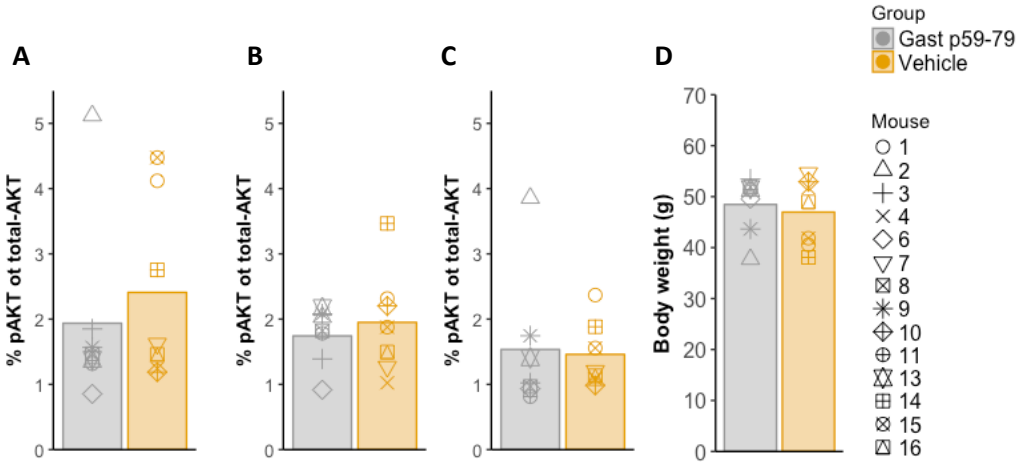

Figure 4.18: Gast p59-79 did not affect pAKT levels in various tissue types. Phosphorylated-AKT (pAKT) expressed as a percentage of total AKT in liver (**A**), skeletal muscle (**B**) and white adipose tissue (WAT) (**C**) 15 minutes after a 0.75 U/kg insulin challenge. (**D**) Individual body weights of mice overlaid on group averages on day of culling for pAKT quantification (day 28). Statistical analysis was performed using a linear regression analysis testing the effect of both treatment group and weight on % pAKT.

4.3.10 ChgA 435-462a and islet peptide content

ChgA 435-462a is almost identical to serpinin which has been shown to be crucial for granule stability through enhancing expression of PN-1 in a pituitary cell line [210]. I hypothesised that ChgA 435-462a may play a similar role in islets as data from Thomsen et al. suggested that amidated ChgA may increase insulin secretion from a β cell line [275]. I incubated islets with increasing concentrations of ChgA 435-462a for 24 hours after which I assessed levels of SST-14, insulin-1 and glucagon in the lysates by LC-MS. Unfortunately, ChgA 435-462a did not seem to affect the islet content of insulin-1, SST-14 or glucagon at any of the concentrations tested (figure 4.19).

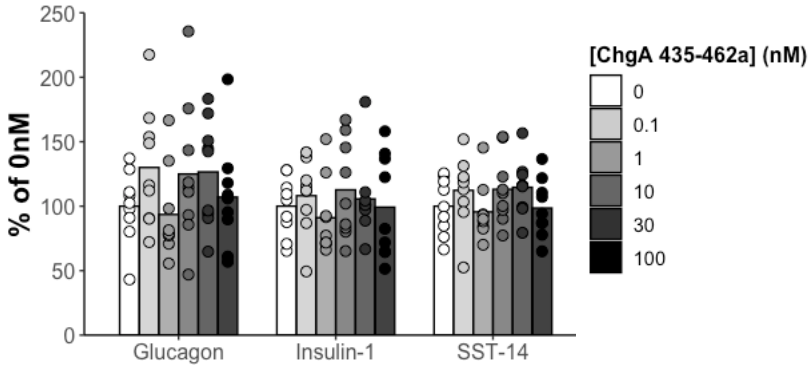

Figure 4.19: Islet content of glucagon, insulin-1 and SST-14 after culturing for 24 hrs in varying concentrations of ChgA 435-426a expressed as a percentage of the control (0 nM of ChgA 435-462a). *Each bar represents n=9 with each sample consisting of 7-8 lysed islets. Statistical analysis carried out using a Kruskal Wallis test to compare islet peptide content at 0.1, 1, 10, 30 and 100 nM ChgA 435-462a to the 0nM condition.*

4.4 Discussion

4.4.1 cAMP accumulation screens

None of the novel peptide candidates activated Gs signalling in hepatocytes, MIN6, αTC1, STC-1 or SK-N-MC cells nor did they activate Gi signalling in SK-N-MC cells. Peptides were screened against MIN6 cells for Gi signalling but results were highly variable and inconclusive. Whilst screening peptides against individual cell lines using a plate-based assay and quantifying intracellular cAMP accumulation was relatively high-throughput, it was flawed as it does not definitively show peptide activity in that cell type. Activity at alternative signalling pathways such as Gq or β-arrestin would not have been detected by these screens. Additionally, antagonist activity would have been missed using the methodology employed for the cAMP screens as peptides were not applied to cells in the presence of a positive control peptide. A more thorough method of screening for activity in various cell types would be to apply peptides and measure a functional response. For example, secretion of hormones from endocrine cells, glucose uptake by hepatocytes or electrical activity of neuronal cells. These functional responses would give an indication of whether a peptide has activity at that cell type regardless of the intracellular mechanism. Unfortunately, these functional studies in different cells require bespoke assays to measure the specific response of that cell type and can be extremely low-throughput. Therefore, using a commercially available kit to quantify cAMP accumulation in various cell types seemed to strike the best balance between throughput and broadness of approach. Activity at 2 common signalling pathways could be assessed whilst maintaining a relatively high-throughput due to the plate-based nature of the assay and little optimisation was needed between cell types. Although it should be mentioned despite using a variety of cell lines, the peptides would not have been exposed to every possible receptor and therefore I can't rule out the possibility that these peptides may target other receptors not expressed by any of the cell lines used.

4.4.2 Priority 1 peptide stability and pharmacokinetics

To aid in the design of PK studies for each priority 1 peptide, their stability in plasma was assessed by spiking the peptides into mouse plasma and quantifying the peptides at various time points over 24 hours. Sst 25-36 and Gast p59-79 were degraded very quickly with ChgA 435-462a showing greater stability. The rapid degradation of Sst 25-36 could be mediated by DPP-IV as the peptide possesses a DPP-IV cleavage site (Ala-Pro) at its N-terminus, although, this is only a theory and I don't have data to back this claim up. PK samples were analysed on the triple quadrupole mass spectrometer and no methods were set up to monitor for metabolites of the peptides. Other peptide substrates of DPP-IV include GLP-1 and GIP, both of which have rapid half-lives [287, 288]. The reason for the rapid

degradation of Gast p59-79 is less clear as the peptide possesses a pyroglutamate residue. The cyclic shape of this residue should help shield the N-terminus from degradation [289]. ChgA 435-462a is amidated on the C-terminus and the resistance to degradation could be aided by this modification [290]. Acidification of plasma with a citrate buffer helped to prevent the degradation of Gast p59-79, Sst 25-35 and ChgA 435-462a whilst also improving their recovery. Addition of citrate buffer would be useful during PK studies therefore to prevent degradation post-blood collection of all three priority 1 peptides.

PK studies were performed to assess the elimination of the peptides from mice. The half-lives calculated were estimated based on the s.c. data and ranged from 7.6-36.0 min with Sst 25-36 being cleared the quickest, followed by Gast p59-79 and then ChgA 435-462a. As a comparison, the half-life for exenatide is estimated to be 144 min [291] so the priority 1 peptides have rapid half-lives, a characteristic to be expected of unmodified, endogenous peptides. This PK data somewhat matched the findings from my *in vitro* test of peptide stability in plasma as in this experiment Sst 25-36 was degraded the fastest followed by Gast p59-79 and then ChgA 435-462a. Using these data, PK models of each peptide were built and the mass infusion rates required to reach a Css of 1 nM were estimated. Levels of gut hormones such as GLP-1, PYY, GIP and PYY in plasma tend to not exceed 0.1 nM [252] even during a GTT and therefore achieving a Css of 1 nM should ensure mice would be exposed to a supraphysiological concentration of the peptide. Chronically exposing mice to supraphysiological levels of these peptides could induce adverse effects or receptor desensitisation. However, it was thought these drawbacks would be worth the risk in order to ensure high exposure of the animals to the peptides. In a study performed by Zhang et al., 5 novel peptides were acutely administered s.c. into mice to monitor food intake and glucose tolerance but no effect of any peptides was found [236]. PK studies were not performed and therefore without information such as bioavailability, clearance and half-life, the authors can't rule out that a lack of efficacy seen wasn't due to poor exposure of the peptides to the mice.

4.4.3 *In vivo* osmotic pump studies

After validating the release of the Gast p59-79 and ChgA 435-462a from osmotic pumps, *in vivo* efficacy studies were performed where mice were chronically infused with one of these two novel peptides. Osmotic pumps were chosen as the method of delivery for the peptides over daily bolus injection as these pumps would ensure consistent exposure of the animal to the peptides. Additionally, use of these pumps would minimise animal handling and therefore stress to the animals. Stress could be a confounding factor when assessing food intake and so reducing stress ensured more reliable data. There is an option to attach a catheter to the osmotic pump and the catheter used to

directly infuse the peptide to a specific region. Peptides can be infused centrally by this method. I opted to administer peptides peripherally, because if the novel peptides were administered centrally, potential peripheral targets may not be exposed to the peptide.

4.4.3.1 *In vivo* effects of Gast p59-79 on glucose and insulin tolerance

Gast p59-79 seemed to improve glucose tolerance in lean mice as demonstrated in osmotic pump studies 1 and 2. Blood glucose levels 30 min post-glucose challenge were consistently and significantly lowered compared to vehicle treated mice. Peak blood glucose levels were only significantly lowered during the first week of osmotic pump study 1 but fasting blood glucose was not significantly altered in any of the IP GTTs across the 2 studies. With these data in mind, and the finding that Gast p59-79 failed to significantly affect islet hormone secretion *in vitro*, I postulated that Gast p59-79 may be altering insulin sensitivity to increase glucose uptake from the circulation. I ruled out the possibility that Gast p59-79 could be acting in a similar manner to gastrin and its effects on β cells [280-285] as the sequence of Gast p59-79 doesn't contain pentagastrin (the amino acids responsible for activity at CCK receptors [277]). CCK receptors are thought to mediate the effects of gastrin on β cells [279] and therefore may be attributed to the control of gastrin in glycemia.

A third osmotic pump study was performed to confirm this in which DIO mice were used in the hope of enhancing the effect size on insulin sensitisation due to the insulin insensitive nature of DIO mice. However, no effect on insulin sensitivity was seen, as levels of a marker of insulin signalling, pAKT, were similar between the two treatment groups in WAT, liver and skeletal muscle 15 minutes after an insulin challenge. Additionally, Gast p59-79 seemed not to affect glucose tolerance in DIO mice suggesting the mechanism through which Gast p59-79 acts is compromised in an obese phenotype. Therefore, the mechanism by which Gast p59-79 may be affecting glucose tolerance in lean mice is not understood although it is unlikely to be through directly affecting islet hormone secretion.

Gast p59-79 exhibited an unusual effect during the ITT as after 30 minutes, blood glucose levels returned to baseline faster than the vehicle treated controls. Alterations in insulin sensitivity between treatment groups would likely manifest as an immediate difference in blood glucose levels post-insulin challenge as this is when levels of plasma insulin are highest as well as insulin signalling [286]. Therefore, a difference in insulin sensitivity between treatment groups is unlikely to be the mechanism at work in the ITT. A study in which a similar effect on insulin tolerance was seen was when α cell secretions and therefore glucagon secretion were impaired upon activation of a Gi-DREADD (designer receptors exclusively activated by designer drugs) receptor expressed in α cells [292]. This

Gi-DREADD receptor was exclusively activated by clozapine N-oxide (CNO), an agent that is otherwise physiologically inert [293-295]. For 30 minutes after co-administration of insulin and CNO to mice expressing Gi-DREAD or wild type control, blood glucose levels were similar. Not until 45 minutes post-challenge did the blood glucose levels of the two groups diverge with blood glucose levels of Gi-DREADD mice continuing to drop but blood glucose levels of wild type mice levelled off. Enhancing glucagon secretion during hypoglycaemia may explain the difference seen between treatment groups in the ITT. However, any effect would likely be indirect as glucagon secretion at 1 mM glucose was not significantly different between Gast p59-79 or vehicle treated islets.

It should be noted that there was an issue with the body weights of mice in osmotic pump study 3. Mice were fattened on a HFD for 16 weeks before osmotic pumps were implanted and dramatic weight loss occurred in all groups over the next week. It is not clear why mice in osmotic pump study 3 exhibited this unexpected weight loss whereas mice in osmotic pump studies 1 and 2 did not. This weight loss may have resulted in the mice changing from an obese/diabetic phenotype towards a leaner/less severe diabetic phenotype. Evidence for this comes from comparing the IP GTT performed on day -3 and the IP GTT on day 7. The AUC is higher for both groups on day -3 (figure 4.17B) than on day 7 (figure 4.17D). Additionally, blood glucose doesn't decrease from peak levels until after 90 minutes post-glucose challenge on day -3 whereas blood glucose drops after 30 minutes post-glucose challenge on day 7 (figure 4.20). From day 7, mice seemed to regain weight but at different rates. This led to a situation on day 28 where there was a high degree of variability between different mice in the study and also potentially variability in the phenotype (figure 4.18D). At day 28, mice #1, 2, 14 and 15 were lighter than the other mice in the cohort and may exhibit better glucose tolerance than the others. Evidence for this divergence in phenotype comes from the quantification of pAKT on day 28 post-insulin challenge. In the liver, mice #1, 2 and 15, and mouse #14 in skeletal muscle, showed considerably higher levels of pAKT than heavier mice that were around 50 g in body weight (figure 4.21). Due to the confounding effect of changing phenotype throughout the 3rd osmotic pump study, the findings should be treated with caution with further studies required to confirm them.

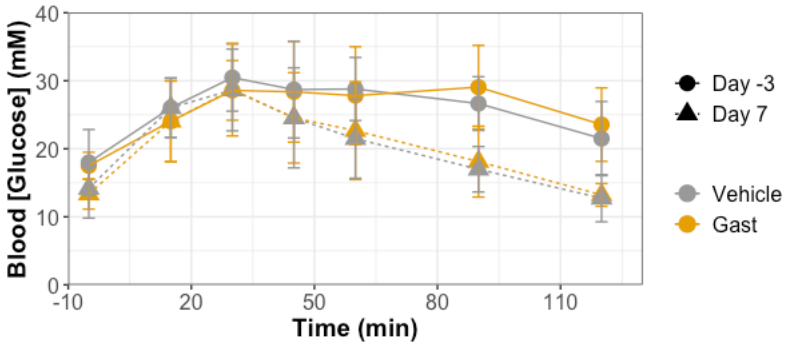

Figure 4.20: Comparison of IP GTT data from 3rd osmotic pump study. *Solid lines with circles represent data from day -3. Dotted lines with triangles represent data from day 7. Each data point is n=7 with standard deviation.*

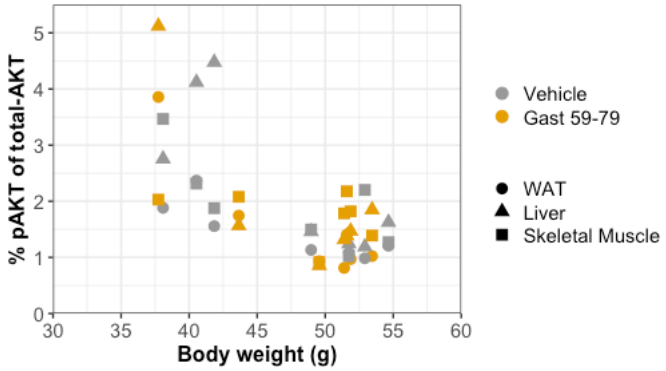

Figure 4.21: Weights of mice versus % pAKT of total AKT in WAT, liver and skeletal muscle on day 28 of study. *% pAKT assessed at 15 minutes after a 0.75 U/kg insulin challenge.*

4.4.3.2 Food intake and body weight

Neither Gast p59-79 nor ChgA 435-462a appeared to affect food intake or body weight throughout the first osmotic pump study and surprisingly neither did exenatide. Exenatide did however induce a strong effect on glucose tolerance and so there did not seem to be an issue with malfunctioning pumps failing to infuse exenatide. It seems that levels of exenatide in the blood were high enough to affect glucose tolerance but not food intake or body weight. This discrepancy in the potency of exenatide to induce different therapeutic effects is backed up by Young et al. [296]. The authors showed that the half-maximal effective dose (ED_{50}) of exenatide to control hyperglycaemia in obese rodents was lower than the ED_{50} for reducing food intake or body weight. An insufficient mass infusion rate or losses of exenatide due to heat instability and binding to the osmotic pump (figure 4.9D) may have prevented exenatide from achieving sufficient levels in the blood to affect food intake. The mass infusion rate used in osmotic pump study 1 was selected based on previous studies. In these studies, 30 µg/kg/day of exenatide induced food intake reductions in DIO rats [269, 297] as well as glucose tolerance improvements in lean mice [270]. No measures were employed in these studies to prevent losses through binding so I assumed these losses would not impact the efficacy of exenatide in my study. Although 30 µg/kg/day was shown to be effective in reducing food intake in DIO rats, perhaps a higher mass infusion rate was needed for lean mice.

4.4.4 Sst 25-36 and neuronostatin

Neuronostatin is a prosomatostatin-derived peptide shown to reduce food intake and improve glucose tolerance in rodents [234, 238] but was not detected in any of the peptidomics data presented in chapter 3. I hypothesised that Sst 25-36 - which overlaps with 6 amino acids on the N-terminus of neuronostatin and is found in EECs - may represent an endogenous version of neuronostatin. Unfortunately, Sst 25-36 was not chronically infused to mice due to unreliable PK data so comparisons cannot be made between the two peptides in their *in vivo* efficacy. However, some comparison can be made on their *in vitro* efficacy as both peptides have been applied to isolated rodent islets. Sst 25-36 was found not to affect glucagon, SST-14 or insulin secretion at 100 nM (figure 4.15). The same concentration of neuronostatin was found to inhibit GSIS in whole islets but not in the β cell line INS1 823/3 [238]. The authors concluded that the inhibitory effect of neuronostatin on GSIS was due to direct effects of neuronostatin on α cells as 1000 nM neuronostatin could stimulate glucagon secretion at 25 mM glucose in whole islets and αTC1 cells. This seems contradictory as an increase in glucagon secretion would likely enhance GSIS through activation of GLP-1 receptors rather than supress GSIS [298]. In any case, based on the lack of efficacy of Sst 25-36 on isolated islets, it is unlikely that Sst 25-36 represents the endogenous version of neuronostatin. In hindsight perhaps I should have

selected a longer peptide from prosomatostatin encompassing the whole sequence of neuronostatin such as Sst 25-51. The sequence necessary for the activity of neuronostatin may be at the C-terminus of the peptide and therefore Sst 25-36 would not possess this active region.

4.4.5 ChgA 435-462a and serpinin

Serpinin is a peptide derived from the C-terminus of ChgA reported to act as a positive inotrope in rat Langendorff heart preparations [211] as well as enhancing granule biogenesis in a pituitary cell line [210]. I postulated that ChgA 435-462a, an amidated and C-terminally extended form of Serpinin, may perform a similar role in islets due to findings by Thomsen et al. showing that knock out of *CHGA* in a human β cell line with siRNA reduced insulin secretion [275]. Thomsen et al. go on to say that amidation of ChgA is crucial as deficiencies in peptidylglycine alpha-amidating monooxygenase (PAM, an enzyme responsible for amidating peptides and proteins) activity reduces insulin content and secretion. Although, it is worth nothing that the authors don't explicitly prove that it is a failure to amidate ChgA which causes the impairment of insulin content in *PAM* deficient β cells. In my peptidomic analysis of mouse islets in chapter 3, 4 amidated peptides derived from ChgA were found, of which ChgA 435-462a was the most prevalent (figure 4.22).

Seeing as the activity of serpinin appears to be reliant on increasing expression of PN-1 [210] and I have already tested if acute incubation of ChgA 435-462a alters secretion of insulin-1, SST-14 or glucagon (figure 4.15), I decided to test if chronic incubation of islets with ChgA 435-462a would alter the content of any of the major islet hormones. Chronic incubation may allow alterations at the transcript level to be translated into visible changes at the peptidomic level hence why acute incubation of ChgA 435-462a with islets may not have shown any effect. Unfortunately, it appears that culturing ChgA 435-462a with islets for 24hrs induced no changes in the islet content of SST-14, insulin-1 or glucagon. It is possible that ChgA 435-462a does not act on a cell surface target but on some intracellular target and so by applying this peptide to islets externally (in the culture media) ChgA 435-462a is not exposed to its target. However, Koshimizu et al. also applied serpinin to the culture media of pituitary cell lines for 24 hrs and observed an increase in PN-1 expression [210]. The authors postulate that serpinin acts at a cell surface receptor which induces a rise in intracellular cAMP and thereby increasing PN-1 expression. If ChgA 435-462a were acting via the same mechanism in β cells, an effect should have been seen. It is more likely that intact amidated ChgA or some other amidated product are responsible for the effects seen in the publication by Thomsen et al.

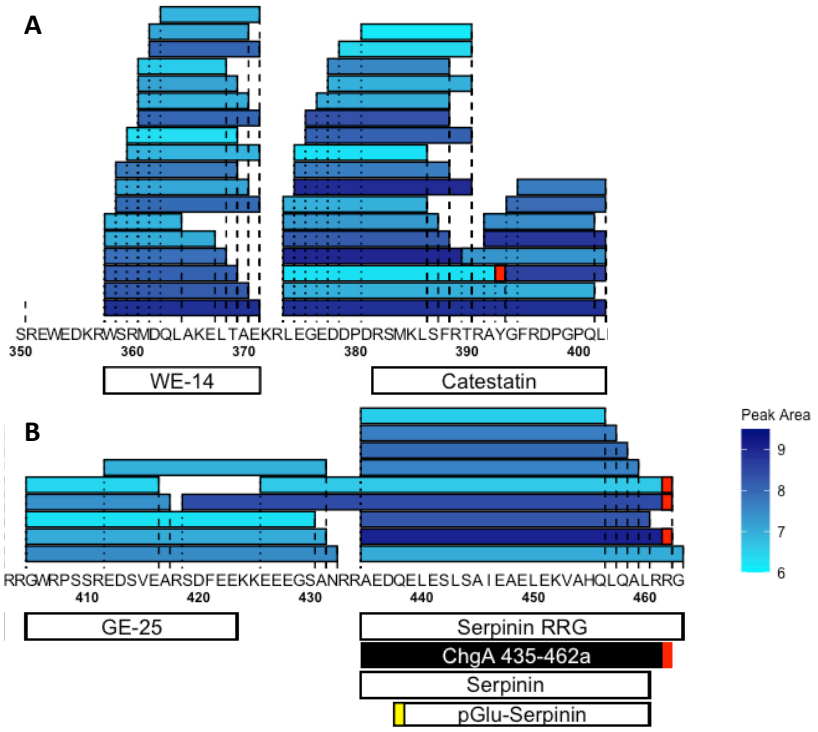

Figure 4.22: Overview of peptides from N-terminus of ChgA proteins in lysed mouse islets. *Peptides derived from positions 358-402 (**A**) and 403-463 (**B**). Shading in blue is a measure of the peptide's peak area (log scale). Red boxes represent amidated residues. For peptidomic coverage of the whole prepropeptide see chapter 3, figure 3.12. However, only 3 other peptides were detected from the rest of the prepropeptide in mouse islets.*

4.4.6 Conclusions

Gast p59-79 may represent a biologically active peptide derived from progastrin as it was shown to improve glucose tolerance when chronically infused to lean mice. A potential effect was seen in DIO mice during an insulin tolerance test, in that blood glucose levels of the Gast p59-79 treated group started to normalise faster than the vehicle controls. The mechanism by which Gast p59-79 may be acting is not understood but seems not to be due to a direct effect on islet secretions or through increased insulin signalling in liver, skeletal muscle or WAT. Further studies are needed to confirm if these effects seen during an ITT can be replicated in mice without confounding effects of weight change. Additionally, plasma glucagon levels during an ITT could be measured to see if Gast p59-79 is indirectly enhancing glucagon secretion to induce these glucose normalising effects seen in the ITT.

Chapter 5: Characterisation of the islet peptidome

5.1 Introduction

Islets of Langerhans are clusters of endocrine cells residing in the pancreas, producing and secreting multiple biologically active peptide hormones. 5 cell populations reside in islets each defined by the peptide hormones they produce. β (insulin and islet amyloid polypeptide (IAPP)), α (glucagon) and δ (somatostatin-14 (SST-14)) are the most studied cell types and constitute the majority of the islet mass [299]. Pancreatic polypeptide (PPY) hormone-producing γ cells and ghrelin-producing ε cells make up the remainder of the islet although the prevalence of the latter cell type in adult islets is markedly reduced in comparison to developing islets [300]. Expression of the intestinal hormone Peptide YY (PYY) has been detected in α, δ and γ cells of mouse islets but not human islets [125, 126].

5.1.1 Intra-islet GLP1 R agonists

There has been much debate over the expression and production of the incretin hormones glucose-dependent insulinotropic polypeptide (GIP) and glucagon-like peptide-1 (GLP-1) in islets. Antibody-dependent methods have found GIP in islets and that this peptide overlaps with glucagon immunoreactivity, indicating α cells are a source of GIP [164, 301]. However, the specificity of these antibodies has been questioned claiming the antibodies also react with proglucagon products such as glicentin and glucagon [302-304]. Furthermore, transcriptomic studies of islets have failed to find expression of *Gip* in human or mouse islets [125, 126, 305] which further adds to the confusion over GIP production in islets.

The evidence for production of active GLP-1 (GLP-1 (7-36 amide) or GLP-1 (7-37)) in islets is more convincing than the evidence for GIP production. Antibody-dependent methods including immunostaining of pancreatic sections or quantification in islet supernatants and homogenised pancreas suggests GLP-1 is produced in α cells [163, 306-310]. Again, these data are not conclusive due the possibility that antibodies targeting active GLP-1 (7-36 amide) may also recognise the inactive longer versions GLP-1 (1-36 amide) and GLP-1 (1-37). In addition, studies by Galsgaard et al. and Svendson et al. used antibody-dependent methods to quantify active GLP-1 in islet supernatants but

were unable to detect the active peptides. In any case, Campbell et al. suggest that inactive or active GLP-1 is produced by a subset of α cells in human islets and that only this subset of GLP-1 producing α cells expresses prohormone convertase 1/3, the enzyme responsible for cleavage of GLP-1 from proglucagon [311]. Functional data provide a more convincing argument for active GLP-1 production in islets. Multiple studies conclude that antagonising the GLP-1 receptor (GLP1 R) attenuates glucose-stimulated insulin secretion (GSIS) [298, 308, 310]. Svendsen et al. take this further to suggest an α cell product is responsible for acting on the GLP1 R, as diphtheria toxin-induced α cell ablation resulted in a similar reduction in GSIS to that seen with GLP1 R antagonism. This functional evidence does not rule out the possibility that glucagon may be acting on the GLP1 R instead and therefore is not direct evidence of intra-islet active GLP-1 production. Glucagon is secreted in abundance from α cells and is an agonist at the GLP1 R albeit with a much lower potency than active GLP-1 [312]. LC-MS-based studies on islets confirmed the presence of active GLP-1 in human islets [163, 166]. However, Marchetti et al. used trypsin to digest human islet extracts meaning the fragments of active GLP-1 (7-36 amide) detected could originate from digestion of longer GLP-1 versions post-tissue collection [163]. Taylor et al. identified active GLP-1 using robust and comprehensive extraction techniques to analyse the peptidomics of islet supernatants but did not quantify any peptides and so the abundance of active forms of GLP-1 is not clear in this study. A direct comparison of active GLP-1 and glucagon would be extremely useful when identifying the predominant α cell product responsible for enhancing GSIS.

5.1.2 Islet peptidome and metabolic disease

The islets can sense and respond to the metabolic state of the body through secretion of specific hormones to help restore homeostasis. When under metabolic stress induced by a chronic caloric excess, the islet cell population adapts to meet the increasing demand for insulin to control glycemia. A caloric excess can lead to obesity and a pre-diabetic state. In obesity, the islets of both humans and mice are known to increase in size due to an expansion of β cell mass [313-316]. Seeing as islet cells are not replenished by a pool of stem cells [317] the source of these additional β cells are believed to be proliferating, mature and fully functional β cells as indicated by lineage tracing experiments [318, 319]. The insulin content of the pancreas therefore increases and so does the insulin output in response to metabolic challenge. In contrast to β cells, the α cell population is not thought to be altered much by an obese/pre-diabetic state. A transcriptomic analysis of FACS purified α and β cells from lean and diet induced obese (DIO) mice found that only 11 genes were differentially expressed in α cells between the two groups [320]. Of these 11, 6 were non-α cell genes such as *Iapp* and *Sst*

and 3 genes have no specific role assigned to them. This was in contrast to the 3192 genes found to be differentially expressed in β cells. Not much is known about the impact of obesity on the other islet cell types.

Once the metabolic demands of the body are no longer being met by the insulin output of the islets, type 2 diabetes (T2D) can ensue [321, 322]. The strain on the endoplasmic reticulum induced by the ever-increasing demand for insulin causes misprocessing of proinsulin and proIAPP leading to a build-up of extracellular amyloid plaques of IAPP although, much like with Alzheimer's disease, it is controversial as to whether these plaques are an indicator of diabetes or a driver [321]. Eventually much of the β cell mass of the islet is lost and hyperglycaemia ensues [323-325]. Growing evidence is emerging that β cells from diabetic mice and humans do not undergo apoptosis but dedifferentiate instead, reverting to a progenitor-like state [326-328]. These dedifferentiated β cells express endocrine progenitor markers such as Neurogenin3 but lose expression of genes key to the function of mature β cells such as *INS*, *FOXO1* and *NKX6.1* [327, 329]. In contrast, the α cell population expands and so too does the glucagon content of the pancreas resulting in hyperglucagonemia, an indicator that an individual has progressed from an obese/prediabetic state to type 2 diabetes (T2D). The source of these additional α cells in T2D is not clear although it could be that loss of β cell transcription factors such as *Nkx6.1* has a knock-on effect on other islet cell types [330]. Some evidence suggests that the source of new α cells is the dedifferentiated β cells as expression of prohormone convertase 1/3 (PC1/3, also known as Nec1) - which is abundant in β cells - is abundant in α cells of T2D individuals [163, 310]. This could also contribute to the increase in GLP-1 seen in T2D as GLP-1 is a PC1/3 cleavage product from proglucagon [163, 306, 310, 311]. However, no study has yet confirmed that the production of GLP-1 (7-36 amide) increases relative to glucagon. This would be a telling sign that dedifferentiated β cells, which retain expression of PC1/3 and PC2 and then start to produce proglucagon, should produce GLP-1 (7-36 amide) and glucagon at fairly similar levels. Furthermore, Wang et al. provide direct evidence against the hypothesis that dedifferentiated β cells assume an α cell phenotype using lineage tracing [328].

5.1.3 LC-MS based studies of the islet peptidome

Given the power of LC-MS to analyse peptidomics and proteomics, LC-MS-based studies of the islet peptidome could be useful to clarify the debate over intra-islet GIP production, compare active GLP-1 levels to glucagon and study how the islet peptidome is altered by metabolic stress. Unfortunately, there have been relatively few studies analysing the islet peptidome, with many of them falling short with room for much improvement in the methodology [166, 226, 331, 332]. Some of these studies

have flaws in the processing of samples prior to LC-MS analysis such as digesting islet supernatants with trypsin [332]. Other studies lack use of specialist software to identify peptides from MS/MS spectra and therefore greatly reduce their ability analyse the whole islet peptidome [226]. Finally, some studies fall short by only analysing islet supernatants and so peptides may not be being analysed in their secreted form as degradation may be occurring in the supernatant during the secretion experiment [261]. Therefore, it seems as though there is gap in the literature in regard to islet peptidomics and a thorough LC-MS-based investigation could help fill this void.

5.1.4 Aims

1. To analyse the peptidome of human and mouse islets.
2. Perform targeted LC-MS analysis searching specifically for intra-islet GLP1 R agonists.
3. Compare the peptidome of islets from diet-induced obese mice to controls.
4. Compare the peptidome of islets from type 2 diabetic humans with non-diabetic controls.

5.2 Methods

5.2.1 Islet lysate peptidomics

Islets were isolated as in section 2.4. After isolating, islets were immediately washed in HBSS with no BSA and 5.5 mM glucose before transferring into a protein LoBind tube (Ependorff) with 250 µL 6M guanidine hydrochloride (GuHCl). Lysates underwent three freeze-thaw cycles to aid cell lysis before a protein crash (see section 2.5.1).

5.2.2 Islet secretion peptidomics

Islets were isolated as in section 2.4. Islets were rested for 1 hour by incubating at 37^{o}C in KRB with 0.1% BSA and 5.5 mM glucose to recover after the isolation process. 15 islets were then transferred to 2 mL protein LoBind Eppendorf tubes for 45 min at 37^{o}C with 300 µL of KRB (section 2.2.1) + 0.001% BSA + one of the following:

1. 1 mM glucose
2. 1 mM glucose + 5 µM adrenaline
3. 6 mM glucose
4. 16.7 mM glucose

At the end of the incubation, 270 µL of supernatant was removed and snap frozen and 9 supernatants from the same condition were pooled together. Care was taken not to remove any islets when removing the supernatant.

5.2.3 Assessing the role of the GLP1 R in GSIS

To assess the role of the GLP1 R in GSIS, an islet secretion experiment was performed where the GLP1 R was antagonised. This islet secretion experiment was carried out as in 5.2.2 except 8-10 islets were used / sample, supernatants were not pooled together and the following conditions were used:

1. 1 mM glucose
2. 16.7 mM glucose
3. 16.7 mM glucose + 300 nM Glp1R0017
4. 16.7 mM glucose + 300 nM NIP228
5. 16.7 mM glucose + 30 nM GLP-1
6. 16.7 mM glucose + 30 nM GLP-1 + 300 nM Glp1R0017

Glp1R0017 is a competitive antagonistic antibody targeting the GLP1 R and was developed by Biggs et al. and synthesised at AstraZeneca [333]. NIP228 is an isotype control antibody.

5.2.4 Peptidomics of sorted β, α and δ cells

5.2.4.1 Mice

To purify the β and α cell populations from islets, *Glu-Venus* mice were used [334]. These mice express GFP under the control of the *Gcg* promoter. To purify δ cells *Sst-Cre/Rosa26*^{EYFP} (referred to as *Sst-Cre)* mice were used [335]. In these *Sst-Cre* mice, Cre recombinase, under the control of the *Sst* promoter, is used to trigger expression of EYFP in *Sst* expressing cells.

5.2.4.2 Single cell digestion

After isolation, islets were transferred to a round bottom polystyrene FACS tube with 1 mL Ca^{2+} free HBSS media with 5.5 mM glucose. Islets were digested to single cells by addition of 0.1 × Trypsin/EDTA in Ca^{2+} free HBSS and incubation at 37^{o}C for 1 minute. The digested islets were then triturated 100 times using a P1000 pipette to aid breakdown of islets into single cells. 100 µL of FBS was then added to inactivate the trypsin.

5.2.4.3 FACS

β, α and δ cell populations were purified by FACS at the flow cytometry group at the Cambridge Institute for Medical Research. Cellular debris and doublets were gated out before selected the cell populations to sort. When sorting cells from *Glu-Venus* mice, α cells were identified as the Venus positive cells and β cells were identified as Venus-negative with high forward scatter and high side scatter. When sorting cells from *Sst-Cre* mice, δ cells were identified as EYFP positive cells. Cells were sorted directly into 200 μL 6M GuHCl and freeze-thawed 3 times before protein crash (see section 2.5.1).

5.2.5 DIO islet peptidomics study

5.2.5.1 Mice

16 male mice were split into 2 groups. One group was fed a high fat diet (HFD) (60% fat, Research Diets) for 13 weeks whilst the other was fed a standard chow diet. At time of death all mice were aged between 22-29 weeks.

5.2.5.2 Tissue collection and islet isolation

After fasting for 6 hours, blood glucose was measured from the tail vein using an AlphaTrak glucosometer. All mice were weighed and culled by rising CO_2. Islets were isolated as in section 2.4.

5.2.5.3 Islet lysis

Immediately after islet isolation, 60 islets from each mouse were washed in HBSS + 5.5 mM glucose (no BSA) and pipetted into 200 μL of 6M GuHCl solution. Three freeze thaw cycles were carried out to aid cell lysis before a protein crash (see section 2.5.1).

5.2.6 T2D vs healthy human islet comparison

Ethical approval was obtained from University of Cambridge Human Biology Research Ethics Committee (application number HBREC.2019.38). De-identified, snap frozen human islets from non-diabetic and T2D donors were obtained from the Alberta Diabetes Institute IsletCore, University of Alberta. Details of the donors are provided in table 5.1. 2000 islet equivalents (IEQ) were obtained per donor. Islets were washed once in HBSS + 0.1 % BSA + 5.5 mM glucose and twice in HBSS + 5.5 mM glucose. Islets were then spun at 200g for 5 min at 4^{o}C and the supernatant discarded. 250 μL of 6M

GuHCl was added to lyse the islets and thoroughly vortexed before three freeze thaw cycles were carried out to aid cell lysis. A protein crash was then performed (see section 2.5.1).

Donor	Condition	Age	Years since diagnosed	Sex	BMI	HbA1c (%)	Purity (%)
R213	T2D	57	22	Male	23.1	6.7	50
R222	T2D	62	5	Male	26.0	10	25
R240	T2D	55	2	Female	30.9	6.9	50
R244	T2D	48	3	Female	30.4	7.5	70
R259	T2D	45	4	Female	33.1	6.4	70
R276	T2D	54	10	Female	24.4	7.2	75
R307	T2D	43	2	Male	25.4	6.5	80
R223	Control	54	-	Male	27.0	5.8	90
R317	Control	54	-	Male	26.4	5.1	90
R343	Control	53	-	Female	32.8	5.7	60
R275	Control	46	-	Male	28.7	4.5	75
R228	Control	45	-	Female	29.6	4.5	70
R234	Control	50	-	Female	31.7	5.7	90
R221	Control	44	-	Male	30.5	5.3	75
R277	Control	47	-	Male	33.8	5.6	75
R327	Control	57	-	Male	33.9	5.8	95

Table 5.1: Donor details for human islet peptidomics study. Purity % relates to what percentage of the isolation was islet tissue. Acinar tissue and ductal cells are likely to contaminate some of the samples.

5.2.7 Sample preparation

Islet supernatants were acidified with of 1% FA to reach a final percentage of 0.1% FA. Whole islet lysates, pooled FACS purified cell lysates and islet secretion supernatants were extracted using SPE (see section 2.5.2). Whole islets and pooled cell lysates were reduced and alkylated (see section 2.5.3) prior to LC-MS analysis whereas islet supernatants were analysed immediately after SPE.

5.2.8 Standard curve preparation

Peptide standards for glucagon and GLP-1 (7-36 amide) were obtained from Bachem and used to prepare standard curves so that these peptides could be assigned a concentration in human and mouse islet lysates. Acinar cell lysates were used as the matrix to make up the standard curves as these cells lack expression of *Gcg* but would provide some background material to prevent binding of the standards to plastics. Internal standards for glucagon and GLP-1 (7-36 amide) were also obtained from Cambridge Research Biochemicals (Billingham, UK) and spiked into the standards and islet lysates at a constant amount.

5.2.9 Nano flow rate analysis on Orbitrap mass spectrometer

Unless otherwise stated, samples were analysed on an Orbitrap mass spectrometer coupled to a nano-LC system. The instruments, chromatography gradient and MS settings were identical to those used in section 2.6.1 apart from multiple product ion scans (also known as parallel reaction monitoring) were used in conjunction to the data-dependent acquisition method described. Product ion scans involve selecting specific ions for the instrument to fragment over the course of the run and then fragments from those specific ions are monitored. Details on these ions are given in table 5.2.

Peptide	**Precursor ion (*m/z*)**	**Normalised collision energy**
Oxyntomodulin	636.600	26
Glucagon	871.600	26
GLP-1 (1-37)	695.840	26
GLP-1 (1-36 amide)	686.170	26
GLP-1 (7-37)	839.600	26
GLP-1 (7-36 amide)	825.400	26
GIP (1-42)	834.422	26
GIP (1-30)	895.220	26
Gip_22-43	516.070	26

Table 5.2: Precursor ions selected for product ion scans. The isolation width for each precursor ion was set at 4 *m/z.*

5.2.10 High flow rate analysis on triple quadrupole mass spectrometer

To assess the effect of antagonising the GLP1 R on GSIS in islets, islet supernatants were analysed using a Xevo TQ-XS triple quadrupole mass spectrometer coupled to H-class Aquity UPLC system. Details on the MS settings and buffers used can be found in section 2.6.2. 40 µL of sample was injected onto the column for 30 seconds with starting conditions set at 90% A and 10% B before the % B was increased to 50% over the course of 7.5 minutes. The column was flushed with 90% B for 2 minutes before initial conditions were restored. Total run time per sample was 10 min. Insulin was the only peptide monitored and the specifications used to monitor this peptide were as follows; precursor ion *(m/z)* = 967.8, product ion (*m/z*) = 331.2, collision energy = 40, dwell time (s) = 0.025.

5.2.11 Data analysis

Raw data files were analysed as in section 2.6.3. LC-MS data obtained on the Orbitrap MS were searched using PEAKS as in section 2.6.4. When peptidomic differences between one or more groups needed to be assessed, the outputs of PEAKS database searches were obtained and analysed by

RStudio (v1.3) and R (v4.0.2). To control for multiple comparisons, P values were adjusted using a permutation based method using Perseus (Max Planck Institute of Biochemistry, v1.6.14.0).

5.3 Results

5.3.1 Mouse islet peptidomics

5.3.1.1 Peptidomics of whole lysed mouse islets

To study the mouse islet peptidome, I first lysed whole islets immediately after isolation and analysed the extracts by LC-MS. This minimised ex-vivo degredation of peptides whilst also removing non-islet derived pancreatic peptides and proteins which could interfere with detection of low abundant analytes. All major hormones known to be produced in islets (glucagon, insulin-1 &-2, PYY (1-36), PYY (3-36), SST-14, IAPP and PPY) were detected and quantified apart from ghrelin, although this was to be expected as adult mice were used (figure 5.1A). Other peptides derived from the propeptides of these hormones were also detected such as oxyntomodulin, GLP-2, GRPP, GLP-1 (1-36 amide) & (1-37), proinsulin 1 & 2 as well as the C-peptides of insulin-1 & -2 (figure 5.1A). Many other peptides not typically associated with islets were also detected and have been quantified in figure 5.1B. Peptides are referred to by the protein from which they originate and the position on the prepropeptide from which the protein is derived. As expected, many peptides derived from granins are seen such as secretogranins (Scg) 1, 2 and 3, Scg5 (7b2) and chromogranin A (ChgA) as well as processing enzymes such as neuroendocrine convertase 1 (Nec1 or PC1/3) and Nec2 (PC2) as well as carboxypeptidase E (CbpE). Although not typically associated with islets, several peptides derived from prourocortin-3 were detected. Fragments from the N-terminus of the propeptide (Ucn3_24-38, Ucn3_46-54 and Ucn3_58-79) as well as a N-terminally truncated fragment of urocortin-3 (Ucn3_138-160a) were detected. The full-length active form of urocortin-3 (Ucn3_123-160a) was not detected. Interestingly, several peptides not previously known to be produced by islets were found. Proenkephalin-B derived peptides such as alpha-neoendorphin (Pdyn_166-175) and rimorphin (Pdyn_221-233) were identified. The levels of many peptides shown in figure 5.1B are extremely low compared to the classic islet hormones of 5.1A and therefore it is difficult to assess the importance of finding these peptides here.

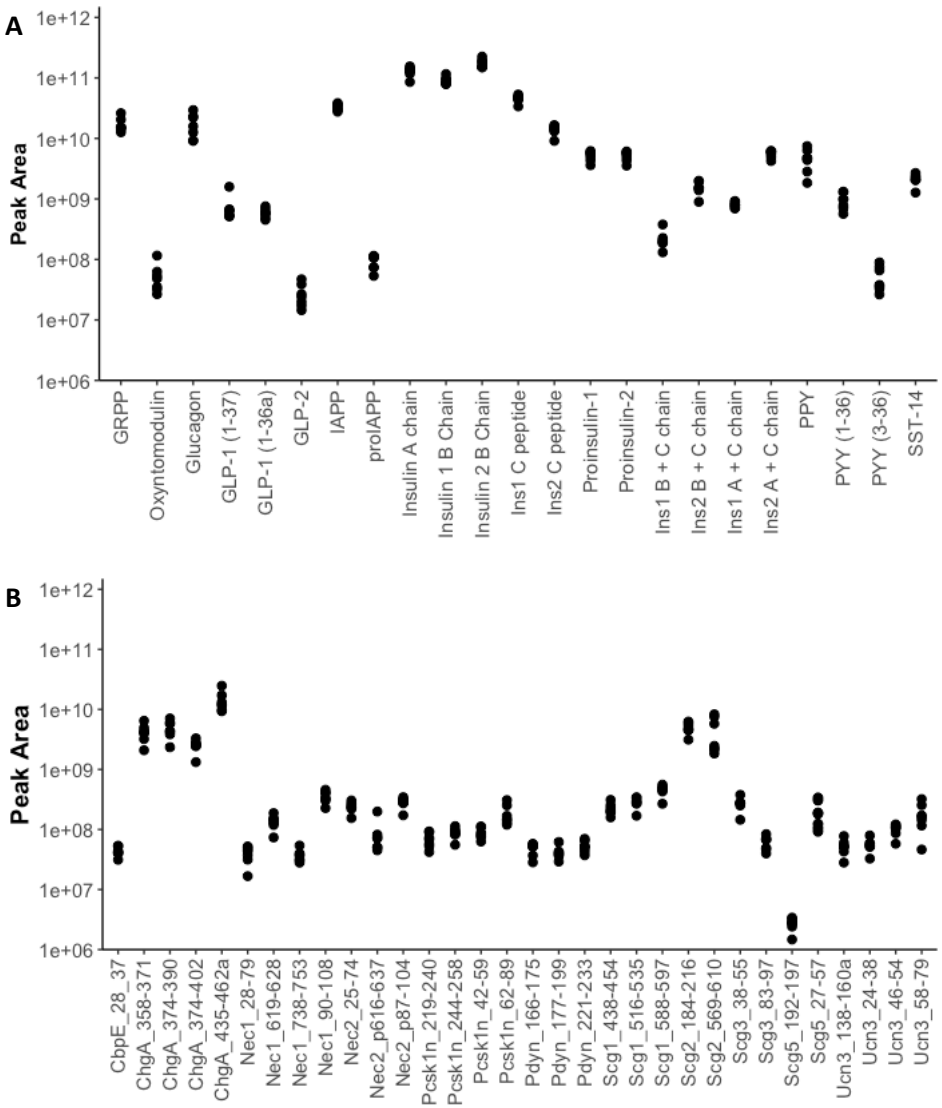

Figure 5.1: Overview of mouse islet peptidomics. *Quantification of peptides derived from the 7 major prohormones of mouse islets (proinsulin-1, proinsulin-2, proglucagon, proIAPP, proPPY, proPYY and prosomatostatin) (**A**) and non-classical islet peptides (**B**). If peptides do not have an assigned name in the literature then peptides are named for their protein of origin as well as their position on the prepropeptide from which the protein is derived. E.g. CbpE_28-37 originates from CbpE (carboxypeptidase E) protein and spans amino acids 282-37 on the prepropeptide. N.B. The chains of insulin-1 an insulin-2 are identical and so only 1 peptide is displayed for the insulin A chain.*

5.3.1.2 Detection and quantification of GLP-1 (7-36 amide)

GLP-1 (7-36 amide) was not detected using data-dependent acquisition (figure 5.1). Therefore, a targeted product ion scan was used to search for this peptide in islets. This approach involved selecting ions specific for GLP-1 (7-36a) for MS/MS analysis and then monitoring for their fragments. Using this approach, active GLP-1 (7-36 amide) was identified (figure 5.2). When monitoring for product ions originating from a precursor ion with a *m/z* of 825.4, a peak can be seen at ~73 min (figure 5.2A). This peak co-elutes with the internal standard for GLP-1 (7-36 amide) and consists of several b and y ions from GLP-1 (7-36 amide) (figure 5.2C). This is irrefutable evidence that mouse islets do produce GLP-1 (7-36 amide). By quantifying other proglucagon derived peptides using a targeted MS method (product ion monitoring) (figure 5.3A), the abundance of GLP-1 (7-36 amide) in relation to these peptides (figure 5.3) can be calculated (figure 5.3B). By running a standard curve for GLP-1 (7-36 amide) and glucagon we can estimate the amount of these peptides in mouse islets. The glucagon content of mouse islets was calculated to be 233 (±70.3) pg/islet. Unfortunately, although GLP-1 (7-36 amide) was detectable, it was below the lower limit of quantitation (0.08 pg/islet). As GLP-1 (7-36 amide) and GLP-1 (7-37) are almost identical in sequence, I used the standard curve of GLP-1 (7-36 amide) to estimate the islet content of GLP-1 (7-37) in pg/islet. Again, although GLP-1 (7-37) was detectable, its abundance was below the lower limit of quantitation (0.08 pg/islet).

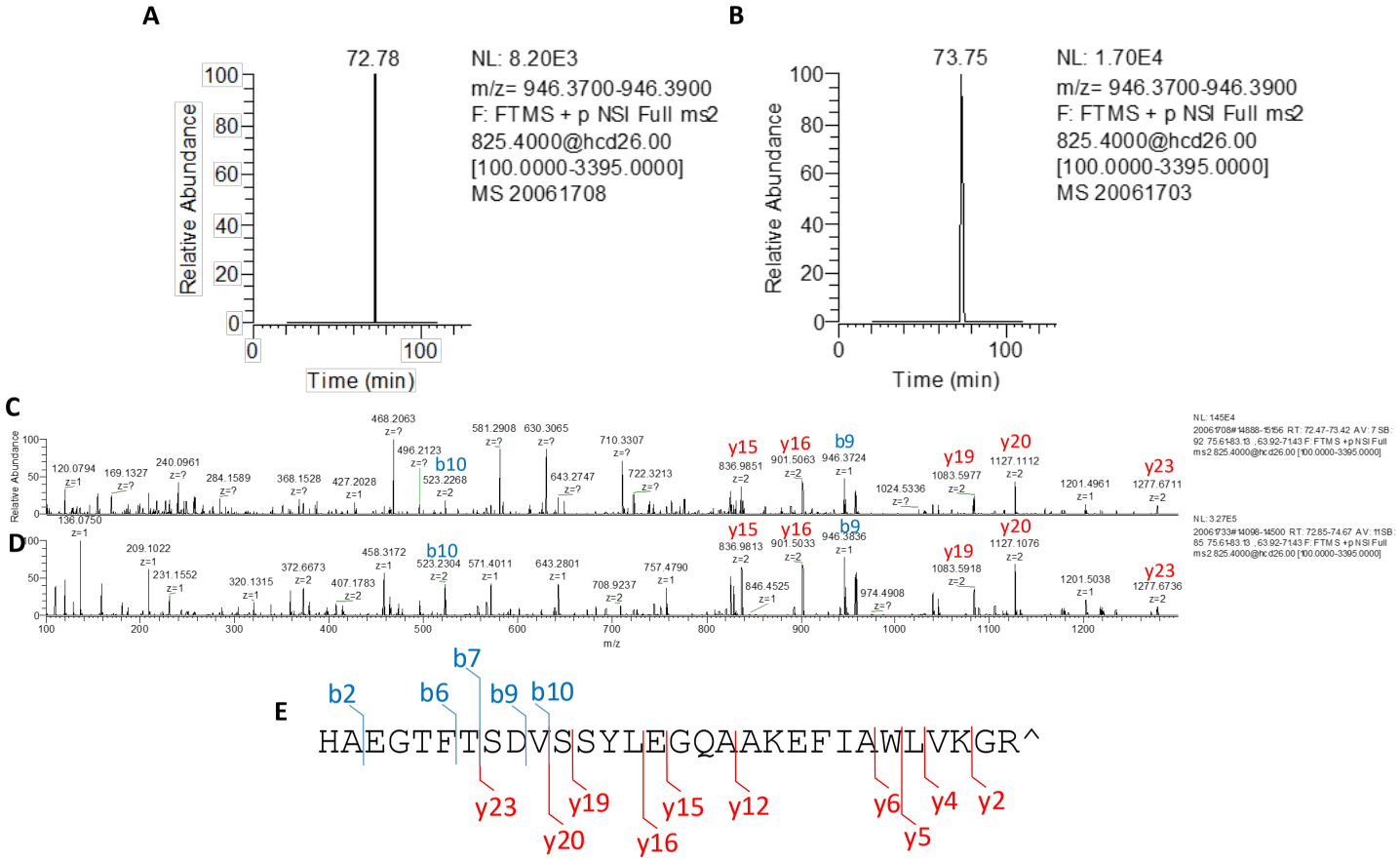

Figure 5.2: GLP-1 (7-36 amide) in mouse islets. *Extracted ion chromatograms from a MS/MS method monitoring for fragments of endogenous GLP-1 (7-36 amide) in mouse islets (**A**) and a GLP-1 (7-36 amide) standard (**B**). Peaks can be seen at 72.78 and 73.75 min in both traces which correspond to GLP-1 (7-36 amide). (**C**) Product ion spectrums corresponding peak at 72.78 min in A. (**D**) Product ion spectrums corresponding peak at 73.75 min in **B**. (**E**) Sequence of GLP-1 (7-36 amide). ^ represents C-terminal amidation. The masses of certain ions shown in **C** and **D** correspond to the masses of b and y ions from GLP-1 (7-36 amide) and have been annotated.*

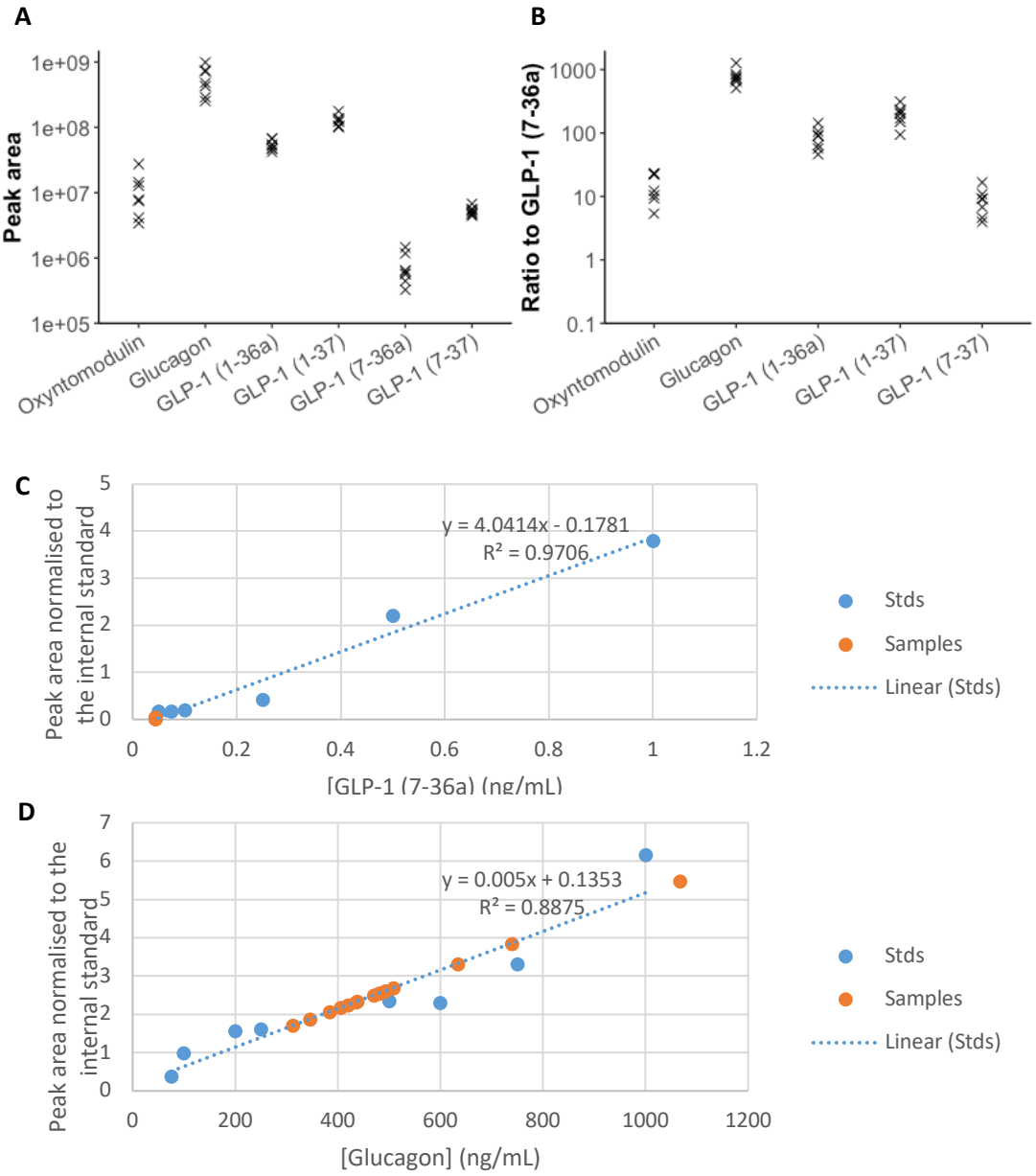

Figure 5.3: Quantification of GLP-1 (7-36a) and comparison with other proglucagon derived peptides in mouse islets. *(**A**) Quantification of proglucagon derived peptides (excluding GRPP) in islet lysates from 7 mice. Each sample contained 60 islets. Peptides quantified by monitoring for specific product ions after fragmenting precursor ions specific to each peptide. (**B**) Ratio of peak areas of proglucagon derived peptides to the peak area of GLP-1 (7-36a). (**C** and **D**) Standard curves for GLP-1 (7-36a) and glucagon respectively with samples plotted.*

Despite the low levels of active GLP-1 present in islets, an intra-islet "incretin effect" was observed, similar to that reported in Traub et al., Svendsen et al. and Hansen et al. [298, 308, 310]. Blocking the GLP1 R using an antagonistic antibody induced a significant decrease in GSIS compared to the isotype control (figure 5.4A, p=0.033).

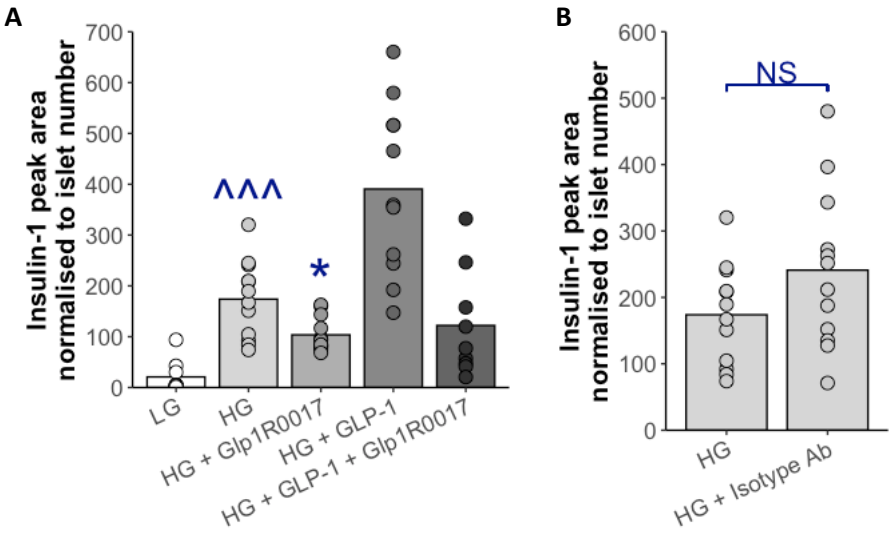

Figure 5.4: Blocking the GLP-1 receptor in mouse islets reduces insulin secretion in response to high glucose. ***(A)*** *Peak area of supernatant Insulin-1 normalized to islet number in 5 different conditions. LG=1 mM glucose, HG=16.7 mM glucose. Isotype Ab and Glp1R0017 concentrations were 300 nM. GLP-1 (7-36a) concentration was 30 nM. (**B**) Effect of isotype antibody on insulin-1 secretion in at 16.7 mM glucose. Data represent n=8-12 over 3 separate experiments. Each replicate is a supernatant from 8-11 islets. Data points were removed if insulin-1 was undetectable in the extracted supernatant. Error bars represent SD. Comparisons between groups were performed using a Kruskal-Wallis analysis with post-hoc Dunn tests. ^^^ represents p<0.005 in comparison to 1 mM glucose. * represent p<0.05 in comparison to 16.7 mM glucose.*

5.3.1.3 Searching for proGIP-derived peptides

Employing a similar approach to the method used to detect active GLP-1 (7-36 amide), proGIP-derived peptides were searched for in mouse islets. Product ion scans were set up for GIP (1-42) (the full-length version of GIP), GIP (1-30) (a C-terminally truncated form of GIP previously described as being present in islets [302]) and the N-terminal peptide of proGIP (Gip_22-44). An extract of homogenised mouse duodenum was analysed using the same product ion scans to serve as a positive control (figures 5.5 A & C, figures 5.6 A & C, figures 5.7 A & C). No ions corresponding to the b or y ions of any of the 3 proGIP-derived peptides could be seen on the ion spectrums of figure 5.5D, 5.6D or 5.7D. Therefore, it is unlikely that mouse islets produce any proGIP.

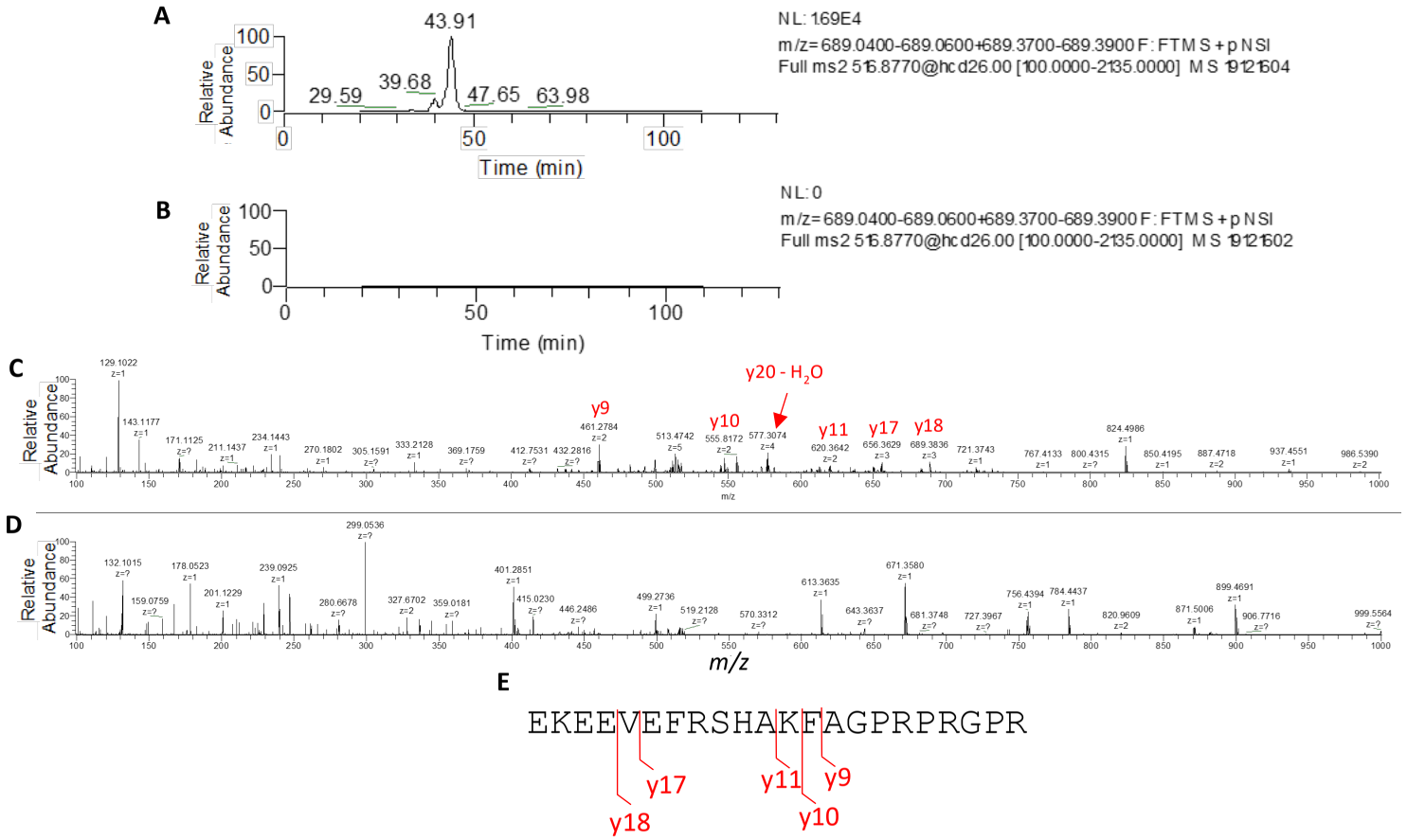
A
43.91
29.59
39.68
47.65
63.98
Relative Abundance
Time (min)
NL: 169E4
m/z= 689.0400-689.0600+689.3700-689.3900 F: FTMS + p NSI
Full ms2 516.8770@hcd26.00 [100.0000-2135.0000] MS 19121604
B
Relative Abundance
Time (min)
NL: 0
m/z= 689.0400-689.0600+689.3700-689.3900 F: FTMS + p NSI
Full ms2 516.8770@hcd26.00 [100.0000-2135.0000] MS 19121602
C
Relative Abundance
y20 - H2O
y9
y10
y11
y17
y18
m/z
D
Relative Abundance
m/z
E
EKEEVEFRSHAKFAGPRPRGPR
y17
y18
y11
y10
y9

Figure 5.5: Searching for the N-terminal propeptide of proGip (Gip 22-43) in mouse islets. *(**A**, **B**) Extracted ion chromatograms from a MS/MS method monitoring for fragments of an ion with a m/z of 516.8770 in either an extract of homogenised mouse duodenum (**A**) or mouse islets (**B**). This 516.8770 precursor ion corresponds to the $[M+5H]^{5}$+ charge state of Gip 22-43. Product ion spectrums from a MS/MS method monitoring for fragments Gip 22-43 in homogenised mouse duodenum (**C**) and lysed mouse islets (**D**). These spectra display ions detected at retention times between 42.7-46.9 min for **A** and **B** respectively. (**E**) Sequence of mouse Gip 22-43 with b and y ions identified in **C** annotated. Gip 22-43 was detectable in mouse duodenum, as multiple b and y ions produced by the fragmentation of Gip 22-43 were detected at a retention time of 43.91 min. No b or y ions produced by the fragmentation of Gip 22-43 were detected at the same retention time in mouse islets.*

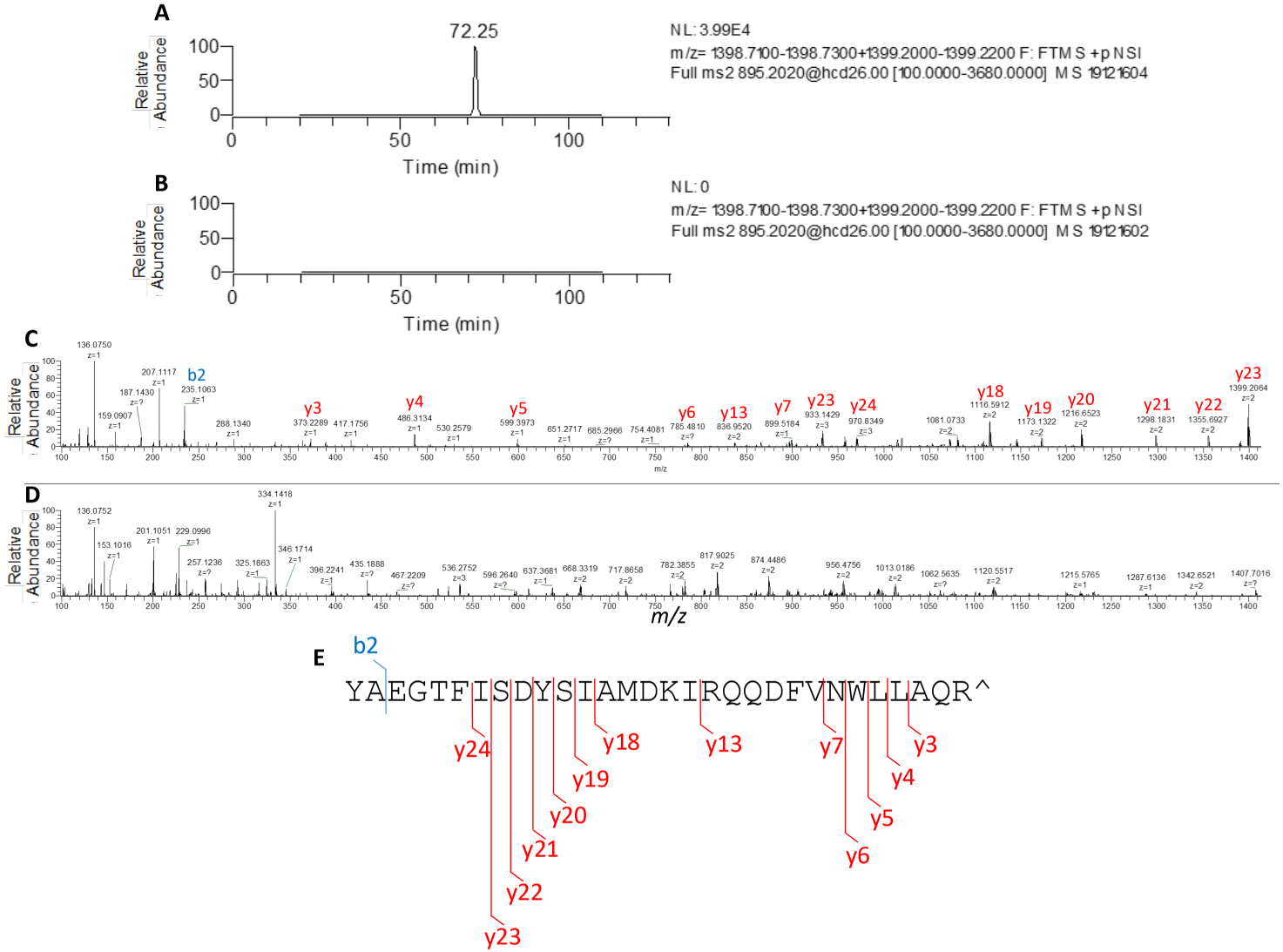
A
72.25
NL: 3.99E4
m/z= 1398.7100-1398.7300+1399.2000-1399.2200 F: FTMS +pNSI
Full ms2 895.2020@hcd26.00 [100.0000-3680.0000] MS 19121604
Relative Abundance
Time (min)
B
NL: 0
m/z= 1398.7100-1398.7300+1399.2000-1399.2200 F: FTMS +pNSI
Full ms2 895.2020@hcd26.00 [100.0000-3680.0000] MS 19121602
C
D
m/z
E
b2
YAEGTFISDYSIAMDKIRQQDFVNWLLAQR^
y24
y23
y22
y21
y20
y19
y18
y13
y7
y6
y5
y4
y3

Figure 5.6: Searching for GIP (1-30) in mouse islets. *(**A, B**) Extracted ion chromatograms from a MS/MS method monitoring for fragments of an ion with a m/z of 895.2020 in either extracts of homogenised mouse duodenum (**A**) or mouse islets (**B**). This 895.2020 precursor ion corresponds to the $[M+4H]^{4}+$ charge state of GIP (1-42). Product ion spectrums from a MS/MS method monitoring for fragments of GIP (1-30) in homogenised mouse duodenum (**C**) and lysed mouse islets (**D**). These spectra display ions detected at retention times between 70.9-74.4 min for **A** and **B** respectively. (**E**) Sequence of mouse GIP (1-30) with b and y ions identified in **C** annotated. ^ represents a C-terminal amidation. GIP (1-30) was detectable in mouse duodenum as multiple b and y ions from GIP (1-30) were detected at a retention time of 72.25 min. No b or y ions originating from GIP (1-30) were detected at the same retention time in mouse islets.*

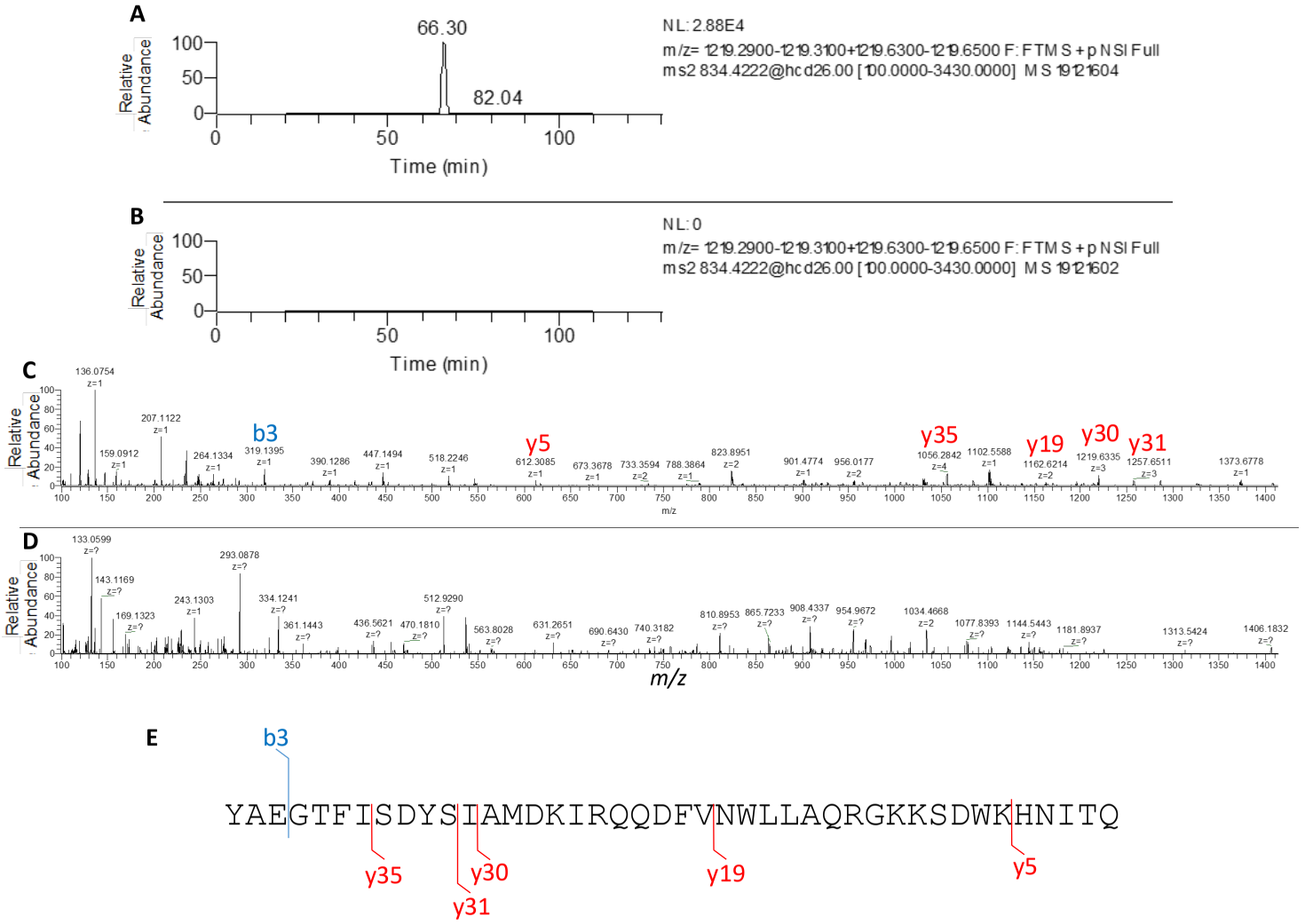
A
66.30
82.04
NL: 2.88E4
m/z= 1219.2900-1219.3100+1219.6300-1219.6500 F: FTMS + p NSI Full ms2 834.4222@hcd26.00 [100.0000-3430.0000] MS 19121604
Relative Abundance
Time (min)
B
NL: 0
m/z= 1219.2900-1219.3100+1219.6300-1219.6500 F: FTMS + p NSI Full ms2 834.4222@hcd26.00 [100.0000-3430.0000] MS 19121602
C
b3
y5
y35
y19
y30
y31
D
m/z
E
b3
YAEGTFISDYSIAMDKIRQQDFVNWLLAQRGKKSDWKHNITQ
y35
y30
y31
y19
y5

Figure 5.7: Searching for GIP (1-42) in mouse islets. *(**A**, **B**) Extracted ion chromatograms from a MS/MS method monitoring for fragments of an ion with a m/z of 834.4222 in either extracts of homogenised mouse duodenum (**A**) or mouse islets (**B**). This 834.4222 precursor ion corresponds to the $[M+6H]^{6}+$ charge state of GIP (1-42). Product ion spectrums from a MS/MS method monitoring for fragments of GIP (1-42) in homogenised mouse duodenum (C) and lysed mouse islets (**D**). These spectra display ions detected at retention times between 62.9-68.5 min for **A** and **B** respectively. (**E**) Sequence of mouse GIP (1-42) with b and y ions identified in **C** annotated. GIP (1-42) was detectable in mouse duodenum as multiple b and y ions produced by the fragmentation of GIP (1-42) were detected at a retention time of 66.30 min. No b or y ions produced by the fragmentation of GIP (1-42) were detected at the same retention time in mouse islets.*

5.3.1.4 Peptidomics of FACS purified α, β and δ cells

The 3 major islet cell populations (α, β and δ) were isolated by FACS, lysed and analysed by LC-MS so that the peptidomic differences between these cell types could be established. α and β cells were purified from *Glu-Venus* mice and δ cells from *Sst-Cre* mice. By quantifying the major islet hormones (glucagon, Insulin-1 and -2, SST-14, PPY and PYY (1-36)), it can be seen that peptides were enriched in their expected cell populations (figure 5.8A). Low levels of PPY were detected in the α and δ populations while low levels of PYY (1-36) were detected in all cell populations. After it was established that good enrichment of each major cell population was achieved, all samples were analysed using PEAKS to identify peptides from the mouse Swissprot database. A total of 999 peptides were matched but peptides not present in at least 2 samples were removed leaving 562 peptides. These 562 peptides were assigned to 1 of 6 clusters by hierarchical clustering on a heatmap (figure 5.8B). Clusters 1, 4 and 6 consist of peptides most abundant in the α, δ and β populations respectively while clusters 2, 3 and 5 represent peptides abundant in 2 cell populations. Cluster 2 contains peptides abundant in the α and δ populations, peptides in cluster 3 are abundant in the α and β populations and peptides in cluster 5 are found in both the β and δ populations. A PCA plot was generated to visualise how each of the 6 populations differ from one another (figure 5.8C).

A selection of peptides has been plotted in figure 5.9 to give an overview of the identity of peptides within each cluster. For the full list of peptides in figure 5.8A see appendix 2. Cluster 1 consists almost entirely of proglucagon-derived peptides as well as a few peptides derived from Nec2 (PC2), proPYY, ChgA and Pcsk1n (proSAAS). However, the most abundant peptides from Nec2, proPYY, ChgA and proSAAS were assigned to a different cluster. Interestingly, proPPY derived peptides reside almost entirely within cluster 2 indicating that both α and δ cells possess low levels of proPPY with a few PC2 derived peptides also residing in cluster 2. Cluster 3 was the smallest cluster consisting of just 4 peptides and therefore could be phenomenon of the analysis rather than the biology. Cluster 4 consisted of many prosomatostatin derived peptides as well as Pcsk1n, Scg1 and Nec2. This was also the cluster where the majority of the proPYY peptides were assigned including PYY (1-36) and (3-36). Cluster 5 consisted largely of Scg2 derived peptides. Unsurprisingly, proinsulin-1, proinsulin-2 and proIAPP derived peptides dominated cluster 6 as well as Scg3 and ChgA derived peptides. Cluster 6 also contained peptides originating from proenkephalin-B and prourocortin-3 indicating these prohormones are likely produced by β cells.

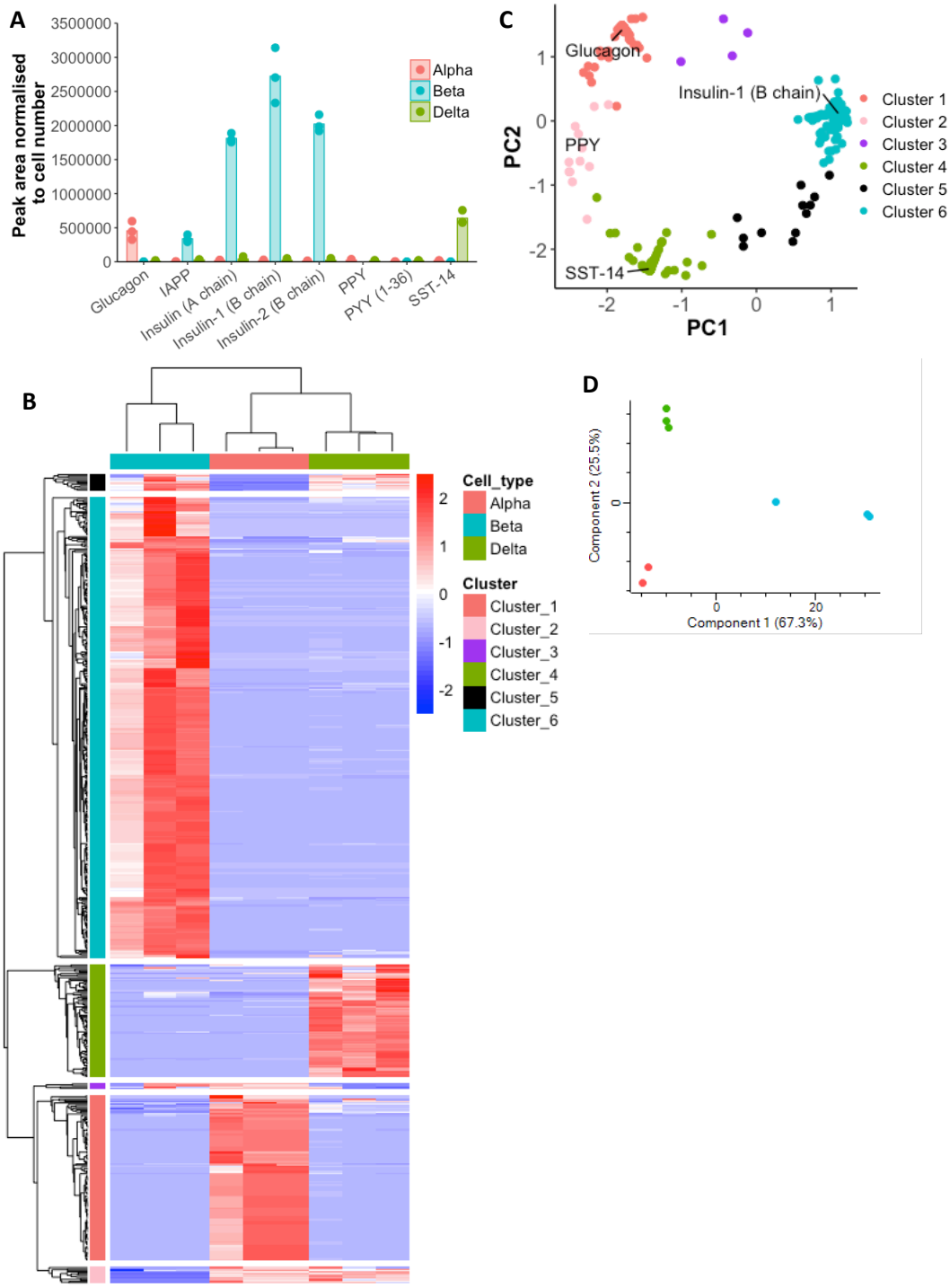

Figure 5.8: Peptidomics of FACS purified mouse alpha beta and delta cells. *(**A**) Abundance of major islet hormones in the three FACS purified islet cell populations. (**B**) Heatmap of all peptides matched through PEAKS database searching in the 3 purified cell populations. Peptides assigned to one of six clusters. (**C**) PCA analysis of matched peptides with colour annotation of cluster assigned in **B**. SST-14, PPY, glucagon and insulin-1 B chain have been annotated. (**D**) PCA analysis of all 9 samples (3 α samples, 3 δ samples and 3 β samples. The peak area of each peptide was normalised to the number of cells in that sample to account for the difference in cell numbers.*

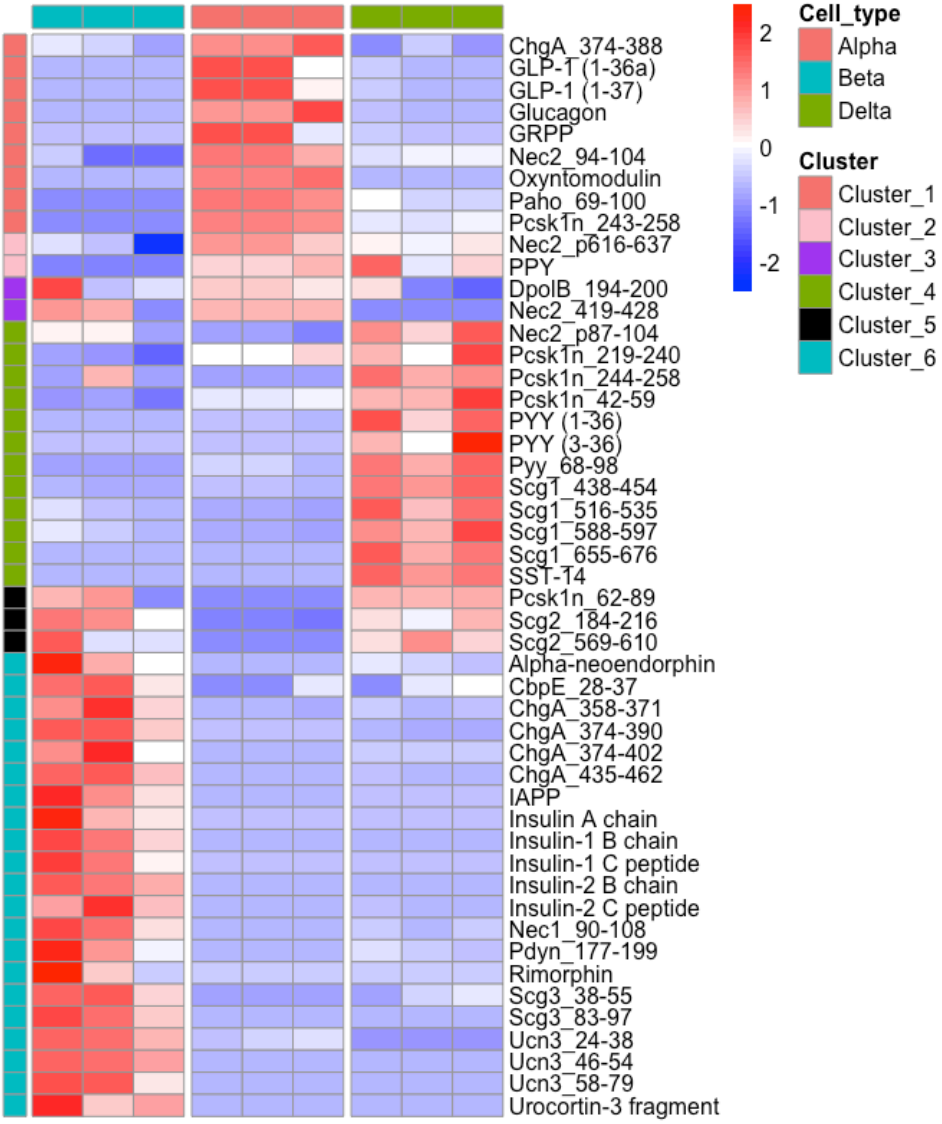

Figure 5.9: Heatmap of selected peptides quantified in FACS purified mouse alpha, beta and delta cells with cluster assigned in figure 5.8 B annotated down the left.

5.3.1.5 Islet secretion peptidomics

To analyse the secreted islet peptidome, islet secretion experiments were performed. 1 mM glucose (LG), 1 mM glucose + 5 μM adrenaline (LG + Adr), 6 mM glucose (MG) and 16.7 mM glucose (HG) were added to the supernatants to stimulate secretion from the different islet cell types. Due to peptide degradation during the secretion experiment and a lack of BSA in the supernatants (BSA was purposefully minimised to reduced interference during LC-MS analysis), peptide abundance in the supernatants was extremely low. Therefore, not all peptides triggered a MS/MS scan and so would not be matched by a PEAKS database search. Peptides were therefore manually quantified and so the number of peptides quantified was greatly reduced compared to those quantified in islet lysates.

Figure 5.10 displays the raw peak area values for numerous peptides quantified in the supernatants. Insulin-1, insulin-2, IAPP and the insulin C peptides are displayed in figure 5.10A and exhibit a >30-fold increase when stimulated with HG compared to either MG or LG. Furthermore, secretion of insulins and IAPP are not stimulated by LG, LG + Adr or MG. ChgA_435-462a exhibits this same pattern of secretion (figure 5.10D). Secretion of proglucagon derived peptides is most strongly stimulated by LG + Adr but seems to be largely unaffected by glucose alone although a slight inhibitory effect was seen at HG (figures 5.10B and 5.11), a pattern which is mimicked by PPY (figure 5.10C). SST-14 secretion exhibits a mild stimulation in HG and is largely unaffected by the other 3 conditions (figure 5.10C). PYY (1-36) and PYY (3-36) secretion is also mildly increased by HG and unaffected by the other conditions however, secretion of PyySP_68-100 seemed to be stimulated by both HG and LG + Adr. None of the major islet hormones (insulin, glucagon, SST-14 or PPY) are stimulated by both HG and LG + Adr indicating that PyySP_68-100 is released by more than one cell type. PyySP_69-100 is the C-terminal peptide of a splice variant of the *Pyy* gene where 2 additional residues (arginine and serine) have been added at the C-terminus of the propeptide. PyySP_68-100 was quantified as the normal C-terminus of proPYY was undetectable due to interference from BSA. ChgA_358-371 exhibited a similar stimulated pattern to PyySP_68-100 indicating this peptide is also present in several cell types (figure 5.10D). Other ChgA-related peptides such as ChgA_374-402 and ChgA_435-462a appear to only be stimulated strongly by HG as well as Nec1_90-108, Nec2_p87-104 and Scg2_569-610 (figures 5.10E and 5.11).

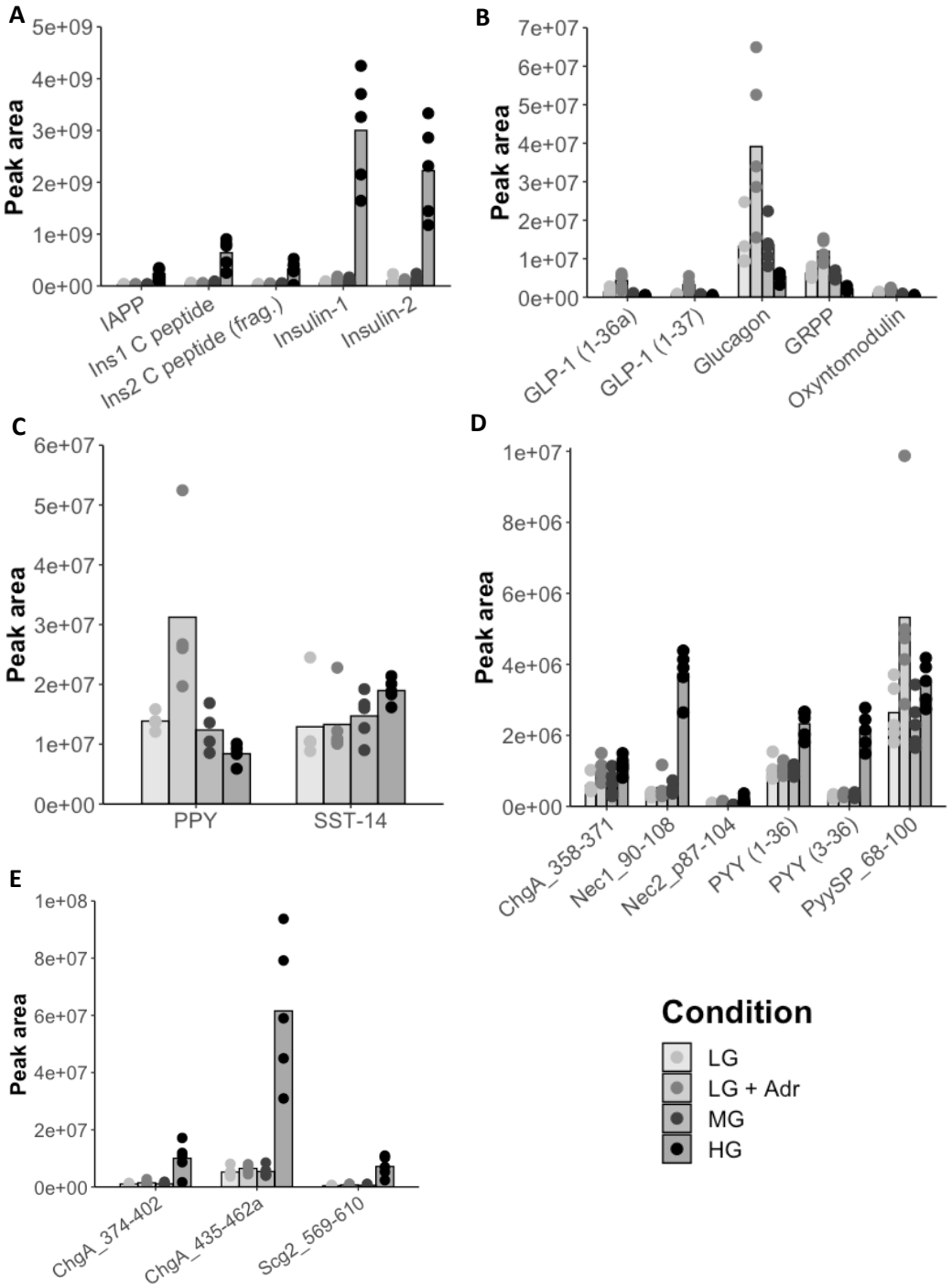

Figure 5.10: Peptidomics of secretions from mouse islets*. Peptides grouped with peptides from same protein or with peptides with similar peak areas. Peak area; of IAPP and insulin-derived peptides (**A**), proglucagon-derived peptides (**B**), PPY and SST-14 (**C**), proPYY-derived peptides along with ChgA_358-371 and Nec-derived peptides (**D**), ChgA_374-402, ChgA_435-462a and Scg2_569-610 (**E**). Individual data points are displayed in each plot along with the mean. Conditions were as follows; LG = 1 mM glucose, LG + Adr = 1mM glucose + 5 µM adrenaline, MG = 6 mM glucose, HG = 16.7 mM glucose. Each data point represents pooled supernatants from 9 tubes containing 15 islets.*

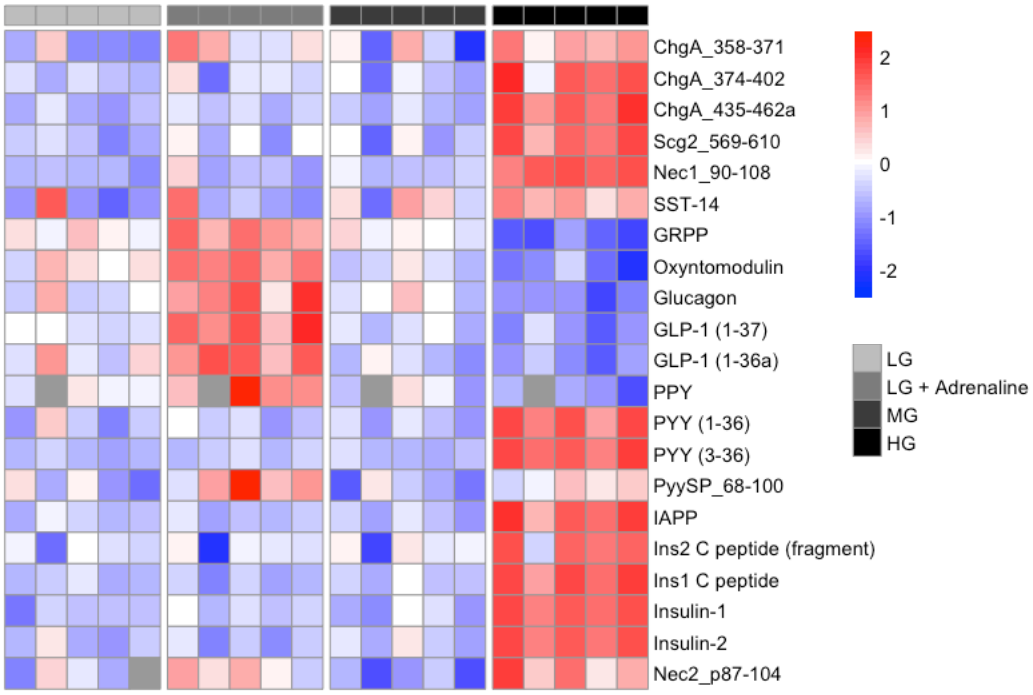

Figure 5.11: Heatmap of mouse islet secretion peptidomics. *Data presented as Z-score of each row. Grey squares within the heatmap indicate where peptides were not detectable within that sample. LG = 1 mM glucose, LG + Adrenaline = 1mM glucose + 5 µM adrenaline, MG = 6 mM glucose, HG = 16.7 mM glucose.*

5.3.1.6 Peptidomics of DIO vs lean mouse islets

After characterising the islet peptidome and establishing the peptidomic differences between islet cell types, I investigated the peptidomic changes in islets induced by obesity in mice. Diet-induced obese (DIO) mice were fattened on a high-fat diet (60% fat) for 13 weeks. At the end of the fattening period the body weight of the HFD-fed mice and fasting blood glucose levels were significantly higher than the lean controls (figures 5.12A and B). Islets were isolated, lysed, analysed by LC-MS and MS/MS data were searched by PEAKS to match peptides against the mouse Swissprot database. 2686 peptides were identified across all samples. Using a filter to exclude peptides not matched in at least 70% of samples in one group, the number of peptides in the final analysis was cut to just 718.

Volcano plots displaying the log2 fold change between groups against the -log10 of the adjusted p value are displayed in figures 5.12C-H. None of the major islet peptides (IAPP, Insulin-1, insulin-2, SST-14, PPY, PYY (1-36) and glucagon) were significantly altered between groups (figure 5.12C). Furthermore, only 3 out of 211 peptides derived from a granin protein (figure 5.12F) or a processing enzyme (figure 5.12G) were significantly altered. However, the majority of peptides significantly altered in DIO mouse islets were derived from a proinsulin or proIAPP indicating that obesity only induced changes to the peptidome of β cells (figure 5.12D).

Therefore, it seems that at the level of the peptidome, only the β cells were affected in the DIO group. To drill down further into this issue, a number of β cell-derived peptides identified from the FACS sorted cells were manually quantified and are displayed in figure 5.13. The islet content of IAPP, Ins2 C peptide, proinsulin-1, proinsulin-2 and a mis-processed form of proinsulin-2 (Ins2_57-110, this is peptide results from a missed cleavage between the A chain and C peptide) are significantly increased in DIO mice (figure 5.13A). However, the levels of other β cell-derived peptides such as prourocortin-3, proenkephalin-B (figure 5.12H and 5.13B) and several ChgA-derived peptides were unaltered between groups. Any potential change to the islet peptidome induced by obesity thus seems restricted to peptides derived from proIAPP and proinsulins.

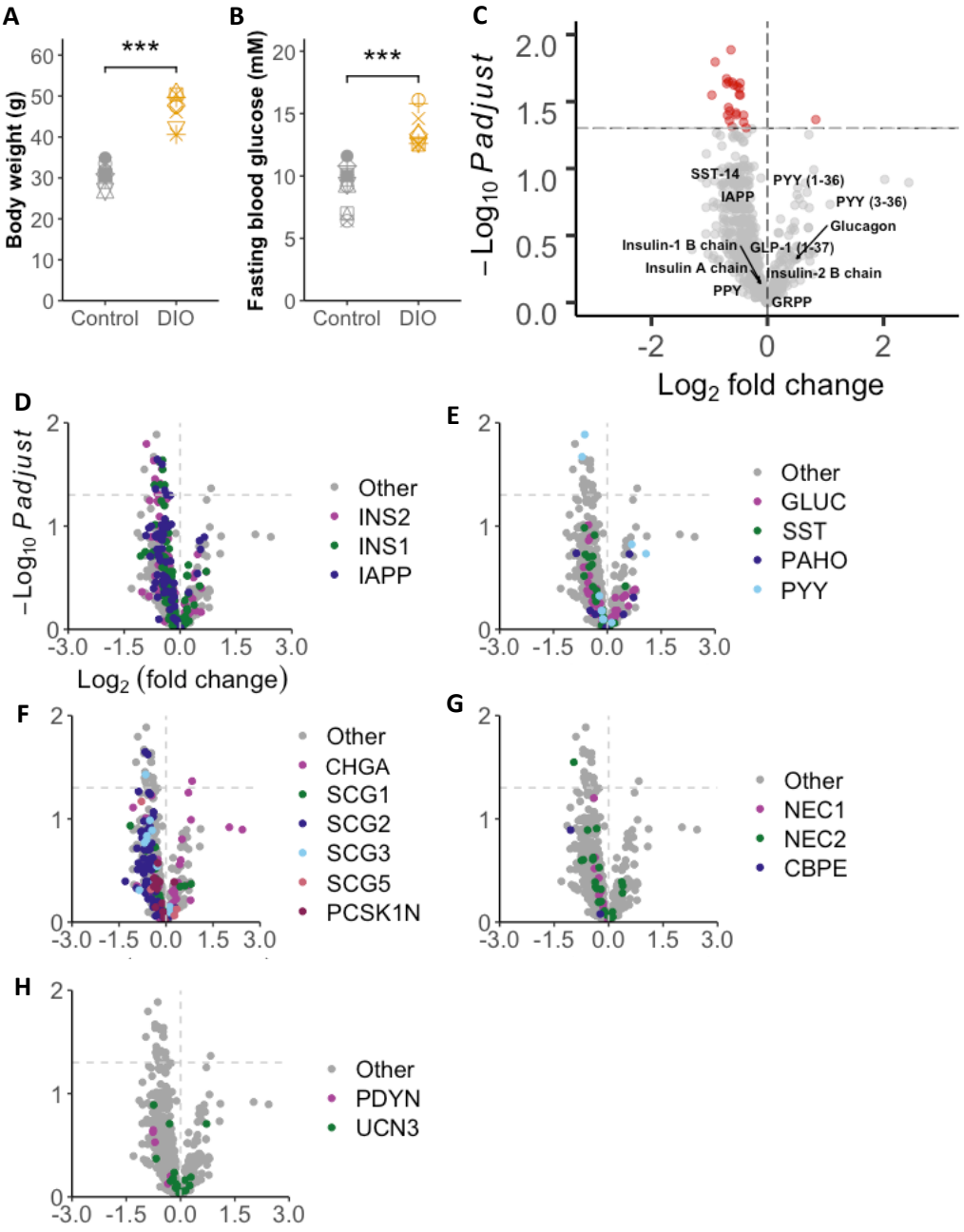

Figure 5.12: Peptidomic comparison of islets from DIO mice and to lean controls. *Body weights (**A**) and fasting blood glucose levels (**B**) of DIO mice vs lean controls. (**C-H**) Volcano plots displaying log_2 fold change vs $–log_{10}$ of the adjusted p value for each peptide. Horizontal dotted line indicates significance threshold of p=0.05. A positive log2 fold change indicates a decrease in DIO mice whereas a negative log2 fold change indicates an increase. 718 t-tests were performed to analyse for significant differences in peptides matched between the groups with a permeation-based method used to adjust for multiple comparisons. Different peptides are coloured in each plot. proIAPP and proinsulin derived peptides in (**D**). Proglucagon (GLUC), prosomatostatin (SMS), proPPY (PAHO) and proPYY (PYY) derived peptides in (**E**). Granin derived peptides in (**F**). Processing enzyme derived peptides in (**G**). Proenkephalin-B (PDYN) and prourocortin-3 (UCN3) derived peptides in H.*

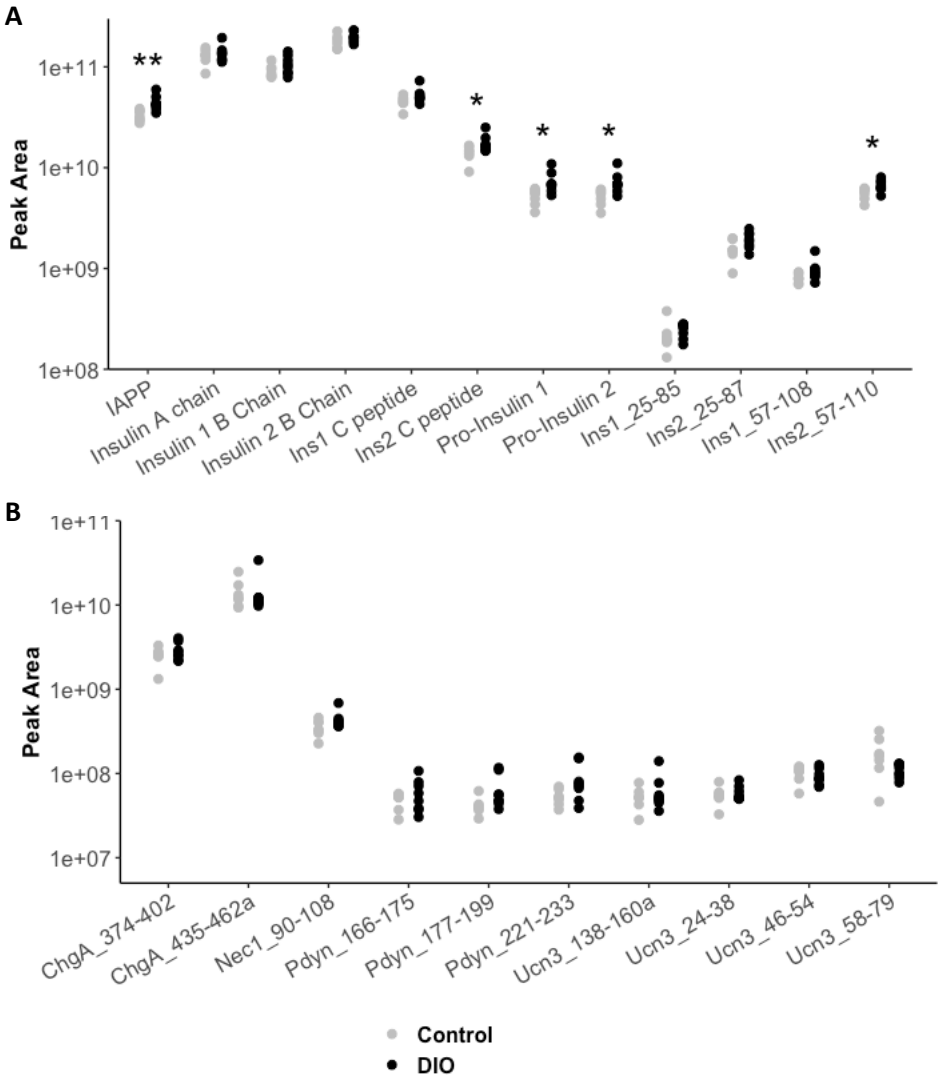

Figure 5.13: Manual quantification of selected β cells peptides from DIO islet peptidomics study. (**A**) Proinsulin-derived peptides along with IAPP. (**B**) Non-proinsulin or proIAPP peptides that were identified as being predominantly produced in β cells in figure 5.9. Statistical comparisons were made using T-tests. * $p<0.05$, ** $p<0.01$.

5.3.2 Human islet peptidomics

5.3.2.1 Peptidomics of lysed whole human islets

After characterising the mouse islet peptidome, the peptidome of human islets was investigated. Human islets were ordered from the Alberta Diabetes Institute IsletCore at the University of Alberta. These snap frozen aliquots of 2000 IEQ were lysed, extracted, analysed by LC-MS and MS/MS data were searched by PEAKS to match spectra against the human Swissprot database. All of the major hormones associated with human islets (glucagon, IAPP, insulin, PPY, SST-14) were detected and quantified (figure 5.14A) including a fragment of ghrelin (GHRL_24-37), although, the full-length version of ghrelin was not detected. In addition to the main islet hormones, alternate processing products from proglucagon and proinsulin could be detected including misprocessed forms of proinsulin (INS_25-87, INS_57-110). In contrast to mouse islets, peptides derived from proPYY prourocortin-3 or proenkephalin-B were not detected in human islets although it is well characterised that human islets don't express *PYY* [125, 126]. Another difference was the detection in human but not mouse islets of peptides derived from a neuroendocrine protein (neurosecretory protein VGF (VGF)), the most abundant of which are quantified in figure 5.14B. Numerous peptides derived from human orthologs of granins and processing enzymes were also detected in human islets (figure 5.14B), but no other major differences were found between the two species.

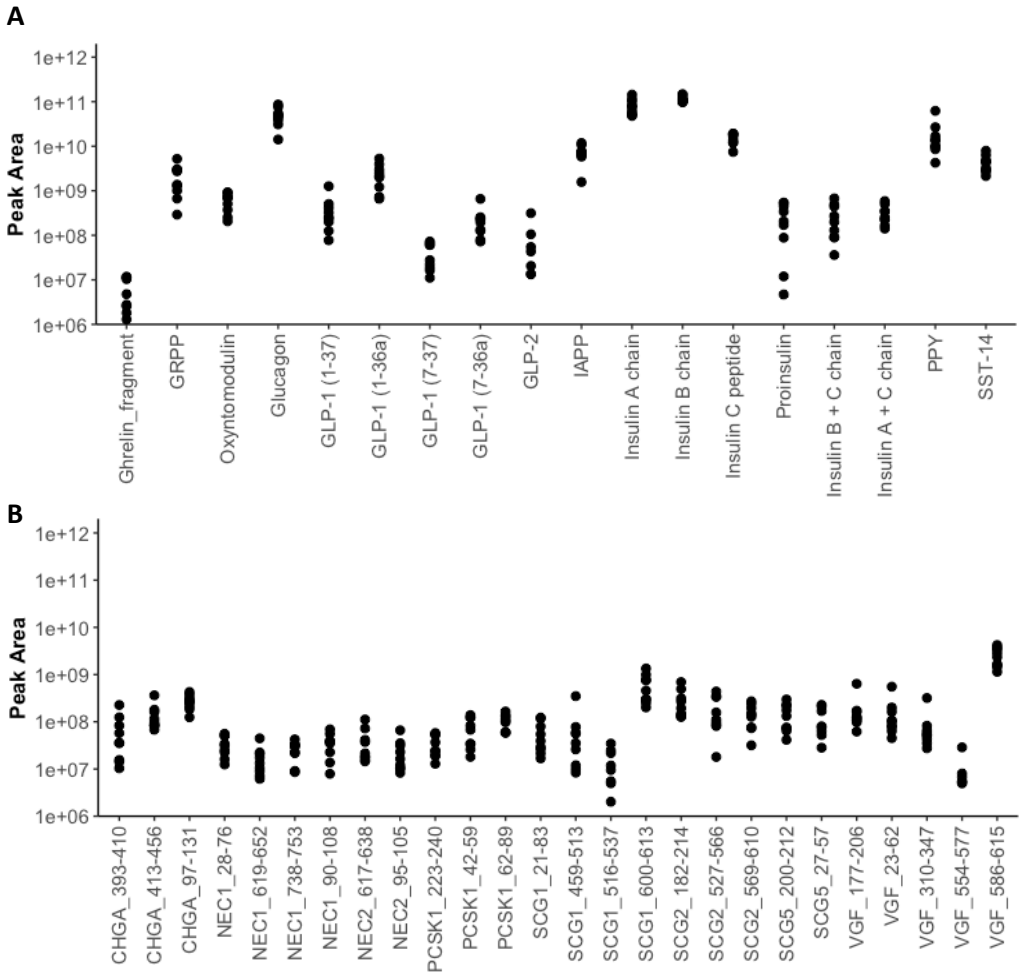

Figure 5.14: Overview of human islet peptidomics. *Quantification of peptides derived from the 6 major prohormones of human islets (proinsulin, proglucagon, proPPY, proIAPP, prosomatostatin) (**A**) and non-classical islet peptides (**B**). If peptides do not have an assigned name, they are named for their protein of origin as well as their position on the prepropeptide the protein is derived from.*

5.3.2.2 Detection and quantification of GLP-1 (7-36 amide) in human islets

Following on from the detection of active GLP-1 in mouse islets, human islets were searched for these active peptides. Both GLP-1 (7-36 amide) and GLP-1 (7-37) were detectable using data-dependent acquisition on the Orbitrap mass spectrometer (figure 5.14A) and a comparison of the abundance of GLP-1 (7-36 amide) with other proglucagon derived peptides is given in figure 5.15A.

As several GLP-1 related peptides were sufficiently abundant to trigger MS/MS scans during data-dependent acquisition, these peptides were identified by the PEAKS database search and are displayed in figure 5.15B in an alignment plot. The most abundant forms of GLP-1 are the inactive GLP-1 (1-36 amide) and (1-37) forms. Non-specific protease activity has generated a peptide ladder of GLP-1 (1-37) forms by sequential degradation at the C-terminus. At the N-terminus, there seems to be specific cleavage between amino acids 97 and 98 which is the annotated cleavage point for PC1/3 on proglucagon. Cleavage of long GLP-1 at this point results in the formation of active forms of GLP-1. Out of all the degradation products of long forms of GLP-1, the active 7-36 amide version is the most abundant.

To assign a concentration to the amount of GLP-1 (7-36 amide) and glucagon in human islets a standard curve was generated. The glucagon content of human islets was estimated to be 3.61 pg/IEQ (±2.39) and the GLP-1 (7-36 amide) content was estimated to be 0.012 pg/IEQ (±0.012). Additionally, using the standard curve of GLP1 (7-36 amide), I calculated that the human islet content of GLP-1 (7-37) was approximately 0.002 (±0.001) pg/IEQ. However, the accuracy of this quantification is questionable due to the fact that many samples fell outside of the standard curve for both glucagon and GLP-1 (7-36 amide) (figure 5.15C & D). Therefore, these calculations assume that the relationship between peak area and concentration is linear outside of limits of the curves.

ProGIP derived peptides were not detected in human islets using a data-dependent acquisition although it should be noted that I did not set up product ion scans to specifically target proGIP peptides in human islets. This was due to the fact that I had already set up product ion scans to search for proglucagon derived peptides such as GLP-1 (7-36 amide) and I didn't want to set up many more for fear of compromising data collection during data-dependent acquisition.

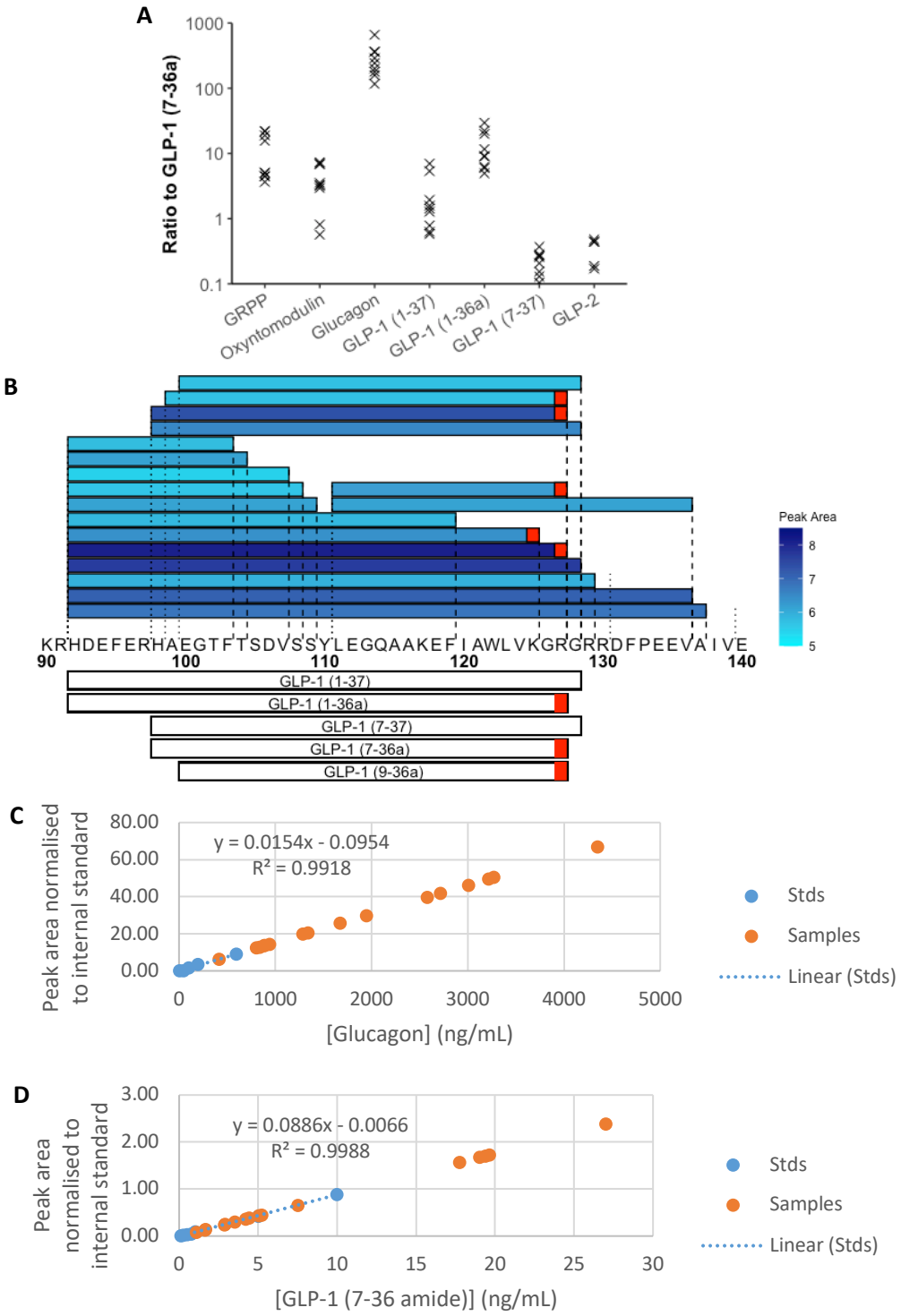

Figure 5.15: Comparison of GLP-1 (7-36a) levels with other proglucagon derived peptides in human islets. *(**A**) Ratios of the peak area of proglucagon (excluding GRPP) derived peptides to the peak area of GLP-1 (7-36a) in lysed human islets. Each sample contained 2000 IEQ. Peptides quantified by monitoring for specific product ions after fragmenting precursor ions specific to each peptide. (**B**) Alignment plot showing peptides identified in human islets by PEAKS from position 90-140 on proglucagon. Shading in blue corresponds to peak area. Red boxes denote amidated amino acids. (**C** and **D**) Standard curves for glucagon and GLP-1 (7-36 amide) respectively with samples plotted.*

5.3.2.3 Peptidomics of T2D vs non-diabetic human islets

Islets from type 2 diabetic (T2D) donors were also obtained from the Alberta Diabetes Institute IsletCore and analysed by nano-LC-MS alongside islets from non-diabetic individuals as controls. All samples were searched by PEAKS against the human Swissprot database to match peptides. Peptides that were not matched in at least 70% of samples of one group were removed leaving 580 peptides for the final analysis. Volcano plots in figure 5.16 display the log2 of the fold change between groups vs the -log10 of the adjusted (figure 5.16A) or unadjusted p values (figures 5.16B-F). No peptide is significantly different between the two groups when adjusting for multiple comparisons (figure 5.16A) and only 3 peptides have adjusted p values below 0.15. Therefore, I examined the unadjusted p values to ascertain if there were any less significant peptidomic differences between the two groups (figure 5.16B). By this analysis, the major hormones produced in β cells (both chains of insulin and IAPP) were decreased in T2D human islets whereas the major α cell hormone (glucagon) was increased. Other proglucagon derived peptides such as oxyntomodulin, GLP-1 (1-36 amide) and (7-36 amide) were also increased in T2D islets but GLP-2, GRPP and GLP-1 (1-37) were similar between groups. No other peptidomic differences between the two groups were seen as no peptides derived from granin proteins (figure 5.16E), processing enzymes (figure 5.16F) δ cells (SST-14) or PP cells (figure 5.16D) reached this lower level of significance. Some non-proIAPP, proinsulin and proglucagon derived peptides did reach this low significance level (figure 5.16D & E), however these peptides were very low in abundance and were not the major product of their prohormone. For example, 3 peptides from proPPY (PAHO_69-82, PAHO_73-88 and PAHO_75-87) were increased in T2D islets but a further 23 peptides from proPPY were not significantly altered. The low percentage of altered peptides from this propeptide suggests that no real change is occurring in the abundance of proPPY derived peptides.

Manual quantification of selected peptides confirmed the findings of the PEAKS peptidomic analysis (figure 5.17). IAPP and proinsulin derived peptides all exhibited between a 1.5-2.5 fold decrease in T2D islets, however only IAPP (p=0.02), insulin A chain (p=0.04), insulin B chain (p=0.006) and INS_57-110 (p=0.009) reached significance. Proglucagon derived peptides were also modestly increased in T2D islets with glucagon increasing by a factor of 1.6 (p=0.04) and GLP-1 (7-36 amide) increasing by a factor of 3.1 (p=0.02). Despite the fold increase of GLP-1 (7-36 amide) in T2D islets being seemingly larger than that of glucagon, no significant difference was seen in the ratio of glucagon:GLP-1 (7-36 amide) in each sample (figure 5.17C).

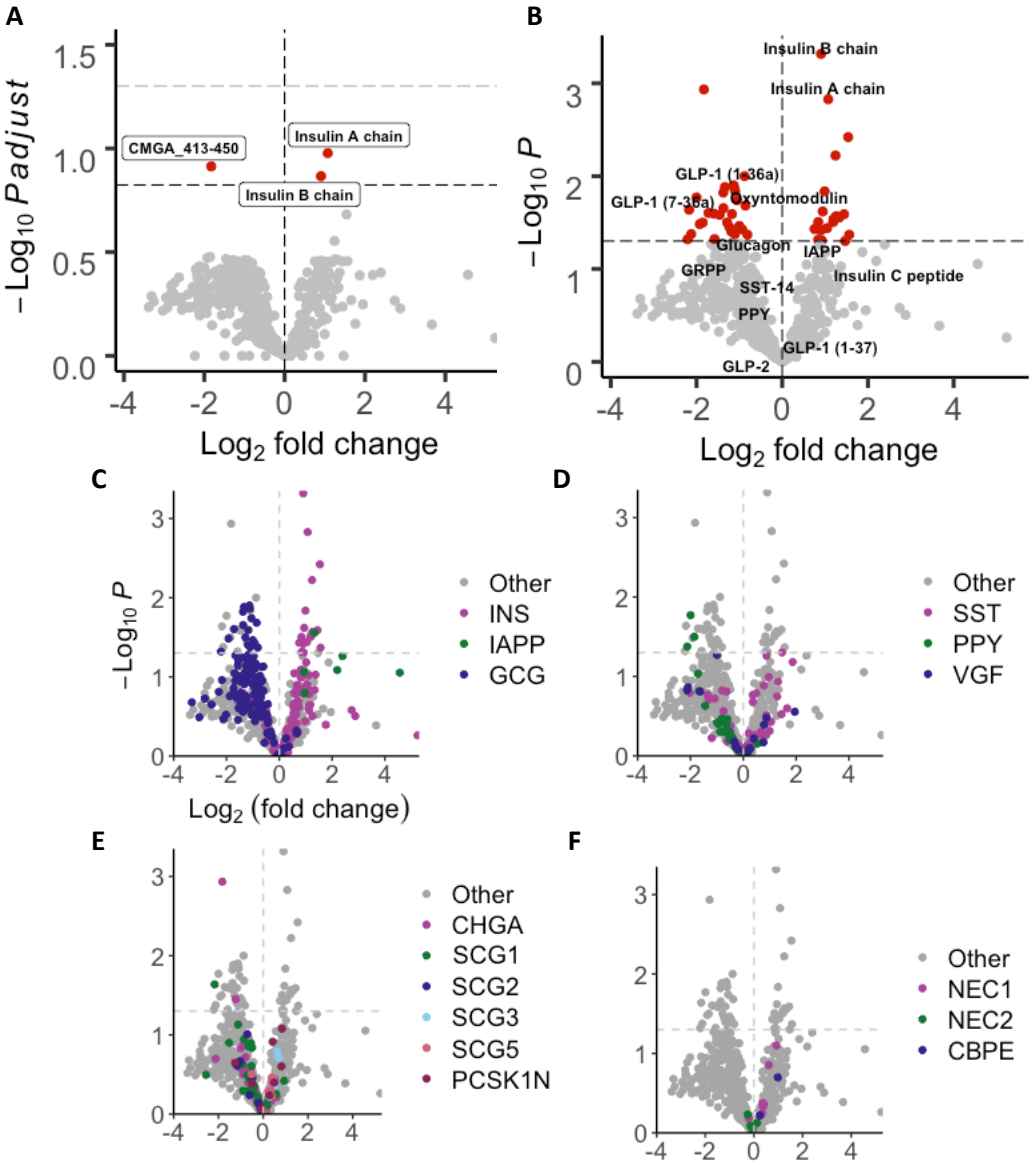

Figure 5.16: Peptidomic comparison of human islets from type 2 diabetic (T2D) individuals compared to non-diabetic controls. *(**A**) Volcano plot displaying log_2 fold change vs $–log_{10}$ of the adjusted p value for each peptide. Black horizontal dotted line indicates p=0.15. Grey horizontal dotted line indicates p=0.05. (**B**-**F**). Volcano plot displaying log_2 fold change vs $–log_{10}$ of the unadjusted p value for each peptide. Horizontal dotted line indicates significance threshold of p=0.05. Major islet hormones are labelled in (**B**), peptides from proIAPP, proinsulin and proglucagon coloured in (**C**), peptides from prosomatostatin (SST), proPPY and proVGF coloured in (**D**), granin derived peptides coloured in (**E**) and processing enzyme derived peptides coloured in (**F**). A positive log2 fold change indicates a decrease in T2D whereas a negative log2 fold change indicates an increase.*

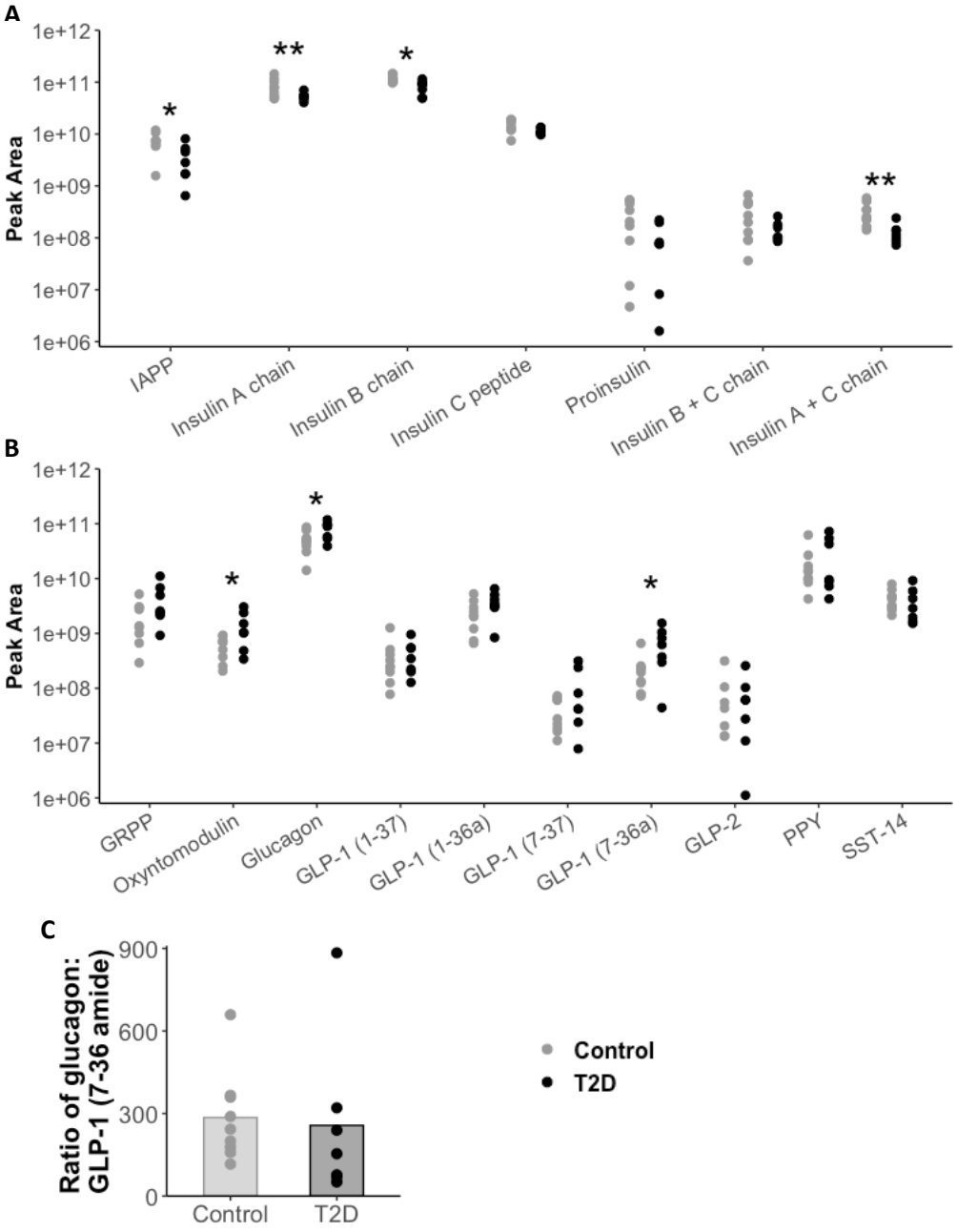

***Figure 5.17: Manual quantification of selected peptides from T2D islet study**. (A) IAPP and proinsulin derived peptides. (B) SST-14, PPY and proglucagon derived peptides. (C) Ratio of glucagon:GLP-1 (7-36 amide). Comparisons between groups performed using a t-test.*

5.4 Discussion

5.4.1 Comparison of human and mouse islet peptidomics

Is this chapter, the human and mouse islet peptidome has been characterised by LC-MS. In both human and mouse islets all classical islets hormones were detected (figure 5.1A & 5.14A). Furthermore, I could detect numerous peptides derived from granin proteins and processing enzymes (figure 5.1B & 5.14B). Aside from the well-known peptidomic differences between human and mice (mouse islets produce 2 forms of insulin as well as active PYY forms), several more differences were discovered. Proenkephalin-B and prourocortin-3 peptides were identified in mouse but not human islets (figure 5.1B) and VGF derived peptides were found in human but not mouse islets (figure 5.14B).

Proenkephalin-B is primarily expressed in the brain [336] and produces multiple opioid receptor agonists such as α-neoendorphin and rimorphin [337, 338], both of which were found in mouse islets. To the best of my knowledge, mouse islets have not been previous shown to produce proenkephalin-B peptides. However, without many functional studies, it is unclear what the relevance of proenkephalin-B derived peptides in mouse islets might be. RNA-seq analysis of human and mouse islets did not find significant levels of opioid receptors in any islet cell type [125, 126] reducing the likelihood that proenkephalin-B peptides are involved islet cell cross-talk. Although, one study found that a proenkephalin-B derived peptide (dynorphin-B) exhibited an inhibitory effect on GSIS in perfused rat pancreata. Perhaps these proenhephalin-B peptides allow retrograde signalling of β cells to autonomic neurones via opioid receptors [339, 340]. Confirmation of opioid receptor expression on mouse pancreatic autonomic neurons would be needed to confirm this theory.

Urocortin-3 is an agonist of the type 2 corticotrophin-releasing factor receptor (CRFR2) and is postulated to be produced by β cells due to the fact that immunoreactivity for urocortin-3 overlaps with insulin in mouse islets [341]. I could not detect full length urocortin-3 in lysed mouse islets but numerous prourocortin-3 derived peptides were detected, including a fragment of urocortin-3 (Ucn3_138-160a) (figure 5.1B). All prourocortin-3 derived peptides were only detected in FACS purified β cells confirming their production in this islet cell type (figure 5.8). Previous studies have already assessed the functional relevance of urocortin-3 in β cells and deem it to have paracrine and indirect autocrine activity. Urocortin-3 inhibits SST-14 secretion, and CRFR2 expression is found exclusively on δ cells in mouse islets [125, 342]. By dampening SST-14 secretion, urocortin-3 can indirectly boost GSIS and glucagon secretion [341, 343].

VGF and its derived peptides are predominantly found in the brain, the adrenal glands and pituitary glands [344] and play roles in energy expenditure, fat storage [345] and memory formation [346]. They have also been identified in IBMX + glucose stimulated human islets [166]. Numerous VGF peptides were found in lysed human islets (figure 5.14B) several of which are annotated as active peptides including neuroendocrine regulatory peptide-2 (VGF_310-347). The relevance of the presence of VGF derived peptides in human islets remains a mystery especially as the receptors for these active VGF-derived peptides are not known. Although, neuroendocrine regulatory peptide-2 is thought to target the orexin receptor [347, 348].

5.4.2 Intra-islet GLP1 receptor agonists

After characterising the human and mouse islet peptidome through untargeted MS methods (data-dependent acquisition), I used product ion scans to specifically search for proGIP peptides as well as forms of GLP-1 to clarify the issue of production of intra-islet GLP1 receptor agonists. Three proGIP-derived peptides, (Gip_22-43, GIP (1-30) and GIP (1-42)) were searched for but were undetectable (figures 5.5-5.7). These 3 proGIP peptides were abundant in mouse duodenal enteroendocrine cells (figures 5.5 A & C, 5.6 A & C, 5.7 A & C). GIP (1-30) and GIP (1-42) have been previously shown to be produced by mouse islets although these data were based on antibody-dependent methods [164, 302]. Seeing as islets express the same processing enzymes as many enteroendocrine cells (PC1/3, PC2 and carboxypeptidases), these 3 proGIP peptides should be present in islets if they produced proGIP. The likelihood that all peptides are undetectable due to shortfalls in our methodology such as ion suppression during ionisation or poor recovery during peptide extraction is extremely low. The more likely scenario is that GIP (1-30) and other proGIP peptides are below the limit of quantitation in our assay or simply not present in islets. I favour the later explanation due to the lack of transcriptomic evidence of *Gip* expression in islets.

Using targeted MS methods, both forms of active GLP-1 (GLP-1 (7-36 amide) and GLP-1 (7-37)) were found in mouse islets. I attempted to assign a concentration to both GLP-1 (7-36 amide) and glucagon by reading off a standard curve for these peptides, however all values for GLP-1 (7-36 amide) and GLP-1 (7-37) were below the lower limit of quantitation (figure 5.3C). Therefore, I can only report that the islet contents of GLP-1 (7-36) and GLP-1 (7-37) are likely to be lower than 0.08 pg/islet, ~2900-fold lower than the islet content of glucagon. It is worth noting however than Traub et al. also calculated that the glucagon content of mouse islets was around 2800-fold higher than active GLP-1 [308]. Although, Traub et al. utilised immunoassays to quantify glucagon and GLP-1 in islet lysates and so may have overestimated GLP-1 content if the antibodies used were not specific for the 7-36 amide

form. In any case, mouse islets do produce GLP-1 (7-36 amide) but at extremely low levels when compared to glucagon

Despite the low levels of active GLP-1, there does seem to be an intra-islet source of GLP1 R agonist, as blockade of the GLP1 receptor during a static islet secretion reduced GSIS (figure 5.4A), a result seen in many previous studies [298, 308, 310]. GLP-1 (7-36 amide) and (7-37) are thought to be equipotent at the GLP1 R and therefore both these peptides could be the basis for the intra-islet GLP1 R agonism [349]. Estimations for the difference in potency between active GLP-1 and glucagon vary but it is thought that active GLP-1 is 100-400 fold more potent at the GLP1 receptor than glucagon [298, 350, 351]. I estimate that glucagon at least ~2900 fold more abundant in mouse islets than either of the two active GLP-1 forms. Therefore, I reach the same conclusion as Svendsen et al., that the intra-islet "incretin effect" witnessed during islet secretion experiments is a result of glucagon acting on the GLP1 R and not GLP-1 (7-36a) [298]. My estimations of the abundance of the two active versions of GLP-1 should be treated with some caution as these two peptides could not be quantified as their abundance was below the lower limit of quantitation. I can only comment that they were each <0.08 pg/islet. Validation of the quantification methods is needed. I am sceptical about the relevance of any intra-islet GLP-1 (7-36 amide) in mice and instead hypothesise that it is produced more by 'accidental' processing of proglucagon than through active synthesis. This is based on the fact that GLP-1 (7-36 amide) is less abundant than the other forms of GLP-1 (figure 5.3B) and it seems unlikely that a cell would not have evolved to maximise the production of such an integral hormone. As α cells produce much proglucagon and express low levels of PC1/3, it seems inevitable that some active GLP-1 will be produced

I next obtained human islets to perform similar peptidomic analysis. All forms of GLP-1 were detectable using the non-targeted data-dependent acquisition method. When calculating the human islet content of glucagon and active GLP-1 in pg/IEQ using standard curves, glucagon appeared to be 373 (±226) and 1954 (±1309) more abundant than GLP-1 (7-36 amide) or GLP-1 (7-37) respectively. I am sceptical to directly compare the islet content of glucagon and active GLP-1 in humans to mice due to a number of factors. Firstly, different methods were used to quantify islet volume for humans and mice. Furthermore, human islet samples spent considerably longer in storage before being processed than mouse islet samples. It is possible that during storage, ex vivo degradation occurred reducing the abundance of islet hormones such as glucagon. These confounding factors make direct comparisons between the human and mouse islets tricky.

Having said this it would appear that GLP-1 (7-36 amide) is more prevalent in human than in mouse islets. Relative to the peak area of other proglucagon derived peptides, GLP-1 (7-36 amide) was 285 (±165) fold lower than glucagon (figure 5.15A) whereas in mice it was 785 (±239) fold lower than

glucagon. These two figures are significantly different when statistical comparison using an unpaired t test was made (p=0.0002). As started in the previous paragraph, there are confounding factors that make a direct comparison between my data on human and mouse islets difficult. However, as other studies find that active GLP-1 is more prevalent in human than mouse pancreases [307, 311], I am more confident that my finding of increased GLP-1 (7-36 amide) relative to glucagon in human islets than in mouse islets is an accurate reflection of the differences in the peptidome of these two species of islet.

It seems conclusive now that human islets produce active GLP-1 but whether this peptide is responsible for the intra-islet "incretin" effect seen in human islet secretion experiments is not clear [310, 311]. Unfortunately, from my data it is difficult to conclude whether the hormone causing this intra-islet "incretin" effect is likely to be active GLP-1 or glucagon due to the large error margins in the estimation of their abundance. In theory, active GLP-1 and glucagon could be sufficiently abundant to activate the GLP1 R as my estimates for the difference in abundance of active GLP-1 and glucagon are within the range of difference in potencies of these peptides at the GLP1 R [350, 351]. The wide error margins in my estimates for the abundance of active GLP-1 and glucagon could have resulted from the variability in the purity of each sample, differing ages/genders of the donors and the time spent in storage prior to processing. The purity of islets in each sample ranged from 25-90% (table 5.1) meaning there was great variability in the abundance of contaminating cell types. Although each sample contained the same number of IEQ, the efficiency of lysing and percentage recovery of peptides could differ between each sample due to differences in the abundance of biological material resulting in greater variability. Additionally, extrapolating the curves for glucagon and GLP-1 (7-36 amide) to estimate concentrations could have introduced error in these values (figure 5.15C & D) as I made the assumption that the relationship between peak area and concentration is linear beyond the limits of the standard curves.

5.4.3 Peptidomics of mouse α, β and δ cells

To analyse the peptidomic differences between mouse islet cell types, I purified α, β and δ cell populations by FACS and analysed the cell lysates by LC-MS. Hierarchical clustering was used to ascertain the cell population each peptide is predominantly produced by, and then a PCA plot was used to visualise different clusters. Based on the data, each peptide was assigned to one of 6 clusters. Four of these clusters were largely defined by peptides derived from one of the following major islet prohormones; proinsulins and proIAPP, proglucagon, prosomatostatin and proPPY and the last two clusters contain a mixture of granin and processing enzyme derived peptides and are not attributed

to one cell type. It was unsurprising to have a cluster defined by each of proinsulin, proglucagon and prosomatostatin derived peptides seeing as the α, β and δ populations were actively separated by FACS, however, the appearance of a cluster defined by proPPY peptides is a little odd. Its presence on the PCA plot (figure 5.8C) suggests that the α and δ cell population produce similarly low levels of proPPY derived peptides. Other peptidomic similarities between α and δ cells included Nec2 (PC2) and proPYY derived peptides. Furthermore, an intermediary population between β and δ cells eludes to the fact that these cell types have some peptidomic similarities including Scg1, Scg2, ChgA and Nec1 derived peptides. Although several peptides were similarly abundant in β and α cells, it appears that these two cell types are peptidomically very different as very few peptides fell into this intermediary β/α cell cluster. Taken together, it seems there is some overlap in the peptidome of δ cells with the other two cell types but the peptidomes of α and β cells are quite distinct.

There were some drawbacks to the methodology and analysis which should be noted. Firstly, even though cell doublets are gated out during FACS, it is impossible to rule out the possibility that some doublets were missed in this gate therefore some of the "cells" sorted were actually doublets of two different cell types. Furthermore, there may be a bias towards the β cell population due to the larger cell volume of β cells compared to α and δ cells. Therefore, the analysis could be skewed by this bias and peptides may not be enriched in β cells, but simply more abundant due to the greater amount of cellular material collected from FACS purified β cells. Lastly, as very few granin derived peptide were assigned to any of the α cell related clusters in figure 5.8, it could be concluded that α cells don't possess granin derived peptides. This was not the case as many granin-derived peptides were detected in FACS purified α cells, but at much lower levels than the other 2 cell populations.

To further assess the peptidomics of the different islet cell types, islet secretion experiments were carried out using several different stimuli. Adrenaline in the presence of 1 mM glucose was used to stimulate α cells and all proglucagon derived peptides were stimulated the strongest in this condition. PPY was also stimulated by adrenaline which is surprising seeing as the main neurotransmitter of the parasympathetic nervous system, acetylcholine, stimulates PPY secretion in islets and PPY is often measured in plasma as an indirect measure of parasympathetic activity [352-354]. It seems counterintuitive therefore that sympathomimetics should stimulate release of PPY and to the best of my knowledge this effect has not been described elsewhere. Although, one study using perifused fragments of chicken pancreas found that 3 adrenergic receptor agonists stimulated PPY secretion [355]. However, in this study by Meglasson et al. the kinetics of PPY release were extremely slow and maximal release of PPY was not reached till between 10-20 min post application of stimulant calling into question the identity of the product they were measuring. Insulin and IAPP related

peptides were secreted very strongly by 16.7 mM glucose but no other condition whilst SST-14 secretion was mildly stimulated 16.7 mM glucose. This is slightly different from the expected secretion pattern of SST-14 as it is reported that SST-14 secretion is stimulated even at 6mM glucose [356]. It is likely that the wide error margins in my data make it difficult to confidently discern fold changes in SST-14 secretion between 1 mM and 6 mM glucose conditions.

Interestingly, different products of proPYY exhibit different patterns of secretion. Secretion of PYY (1-36) and (3-36) is only induced moderately by 16.7 mM glucose whilst secretion of a C-terminal fragment is stimulated by both 16.7 mM and by adrenaline. This suggests the possibility that active forms of PYY are secreted by just one cell type whereas the C-terminus is secreted by multiple. ProPYY derived peptides were detected in both FACS purified α and δ cells although appeared to be more abundant in the δ cell population. Nevertheless, this indicates that both α and δ cells can produce proPYY peptides and from this secretion data it seems as though there is a difference in processing of this propeptide between these cell types. α cells (or possibly PP cells based on the fact that adrenaline also stimulates PPY) and δ cells secrete both the C- and N-termini whereas only δ cells secrete active PYY. Differences in the processing of other propeptides between cell types can be seen in this data. ChgA_435-462a and ChgA_374-402 are only secreted in response to 16.7 mM glucose indicating release from β or δ cells. However, ChgA_358-371 is secreted in response to adrenaline and at 16.7 mM glucose suggesting release from α or PP cells as well as β or δ cells. As there is overlap between the cell types stimulated by the different conditions, more as well as more-specific stimuli are needed to discern the cell types from which some of these peptides are being primarily released. For example, ghrelin could be used to selectively stimulate the δ cell population [125]. I avoided using ghrelin or ghrelin receptor agonists as these secretagogues could be retained by the extraction methods and therefore overload the nano-LC column when loaded onto it. This would cause issues such as ion suppression and compromise data acquisition. Small molecules are not precipitated by the ACN crash and the SPE plate used retains molecules that have low pKa values in acidic conditions (this is not an issue for adrenaline as the pKa is high in acidic conditions). Therefore, ghrelin and ghrelin receptor agonists were avoided.

I should note that this secretion data highlights an issue with analysis of the peptidomics of FACS purified α, β and δ cells. In the secretion peptidomics data, secretion of the C-terminus of proPYY appears to be induced by adrenaline and 16.7 mM glucose indicating release from several different cell types. The same can be said for ChgA_358-371. However, in the peptidomics analysis of FACS purified islet cells, the C-terminus of proPYY appears to only be found in δ cells whereas ChgA 358-371 appears to only be in β cells. This is misleading as these peptides were found in other cell types and so the analysis of FACS purified islet cells should be treated with caution.

5.4.4 Peptidomic assessment of metabolically stressed islets

After characterising the peptidome of healthy islets and peptidomic differences between 3 of the major islet cell types, I applied the same methods to assess how the islet peptidome is altered when metabolically stressed. First of all, islets from a mouse model of obesity were assessed. Islets from DIO mice seemed to have a higher content of many proinsulin and proIAPP-derived peptides than their lean controls (figure 5.12D & 5.13A). This could indicate an increase in the islet β cell population which is in line with previous literature [357]. Although it should be noted that I am unable to attribute any changes in the peptidome of DIO islets to β cell hyperplasia islets due to my methodology. Islets from DIO mice were size matched with their lean controls as a method of normalising the data. Therefore I would have negatively selected against larger islets that may exhibit hyperplasia of β cells by trying to obtain the same proportions of islet sizes in all samples. Despite this, I did observe a significant increase in many proinsulin derived peptides and so some changes did seem to be induced in DIO islets independent of β cell hyperplasia. The hyperglycaemia exhibited by the DIO mice may be increasing the expression of *Ins1* and *Ins2* as these genes have been shown to respond to circulating glucose levels [358]. Furthermore, the growing demand for insulin to control the hyperglycaemia may be leading to increased misprocessing of proinsulins as a result of the increased stress on the endoplasmic reticulum (figure 5.13A). Together, increased expression of *Ins1* and Ins2 as well as increased misprocessing of insulin may account for why the levels of correctly processed levels of insulins are unchanged but levels of proinsulins are increased (figure 5.13A).

Aside from β cells, no other islet cell type seems to be peptidomically altered in DIO mice as the islet contents of glucagon, PPY and SST-14 were unchanged (figure 5.12E). This backs up transcriptomic data from Dusaulcy et al. who did not find any major transcriptomic differences in α cells between DIO mice and lean controls [320]. However, to the best of my knowledge, this is the first time δ or PP cells have been assessed in mouse model of obesity using a peptidomic based method. Further studies using alternative approaches to assess δ or PP cells such as transcriptomics or immunofluorescence are needed to confirm my findings for these cell types.

It should be noted though that the effect of obesity on islets varies depending on the mouse model used. Burke et al. assessed the impact of obesity on islets from DIO mice as well as *db/db* mice and compared them to their controls [357, 359]. In *db/db* mice, the glucagon content of islets increased as opposed to the DIO mice where only islet insulin content was increased. *Db/db* but not DIO mouse islets, displayed decreased expression of *Nkx6.1* which is an indicator of β cell dedifferentiation [329]. All together this indicates that when assessing the effect of metabolic stress

on islets, the *db/db* model may better resemble human T2D however the DIO model may exhibit a phenotype closer to human obesity and a pre-diabetic state.

I next assessed peptidomic differences between islets from T2D patients and non-diabetic donors. Insulin and IAPP islet contents were decreased but the islet contents of certain proglucagon-derived peptides (glucagon, oxyntomodulin, GLP-1 (7-36 amide)) was increased (figure 5.16B). No other peptidomic differences were seen between the two groups (figure 5.16D-F). This seems to corroborate the literature as it is thought that in T2D β cells undergo dedifferentiation returning to an early progenitor like-phenotype and lose their ability to produce insulin [326-328]. However these dedifferentiated β cells maintain some phenotypic markers of endocrine cells such as expression of granins and processing enzymes and so levels of peptides derived from these proteins should not be altered [326]. It is worth noting here that these conclusions from the human islet results are based on non-adjusted p values and therefore will contain some false positives.

Interestingly no increases in the amount of mis-processed insulin forms were seen in T2D islets (figure 5.17A). It is thought that additional ER stress on β cells can induce misprocessing of proinsulin and indeed elevated plasma proinsulin is a well-known indicator of insulin resistance and T2D [88, 360, 361]. However, it seems as though T2D islets in this study had transitioned into a state of β cell dedifferentiation due to the decreased levels of almost all insulin associated peptides as well as IAPP.

Another point of note is that active GLP-1 (7-36 amide) was increased in T2D islets (figure 5.16B & 5.17B) as has been described in many previous studies. What is interesting is that the ratio between glucagon and GLP-1 (7-36 amide) did not significantly change in T2D (figure 5.17C). Some studies suggest that dedifferentiated β cells take on an α cell phenotype and express *GCG* whilst maintaining high expression levels of *Pcsk1* (the gene coding for PC1/3) [326, 362]. The result of an increase in the number of cells co-expressing *GCG* and *PC1/3* cells should be an increase in GLP-1 (7-36 amide) relative to glucagon seeing as PC1/3 cleaves proglucagon to form active GLP-1. Assumption of an α cell phenotype by dedifferentiated β cells is not supported by my data because GLP-1 (7-36 amide) and glucagon seem to rise proportionally in T2D islets, although it is possible that my methods were not sensitive enough to pick up small differences in the data. It is also possible the treatments the T2D donors were taking helped to restore the proportions of islet cell types to something more similar to a non-diabetic state.

5.4.5 Normalising data to islet number

On a number of occasions throughout this chapter, the peak area of many islet derived peptides has been normalised to islet number. Although a commonly used technique to normalise the abundance

of islet derived peptides, this method is not perfect due to the heterogenicity in islet sizes and proportions of islet cell types within islets. A more robust method of normalisation is to quantify one of the following in lysates; insulin, DNA or total protein and normalise to that as this gives a more accurate representation of the cellular content in each sample. I did not try normalisation to insulin content as this only gives an idea of the β cell content of each sample and so would not be useful for normalising non-β cell peptides. I also tried normalising to protein content using a Bradford assay but the protein content of lysates of <=60 islets was below the limit of quantitation of the assay. I did not try normalising to DNA content, however.

5.4.6 Conclusions

To summarise, in this chapter the islet peptidome has been extensively studied, using extracts from whole islets, FACS purified β, α and δ cells and islet supernatants. The presence of active GLP-1 was confirmed in both mouse and human islets although the levels of these peptides were very low when compared to glucagon in mice and so its functional relevance is questionable. In humans, however, active GLP-1 may take on more relevance. Islets from DIO mice were found to display peptidomic differences only in the β cell population, whilst islets from T2D human donors were found to display differences in the peptidome of both α and β cells. Although no major new findings were uncovered, these results provide clarity over how the islet peptidome changes during metabolic stress, and refute previous suggestions that islet cells produce either GIP or high levels of active GLP-1.

Chapter 6: General discussion

6.1 Thesis summary

The peptidomic characterisation of murine and human tissue types has been central to this thesis with the aim of discovering novel bioactive peptides and uncovering peptidomic differences induced by metabolic disease. To achieve these aims several projects were undertaken. The first started off by characterising the peptidome of murine EECs and the human GI epithelium to identify promising peptide candidates. A number of peptides were synthesised, and their activity explored using various *in vitro* and *in vivo* tests. One peptide, Gast p59-79, seemed to modestly improve glucose tolerance in lean mice but not in diet-induced obese mice. Unfortunately, I could not shed light on the potential mechanism of action of this peptide as Gast p59-79 did not appear to directly alter secretion of islet hormones or alter insulin signalling in various tissue types. The second project focused specifically on characterising the islet peptidome and moved beyond trying to identify potentially novel hormones to identifying peptidomic differences induced by obesity and diabetes. In both humans and mouse islets, I was able to detect the incretin hormone GLP-1 (7-36 amide), albeit at extremely low levels. Unfortunately, no novel peptidomic differences induced by metabolic stress were detected upon analysing islets from type 2 diabetic donors and diet-induced obese mice.

In this chapter, the main findings of these projects are summarised and contextualised. Furthermore, alternative approaches to novel peptide discovery and further experiments are discussed.

6.2 Searching for novel peptides

As chapter 3 discussed, several studies have aimed to identify novel hormones through a variety of methods. Some used a computational approach [234, 237], others relied on transciptomic data to guide their candidate selection [236] and a few have performed peptidomic analyses [166, 331]. In this thesis, I aimed to identify novel hormones through a comprehensive peptidomic characterisation of the GI epithelium of humans and mice as well as the islets of Langerhans. It was hoped that analysing the peptidome of the cells known to produce hormones would enable me to select endogenously produced peptides and not theoretical peptides based on computational analysis. Therefore, FACS purified murine EECs were the main focus of chapter 3, supplemented by data from human GI epithelium, secretions from mixed GI epithelial cultures and whole mouse islets. By using a

variety of tissues, I hoped that any novel peptide hormone would be detected and therefore be within this data set. From here, I selected 13 candidates to be synthesised and characterised by *in vivo* and/or *in vitro* experiments.

It should be noted that these candidates were selected manually meaning no computational aspect guided our selection. The data was manually combed, and candidates picked out by our own knowledge of known traits of hormones. Therefore, our candidate selection is prone to human error and could have missed promising candidates. For example, we did not see the fact that the mono-basic cleavage site at the C-terminus of Gast p59-79 is not conserved in humans. While this peptide may be theoretically well conserved, it is unlikely this peptide is produced in human EECs at the same levels it is in mice and so is less likely to represent a novel peptide hormone. Gast p59-73 may have been a better candidate as the dibasic cleavage site at its C-terminus is conserved in humans.

Despite errors in the candidate selection, the dataset still represents a comprehensive overview of the peptidome of human and mouse endocrine tissue in the GI tract. It represents a vast improvement on previous studies which have sought to characterise the peptidome of EECs due to the preventative methods used to prevent post-sample collection degradation of peptides and breadth of tissue types analysed [82, 363]. A manuscript is currently in preparation which will detail the processing of all prohomornes, granins and processing enzymes found in murine EECs and human GI epithelium. Much of the data has already been made available online to the ProteomeXchange Consortium via the PRIDE partner repository (identifiers PXD009788 (10.6019/PXD009788) and PXD009796 (10.6019/PXD009796)) [193]. It is hoped that other studies may be able to use this data to guide their search for novel peptide hormones. Machine learning algorithms such as artificial neural networks (ANNs) are making great advances across in peptidomics and proteomics [256, 257]. With the right expertise, ANNs could be trained using our peptidomic data set to search for novel peptide hormones which exhibit similar characteristics to known hormones. Machine learning algorithms can avoid the pitfalls of other computational methods such as those used by Samson et al. as they will not be restricted to look for peptides fitting a static and restrictive set of criteria [234]. Instead, ANNs can adapt based on the training data they are supplied. In theory, they could incorporate traits found in our peptidomic data set such as the presence of a clear cleavage site to guide its candidate selection. Therefore, machine learning algorithms represent a great opportunity for the identification of novel peptide hormones and future studies could utilise our data to train their algorithms.

6.3 Characterising activity of novel hormones

In chapter 4 the peptides selected in chapter 3 were synthesised and simultaneously characterised *in vitro* and *in vivo*. Ideally, all novel agents would be screened extensively *in vitro* to identify receptors, enzymes, ion channels etc. which these agents may target. That way an idea of the whole-body effects of the agent could be gauged before administering to animals and so studies could be designed and powered to pick up these physiological effects and unwanted side effects might be predicted. However, such *in vitro* testing requires high-throughput screening platforms with vast libraries of GPCRs, ion channel, enzymes and other targets. These platforms are not widely available and therefore to get the same exposure to an array of targets, the next best screening platform is an animal model. Administration of the agent to the circulation can expose it to all tissue types and provide a fast answer to if the agent is biologically active. An interaction with a receptor/enzyme during high-throughput *in* vitro testing is meaningless if that agent shows no efficacy during *in vivo* testing. The only high throughput screening assays available were to test for Gs or Gi activity in various cell lines. However, these assays are narrow in that peptides acting through alternate signalling pathways such as G_q, ERK, β-arrestin would be missed. Therefore, in the absence of any high-throughput binding assays or thorough activity efficacy screening assays, I opted to administer the peptides *in vivo* to assess their ability to control food intake and glucose tolerance.

6.4 Is Gast p59-79 a gut hormone?

One of the novel peptides, Gast p59-79, was shown to improve glucose tolerance in lean mice but no mechanism of action of this peptide could be found despite several follow up tests. Therefore, despite the fact that Gast p59-79 satisfies several characteristics of a novel hormone (highly expressed in the tissue type its predominantly found in as well as being secreted in response to a stimulus) it is a long way off being considered as a novel gut hormone. A specific receptor and cell type that Gast p59-79 is targeting needs to be identified and the physiological role of Gast p59-79 should be investigated. Although Gast p59-79 did improve glucose tolerance, this was only an extremely modest effect and so whether this is physiologically relevant is unclear. If a receptor could be identified then an antagonist could be used to block the receptor during an intraperitoneal (IP) GTT and therefore the physiological role of Gast p59-79 could be examined. This is provided that no other hormones also target the same receptor.

Finding the specific target of Gast p59-79 may prove tricky as high throughput binding screens are not financially feasible (discussed above) but if the specific tissue or cell type Gast p59-79 is acting

on could be identified then this may help narrow it down. To that end, I assessed if Gast p59-79 could improve glucose tolerance by either altering insulin sensitivity in various tissue types or directly affecting secretions from islets. No effect of Gast p59-79 was seen in any of these tissue types. Perhaps further experiments could focus on how Gast p59-79 indirectly affects secretions from islets. A very similar study to the osmotic pump studies performed in chapter 4 could be performed where a glucose tolerance test is performed on mice receiving Gast p59-79 or vehicle but blood samples are taken to assess if levels of islet hormones such as insulin, glucagon and somatostatin-14 are altered by Gast p59-79 infusion. Although it is speculative, perhaps Gast p59-79 is having a similar indirect effect on islets to the autonomic nerves system (ANS). The ANS controls blood flow to the islets thereby regulating hormone release [149]. By assessing levels of islet hormones in the circulation in mice infused with Gast p59-79, evidence of this indirect effect may be gained.

Another experiment which may add weight to the argument that Gast p59-79 is a novel hormone is measuring the endogenous levels of this peptide in plasma. For this, a more sensitive assay to quantify Gast p59-79 would be needed as my LC-MS based method could not detect Gast p59-79 below 10 nM and endogenous gut hormones often peak in the circulation at <100 pM [364]. Such an assay could help identify the physiological stimuli required to induce the release of this peptide and may shed light on the potential physiological role of the peptide.

In summary, many further experiments to identify the target of Gast p59-79 and then to assess physiological role of this peptide are needed before it can be considered as a gut hormone.

6.5 Therapeutic use of Gast p59-79

Gast p59-79 infused lean mice exhibited a modest improvement in glucose tolerance. Therapies based on other gut hormones that improve glucose tolerance such as GLP-1 have been developed for the treatment of obesity and diabetes and so I will briefly discuss if Gast p59-79 has any therapeutic potential. In short, probably not. If we thought the road to proving Gast p59-79 is a novel gut hormone is long, it is nothing compared to the journey necessary to develop Gast p59-79 as a therapeutic. First of all, its therapeutic effect was marginal and only induced an extremely modest improvement in glucose tolerance in lean mice. In comparison, exenatide induced a much larger improvement in glucose tolerance. Whilst we did not observe any effect on food intake of exenatide, its ability to induce weight loss and reduce food intake is well characterised and is therefore extremely useful therapeutically in treating the co-morbidities of diabetes and obesity. Gast p59-79 does not have this advantage. Furthermore, Gast p59-79 was not efficacious in an obese model meaning it is unlikely to

have any therapeutic use in type 2 diabetic (T2D) individuals as this disease is associated with obesity. Type 1 diabetic (T1D) individuals may benefit from Gast p59-79 as this disease is not associated with obesity. More information is needed as to whether insulin is required for the the mechanism of action of Gast p59-79 as T1D lack active circulating insulin. In summary, due to a small therapeutic effect and lack of efficacy in obese mice, the therapeutic potential of Gast p59-79 is almost non-existent.

6.6 Intra-islet incretins and implications

In chapter 5, I use targeted LC-MS/MS methods to search for incretins such as GIP and GLP-1 in islets. The presence of an intra-islet incretin is indisputable as *in vitro* studies have consistently proved that pharmacological blockade of the GLP1 receptor on islets from humans and mice leads to a decrease in glucose stimulated insulin secretion (GSIS) [298, 308, 310]. However, the identity of this incretin has been of some dispute with studies claiming active GLP-1 is produced in abundance in islets and therefore must be the primary intra-islet incretin [163, 307]. Others propose glucagon [298] or GIP [164, 302] could be this intra-islet incretin. By performing an LC-MS/MS analysis of human and mouse islets, I hoped to be able to shed light on this debate by removing the issue of antibody promiscuity in the detection and quantification of these incretin 'candidates'. I concluded that in mouse islets, glucagon is likely to be the primary peptide acting on the GLP1 receptor to enhance GSIS. However, due to wide error margins in the estimations of glucagon and GLP-1 human islet content and the difference in potency between these two peptides at the GLP1 receptor [298, 350, 351], I could not say which peptide may be the primary intra-islet incretin in humans. Further experiments could resolve which of glucagon or GLP-1 (7-36 amide) is more important for this intra-islet incretin effect in human islet by using an antibody to immunoneutralise glucagon in *in vitro* islet secretion experiments. With glucagon selectively neutralised, the role of the GLP1 receptor in GSIS could be assessed and therefore clarifying the identity of the intra-islet incretin.

It is important to discuss the implication of an intra-islet incretin in glucose homeostasis. GLP-1 (7-36 amide) is primarily released from L-cells of the distal intestines but is degraded rapidly to the antagonistic version GLP-1 (9-36 amide) by dipeptidyl peptidase IV (DPP-IV) [365]. Consequently, it could be that very little intestinally derived GLP-1 (7-36 amide) reaches the islets [288]. Therefore, the presence of an intra-islet incretin may be crucial to the maintenance of glucose homeostasis. This is the stance taken by Chambers et al. in their controversial paper in 2017 [366]. In this paper, the authors reactivated *Gcg* expression in intestines versus the pancreas of *Gcg* $^{-/-}$ mice and then infused an antagonist at the GLP-1 receptor (exendin 9-39) to these mice to assess the importance of *Gcg* expression in these two tissue types in glucose tolerance. They found that exendin (9-39) was able to

impair glucose tolerance during oral and IP GTTs when *Gcg* was reactivated in the pancreas but not upon intestinal *Gcg* reactivation. Although the finding that intestinal derived proglucagon peptides were unimportant for glucose tolerance have been rebutted by data from the same laboratory [307], the findings by Chambers et al. do highlight the importance of an intra-islet incretin in maintenance of glucose homeostasis. Zhu et al. also highlight the importance of an intra-islet incretin in the glucose homeostasis by using a G_i-coupled designer receptor exclusively activated by designer drugs (DREADD) expressed selectively in α cells [292]. Activation of this G_i coupled DREADD in α cells during an IP GTT resulted in impaired glucose tolerance. Therefore, despite the fact that active GLP-1 and GIP are primarily produced in the intestines, intra-islet incretins still play a crucial role in glucose homeostasis.

6.7 Lessons from peptidomics of metabolically stressed islets

In chapter 5, islets from T2D individuals were peptidomically compared to non-diabetic donors in order to understand how this metabolic disorder alters the islet peptidome. The only peptidomic alterations found in T2D islets were those that were already well characterised (proglucagon derived peptides increase, insulin content decreases) [311, 326-328, 362]. Although this was a little disappointing, it is hoped that this slight advancement in the knowledge will ultimately lead to a better understanding of how T2D affects the islets and enable better treatments for individuals afflicted by this disease.

I also compared the peptidome of islets from diet-induced obese (DIO) mice and lean mice. The results from this study highlight how mice and humans can respond very differently to a caloric excess and metabolic stress. A chronic caloric excess and hyperglycaemia can induce T2D in humans leading to a loss of β cell mass and an increase in the α cell mass of the islet (as highlight in previous paragraph). In mice, a chronic caloric excess and hyperglycaemia (similar to that induced in my DIO mouse study) seems to induce a different phenotype at the level of the islet. The content of β cell associated peptides seems to increase whereas the content of α cell associated peptides is unaltered. Findings by Burke et al. seem to support this as even after 20 weeks on a HFD, DIO mouse islets did not exhibit similar phenotypic markers of human diabetes [357]. Instead, *db/db* mouse islets (leptin receptor deficient mice) seemed to exhibit more similarities to human T2D islets as these *db/db* mouse islets exhibited increases in markers of β cell dedifferentiation and numbers of α cells. This coupled with slight differences in the peptidome of humans and mice (mouse islets produce PYY, human islets seem to produce more active GLP-1 relative to glucagon) means that care should be taken when using mouse islets in lieu of humans to study the biology of islets.

6.8 Mass spectrometry in peptidomics

LC/MS has been a common theme throughout this thesis and has been used for a variety of functions. In chapters 3 and 5 a broad peptidomic analysis of the endocrine components of murine and human pancreas and GI tract was performed. These analyses were performed using almost identical methods, but the purpose of the data was very different. The peptidomic analysis performed in chapter 3 was to identify novel peptides, however, the analysis in chapter 5 was focused on detecting peptidomic differences induced by a disease state. This demonstrates the data obtained by almost identical methodologies can be multi-functional and used to address different biological questions. Furthermore, by using the same extraction methodology but tweaking the analysis settings on the mass spectrometer (product ion scans as opposed to data-dependent acquisition) or by using a different instrument (using a triple quadrupole mass analyser instead of an Orbitrap mass analyser), the focus of the data analysis can be shifted to targeted peptide identification and quantification. Further tweaking the methodology to introduce a standard curve and stable isotope labelled peptides enables absolute quantification of peptides. Therefore LC/MS can serve a similar quantitative purpose to ELISAs or RIAs but without the issues of antibody promiscuity and off-target binding.

Overall, LC/MS is an invaluable technology in the field of peptidomics capable of providing information on peptide or protein sequences, post-translational modifications and abundance for potentially 1000s of peptides in a single sample. I sincerely hope I have been able to utilise it to close to its full potential in this thesis and provide new insights into the peptidome of the endocrine pancreas and GI tract.

6.9 Concluding remarks

This thesis has focused heavily on the peptidomics analysis of various tissue types. I first characterised the peptidome murine EECs and the human GI epithelium in the hope of identifying novel gut hormones. The data and analysis from this study is being published and made available to the wider scientific community. It is hoped that future studies seeking to identify novel peptides could utilise this data set to help guide their search. Several promising candidates were synthesised and tested *in vivo* and/or *in vitro* with one peptide showing promise in *in vivo* studies by slightly improving glucose tolerance in lean mice. Much work needs to be done however before this peptide could be considered a novel hormone though. Lastly, the peptidome of islets were analysed in detail shedding new light on intra-islet cross talk and hormonal changes induced by metabolic stress. I hope that this thesis

advances the knowledge surrounding the peptidome of the endocrine pancreas and gut truly showcases the power of LC-MS in the field of peptidomics.

References

1. OpenStax. *Anatomy & Physiology*. 2016; Available from: https://cnx.org/contents/FPtK1zmh@8.25:Qw2OWvaZ@4/The-Small-and-Large-Intestines.
2. Rao, M. and M.D. Gershon, *The bowel and beyond: the enteric nervous system in neurological disorders.* Nat Rev Gastroenterol Hepatol, 2016. **13**(9): p. 517-28.
3. Furness, J.B., *The enteric nervous system and neurogastroenterology.* Nat Rev Gastroenterol Hepatol, 2012. **9**(5): p. 286-94.
4. Dockray, G.J., *Enteroendocrine cell signalling via the vagus nerve.* Current Opinion in Pharmacology, 2013. **13**(6): p. 954-958.
5. Brubaker, P.L. and Y. Anini, *Direct and indirect mechanisms regulating secretion of glucagon-like peptide-1 and glucagon-like peptide-2.* Can J Physiol Pharmacol, 2003. **81**(11): p. 1005-12.
6. Sandoval, D., et al., *Impact of intestinal electrical stimulation on nutrient-induced GLP-1 secretionin vivo.* Neurogastroenterology & Motility, 2013. **25**(8): p. 700-e513.
7. Furness, J.B., et al., *The enteric nervous system and gastrointestinal innervation: integrated local and central control.* Adv Exp Med Biol, 2014. **817**: p. 39-71.
8. Gehart, H. and H. Clevers, *Tales from the crypt: new insights into intestinal stem cells.* Nat Rev Gastroenterol Hepatol, 2019. **16**(1): p. 19-34.
9. Kim, T.H. and R.A. Shivdasani, *Stomach development, stem cells and disease.* Development, 2016. **143**(4): p. 554-65.
10. Barker, N., et al., *Identification of stem cells in small intestine and colon by marker gene Lgr5.* Nature, 2007. **449**(7165): p. 1003-7.
11. Flanagan, D., et al., *Wnt Signalling in Gastrointestinal Epithelial Stem Cells.* Genes, 2018. **9**(4): p. 178.
12. Valenta, T., et al., *Wnt Ligands Secreted by Subepithelial Mesenchymal Cells Are Essential for the Survival of Intestinal Stem Cells and Gut Homeostasis.* Cell Rep, 2016. **15**(5): p. 911-918.
13. Stzepourginski, I., et al., *CD34+ mesenchymal cells are a major component of the intestinal stem cells niche at homeostasis and after injury.* Proc Natl Acad Sci U S A, 2017. **114**(4): p. E506-E513.
14. Crosnier, C., et al., *Delta-Notch signalling controls commitment to a secretory fate in the zebrafish intestine.* Development, 2005. **132**(5): p. 1093-104.
15. Sato, T., et al., *Paneth cells constitute the niche for Lgr5 stem cells in intestinal crypts.* Nature, 2011. **469**(7330): p. 415-8.
16. Wong, V.W., et al., *Lrig1 controls intestinal stem-cell homeostasis by negative regulation of ErbB signalling.* Nat Cell Biol, 2012. **14**(4): p. 401-8.
17. Pines, G., W.J. Köstler, and Y. Yarden, *Oncogenic mutant forms of EGFR: Lessons in signal transduction and targets for cancer therapy.* FEBS Letters, 2010. **584**(12): p. 2699-2706.
18. He, X.C., et al., *BMP signaling inhibits intestinal stem cell self-renewal through suppression of Wnt-beta-catenin signaling.* Nat Genet, 2004. **36**(10): p. 1117-21.
19. Kosinski, C., et al., *Gene expression patterns of human colon tops and basal crypts and BMP antagonists as intestinal stem cell niche factors.* Proc Natl Acad Sci U S A, 2007. **104**(39): p. 15418-23.
20. Haramis, A.P., et al., *De novo crypt formation and juvenile polyposis on BMP inhibition in mouse intestine.* Science, 2004. **303**(5664): p. 1684-6.
21. Hardwick, J.C., et al., *Bone morphogenetic protein 2 is expressed by, and acts upon, mature epithelial cells in the colon.* Gastroenterology, 2004. **126**(1): p. 111-21.
22. Barker, N., et al., *Lgr5(+ve) stem cells drive self-renewal in the stomach and build long-lived gastric units in vitro.* Cell Stem Cell, 2010. **6**(1): p. 25-36.

23. Bartfeld, S. and B.K. Koo, *Adult gastric stem cells and their niches.* Wiley Interdiscip Rev Dev Biol, 2017. **6**(2).
24. Hayakawa, Y., et al., *Mist1 Expressing Gastric Stem Cells Maintain the Normal and Neoplastic Gastric Epithelium and Are Supported by a Perivascular Stem Cell Niche.* Cancer Cell, 2015. **28**(6): p. 800-814.
25. Stange, D.E., et al., *Differentiated Troy+ chief cells act as reserve stem cells to generate all lineages of the stomach epithelium.* Cell, 2013. **155**(2): p. 357-68.
26. Demitrack, E.S., et al., *Notch signaling regulates gastric antral LGR5 stem cell function.* EMBO J, 2015. **34**(20): p. 2522-36.
27. van den Brink, G.R., et al., *Sonic hedgehog regulates gastric gland morphogenesis in man and mouse.* Gastroenterology, 2001. **121**(2): p. 317-28.
28. Li, Q., S.M. Karam, and J.I. Gordon, *Diphtheria toxin-mediated ablation of parietal cells in the stomach of transgenic mice.* J Biol Chem, 1996. **271**(7): p. 3671-6.
29. Bellusci, S., et al., *Fibroblast growth factor 10 (FGF10) and branching morphogenesis in the embryonic mouse lung.* Development, 1997. **124**(23): p. 4867-78.
30. Nyeng, P., et al., *FGF10 signaling controls stomach morphogenesis.* Dev Biol, 2007. **303**(1): p. 295-310.
31. Goodlad, R.A., et al., *Proliferative effects of urogastrone-EGF on the intestinal epithelium.* Gut, 1987. **28 Suppl**: p. 37-43.
32. Giannakis, M., et al., *Molecular properties of adult mouse gastric and intestinal epithelial progenitors in their niches.* J Biol Chem, 2006. **281**(16): p. 11292-300.
33. Schubert, M.L., *Gastric exocrine and endocrine secretion.* Curr Opin Gastroenterol, 2009. **25**(6): p. 529-36.
34. Wilkes, J.M., et al., *Muscarinic responses of gastric parietal cells.* J Membr Biol, 1991. **122**(2): p. 97-110.
35. Cherner, J.A., et al., *Functionally distinct receptors for cholecystokinin and gastrin on dispersed chief cells from guinea pig stomach.* Am J Physiol, 1988. **254**(2 Pt 1): p. G151-5.
36. Dockray, G.J., *Topical review. Gastrin and gastric epithelial physiology.* J Physiol, 1999. **518 (Pt 2)**: p. 315-24.
37. Kopin, A.S., et al., *Expression cloning and characterization of the canine parietal cell gastrin receptor.* Proc Natl Acad Sci U S A, 1992. **89**(8): p. 3605-9.
38. Raufman, J.P., et al., *Pepsinogen secretion from dispersed chief cells from guinea pig stomach.* Am J Physiol, 1984. **247**(1 Pt 1): p. G95-104.
39. Raufman, J.P. and L. Cosowsky, *Interaction between the calcium and adenylate cyclase messenger systems in dispersed chief cells from guinea pig stomach. Possible cellular mechanism for potentiation of pepsinogen secretion.* J Biol Chem, 1987. **262**(13): p. 5957-62.
40. Schubert, M.L., *Regulation of gastric acid secretion.* Curr Opin Gastroenterol, 1999. **15**(6): p. 457-62.
41. Kellett, G.L., et al., *Sugar absorption in the intestine: the role of GLUT2.* Annu Rev Nutr, 2008. **28**: p. 35-54.
42. Ma, T. and A.S. Verkman, *Aquaporin water channels in gastrointestinal physiology.* J Physiol, 1999. **517 (Pt 2)**: p. 317-26.
43. Giammanco, A., et al., *The pathophysiology of intestinal lipoprotein production.* Front Physiol, 2015. **6**: p. 61.
44. Yu, Q.H. and Q. Yang, *Diversity of tight junctions (TJs) between gastrointestinal epithelial cells and their function in maintaining the mucosal barrier.* Cell Biol Int, 2009. **33**(1): p. 78-82.
45. Gerbe, F., et al., *Intestinal epithelial tuft cells initiate type 2 mucosal immunity to helminth parasites.* Nature, 2016. **529**(7585): p. 226-30.
46. Kaske, S., et al., *TRPM5, a taste-signaling transient receptor potential ion-channel, is a ubiquitous signaling component in chemosensory cells.* BMC Neurosci, 2007. **8**: p. 49.

47. Andreu, P., et al., *A genetic study of the role of the Wnt/beta-catenin signalling in Paneth cell differentiation.* Dev Biol, 2008. **324**(2): p. 288-96.
48. Gassler, N., *Paneth cells in intestinal physiology and pathophysiology.* World J Gastrointest Pathophysiol, 2017. **8**(4): p. 150-160.
49. Ayabe, T., et al., *Secretion of microbicidal alpha-defensins by intestinal Paneth cells in response to bacteria.* Nat Immunol, 2000. **1**(2): p. 113-8.
50. Satoh, Y., et al., *Carbamylcholine- and catecholamine-induced intracellular calcium dynamics of epithelial cells in mouse ileal crypts.* Gastroenterology, 1995. **108**(5): p. 1345-56.
51. Durand, A., et al., *Functional intestinal stem cells after Paneth cell ablation induced by the loss of transcription factor Math1 (Atoh1).* Proc Natl Acad Sci U S A, 2012. **109**(23): p. 8965-70.
52. Gregorieff, A., et al., *Expression pattern of Wnt signaling components in the adult intestine.* Gastroenterology, 2005. **129**(2): p. 626-38.
53. Sancho, R., C.A. Cremona, and A. Behrens, *Stem cell and progenitor fate in the mammalian intestine: Notch and lateral inhibition in homeostasis and disease.* EMBO Rep, 2015. **16**(5): p. 571-81.
54. Noah, T.K., B. Donahue, and N.F. Shroyer, *Intestinal development and differentiation.* Exp Cell Res, 2011. **317**(19): p. 2702-10.
55. Ambort, D., et al., *Calcium and pH-dependent packing and release of the gel-forming MUC2 mucin.* Proc Natl Acad Sci U S A, 2012. **109**(15): p. 5645-50.
56. Corfield, A.P., *Mucins: a biologically relevant glycan barrier in mucosal protection.* Biochim Biophys Acta, 2015. **1850**(1): p. 236-52.
57. Deplancke, B. and H.R. Gaskins, *Microbial modulation of innate defense: goblet cells and the intestinal mucus layer.* Am J Clin Nutr, 2001. **73**(6): p. 1131S-1141S.
58. Shirazi, T., et al., *Mucins and inflammatory bowel disease.* Postgrad Med J, 2000. **76**(898): p. 473-8.
59. Radtke, F. and H. Clevers, *Self-renewal and cancer of the gut: two sides of a coin.* Science, 2005. **307**(5717): p. 1904-9.
60. Johansson, M.E., H. Sjövall, and G.C. Hansson, *The gastrointestinal mucus system in health and disease.* Nat Rev Gastroenterol Hepatol, 2013. **10**(6): p. 352-61.
61. Johansson, M.E.V., et al., *The inner of the two Muc2 mucin-dependent mucus layers in colon is devoid of bacteria.* Proceedings of the National Academy of Sciences, 2008. **105**(39): p. 15064-15069.
62. McCauley, H.A. and G. Guasch, *Three cheers for the goblet cell: maintaining homeostasis in mucosal epithelia.* Trends Mol Med, 2015. **21**(8): p. 492-503.
63. Hoffmann, W., *Self-renewal of the gastric epithelium from stem and progenitor cells.* Front Biosci (Schol Ed), 2013. **5**: p. 720-31.
64. Mueller, A., et al., *Profiling of microdissected gastric epithelial cells reveals a cell type-specific response to Helicobacter pylori infection.* Gastroenterology, 2004. **127**(5): p. 1446-62.
65. Gunawardene, A.R., B.M. Corfe, and C.A. Staton, *Classification and functions of enteroendocrine cells of the lower gastrointestinal tract.* Int J Exp Pathol, 2011. **92**(4): p. 219-31.
66. van der Flier, L.G. and H. Clevers, *Stem cells, self-renewal, and differentiation in the intestinal epithelium.* Annu Rev Physiol, 2009. **71**: p. 241-60.
67. Gehart, H., et al., *Identification of Enteroendocrine Regulators by Real-Time Single-Cell Differentiation Mapping.* Cell, 2019. **176**(5): p. 1158-1173.e16.
68. Cheng, H. and C.P. Leblond, *Origin, differentiation and renewal of the four main epithelial cell types in the mouse small intestine. III. Entero-endocrine cells.* Am J Anat, 1974. **141**(4): p. 503-19.
69. Thompson, E.M., Y.E. Price, and N.A. Wright, *Kinetics of enteroendocrine cells with implications for their origin: a study of the cholecystokinin and gastrin subpopulations*

combining tritiated thymidine labelling with immunocytochemistry in the mouse. Gut, 1990. **31**(4): p. 406-11.
70. Gribble, F.M. and F. Reimann, *Enteroendocrine Cells: Chemosensors in the Intestinal Epithelium.* Annu Rev Physiol, 2016. **78**: p. 277-99.
71. Psichas, A., et al., *Chylomicrons stimulate incretin secretion in mouse and human cells.* Diabetologia, 2017. **60**(12): p. 2475-2485.
72. Gribble, F.M. and F. Reimann, *Function and mechanisms of enteroendocrine cells and gut hormones in metabolism.* Nature Reviews Endocrinology, 2019. **15**(4): p. 226-237.
73. Christensen, L.W., et al., *Vascular, but not luminal, activation of FFAR1 (GPR40) stimulates GLP-1 secretion from isolated perfused rat small intestine.* Physiological Reports, 2015. **3**(9): p. e12551.
74. Tough, I.R., et al., *Bidirectional GPR119 Agonism Requires Peptide YY and Glucose for Activity in Mouse and Human Colon Mucosa.* Endocrinology, 2018. **159**(4): p. 1704-1717.
75. Wheeler, S.E., et al., *The SNARE Protein Syntaxin-1a Plays an Essential Role in Biphasic Exocytosis of the Incretin Hormone Glucagon-Like Peptide 1.* Diabetes, 2017. **66**(9): p. 2327-2338.
76. Bohórquez, D.V., et al., *Characterization of basal pseudopod-like processes in ileal and colonic PYY cells.* J Mol Histol, 2011. **42**(1): p. 3-13.
77. Bohórquez, D.V., et al., *An enteroendocrine cell-enteric glia connection revealed by 3D electron microscopy.* PLoS One, 2014. **9**(2): p. e89881.
78. Bohórquez, D.V., et al., *Neuroepithelial circuit formed by innervation of sensory enteroendocrine cells.* J Clin Invest, 2015. **125**(2): p. 782-6.
79. Chandra, R., et al., *Pseudopod-like basal cell processes in intestinal cholecystokinin cells.* Cell Tissue Res, 2010. **341**(2): p. 289-97.
80. Furness, J.B., et al., *The gut as a sensory organ.* Nat Rev Gastroenterol Hepatol, 2013. **10**(12): p. 729-40.
81. Cho, H.J., et al., *Differences in hormone localisation patterns of K and L type enteroendocrine cells in the mouse and pig small intestine and colon.* Cell Tissue Res, 2015. **359**(2): p. 693-8.
82. Egerod, K.L., et al., *A major lineage of enteroendocrine cells coexpress CCK, secretin, GIP, GLP-1, PYY, and neurotensin but not somatostatin.* Endocrinology, 2012. **153**(12): p. 5782-95.
83. Habib, A.M., et al., *Overlap of endocrine hormone expression in the mouse intestine revealed by transcriptional profiling and flow cytometry.* Endocrinology, 2012. **153**(7): p. 3054-65.
84. Svendsen, B., et al., *An analysis of cosecretion and coexpression of gut hormones from male rat proximal and distal small intestine.* Endocrinology, 2015. **156**(3): p. 847-57.
85. Haber, A.L., et al., *A single-cell survey of the small intestinal epithelium.* Nature, 2017. **551**(7680): p. 333-339.
86. Murphy, K.G. and S.R. Bloom, *Gut hormones and the regulation of energy homeostasis.* Nature, 2006. **444**(7121): p. 854-9.
87. Coleman, J., M. Inukai, and M. Inouye, *Dual functions of the signal peptide in protein transfer across the membrane.* Cell, 1985. **43**(1): p. 351-60.
88. Baldwin, G.S., et al., *Biologically active recombinant human progastrin(6-80) contains a tightly bound calcium ion.* J Biol Chem, 2001. **276**(11): p. 7791-6.
89. Gagnon, J., et al., *Expression of PCSK1 (PC1/3), PCSK2 (PC2) and PCSK3 (furin) in mouse small intestine.* Regul Pept, 2009. **152**(1-3): p. 54-60.
90. Eipper, B.A., et al., *Peptidylglycine alpha-amidating monooxygenase: a multifunctional protein with catalytic, processing, and routing domains.* Protein Sci, 1993. **2**(4): p. 489-97.
91. Patel, O., et al., *Stimulation of proliferation and migration of a colorectal cancer cell line by amidated and glycine-extended gastrin-releasing peptide via the same receptor.* Biochem Pharmacol, 2004. **68**(11): p. 2129-42.
92. Liu, Y.D., et al., *N-terminal glutamate to pyroglutamate conversion in vivo for human IgG2 antibodies.* J Biol Chem, 2011. **286**(13): p. 11211-7.

93. Sevier, C.S. and C.A. Kaiser, *Formation and transfer of disulphide bonds in living cells.* Nature Reviews Molecular Cell Biology, 2002. **3**(11): p. 836-847.
94. Schilling, S., C. Wasternack, and H.U. Demuth, *Glutaminyl cyclases from animals and plants: a case of functionally convergent protein evolution.* Biol Chem, 2008. **389**(8): p. 983-91.
95. Kojima, M., et al., *Ghrelin is a growth-hormone-releasing acylated peptide from stomach.* Nature, 1999. **402**(6762): p. 656-60.
96. Knudsen, L.B. and L. Pridal, *Glucagon-like peptide-1-(9-36) amide is a major metabolite of glucagon-like peptide-1-(7-36) amide after in vivo administration to dogs, and it acts as an antagonist on the pancreatic receptor.* Eur J Pharmacol, 1996. **318**(2-3): p. 429-35.
97. Berglund, M.M., P.A. Hipskind, and D.R. Gehlert, *Recent Developments in Our Understanding of the Physiological Role of PP-Fold Peptide Receptor Subtypes.* Experimental Biology and Medicine, 2003. **228**(3): p. 217-244.
98. Keire, D.A., et al., *Solution Structure of Monomeric Peptide YY Supports the Functional Significance of the PP-Fold†,‡.* Biochemistry, 2000. **39**(32): p. 9935-9942.
99. Pedragosa-Badia, X., J. Stichel, and A.G. Beck-Sickinger, *Neuropeptide Y receptors: how to get subtype selectivity.* Frontiers in Endocrinology, 2013. **4**.
100. Tang-Christensen, M., et al., *Central administration of GLP-1-(7-36) amide inhibits food and water intake in rats.* Am J Physiol, 1996. **271**(4 Pt 2): p. R848-56.
101. Turton, M.D., et al., *A role for glucagon-like peptide-1 in the central regulation of feeding.* Nature, 1996. **379**(6560): p. 69-72.
102. Orskov, C., et al., *Glucagon-Like Peptide I Receptors in the Subfornical Organ and the Area Postrema Are Accessible to Circulating Glucagon-Like Peptide I.* Diabetes, 1996. **45**(6): p. 832-835.
103. Yamamoto, H., et al., *Glucagon-like peptide-1 receptor stimulation increases blood pressure and heart rate and activates autonomic regulatory neurons.* 2002. **110**(1): p. 43-52.
104. Meier, J.J., et al., *Normalization of glucose concentrations and deceleration of gastric emptying after solid meals during intravenous glucagon-like peptide 1 in patients with type 2 diabetes.* J Clin Endocrinol Metab, 2003. **88**(6): p. 2719-25.
105. Nauck, M.A., et al., *Glucagon-like peptide 1 inhibition of gastric emptying outweighs its insulinotropic effects in healthy humans.* Am J Physiol, 1997. **273**(5 Pt 1): p. E981-8.
106. Schirra, J., et al., *Effects of glucagon-like peptide-1(7-36)amide on motility and sensation of the proximal stomach in humans.* Gut, 2002. **50**(3): p. 341-8.
107. Richards, P., et al., *Identification and characterization of GLP-1 receptor-expressing cells using a new transgenic mouse model.* Diabetes, 2014. **63**(4): p. 1224-33.
108. Moran, T.H., et al., *Peptide YY(3-36) inhibits gastric emptying and produces acute reductions in food intake in rhesus monkeys.* Am J Physiol Regul Integr Comp Physiol, 2005. **288**(2): p. R384-8.
109. Tough, I., et al., *Endogenous peptide YY and neuropeptide Y inhibit colonic ion transport, contractility and transit differentially via Y1 and Y2 receptors.* British Journal of Pharmacology, 2011. **164**(2b): p. 471-484.
110. Wang, L., et al., *Peripheral peptide YY inhibits propulsive colonic motor function through Y2 receptor in conscious mice.* Am J Physiol Gastrointest Liver Physiol, 2010. **298**(1): p. G45-56.
111. Nonaka, N., et al., *Characterization of blood-brain barrier permeability to PYY3-36 in the mouse.* J Pharmacol Exp Ther, 2003. **306**(3): p. 948-53.
112. Batterham, R.L., et al., *PYY modulation of cortical and hypothalamic brain areas predicts feeding behaviour in humans.* Nature, 2007. **450**(7166): p. 106-109.
113. Shi, Y.-C., et al., *PYY3-36 and pancreatic polypeptide reduce food intake in an additive manner via distinct hypothalamic dependent pathways in mice.* Obesity, 2013. **21**(12): p. E669-E678.
114. Kamegai, J., et al., *Central Effect of Ghrelin, an Endogenous Growth Hormone Secretagogue, on Hypothalamic Peptide Gene Expression.* Endocrinology, 2000. **141**(12): p. 4797-4800.

115. Nakazato, M., et al., *A role for ghrelin in the central regulation of feeding.* Nature, 2001. **409**(6817): p. 194-198.
116. Wang, L., D.H. Saint-Pierre, and Y. Taché, *Peripheral ghrelin selectively increases Fos expression in neuropeptide Y - synthesizing neurons in mouse hypothalamic arcuate nucleus.* Neurosci Lett, 2002. **325**(1): p. 47-51.
117. Page, A.J., et al., *Ghrelin selectively reduces mechanosensitivity of upper gastrointestinal vagal afferents.* Am J Physiol Gastrointest Liver Physiol, 2007. **292**(5): p. G1376-84.
118. Carreira, M.C., et al., *Agonist-Specific Coupling of Growth Hormone Secretagogue Receptor Type 1a to Different Intracellular Signaling Systems.* Neuroendocrinology, 2004. **79**(1): p. 13-25.
119. Skibicka, K.P., et al., *Role of ghrelin in food reward: impact of ghrelin on sucrose self-administration and mesolimbic dopamine and acetylcholine receptor gene expression.* Addict Biol, 2012. **17**(1): p. 95-107.
120. Zhang, L., et al., *Protein kinase C pathway mediates the protective effects of glucagon-like peptide-1 on the apoptosis of islet β-cells.* Mol Med Rep, 2015. **12**(5): p. 7589-94.
121. Fusco, J., et al., *GLP-1/Exendin-4 induces β-cell proliferation via the epidermal growth factor receptor.* Sci Rep, 2017. **7**(1): p. 9100.
122. de Heer, J., et al., *Glucagon-like peptide-1, but not glucose-dependent insulinotropic peptide, inhibits glucagon secretion via somatostatin (receptor subtype 2) in the perfused rat pancreas.* Diabetologia, 2008. **51**(12): p. 2263-70.
123. Chia, C.W., et al., *Exogenous glucose-dependent insulinotropic polypeptide worsens post prandial hyperglycemia in type 2 diabetes.* Diabetes, 2009. **58**(6): p. 1342-9.
124. Burnicka-Turek, O., et al., *INSL5-deficient mice display an alteration in glucose homeostasis and an impaired fertility.* Endocrinology, 2012. **153**(10): p. 4655-65.
125. Adriaenssens, A.E., et al., *Transcriptomic profiling of pancreatic alpha, beta and delta cell populations identifies delta cells as a principal target for ghrelin in mouse islets.* Diabetologia, 2016. **59**(10): p. 2156-65.
126. Baron, M., et al., *A Single-Cell Transcriptomic Map of the Human and Mouse Pancreas Reveals Inter- and Intra-cell Population Structure.* Cell Syst, 2016. **3**(4): p. 346-360.e4.
127. Toouli, J., *Sphincter of Oddi: Function, dysfunction, and its management.* J Gastroenterol Hepatol, 2009. **24 Suppl 3**: p. S57-62.
128. Benjamin, M.A., et al., *Glucagon-like peptide-2 enhances intestinal epithelial barrier function of both transcellular and paracellular pathways in the mouse.* Gut, 2000. **47**(1): p. 112-9.
129. Batterham, R.L., et al., *Gut hormone PYY(3-36) physiologically inhibits food intake.* Nature, 2002. **418**(6898): p. 650-4.
130. Batterham, R.L., et al., *Inhibition of food intake in obese subjects by peptide YY3-36.* N Engl J Med, 2003. **349**(10): p. 941-8.
131. Borg, C.M., et al., *Progressive rise in gut hormone levels after Roux-en-Y gastric bypass suggests gut adaptation and explains altered satiety.* Br J Surg, 2006. **93**(2): p. 210-5.
132. le Roux, C.W., et al., *Gut hormone profiles following bariatric surgery favor an anorectic state, facilitate weight loss, and improve metabolic parameters.* Ann Surg, 2006. **243**(1): p. 108-14.
133. le Roux, C.W., et al., *Gut hormones as mediators of appetite and weight loss after Roux-en-Y gastric bypass.* Ann Surg, 2007. **246**(5): p. 780-5.
134. Parlevliet, E.T., et al., *Oxyntomodulin ameliorates glucose intolerance in mice fed a high-fat diet.* Am J Physiol Endocrinol Metab, 2008. **294**(1): p. E142-7.
135. Tan, T.M., et al., *Coadministration of glucagon-like peptide-1 during glucagon infusion in humans results in increased energy expenditure and amelioration of hyperglycemia.* Diabetes, 2013. **62**(4): p. 1131-8.
136. Druce, M.R., et al., *Investigation of structure-activity relationships of Oxyntomodulin (Oxm) using Oxm analogs.* Endocrinology, 2009. **150**(4): p. 1712-22.

137. Pocai, A., et al., *Glucagon-like peptide 1/glucagon receptor dual agonism reverses obesity in mice.* Diabetes, 2009. **58**(10): p. 2258-66.
138. Santoprete, A., et al., *DPP-IV-resistant, long-acting oxyntomodulin derivatives.* J Pept Sci, 2011. **17**(4): p. 270-80.
139. Alexiadou, K., O. Anyiam, and T. Tan, *Cracking the combination: Gut hormones for the treatment of obesity and diabetes.* Journal of Neuroendocrinology, 2019. **31**(5): p. e12664.
140. Ambery, P., et al., *MEDI0382, a GLP-1 and glucagon receptor dual agonist, in obese or overweight patients with type 2 diabetes: a randomised, controlled, double-blind, ascending dose and phase 2a study.* The Lancet, 2018. **391**(10140): p. 2607-2618.
141. Tillner, J., et al., *A novel dual glucagon-like peptide and glucagon receptor agonist SAR425899: Results of randomized, placebo-controlled first-in-human and first-in-patient trials.* Diabetes, Obesity and Metabolism, 2019. **21**(1): p. 120-128.
142. Finan, B., et al., *Unimolecular dual incretins maximize metabolic benefits in rodents, monkeys, and humans.* Sci Transl Med, 2013. **5**(209): p. 209ra151.
143. Coskun, T., et al., *LY3298176, a novel dual GIP and GLP-1 receptor agonist for the treatment of type 2 diabetes mellitus: From discovery to clinical proof of concept.* Mol Metab, 2018. **18**: p. 3-14.
144. Frias, J.P., et al., *Efficacy and safety of LY3298176, a novel dual GIP and GLP-1 receptor agonist, in patients with type 2 diabetes: a randomised, placebo-controlled and active comparator-controlled phase 2 trial.* Lancet, 2018. **392**(10160): p. 2180-2193.
145. Frias, J.P., et al., *Efficacy and tolerability of tirzepatide, a dual glucose-dependent insulinotropic peptide and glucagon-like peptide-1 receptor agonist in patients with type 2 diabetes: A 12-week, randomized, double-blind, placebo-controlled study to evaluate different dose-escalation regimens.* Diabetes Obes Metab, 2020.
146. Longnecker, D., *Anatomy and Histology of the Pancreas.* Pancrepedia, 2014. **1**.
147. Love, J.A., E. Yi, and T.G. Smith, *Autonomic pathways regulating pancreatic exocrine secretion.* Auton Neurosci, 2007. **133**(1): p. 19-34.
148. Tiscornia, O.M., *The neural control of exocrine and endocrine pancreas.* Am J Gastroenterol, 1977. **67**(6): p. 541-60.
149. Molina, J., et al., *Control of insulin secretion by cholinergic signaling in the human pancreatic islet.* Diabetes, 2014. **63**(8): p. 2714-26.
150. Rodriguez-Diaz, R., et al., *Alpha cells secrete acetylcholine as a non-neuronal paracrine signal priming beta cell function in humans.* Nat Med, 2011. **17**(7): p. 888-92.
151. Dolenšek, J., M.S. Rupnik, and A. Stožer, *Structural similarities and differences between the human and the mouse pancreas.* Islets, 2015. **7**(1): p. e1024405.
152. Williams, J.A., *Regulation of acinar cell function in the pancreas.* Curr Opin Gastroenterol, 2010. **26**(5): p. 478-83.
153. Korc, M., et al., *Insulin receptors in isolated mouse pancreatic acini.* Biochem Biophys Res Commun, 1978. **84**(2): p. 293-9.
154. Korc, M., et al., *Insulin action in pancreatic acini from streptozotocin-treated rats. I. Stimulation of protein synthesis.* Am J Physiol, 1981. **240**(1): p. G56-62.
155. Sankaran, H., et al., *Insulin action in pancreatic acini from streptozotocin-treated rats. II. Binding of 125I-insulin to receptors.* Am J Physiol, 1981. **240**(1): p. G63-8.
156. OpenStax. *Anatomy & Physiology*. 2016; Available from: https://openstax.org/books/anatomy-and-physiology/pages/17-9-the-endocrine-pancreas.
157. Afelik, S. and J. Jensen, *Notch signaling in the pancreas: patterning and cell fate specification.* Wiley Interdiscip Rev Dev Biol, 2013. **2**(4): p. 531-44.
158. Gradwohl, G., et al., *neurogenin3 is required for the development of the four endocrine cell lineages of the pancreas.* Proc Natl Acad Sci U S A, 2000. **97**(4): p. 1607-11.
159. Sosa-Pineda, B., *The gene Pax4 is an essential regulator of pancreatic beta-cell development.* Mol Cells, 2004. **18**(3): p. 289-94.

160. Wilcox, C.L., et al., *Pancreatic α-cell specific deletion of mouse Arx leads to α-cell identity loss.* PLoS One, 2013. **8**(6): p. e66214.
161. Collombat, P., et al., *Embryonic endocrine pancreas and mature beta cells acquire alpha and PP cell phenotypes upon Arx misexpression.* J Clin Invest, 2007. **117**(4): p. 961-70.
162. Napolitano, T., et al., *Pax4 acts as a key player in pancreas development and plasticity.* Semin Cell Dev Biol, 2015. **44**: p. 107-14.
163. Marchetti, P., et al., *A local glucagon-like peptide 1 (GLP-1) system in human pancreatic islets.* Diabetologia, 2012. **55**(12): p. 3262-72.
164. Fujita, Y., et al., *Glucose-dependent insulinotropic polypeptide is expressed in pancreatic islet alpha-cells and promotes insulin secretion.* Gastroenterology, 2010. **138**(5): p. 1966-75.
165. Lan, H., et al., *Gene expression profiles of nondiabetic and diabetic obese mice suggest a role of hepatic lipogenic capacity in diabetes susceptibility.* Diabetes, 2003. **52**(3): p. 688-700.
166. Taylor, S.W., et al., *Peptidomic profiling of secreted products from pancreatic islet culture results in a higher yield of full-length peptide hormones than found using cell lysis procedures.* J Proteome Res, 2013. **12**(8): p. 3610-9.
167. Da Silva Xavier, G., *The Cells of the Islets of Langerhans.* J Clin Med, 2018. **7**(3).
168. Akter, R., et al., *Islet Amyloid Polypeptide: Structure, Function, and Pathophysiology.* J Diabetes Res, 2016. **2016**: p. 2798269.
169. Greenberg, G.R., et al., *Inhibition of pancreas and gallbladder by pancreatic polypeptide.* Lancet, 1978. **2**(8103): p. 1280-2.
170. Edelman, S., H. Maier, and K. Wilhelm, *Pramlintide in the treatment of diabetes mellitus.* BioDrugs, 2008. **22**(6): p. 375-86.
171. Aronne, L., et al., *Progressive reduction in body weight after treatment with the amylin analog pramlintide in obese subjects: a phase 2, randomized, placebo-controlled, dose-escalation study.* J Clin Endocrinol Metab, 2007. **92**(8): p. 2977-83.
172. Chaudhri, O.B., K. Wynne, and S.R. Bloom, *Can gut hormones control appetite and prevent obesity?* Diabetes Care, 2008. **31 Suppl 2**: p. S284-9.
173. Batterham, R.L., et al., *Pancreatic polypeptide reduces appetite and food intake in humans.* J Clin Endocrinol Metab, 2003. **88**(8): p. 3989-92.
174. McLaughlin, C.L. and C.A. Baile, *Obese mice and the satiety effects of cholecystokinin, bombesin and pancreatic polypeptide.* Physiol Behav, 1981. **26**(3): p. 433-7.
175. Berntson, G.G., et al., *Pancreatic polypeptide infusions reduce food intake in Prader-Willi syndrome.* Peptides, 1993. **14**(3): p. 497-503.
176. Bellmann-Sickert, K., et al., *Long-acting lipidated analogue of human pancreatic polypeptide is slowly released into circulation.* J Med Chem, 2011. **54**(8): p. 2658-67.
177. Tan, T.M., et al., *Pharmacokinetics, adverse effects and tolerability of a novel analogue of human pancreatic polypeptide, PP 1420.* Br J Clin Pharmacol, 2012. **73**(2): p. 232-9.
178. Cabrera, O., et al., *The unique cytoarchitecture of human pancreatic islets has implications for islet cell function.* Proceedings of the National Academy of Sciences, 2006. **103**(7): p. 2334-2339.
179. Ballian, N. and F.C. Brunicardi, *Islet vasculature as a regulator of endocrine pancreas function.* World J Surg, 2007. **31**(4): p. 705-14.
180. Kebarle, P., *A brief overview of the present status of the mechanisms involved in electrospray mass spectrometry.* J Mass Spectrom, 2000. **35**(7): p. 804-17.
181. Hillenkamp, F. and M. Karas, *Mass spectrometry of peptides and proteins by matrix-assisted ultraviolet laser desorption/ionization.* Methods Enzymol, 1990. **193**: p. 280-95.
182. Fung, K.Y., et al., *A simple and inexpensive approach to interfacing high-performance liquid chromatography and matrix-assisted laser desorption/ionization-time of flight-mass spectrometry.* Proteomics, 2004. **4**(10): p. 3121-7.

183. El-Aneed, A., A. Cohen, and J. Banoub, *Mass Spectrometry, Review of the Basics: Electrospray, MALDI, and Commonly Used Mass Analyzers*. 2009: Applied Spectroscopy Reviews. p. 210-230.
184. Hu, Q., et al., *The Orbitrap: a new mass spectrometer.* J Mass Spectrom, 2005. **40**(4): p. 430-43.
185. Demartini, D.R., G. Pasquali, and C.R. Carlini, *An overview of proteomics approaches applied to biopharmaceuticals and cyclotides research.* J Proteomics, 2013. **93**: p. 224-33.
186. Chambers, E.E., et al., *Multidimensional LC-MS/MS enables simultaneous quantification of intact human insulin and five recombinant analogs in human plasma.* Anal Chem, 2014. **86**(1): p. 694-702.
187. Howard, J.W., et al., *Development of a UHPLC-MS/MS (SRM) method for the quantitation of endogenous glucagon and dosed GLP-1 from human plasma.* Bioanalysis, 2017. **9**(9): p. 733-751.
188. Lee, A.Y., et al., *Multiplexed Quantification of Proglucagon-Derived Peptides by Immunoaffinity Enrichment and Tandem Mass Spectrometry after a Meal Tolerance Test.* Clin Chem, 2016. **62**(1): p. 227-35.
189. Cox, J.M., et al., *Characterization and quantification of oxyntomodulin in human and rat plasma using high-resolution accurate mass LC-MS.* Bioanalysis, 2016. **8**(15): p. 1579-1595.
190. Zhang, J., et al., *Peptidomic Analysis of Fetal Heart Tissue for Identification of Endogenous Peptides Involved in Tetralogy of Fallot.* DNA Cell Biol, 2017.
191. Billing, L.J., et al., *Co-storage and release of insulin-like peptide-5, glucagon-like peptide-1 and peptideYY from murine and human colonic enteroendocrine cells.* Mol Metab, 2018. **16**: p. 65-75.
192. Svensson, M., et al., *Peptidomics-based discovery of novel neuropeptides.* J Proteome Res, 2003. **2**(2): p. 213-9.
193. Roberts, G.P., et al., *Comparison of Human and Murine Enteroendocrine Cells by Transcriptomic and Peptidomic Profiling.* Diabetes, 2019. **68**(5): p. 1062-1072.
194. Machado, J.D., et al., *Chromogranins A and B as regulators of vesicle cargo and exocytosis.* Cell Mol Neurobiol, 2010. **30**(8): p. 1181-7.
195. HILLARP, N.A., *Further observations on the state of the catechol amines stored in the adrenal medullary granules.* Acta Physiol Scand, 1959. **47**: p. 271-9.
196. Helle, K.B., et al., *Osmotic properties of the chromogranins and relation to osmotic pressure in catecholamine storage granules.* Acta Physiol Scand, 1985. **123**(1): p. 21-33.
197. Doblinger, A., et al., *Proteolytic processing of chromogranin A by the prohormone convertase PC2.* Regul Pept, 2003. **111**(1-3): p. 111-6.
198. Eskeland, N.L., et al., *Chromogranin A processing and secretion: specific role of endogenous and exogenous prohormone convertases in the regulated secretory pathway.* J Clin Invest, 1996. **98**(1): p. 148-56.
199. Udupi, V., et al., *Prohormone convertase-1 is essential for conversion of chromogranin A to pancreastatin.* Regul Pept, 1999. **83**(2-3): p. 123-7.
200. Aardal, S. and K.B. Helle, *The vasoinhibitory activity of bovine chromogranin A fragment (vasostatin) and its independence of extracellular calcium in isolated segments of human blood vessels.* Regul Pept, 1992. **41**(1): p. 9-18.
201. Drees, B.M., et al., *Bovine parathyroid glands secrete a 26-kDa N-terminal fragment of chromogranin-A which inhibits parathyroid cell secretion.* Endocrinology, 1991. **129**(6): p. 3381-7.
202. Lugardon, K., et al., *Antibacterial and antifungal activities of vasostatin-1, the N-terminal fragment of chromogranin A.* J Biol Chem, 2000. **275**(15): p. 10745-53.
203. Metz-Boutigue, M.H., et al., *Antibacterial peptides are present in chromaffin cell secretory granules.* Cell Mol Neurobiol, 1998. **18**(2): p. 249-66.

204. Sanchez, V., J.R. Calvo, and R. Goberna, *Glycogenolytic effect of pancreastatin in the rat.* Biosci Rep, 1990. **10**(1): p. 87-91.
205. Sánchez-Margalet, V. and C. González-Yanes, *Pancreastatin inhibits insulin action in rat adipocytes.* Am J Physiol, 1998. **275**(6): p. E1055-60.
206. Funakoshi, A., et al., *Bioactivity of synthetic C-terminal fragment of rat pancreastatin on endocrine pancreas.* Biochem Biophys Res Commun, 1989. **158**(3): p. 844-9.
207. Mahata, S.K., et al., *Novel autocrine feedback control of catecholamine release. A discrete chromogranin a fragment is a noncompetitive nicotinic cholinergic antagonist.* J Clin Invest, 1997. **100**(6): p. 1623-33.
208. Stadinski, B.D., et al., *Chromogranin A is an autoantigen in type 1 diabetes.* Nat Immunol, 2010. **11**(3): p. 225-31.
209. Fasciotto, B.H., et al., *Parastatin (porcine chromogranin A347-419), a novel chromogranin A-derived peptide, inhibits parathyroid cell secretion.* Endocrinology, 1993. **133**(2): p. 461-6.
210. Koshimizu, H., et al., *Serpinin: a novel chromogranin A-derived, secreted peptide up-regulates protease nexin-1 expression and granule biogenesis in endocrine cells.* Mol Endocrinol, 2011. **25**(5): p. 732-44.
211. Tota, B., et al., *The novel chromogranin A-derived serpinin and pyroglutaminated serpinin peptides are positive cardiac β-adrenergic-like inotropes.* FASEB J, 2012. **26**(7): p. 2888-98.
212. Russell, J., et al., *Inhibition of parathyroid hormone secretion by amino-terminal chromogranin peptides.* Endocrinology, 1994. **135**(1): p. 337-42.
213. Kroesen, S., et al., *Rat brain: distribution of immunoreactivity of PE-11, a peptide derived from chromogranin B.* Eur J Neurosci, 1996. **8**(12): p. 2679-89.
214. Flanagan, T., et al., *A novel 1745-dalton pyroglutamyl peptide derived from chromogranin B is in the bovine adrenomedullary chromaffin vesicle.* Cell Mol Neurobiol, 1990. **10**(4): p. 507-23.
215. Strub, J.M., et al., *Processing of chromogranin B in bovine adrenal medulla. Identification of secretolytin, the endogenous C-terminal fragment of residues 614-626 with antibacterial activity.* Eur J Biochem, 1995. **229**(2): p. 356-68.
216. Zhao, E., et al., *Secretoneurin stimulates the production and release of luteinizing hormone in mouse L{beta}T2 gonadotropin cells.* Am J Physiol Endocrinol Metab, 2011. **301**(2): p. E288-97.
217. Yajima, A., et al., *Manserin, a novel peptide from secretogranin II in the neuroendocrine system.* Neuroreport, 2004. **15**(11): p. 1755-9.
218. Yajima, A., N. Narita, and M. Narita, *Recently identified a novel neuropeptide manserin colocalize with the TUNEL-positive cells in the top villi of the rat duodenum.* J Pept Sci, 2008. **14**(6): p. 773-6.
219. Tano, K., et al., *Manserin, a secretogranin II-derived peptide, distributes in the rat endocrine pancreas colocalized with islet-cell specific manner.* Histochem Cell Biol, 2010. **134**(1): p. 53-7.
220. Feng, Y., S.E. Reznik, and L.D. Fricker, *Distribution of proSAAS-derived peptides in rat neuroendocrine tissues.* Neuroscience, 2001. **105**(2): p. 469-78.
221. Basak, A., et al., *Inhibitory specificity and potency of proSAAS-derived peptides toward proprotein convertase 1.* J Biol Chem, 2001. **276**(35): p. 32720-8.
222. Pritchard, L.E., A.V. Turnbull, and A. White, *Pro-opiomelanocortin processing in the hypothalamus: impact on melanocortin signalling and obesity.* J Endocrinol, 2002. **172**(3): p. 411-21.
223. Karra, E., K. Chandarana, and R.L. Batterham, *The role of peptide YY in appetite regulation and obesity.* J Physiol, 2009. **587**(1): p. 19-25.
224. Glass, L.L., et al., *Single-cell RNA-sequencing reveals a distinct population of proglucagon-expressing cells specific to the mouse upper small intestine.* Mol Metab, 2017. **6**(10): p. 1296-1303.

225. Corbière, A., et al., *Strategies for the Identification of Bioactive Neuropeptides in Vertebrates.* Front Neurosci, 2019. **13**: p. 948.
226. Stewart, K.W., et al., *A simple and rapid method for identifying and semi-quantifying peptide hormones in isolated pancreatic islets by direct-tissue matrix-assisted laser desorption ionization time-of-flight mass spectrometry.* Rapid Commun Mass Spectrom, 2011. **25**(22): p. 3387-95.
227. Secher, A., et al., *Analytic framework for peptidomics applied to large-scale neuropeptide identification.* Nat Commun, 2016. **7**: p. 11436.
228. Brazeau, P., et al., *Hypothalamic polypeptide that inhibits the secretion of immunoreactive pituitary growth hormone.* Science, 1973. **179**(4068): p. 77-9.
229. Sakurai, T., et al., *Orexins and orexin receptors: a family of hypothalamic neuropeptides and G protein-coupled receptors that regulate feeding behavior.* Cell, 1998. **92**(4): p. 573-85.
230. Tatemoto, K., et al., *Isolation and characterization of cholecystokinin-58 (CCK-58) from porcine brain.* FEBS Lett, 1984. **174**(2): p. 289-93.
231. Tatemoto, K., M. Carlquist, and V. Mutt, *Neuropeptide Y--a novel brain peptide with structural similarities to peptide YY and pancreatic polypeptide.* Nature, 1982. **296**(5858): p. 659-60.
232. Coulouarn, Y., et al., *Cloning of the cDNA encoding the urotensin II precursor in frog and human reveals intense expression of the urotensin II gene in motoneurons of the spinal cord.* Proc Natl Acad Sci U S A, 1998. **95**(26): p. 15803-8.
233. Lund, P.K., et al., *Pancreatic preproglucagon cDNA contains two glucagon-related coding sequences arranged in tandem.* Proc Natl Acad Sci U S A, 1982. **79**(2): p. 345-9.
234. Samson, W.K., et al., *Neuronostatin encoded by the somatostatin gene regulates neuronal, cardiovascular, and metabolic functions.* J Biol Chem, 2008. **283**(46): p. 31949-59.
235. Li, H.J., et al., *Notch signaling differentially regulates the cell fate of early endocrine precursor cells and their maturing descendants in the mouse pancreas and intestine.* Dev Biol, 2012. **371**(2): p. 156-69.
236. Zhang, C., et al., *The preprohormone expression profile of enteroendocrine cells following Roux-en-Y gastric bypass in rats.* Peptides, 2019. **118**: p. 170100.
237. Yosten, G.L., et al., *A novel reproductive peptide, phoenixin.* J Neuroendocrinol, 2013. **25**(2): p. 206-15.
238. Salvatori, A.S., et al., *Neuronostatin inhibits glucose-stimulated insulin secretion via direct action on the pancreatic α-cell.* Am J Physiol Endocrinol Metab, 2014. **306**(11): p. E1257-63.
239. Su, S.F., et al., *Intracerebroventricular administration of neuronostatin delays gastric emptying and gastrointestinal transit in mice.* Peptides, 2012. **35**(1): p. 31-5.
240. Vainio, L., et al., *Neuronostatin, a novel peptide encoded by somatostatin gene, regulates cardiac contractile function and cardiomyocyte survival.* J Biol Chem, 2012. **287**(7): p. 4572-80.
241. Troger, J., et al., *Granin-derived peptides.* Prog Neurobiol, 2017. **154**: p. 37-61.
242. Helle, K.B., et al., *Chromogranins: from discovery to current times.* Pflugers Arch, 2018. **470**(1): p. 143-154.
243. Yosten, G.L., et al., *Understanding peptide biology: The discovery and characterization of the novel hormone, neuronostatin.* Peptides, 2015. **72**: p. 192-5.
244. Hua, Y., et al., *Neuronostatin inhibits cardiac contractile function via a protein kinase A- and JNK-dependent mechanism in murine hearts.* Am J Physiol Regul Integr Comp Physiol, 2009. **297**(3): p. R682-9.
245. Yosten, G.L., *Novel neuropeptides in the control of food intake: neuronostatin and nesfatin-1.* Vitam Horm, 2013. **92**: p. 1-25.
246. Cummings, D.E., J. Overduin, and K.E. Foster-Schubert, *Gastric bypass for obesity: mechanisms of weight loss and diabetes resolution.* J Clin Endocrinol Metab, 2004. **89**(6): p. 2608-15.
247. Hammer, H.F., *Medical complications of bariatric surgery: focus on malabsorption and dumping syndrome.* Dig Dis, 2012. **30**(2): p. 182-6.

248. Holst, J.J., et al., *Mechanisms in bariatric surgery: Gut hormones, diabetes resolution, and weight loss.* Surg Obes Relat Dis, 2018. **14**(5): p. 708-714.
249. Spinelli, V., et al., *Influence of Roux-en-Y gastric bypass on plasma bile acid profiles: a comparative study between rats, pigs and humans.* Int J Obes (Lond), 2016. **40**(8): p. 1260-7.
250. Hankir, M.K., et al., *Brain Feeding Circuits after Roux-en-Y Gastric Bypass.* Trends Endocrinol Metab, 2018. **29**(4): p. 218-237.
251. Jacobsen, S.H., et al., *Changes in gastrointestinal hormone responses, insulin sensitivity, and beta-cell function within 2 weeks after gastric bypass in non-diabetic subjects.* Obes Surg, 2012. **22**(7): p. 1084-96.
252. Roberts, G.P., et al., *Gastrectomy with Roux-en-Y reconstruction as a lean model of bariatric surgery.* Surg Obes Relat Dis, 2018. **14**(5): p. 562-568.
253. Yan, W., et al., *Effects of meal size on the release of GLP-1 and PYY after Roux-en-Y gastric bypass surgery in obese subjects with or without type 2 diabetes.* Obes Surg, 2014. **24**(11): p. 1969-74.
254. Fend, F. and M. Raffeld, *Laser capture microdissection in pathology.* J Clin Pathol, 2000. **53**(9): p. 666-72.
255. Svensson, M., et al., *Heat stabilization of the tissue proteome: a new technology for improved proteomics.* J Proteome Res, 2009. **8**(2): p. 974-81.
256. Tran, N.H., et al., *De novo peptide sequencing by deep learning.* Proc Natl Acad Sci U S A, 2017. **114**(31): p. 8247-8252.
257. Wen, B., et al., *Deep Learning in Proteomics.* Proteomics, 2020. **20**(21-22): p. e1900335.
258. Pappireddi, N., L. Martin, and M. Wühr, *A Review on Quantitative Multiplexed Proteomics.* ChemBioChem, 2019. **20**(10): p. 1210-1224.
259. Muntel, J., et al., *Abundance-based classifier for the prediction of mass spectrometric peptide detectability upon enrichment (PPA).* Mol Cell Proteomics, 2015. **14**(2): p. 430-40.
260. Anlauf, M., et al., *Localization of xenin-immunoreactive cells in the duodenal mucosa of humans and various mammals.* J Histochem Cytochem, 2000. **48**(12): p. 1617-26.
261. Taylor, A.I., et al., *Evaluation of the degradation and metabolic effects of the gut peptide xenin on insulin secretion, glycaemic control and satiety.* J Endocrinol, 2010. **207**(1): p. 87-93.
262. Parthsarathy, V., et al., *A novel chemically modified analogue of xenin-25 exhibits improved glucose-lowering and insulin-releasing properties.* Biochim Biophys Acta, 2016. **1860**(4): p. 757-64.
263. Veronese, F.M., *Peptide and protein PEGylation: a review of problems and solutions.* Biomaterials, 2001. **22**(5): p. 405-17.
264. Theeuwes, F. and S.I. Yum, *Principles of the design and operation of generic osmotic pumps for the delivery of semisolid or liquid drug formulations.* Ann Biomed Eng, 1976. **4**(4): p. 343-53.
265. Li, Y., et al., *Secretin-Activated Brown Fat Mediates Prandial Thermogenesis to Induce Satiation.* Cell, 2018. **175**(6): p. 1561-1574.e12.
266. Adams, S.H., et al., *PYY[3-36] administration decreases the respiratory quotient and reduces adiposity in diet-induced obese mice.* J Nutr, 2006. **136**(1): p. 195-201.
267. Frikke-Schmidt, H., et al., *Adipose weight gain during chronic insulin treatment of mice results from changes in lipid storage without affecting de novo synthesis of palmitate.* PLoS One, 2013. **8**(9): p. e76060.
268. Unniappan, S., M. Speck, and T.J. Kieffer, *Metabolic effects of chronic obestatin infusion in rats.* Peptides, 2008. **29**(8): p. 1354-61.
269. Mack, C.M., et al., *Antiobesity action of peripheral exenatide (exendin-4) in rodents: effects on food intake, body weight, metabolic status and side-effect measures.* Int J Obes (Lond), 2006. **30**(9): p. 1332-40.
270. Shang, J., et al., *Induction of miR-132 and miR-212 Expression by Glucagon-Like Peptide 1 (GLP-1) in Rodent and Human Pancreatic β-Cells.* Mol Endocrinol, 2015. **29**(9): p. 1243-53.

271. Pittner, R.A., et al., *Effects of PYY[3-36] in rodent models of diabetes and obesity.* Int J Obes Relat Metab Disord, 2004. **28**(8): p. 963-71.
272. Nishizawa, N., et al., *Antiobesity Effect of a Short-Length Peptide YY Analogue after Continuous Administration in Mice.* ACS Med Chem Lett, 2017. **8**(6): p. 628-631.
273. Elrick, M.M., et al., *Neuronostatin acts via GPR107 to increase cAMP-independent PKA phosphorylation and proglucagon mRNA accumulation in pancreatic α-cells.* Am J Physiol Regul Integr Comp Physiol, 2016. **310**(2): p. R143-55.
274. Kim, T. and Y.P. Loh, *Protease nexin-1 promotes secretory granule biogenesis by preventing granule protein degradation.* Mol Biol Cell, 2006. **17**(2): p. 789-98.
275. Thomsen, S.K., et al., *Type 2 diabetes risk alleles in PAM impact insulin release from human pancreatic β-cells.* Nature Genetics, 2018. **50**(8): p. 1122-1131.
276. Rehfeld, J.F., et al., *Naming progastrin-derived peptides.* Regul Pept, 2004. **120**(1-3): p. 177-83.
277. Johnsen, A.H., *Phylogeny of the cholecystokinin/gastrin family.* Front Neuroendocrinol, 1998. **19**(2): p. 73-99.
278. Schubert, M.L. and J.F. Rehfeld, *Gastric Peptides-Gastrin and Somatostatin.* Compr Physiol, 2019. **10**(1): p. 197-228.
279. Lenz, A., et al., *Islets from human donors with higher but not lower hemoglobin A1c levels respond to gastrin treatment in vitro.* PLoS One, 2019. **14**(8): p. e0221456.
280. Dalbøge, L.S., et al., *The novel GLP-1-gastrin dual agonist ZP3022 improves glucose homeostasis and increases β-cell mass without affecting islet number in db/db mice.* J Pharmacol Exp Ther, 2014. **350**(2): p. 353-60.
281. Rooman, I. and L. Bouwens, *Combined gastrin and epidermal growth factor treatment induces islet regeneration and restores normoglycaemia in C57Bl6/J mice treated with alloxan.* Diabetologia, 2004. **47**(2): p. 259-65.
282. Suarez-Pinzon, W.L., et al., *Combination therapy with epidermal growth factor and gastrin induces neogenesis of human islet {beta}-cells from pancreatic duct cells and an increase in functional {beta}-cell mass.* J Clin Endocrinol Metab, 2005. **90**(6): p. 3401-9.
283. Suarez-Pinzon, W.L., J.R. Lakey, and A. Rabinovitch, *Combination therapy with glucagon-like peptide-1 and gastrin induces beta-cell neogenesis from pancreatic duct cells in human islets transplanted in immunodeficient diabetic mice.* Cell Transplant, 2008. **17**(6): p. 631-40.
284. Téllez, N., et al., *Gastrin treatment stimulates β-cell regeneration and improves glucose tolerance in 95% pancreatectomized rats.* Endocrinology, 2011. **152**(7): p. 2580-8.
285. Wang, T.C., et al., *Pancreatic gastrin stimulates islet differentiation of transforming growth factor alpha-induced ductular precursor cells.* J Clin Invest, 1993. **92**(3): p. 1349-56.
286. Agouni, A., et al., *In vivo differential effects of fasting, re-feeding, insulin and insulin stimulation time course on insulin signaling pathway components in peripheral tissues.* Biochem Biophys Res Commun, 2010. **401**(1): p. 104-11.
287. De Meester, I., et al., *Natural substrates of dipeptidyl peptidase IV.* Adv Exp Med Biol, 2000. **477**: p. 67-87.
288. Meier, J.J., et al., *Secretion, degradation, and elimination of glucagon-like peptide 1 and gastric inhibitory polypeptide in patients with chronic renal insufficiency and healthy control subjects.* Diabetes, 2004. **53**(3): p. 654-62.
289. Vanhoof, G., et al., *Proline motifs in peptides and their biological processing.* FASEB J, 1995. **9**(9): p. 736-44.
290. Vishwanatha, S., R. Mains, and B. Eipper, *Chapter 244-Peptidylglycine Amidating Monooxygenase (PAM)*. Handbook of Biologically Active Peptides (Second Edition). 2013, Academic Press.
291. *Drug bank-Exenatide*. Available from: https://www.drugbank.ca/drugs/DB01276#label-reference.

292. Zhu, L., et al., *Intra-islet glucagon signaling is critical for maintaining glucose homeostasis.* JCI Insight, 2019. **5**.
293. Urban, D.J. and B.L. Roth, *DREADDs (designer receptors exclusively activated by designer drugs): chemogenetic tools with therapeutic utility.* Annu Rev Pharmacol Toxicol, 2015. **55**: p. 399-417.
294. Wess, J., K. Nakajima, and S. Jain, *Novel designer receptors to probe GPCR signaling and physiology.* Trends Pharmacol Sci, 2013. **34**(7): p. 385-92.
295. Armbruster, B.N., et al., *Evolving the lock to fit the key to create a family of G protein-coupled receptors potently activated by an inert ligand.* Proc Natl Acad Sci U S A, 2007. **104**(12): p. 5163-8.
296. Young, A.A., et al., *Glucose-lowering and insulin-sensitizing actions of exendin-4: studies in obese diabetic (ob/ob, db/db) mice, diabetic fatty Zucker rats, and diabetic rhesus monkeys (Macaca mulatta).* Diabetes, 1999. **48**(5): p. 1026-34.
297. Vickers, S.P., et al., *Effects of the DPP-4 inhibitor, linagliptin, in diet-induced obese rats: a comparison in naive and exenatide-treated animals.* Clin Lab, 2012. **58**(7-8): p. 787-99.
298. Svendsen, B., et al., *Insulin Secretion Depends on Intra-islet Glucagon Signaling.* Cell Rep, 2018. **25**(5): p. 1127-1134.e2.
299. Mastracci, T.L. and L. Sussel, *The Endocrine Pancreas: insights into development, differentiation and diabetes.* Wiley Interdiscip Rev Membr Transp Signal, 2012. **1**(5): p. 609-628.
300. Wierup, N., et al., *The ghrelin cell: a novel developmentally regulated islet cell in the human pancreas.* Regulatory Peptides, 2002. **107**(1-3): p. 63-69.
301. Alumets, J., et al., *Is GIP a glucagon cell constituent?* Histochemistry, 1978. **58**(4): p. 253-7.
302. Fujita, Y., et al., *Alternative form of glucose-dependent insulinotropic polypepide and its physiology.* J Diabetes Investig, 2016. **7 Suppl 1**: p. 33-7.
303. Larsson, L.I. and A.J. Moody, *Glicentin and gastric inhibitory polypeptide immunoreactivity in endocrine cells of the gut and pancreas.* J Histochem Cytochem, 1980. **28**(9): p. 925-33.
304. Buchan, A.M., et al., *A comparison of the ability of serum and monoclonal antibodies to gastric inhibitory polypeptide to detect immunoreactive cells in the gastroenteropancreatic system of mammals and reptiles.* Histochemistry, 1982. **76**(3): p. 341-9.
305. Segerstolpe, Å., et al., *Single-Cell Transcriptome Profiling of Human Pancreatic Islets in Health and Type 2 Diabetes.* Cell Metab, 2016. **24**(4): p. 593-607.
306. O'Malley, T.J., et al., *Progressive change of intra-islet GLP-1 production during diabetes development.* Diabetes Metab Res Rev, 2014. **30**(8): p. 661-8.
307. Song, Y., et al., *Gut-Proglucagon-Derived Peptides Are Essential for Regulating Glucose Homeostasis in Mice.* Cell Metab, 2019. **30**(5): p. 976-986.e3.
308. Traub, S., et al., *Pancreatic α Cell-Derived Glucagon-Related Peptides Are Required for β Cell Adaptation and Glucose Homeostasis.* Cell Rep, 2017. **18**(13): p. 3192-3203.
309. Whalley, N.M., et al., *Processing of proglucagon to GLP-1 in pancreatic α-cells: is this a paracrine mechanism enabling GLP-1 to act on β-cells?* J Endocrinol, 2011. **211**(1): p. 99-106.
310. Hansen, A.M., et al., *Upregulation of alpha cell glucagon-like peptide 1 (GLP-1) in Psammomys obesus--an adaptive response to hyperglycaemia?* Diabetologia, 2011. **54**(6): p. 1379-87.
311. Campbell, S.A., et al., *Human islets contain a subpopulation of glucagon-like peptide-1 secreting α cells that is increased in type 2 diabetes.* Mol Metab, 2020. **39**: p. 101014.
312. Chepurny, O.G., et al., *Nonconventional glucagon and GLP-1 receptor agonist and antagonist interplay at the GLP-1 receptor revealed in high-throughput FRET assays for cAMP.* J Biol Chem, 2019. **294**(10): p. 3514-3531.
313. Hull, R.L., et al., *Increased dietary fat promotes islet amyloid formation and beta-cell secretory dysfunction in a transgenic mouse model of islet amyloid.* Diabetes, 2003. **52**(2): p. 372-9.

314. Muoio, D.M. and C.B. Newgard, *Mechanisms of disease:Molecular and metabolic mechanisms of insulin resistance and beta-cell failure in type 2 diabetes.* Nat Rev Mol Cell Biol, 2008. **9**(3): p. 193-205.
315. Sharma, R.B., et al., *Insulin demand regulates β cell number via the unfolded protein response.* J Clin Invest, 2015. **125**(10): p. 3831-46.
316. Butler, A.E., et al., *Beta-cell deficit and increased beta-cell apoptosis in humans with type 2 diabetes.* Diabetes, 2003. **52**(1): p. 102-10.
317. Butler, A.E., et al., *Hematopoietic stem cells derived from adult donors are not a source of pancreatic beta-cells in adult nondiabetic humans.* Diabetes, 2007. **56**(7): p. 1810-6.
318. Dor, Y., et al., *Adult pancreatic beta-cells are formed by self-duplication rather than stem-cell differentiation.* Nature, 2004. **429**(6987): p. 41-6.
319. Georgia, S. and A. Bhushan, *Beta cell replication is the primary mechanism for maintaining postnatal beta cell mass.* J Clin Invest, 2004. **114**(7): p. 963-8.
320. Dusaulcy, R., et al., *High-fat diet impacts more changes in beta-cell compared to alpha-cell transcriptome.* PLoS One, 2019. **14**(3): p. e0213299.
321. Costes, S., et al., *β-Cell failure in type 2 diabetes: a case of asking too much of too few?* Diabetes, 2013. **62**(2): p. 327-35.
322. Weir, G.C. and S. Bonner-Weir, *Islet β cell mass in diabetes and how it relates to function, birth, and death.* Ann N Y Acad Sci, 2013. **1281**: p. 92-105.
323. Back, S.H. and R.J. Kaufman, *Endoplasmic reticulum stress and type 2 diabetes.* Annu Rev Biochem, 2012. **81**: p. 767-93.
324. Eizirik, D.L. and M. Cnop, *ER stress in pancreatic beta cells: the thin red line between adaptation and failure.* Sci Signal, 2010. **3**(110): p. pe7.
325. Papa, F.R., *Endoplasmic reticulum stress, pancreatic β-cell degeneration, and diabetes.* Cold Spring Harb Perspect Med, 2012. **2**(9): p. a007666.
326. Cinti, F., et al., *Evidence of β-Cell Dedifferentiation in Human Type 2 Diabetes.* J Clin Endocrinol Metab, 2016. **101**(3): p. 1044-54.
327. Talchai, C., et al., *Pancreatic β cell dedifferentiation as a mechanism of diabetic β cell failure.* Cell, 2012. **150**(6): p. 1223-34.
328. Wang, Z., et al., *Pancreatic β cell dedifferentiation in diabetes and redifferentiation following insulin therapy.* Cell Metab, 2014. **19**(5): p. 872-82.
329. Taylor, B.L., F.F. Liu, and M. Sander, *Nkx6.1 is essential for maintaining the functional state of pancreatic beta cells.* Cell Rep, 2013. **4**(6): p. 1262-75.
330. Unger, R.H. and L. Orci, *The essential role of glucagon in the pathogenesis of diabetes mellitus.* Lancet, 1975. **1**(7897): p. 14-6.
331. Boonen, K., et al., *Neuropeptides of the islets of Langerhans: a peptidomics study.* Gen Comp Endocrinol, 2007. **152**(2-3): p. 231-41.
332. Waanders, L.F., et al., *Quantitative proteomic analysis of single pancreatic islets.* Proc Natl Acad Sci U S A, 2009. **106**(45): p. 18902-7.
333. Biggs, E.K., et al., *Development and characterisation of a novel glucagon like peptide-1 receptor antibody.* Diabetologia, 2018. **61**(3): p. 711-721.
334. Reimann, F., et al., *Glucose sensing in L cells: a primary cell study.* Cell Metab, 2008. **8**(6): p. 532-9.
335. Adriaenssens, A., et al., *A Transcriptome-Led Exploration of Molecular Mechanisms Regulating Somatostatin-Producing D-Cells in the Gastric Epithelium.* Endocrinology, 2015. **156**(11): p. 3924-36.
336. *The Human Protein Atlas: PDYN expression*. Available from: https://www.proteinatlas.org/ENSG00000101327-PDYN/tissue.
337. Li, S., et al., *Molecular cloning and expression of a rat kappa opioid receptor.* Biochem J, 1993. **295 (Pt 3)**: p. 629-33.

338. Zhu, J., et al., *Cloning of a human kappa opioid receptor from the brain.* Life Sci, 1995. **56**(9): p. PL201-7.
339. Rodriguez-Diaz, R., et al., *Innervation patterns of autonomic axons in the human endocrine pancreas.* Cell Metab, 2011. **14**(1): p. 45-54.
340. Rodriguez-Diaz, R. and A. Caicedo, *Neural control of the endocrine pancreas.* Best Pract Res Clin Endocrinol Metab, 2014. **28**(5): p. 745-56.
341. Li, C., et al., *Urocortin III is expressed in pancreatic beta-cells and stimulates insulin and glucagon secretion.* Endocrinology, 2003. **144**(7): p. 3216-24.
342. van der Meulen, T., et al., *Urocortin3 mediates somatostatin-dependent negative feedback control of insulin secretion.* Nat Med, 2015. **21**(7): p. 769-76.
343. Li, C., et al., *Urocortin 3 regulates glucose-stimulated insulin secretion and energy homeostasis.* Proc Natl Acad Sci U S A, 2007. **104**(10): p. 4206-11.
344. *The Human Protein Atlas: VGF expression*.
345. Watson, E., et al., *Analysis of knockout mice suggests a role for VGF in the control of fat storage and energy expenditure.* BMC Physiol, 2009. **9**: p. 19.
346. Lin, W.J., et al., *VGF and Its C-Terminal Peptide TLQP-62 Regulate Memory Formation in Hippocampus via a BDNF-TrkB-Dependent Mechanism.* J Neurosci, 2015. **35**(28): p. 10343-56.
347. Namkoong, C., et al., *NERP-2 regulates gastric acid secretion and gastric emptying via the orexin pathway.* Biochem Biophys Res Commun, 2017. **485**(2): p. 409-413.
348. Toshinai, K., et al., *Neuroendocrine regulatory peptide-2 regulates feeding behavior via the orexin system in the hypothalamus.* Am J Physiol Endocrinol Metab, 2010. **299**(3): p. E394-401.
349. Orskov, C., A. Wettergren, and J.J. Holst, *Biological Effects and Metabolic Rates of Glucagonlike Peptide-1 7-36 Amide and Glucagonlike Peptide-1 7-37 in Healthy Subjects Are Indistinguishable.* Diabetes, 1993. **42**(5): p. 658-661.
350. Chepurny, O.G., et al., *Correction: Nonconventional glucagon and GLP-1 receptor agonist and antagonist interplay at the GLP-1 receptor revealed in high-throughput FRET assays for cAMP.* J Biol Chem, 2019. **294**(22): p. 8714.
351. Runge, S., et al., *Different domains of the glucagon and glucagon-like peptide-1 receptors provide the critical determinants of ligand selectivity.* Br J Pharmacol, 2003. **138**(5): p. 787-94.
352. Ahrén, B., *Autonomic regulation of islet hormone secretion--implications for health and disease.* Diabetologia, 2000. **43**(4): p. 393-410.
353. Gingerich, R.L., et al., *A new in vitro model for studies of pancreatic polypeptide secretion and biochemistry.* Regul Pept, 1982. **5**(1): p. 13-25.
354. Schwartz, T.W., et al., *Vagal, cholinergic regulation of pancreatic polypeptide secretion.* J Clin Invest, 1978. **61**(3): p. 781-9.
355. Meglasson, M.D. and R.L. Hazelwood, *Adrenergic regulation of avian pancreatic polypeptide secretion in vitro.* Am J Physiol, 1983. **244**(4): p. E408-13.
356. Vieira, E., A. Salehi, and E. Gylfe, *Glucose inhibits glucagon secretion by a direct effect on mouse pancreatic alpha cells.* Diabetologia, 2007. **50**(2): p. 370-9.
357. Burke, S.J., et al., *db / db Mice Exhibit Features of Human Type 2 Diabetes That Are Not Present in Weight-Matched C57BL/6J Mice Fed a Western Diet.* J Diabetes Res, 2017. **2017**: p. 8503754.
358. Docherty, K. and A.R. Clark, *Nutrient regulation of insulin gene expression.* The FASEB Journal, 1994. **8**(1): p. 20-27.
359. Burke, S.J., M.D. Karlstad, and J.J. Collier, *Pancreatic Islet Responses to Metabolic Trauma.* Shock, 2016. **46**(3): p. 230-8.
360. Pfützner, A., et al., *Role of intact proinsulin in diagnosis and treatment of type 2 diabetes mellitus.* Diabetes Technol Ther, 2004. **6**(3): p. 405-12.
361. Pfützner, A., et al., *IRIS II study: intact proinsulin is confirmed as a highly specific indicator for insulin resistance in a large cross-sectional study design.* Diabetes Technol Ther, 2005. **7**(3): p. 478-86.

362. Mezza, T., et al., *β-Cell Fate in Human Insulin Resistance and Type 2 Diabetes: A Perspective on Islet Plasticity.* Diabetes, 2019. **68**(6): p. 1121-1129.
363. Beumer, J., et al., *High-Resolution mRNA and Secretome Atlas of Human Enteroendocrine Cells.* Cell, 2020.
364. Larraufie, P., et al., *Important Role of the GLP-1 Axis for Glucose Homeostasis after Bariatric Surgery.* Cell Reports, 2019. **26**(6): p. 1399-1408.e6.
365. Hansen, L., et al., *Glucagon-Like Peptide-1-(7–36)Amide Is Transformed to Glucagon-Like Peptide-1-(9–36)Amide by Dipeptidyl Peptidase IV in the Capillaries Supplying the L Cells of the Porcine Intestine1.* Endocrinology, 1999. **140**(11): p. 5356-5363.
366. Chambers, A.P., et al., *The Role of Pancreatic Preproglucagon in Glucose Homeostasis in Mice.* Cell Metabolism, 2017. **25**(4): p. 927-934.e3.

Appendix 1

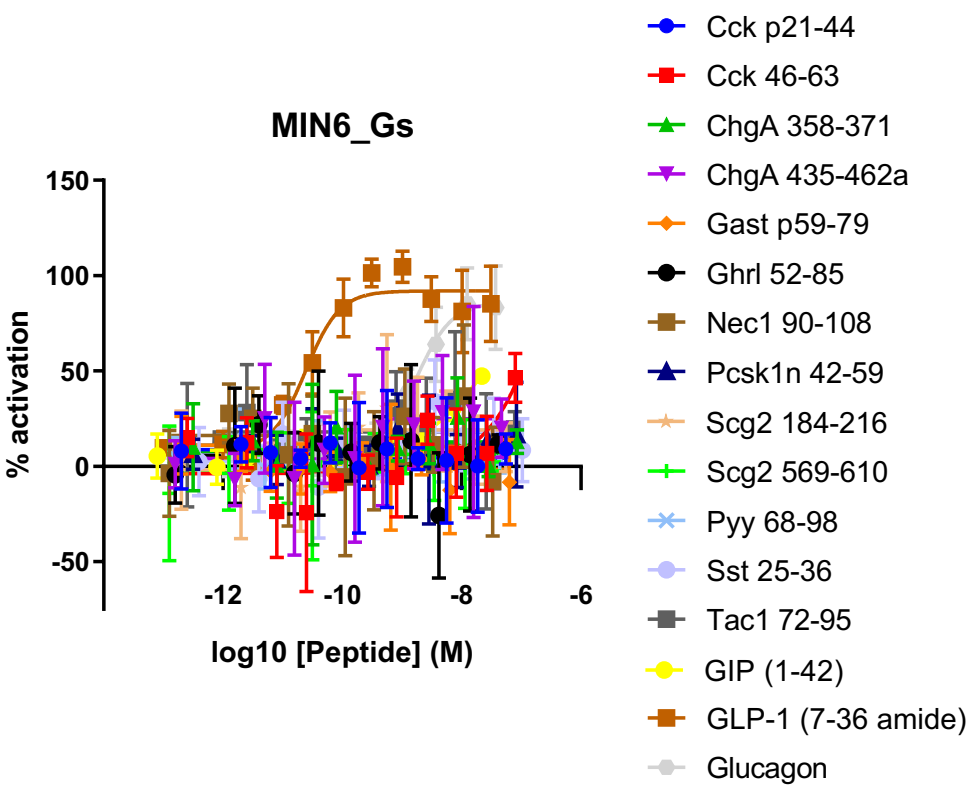

Supplementary figure 1: Screening for Gs activity in MIN6 cell line. *Glucagon, GLP-1 (7-36 amide) and GIP (1-42) were used as positive controls.*

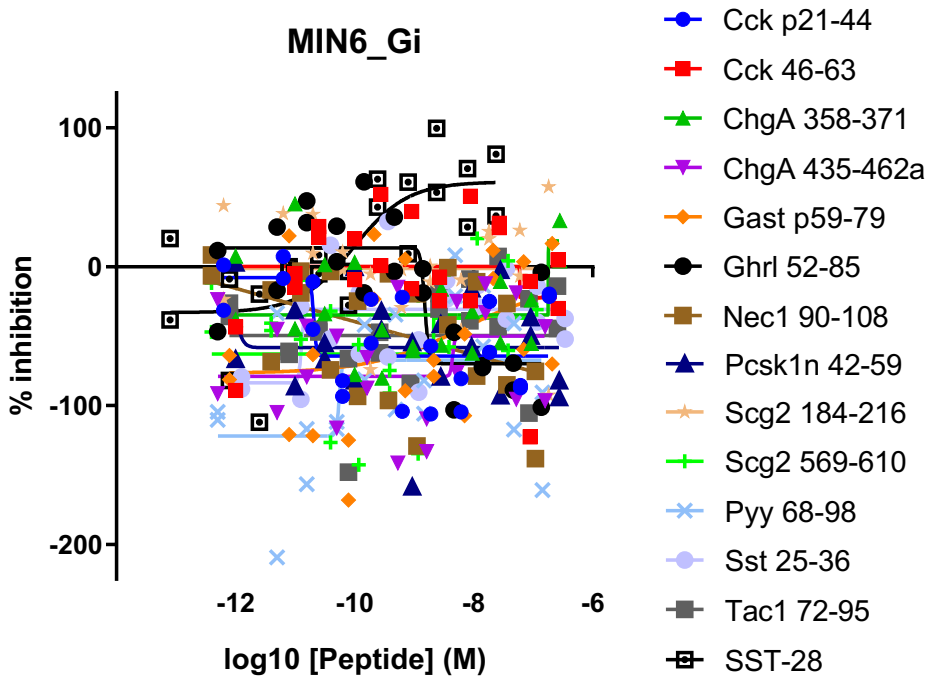

Supplementary figure 2: Screening for Gi activity in MIN6 cell line. *SST-28 used as positive control.*

Appendix 2

Peptide	Beta (Z score)	Alpha (Z score)	Delta (Z score)	Cluster
CBPE_28-37	1.105	-0.730	-0.375	Cluster 6
CMGA_139-151	1.298	-0.690	-0.608	Cluster 6
CMGA_358-368	1.254	-0.627	-0.627	Cluster 6
CMGA_358-369	1.069	-0.532	-0.537	Cluster 6
CMGA_358-370	1.203	-0.549	-0.654	Cluster 6
CMGA_358-371	1.206	-0.665	-0.542	Cluster 6
CMGA_358-371.1	1.147	-0.872	-0.275	Cluster 6
CMGA_359-369	1.227	-0.613	-0.613	Cluster 6
CMGA_359-370	1.267	-0.634	-0.634	Cluster 6
CMGA_359-371	1.241	-0.537	-0.704	Cluster 6
CMGA_360-371	1.002	-0.501	-0.501	Cluster 6
CMGA_361-369	1.101	-0.266	-0.835	Cluster 6
CMGA_361-370	1.273	-0.478	-0.795	Cluster 6
CMGA_361-371	1.176	-0.539	-0.638	Cluster 6
CMGA_361-371.1	1.261	-0.614	-0.647	Cluster 6
CMGA_362-370	1.324	-0.662	-0.662	Cluster 6
CMGA_362-371	1.260	-0.630	-0.630	Cluster 6
CMGA_363-371	1.226	-0.613	-0.613	Cluster 6
CMGA_374-388	-0.466	1.270	-0.804	Cluster 1
CMGA_374-388.1	0.494	0.517	-1.010	Cluster 3
CMGA_374-390	1.289	-0.583	-0.706	Cluster 6
CMGA_374-390.1	1.261	-0.534	-0.728	Cluster 6
CMGA_374-401	1.047	-0.743	-0.304	Cluster 6
CMGA_374-402	1.154	-0.705	-0.449	Cluster 6
CMGA_374-402.1	1.132	-0.658	-0.474	Cluster 6
CMGA_375-388	1.242	-0.621	-0.621	Cluster 6
CMGA_375-388.1	1.255	-0.554	-0.701	Cluster 6
CMGA_375-390	1.289	-0.630	-0.659	Cluster 6
CMGA_375-390.1	1.283	-0.633	-0.650	Cluster 6
CMGA_376-388	1.249	-0.609	-0.639	Cluster 6
CMGA_376-388.1	1.257	-0.629	-0.629	Cluster 6
CMGA_376-390	1.224	-0.552	-0.672	Cluster 6
CMGA_378-388	1.225	-0.621	-0.604	Cluster 6
CMGA_390-402	1.252	-0.540	-0.712	Cluster 6
CMGA_392-400	-0.573	1.326	-0.753	Cluster 1
CMGA_392-401	0.696	-1.315	0.619	Cluster 5
CMGA_392-402	1.280	-0.686	-0.595	Cluster 6

Peptide	Beta (Z score)	Alpha (Z score)	Delta (Z score)	Cluster
CMGA_393-402	1.264	-0.616	-0.648	Cluster 6
CMGA_394-402	1.225	-0.523	-0.701	Cluster 6
CMGA_395-402	1.215	-0.571	-0.644	Cluster 6
CMGA_405-417	1.226	-0.613	-0.613	Cluster 6
CMGA_419-462	1.225	-0.552	-0.673	Cluster 6
CMGA_435-457	1.230	-0.528	-0.702	Cluster 6
CMGA_435-458	1.177	-0.705	-0.472	Cluster 6
CMGA_435-459	1.049	-0.541	-0.508	Cluster 6
CMGA_435-460	1.196	-0.697	-0.499	Cluster 6
CMGA_435-461	1.163	-0.581	-0.581	Cluster 6
CMGA_435-462	1.282	-0.667	-0.616	Cluster 6
CMGA_435-463	-0.620	1.240	-0.620	Cluster 1
CYTC_21-43	1.268	-0.634	-0.634	Cluster 6
CYTC_46-64	1.235	-0.617	-0.617	Cluster 6
CYTC_50-72	1.319	-0.731	-0.589	Cluster 6
DPOLB_194-200	0.326	0.438	-0.765	Cluster 3
FAS_273-289	1.237	-0.639	-0.598	Cluster 6
GLUC_131-142	-0.658	1.315	-0.658	Cluster 1
GLUC_131-143	-0.656	1.312	-0.656	Cluster 1
GLUC_131-145	-0.157	0.707	-0.549	Cluster 3
GLUC_147-178	-0.470	0.940	-0.470	Cluster 1
GLUC_163-170	-0.659	1.317	-0.659	Cluster 1
GLUC_163-171	-0.665	1.330	-0.665	Cluster 1
GLUC_166-178	-0.662	1.325	-0.662	Cluster 1
GLUC_167-178	-0.654	1.308	-0.654	Cluster 1
GLUC_168-178	-0.666	1.333	-0.666	Cluster 1
GLUC_18-50	-0.632	1.263	-0.632	Cluster 1
GLUC_21-35	-0.655	1.309	-0.655	Cluster 1
GLUC_21-36	-0.654	1.308	-0.654	Cluster 1
GLUC_21-43	-0.670	1.307	-0.637	Cluster 1
GLUC_21-45	-0.656	1.311	-0.656	Cluster 1
GLUC_21-46	-0.712	1.329	-0.617	Cluster 1
GLUC_21-47	-0.666	1.332	-0.666	Cluster 1
GLUC_21-47.1	-0.706	1.329	-0.623	Cluster 1
GLUC_21-48	-0.684	1.313	-0.629	Cluster 1
GLUC_21-48.1	-0.659	1.309	-0.649	Cluster 1
GLUC_21-49	-0.696	1.328	-0.632	Cluster 1
GLUC_21-49.1	-0.746	1.293	-0.547	Cluster 1
GLUC_21-49.2	-0.656	1.311	-0.656	Cluster 1
GLUC_21-50	-0.576	1.116	-0.540	Cluster 1
GLUC_21-50.1	-0.661	1.285	-0.625	Cluster 1

Peptide	Beta (Z score)	Alpha (Z score)	Delta (Z score)	Cluster
GLUC_21-50.2	-0.662	1.325	-0.662	Cluster 1
GLUC_22-46	-0.667	1.333	-0.667	Cluster 1
GLUC_22-49	-0.650	1.267	-0.617	Cluster 1
GLUC_22-50	-0.665	1.329	-0.665	Cluster 1
GLUC_23-35	-0.644	1.287	-0.644	Cluster 1
GLUC_23-36	-0.631	1.262	-0.631	Cluster 1
GLUC_23-43	-0.643	1.286	-0.643	Cluster 1
GLUC_23-45	-0.647	1.294	-0.647	Cluster 1
GLUC_23-46	-0.672	1.323	-0.651	Cluster 1
GLUC_23-47	-0.657	1.314	-0.657	Cluster 1
GLUC_23-47.1	-0.663	1.326	-0.663	Cluster 1
GLUC_23-48	-0.638	1.268	-0.630	Cluster 1
GLUC_23-48.1	-0.649	1.297	-0.649	Cluster 1
GLUC_23-49	-0.658	1.276	-0.618	Cluster 1
GLUC_23-49.1	-0.654	1.300	-0.646	Cluster 1
GLUC_23-50	-0.626	1.248	-0.622	Cluster 1
GLUC_23-50.1	-0.674	1.333	-0.659	Cluster 1
GLUC_24-49	-0.645	1.290	-0.645	Cluster 1
GLUC_24-49.1	-0.677	1.333	-0.656	Cluster 1
GLUC_24-50	-0.621	1.242	-0.621	Cluster 1
GLUC_24-50.1	-0.662	1.324	-0.662	Cluster 1
GLUC_25-43	-0.630	1.260	-0.630	Cluster 1
GLUC_25-45	-0.642	1.284	-0.642	Cluster 1
GLUC_25-46	-0.623	1.246	-0.623	Cluster 1
GLUC_25-49	-0.642	1.285	-0.642	Cluster 1
GLUC_26-49	-0.656	1.312	-0.656	Cluster 1
GLUC_26-49.1	-0.667	1.333	-0.667	Cluster 1
GLUC_26-50	-0.640	1.279	-0.640	Cluster 1
GLUC_30-49	-0.640	1.281	-0.640	Cluster 1
GLUC_30-49.1	-0.645	1.290	-0.645	Cluster 1
GLUC_30-50	-0.609	1.219	-0.609	Cluster 1
GLUC_32-46	-0.665	1.331	-0.665	Cluster 1
GLUC_32-47	-0.692	1.326	-0.634	Cluster 1
GLUC_32-47.1	-0.665	1.330	-0.665	Cluster 1
GLUC_32-48	-0.665	1.329	-0.665	Cluster 1
GLUC_32-48.1	-0.666	1.332	-0.666	Cluster 1
GLUC_32-49	-0.691	1.328	-0.638	Cluster 1
GLUC_32-49.1	-0.686	1.332	-0.646	Cluster 1
GLUC_32-50	-0.667	1.300	-0.633	Cluster 1
GLUC_32-50.1	-0.676	1.332	-0.657	Cluster 1
GLUC_33-49	-0.654	1.309	-0.654	Cluster 1

Peptide	Beta (Z score)	Alpha (Z score)	Delta (Z score)	Cluster
GLUC_33-50	-0.664	1.329	-0.664	Cluster 1
GLUC_53-65	-0.642	1.284	-0.642	Cluster 1
GLUC_53-66	-0.659	1.318	-0.659	Cluster 1
GLUC_53-67	-0.638	1.276	-0.638	Cluster 1
GLUC_53-68	-0.678	1.297	-0.620	Cluster 1
GLUC_53-69	-0.624	1.247	-0.624	Cluster 1
GLUC_53-70	-0.531	1.062	-0.531	Cluster 1
GLUC_53-71	-0.662	1.324	-0.662	Cluster 1
GLUC_53-72	-0.660	1.319	-0.660	Cluster 1
GLUC_53-73	-0.660	1.320	-0.660	Cluster 1
GLUC_53-74	-0.662	1.324	-0.662	Cluster 1
GLUC_53-76	-0.634	1.268	-0.634	Cluster 1
GLUC_53-77	-0.685	1.328	-0.643	Cluster 1
GLUC_53-78	-0.684	1.331	-0.647	Cluster 1
GLUC_53-79	-0.660	1.321	-0.660	Cluster 1
GLUC_53-80	-0.659	1.318	-0.659	Cluster 1
GLUC_53-81	-0.654	1.308	-0.654	Cluster 1
GLUC_53-81.1	-0.678	1.299	-0.622	Cluster 1
GLUC_53-81.2	-0.685	1.332	-0.648	Cluster 1
GLUC_53-84	-0.547	1.095	-0.547	Cluster 1
GLUC_53-89	-0.665	1.331	-0.665	Cluster 1
GLUC_54-66	-0.667	1.333	-0.667	Cluster 1
GLUC_54-68	-0.666	1.332	-0.666	Cluster 1
GLUC_54-81	-0.650	1.301	-0.650	Cluster 1
GLUC_54-81.1	-0.654	1.307	-0.654	Cluster 1
GLUC_55-68	-0.624	1.248	-0.624	Cluster 1
GLUC_55-81	-0.609	1.218	-0.609	Cluster 1
GLUC_56-81	-0.647	1.294	-0.647	Cluster 1
GLUC_59-73	-0.665	1.331	-0.665	Cluster 1
GLUC_59-81	-0.658	1.316	-0.658	Cluster 1
GLUC_68-81	-0.665	1.330	-0.665	Cluster 1
GLUC_70-81	-0.686	1.320	-0.633	Cluster 1
GLUC_71-78	-0.667	1.333	-0.667	Cluster 1
GLUC_71-81	-0.687	1.320	-0.633	Cluster 1
GLUC_71-81.1	-0.677	1.321	-0.644	Cluster 1
GLUC_92-119	-0.647	1.294	-0.647	Cluster 1
GLUC_92-127	-0.603	1.167	-0.565	Cluster 1
GLUC_92-128	-0.615	1.189	-0.573	Cluster 1
GLUC_92-129	-0.667	1.333	-0.667	Cluster 1
GLUC_98-127	-0.634	1.269	-0.634	Cluster 1
HNRPM_596-616	1.258	-0.629	-0.629	Cluster 6

Peptide	Beta (Z score)	Alpha (Z score)	Delta (Z score)	Cluster
IAPP_38-52	1.218	-0.644	-0.575	Cluster 6
IAPP_38-53	1.231	-0.649	-0.581	Cluster 6
IAPP_38-54	1.236	-0.662	-0.573	Cluster 6
IAPP_38-55	1.005	-0.531	-0.474	Cluster 6
IAPP_38-59	1.210	-0.605	-0.605	Cluster 6
IAPP_38-74	1.198	-0.657	-0.540	Cluster 6
IAPP_39-52	1.161	-0.580	-0.580	Cluster 6
IAPP_39-53	1.158	-0.579	-0.579	Cluster 6
IAPP_39-54	1.146	-0.573	-0.573	Cluster 6
IAPP_41-52	1.274	-0.637	-0.637	Cluster 6
IAPP_41-53	1.280	-0.640	-0.640	Cluster 6
IAPP_41-54	1.287	-0.644	-0.644	Cluster 6
IAPP_41-74	1.286	-0.643	-0.643	Cluster 6
IAPP_49-55	1.064	-0.724	-0.340	Cluster 6
IAPP_52-74	1.297	-0.648	-0.648	Cluster 6
IAPP_53-74	1.258	-0.701	-0.556	Cluster 6
IAPP_54-74	1.209	-0.722	-0.488	Cluster 6
IAPP_56-72	1.200	-0.600	-0.600	Cluster 6
IAPP_56-73	1.217	-0.609	-0.609	Cluster 6
IAPP_56-74	1.246	-0.674	-0.572	Cluster 6
IAPP_57-74	1.190	-0.595	-0.595	Cluster 6
IAPP_58-74	1.172	-0.586	-0.586	Cluster 6
IAPP_59-74	1.288	-0.644	-0.644	Cluster 6
IAPP_64-74	1.189	-0.595	-0.595	Cluster 6
IAPP_78-90	1.264	-0.703	-0.560	Cluster 6
IAPP_78-90.1	1.270	-0.635	-0.635	Cluster 6
IAPP_78-91	1.064	-0.914	-0.149	Cluster 6
IAPP_78-92	0.944	-1.113	0.169	Cluster 5
IAPP_78-93	0.730	-1.267	0.537	Cluster 5
IAPP_79-90	1.279	-0.661	-0.618	Cluster 6
IAPP_79-93	1.235	-0.741	-0.494	Cluster 6
IAPP_80-90	1.263	-0.654	-0.608	Cluster 6
IAPP_80-91	1.233	-0.617	-0.617	Cluster 6
IAPP_80-93	1.253	-0.881	-0.372	Cluster 6
IAPP_81-90	1.298	-0.671	-0.627	Cluster 6
IAPP_81-91	1.237	-0.661	-0.576	Cluster 6
IAPP_81-92	1.298	-0.682	-0.617	Cluster 6
IAPP_81-93	1.327	-0.758	-0.569	Cluster 6
IAPP_82-90	1.282	-0.671	-0.611	Cluster 6
IAPP_82-91	1.272	-0.636	-0.636	Cluster 6
IAPP_82-92	1.324	-0.725	-0.600	Cluster 6

Peptide	Beta (Z score)	Alpha (Z score)	Delta (Z score)	Cluster
IAPP_83-91	1.233	-0.654	-0.579	Cluster 6
IAPP_83-92	1.199	-0.738	-0.461	Cluster 6
IAPP_84-90	1.248	-0.624	-0.624	Cluster 6
IAPP_84-91	1.229	-0.614	-0.614	Cluster 6
IAPP_84-92	1.246	-0.630	-0.615	Cluster 6
IAPP_84-93	1.195	-0.611	-0.585	Cluster 6
IAPP_85-91	1.240	-0.620	-0.620	Cluster 6
IAPP_85-92	1.218	-0.609	-0.609	Cluster 6
IAPP_85-93	1.267	-0.634	-0.634	Cluster 6
INS1_25-40	1.222	-0.611	-0.611	Cluster 6
INS1_25-54	1.247	-0.627	-0.621	Cluster 6
INS1_26-54	1.325	-0.663	-0.663	Cluster 6
INS1_41-49	1.263	-0.632	-0.632	Cluster 6
INS1_41-54	1.266	-0.633	-0.633	Cluster 6
INS1_47-54	1.088	-0.544	-0.544	Cluster 6
INS1_57-67	1.248	-0.624	-0.624	Cluster 6
INS1_57-68	1.210	-0.605	-0.605	Cluster 6
INS1_57-70	0.972	-0.486	-0.486	Cluster 6
INS1_57-73	1.281	-0.641	-0.641	Cluster 6
INS1_57-74	1.277	-0.638	-0.638	Cluster 6
INS1_57-75	1.310	-0.658	-0.652	Cluster 6
INS1_57-76	1.291	-0.646	-0.644	Cluster 6
INS1_57-77	1.244	-0.623	-0.620	Cluster 6
INS1_57-78	1.265	-0.635	-0.630	Cluster 6
INS1_57-79	1.268	-0.637	-0.632	Cluster 6
INS1_57-80	1.251	-0.627	-0.624	Cluster 6
INS1_57-81	1.263	-0.632	-0.632	Cluster 6
INS1_57-82	1.131	-0.565	-0.565	Cluster 6
INS1_57-83	1.214	-0.607	-0.607	Cluster 6
INS1_57-85	1.180	-0.598	-0.583	Cluster 6
INS1_58-66	1.248	-0.624	-0.624	Cluster 6
INS1_58-68	1.259	-0.629	-0.629	Cluster 6
INS1_58-74	1.308	-0.654	-0.654	Cluster 6
INS1_58-75	1.289	-0.647	-0.642	Cluster 6
INS1_58-76	1.252	-0.626	-0.626	Cluster 6
INS1_58-77	1.250	-0.628	-0.622	Cluster 6
INS1_58-78	1.238	-0.622	-0.616	Cluster 6
INS1_58-79	1.318	-0.665	-0.653	Cluster 6
INS1_58-80	1.304	-0.659	-0.646	Cluster 6
INS1_58-85	1.286	-0.643	-0.643	Cluster 6
INS1_59-76	1.249	-0.625	-0.625	Cluster 6

Peptide	Beta (Z score)	Alpha (Z score)	Delta (Z score)	Cluster
INS1_59-77	1.261	-0.630	-0.630	Cluster 6
INS1_59-78	1.247	-0.624	-0.624	Cluster 6
INS1_59-79	1.313	-0.657	-0.657	Cluster 6
INS1_59-80	1.306	-0.653	-0.653	Cluster 6
INS1_60-77	1.245	-0.635	-0.611	Cluster 6
INS1_60-78	1.269	-0.647	-0.622	Cluster 6
INS1_60-79	1.272	-0.643	-0.629	Cluster 6
INS1_60-80	1.315	-0.664	-0.651	Cluster 6
INS1_61-75	1.276	-0.638	-0.638	Cluster 6
INS1_61-76	1.225	-0.612	-0.612	Cluster 6
INS1_61-77	1.264	-0.635	-0.629	Cluster 6
INS1_61-78	1.318	-0.659	-0.659	Cluster 6
INS1_61-79	1.321	-0.664	-0.657	Cluster 6
INS1_61-80	1.317	-0.663	-0.654	Cluster 6
INS1_61-85	1.281	-0.640	-0.640	Cluster 6
INS1_62-75	1.248	-0.624	-0.624	Cluster 6
INS1_62-76	1.276	-0.638	-0.638	Cluster 6
INS1_62-77	1.318	-0.659	-0.659	Cluster 6
INS1_62-77.1	1.245	-0.622	-0.622	Cluster 6
INS1_62-78	1.229	-0.614	-0.614	Cluster 6
INS1_62-79	1.232	-0.616	-0.616	Cluster 6
INS1_62-80	0.990	-0.495	-0.495	Cluster 6
INS1_63-75	1.264	-0.632	-0.632	Cluster 6
INS1_63-76	1.223	-0.612	-0.612	Cluster 6
INS1_63-77	1.218	-0.606	-0.612	Cluster 6
INS1_63-78	1.189	-0.595	-0.595	Cluster 6
INS1_63-79	1.221	-0.611	-0.611	Cluster 6
INS1_65-76	1.230	-0.615	-0.615	Cluster 6
INS1_65-77	1.229	-0.615	-0.615	Cluster 6
INS1_65-79	1.244	-0.622	-0.622	Cluster 6
INS1_65-80	1.289	-0.645	-0.645	Cluster 6
INS1_66-76	1.224	-0.612	-0.612	Cluster 6
INS1_66-77	1.201	-0.601	-0.601	Cluster 6
INS1_66-78	1.197	-0.599	-0.599	Cluster 6
INS1_67-77	1.222	-0.618	-0.605	Cluster 6
INS1_67-79	1.244	-0.622	-0.622	Cluster 6
INS1_68-78	1.201	-0.600	-0.600	Cluster 6
INS1_69-79	1.276	-0.638	-0.638	Cluster 6
INS1_69-85	1.269	-0.634	-0.634	Cluster 6
INS1_70-80	1.245	-0.623	-0.623	Cluster 6
INS1_71-79	1.264	-0.632	-0.632	Cluster 6

Peptide	Beta (Z score)	Alpha (Z score)	Delta (Z score)	Cluster
INS1_88-100	1.240	-0.620	-0.620	Cluster 6
INS1_88-101	1.200	-0.600	-0.600	Cluster 6
INS1_88-105	1.195	-0.597	-0.597	Cluster 6
INS1_88-106	1.223	-0.612	-0.612	Cluster 6
INS1_88-108	1.129	-0.568	-0.561	Cluster 6
INS1_88-98	1.260	-0.630	-0.630	Cluster 6
INS1_89-108	1.324	-0.662	-0.662	Cluster 6
INS1_93-108	1.205	-0.603	-0.603	Cluster 6
INS1_94-108	1.208	-0.604	-0.604	Cluster 6
INS1_99-108	1.233	-0.617	-0.617	Cluster 6
INS2_101-110	1.233	-0.617	-0.617	Cluster 6
INS2_25-39	1.259	-0.629	-0.629	Cluster 6
INS2_25-40	1.322	-0.661	-0.661	Cluster 6
INS2_25-42	1.307	-0.653	-0.653	Cluster 6
INS2_25-43	1.264	-0.632	-0.632	Cluster 6
INS2_25-48	1.135	-0.568	-0.568	Cluster 6
INS2_25-53	1.149	-0.574	-0.574	Cluster 6
INS2_25-53.1	1.153	-0.576	-0.576	Cluster 6
INS2_25-54	1.314	-0.665	-0.649	Cluster 6
INS2_25-54.1	1.306	-0.657	-0.649	Cluster 6
INS2_25-54.2	1.270	-0.635	-0.635	Cluster 6
INS2_31-54	1.187	-0.593	-0.593	Cluster 6
INS2_40-54	1.260	-0.630	-0.630	Cluster 6
INS2_41-49	1.263	-0.632	-0.632	Cluster 6
INS2_41-54	1.273	-0.637	-0.637	Cluster 6
INS2_41-54.1	1.255	-0.627	-0.627	Cluster 6
INS2_43-54	1.296	-0.648	-0.648	Cluster 6
INS2_44-54	1.309	-0.655	-0.655	Cluster 6
INS2_44-54.1	1.304	-0.652	-0.652	Cluster 6
INS2_57-110	1.286	-0.643	-0.643	Cluster 6
INS2_57-66	1.174	-0.587	-0.587	Cluster 6
INS2_57-67	1.254	-0.627	-0.627	Cluster 6
INS2_57-71	1.205	-0.603	-0.603	Cluster 6
INS2_57-72	1.091	-0.537	-0.553	Cluster 6
INS2_57-73	1.274	-0.637	-0.637	Cluster 6
INS2_57-74	1.285	-0.642	-0.642	Cluster 6
INS2_57-75	1.266	-0.633	-0.633	Cluster 6
INS2_57-76	1.282	-0.645	-0.638	Cluster 6
INS2_57-77	1.298	-0.653	-0.645	Cluster 6
INS2_57-78	1.253	-0.628	-0.626	Cluster 6
INS2_57-79	1.251	-0.631	-0.620	Cluster 6

Peptide	Beta (Z score)	Alpha (Z score)	Delta (Z score)	Cluster
INS2_57-80	1.256	-0.636	-0.621	Cluster 6
INS2_57-81	1.291	-0.651	-0.639	Cluster 6
INS2_57-82	1.221	-0.616	-0.605	Cluster 6
INS2_57-84	1.305	-0.652	-0.652	Cluster 6
INS2_57-86	1.270	-0.635	-0.635	Cluster 6
INS2_57-87	1.235	-0.628	-0.607	Cluster 6
INS2_58-66	1.221	-0.611	-0.611	Cluster 6
INS2_58-72	1.093	-0.539	-0.553	Cluster 6
INS2_58-75	1.275	-0.638	-0.638	Cluster 6
INS2_58-77	1.245	-0.629	-0.616	Cluster 6
INS2_58-78	1.223	-0.616	-0.607	Cluster 6
INS2_58-79	1.224	-0.622	-0.602	Cluster 6
INS2_58-80	1.294	-0.659	-0.635	Cluster 6
INS2_58-81	1.303	-0.661	-0.642	Cluster 6
INS2_58-82	1.310	-0.662	-0.648	Cluster 6
INS2_58-87	1.213	-0.606	-0.606	Cluster 6
INS2_59-72	1.098	-0.544	-0.554	Cluster 6
INS2_59-76	1.241	-0.621	-0.621	Cluster 6
INS2_59-77	1.185	-0.593	-0.593	Cluster 6
INS2_59-78	1.234	-0.617	-0.617	Cluster 6
INS2_59-79	1.145	-0.575	-0.569	Cluster 6
INS2_59-80	1.130	-0.565	-0.565	Cluster 6
INS2_59-81	1.198	-0.599	-0.599	Cluster 6
INS2_59-82	1.235	-0.618	-0.618	Cluster 6
INS2_59-87	1.194	-0.597	-0.597	Cluster 6
INS2_60-72	1.138	-0.569	-0.569	Cluster 6
INS2_60-77	1.283	-0.661	-0.622	Cluster 6
INS2_60-78	1.160	-0.580	-0.580	Cluster 6
INS2_60-79	1.243	-0.634	-0.609	Cluster 6
INS2_60-80	1.241	-0.632	-0.610	Cluster 6
INS2_60-81	1.255	-0.635	-0.620	Cluster 6
INS2_60-82	1.281	-0.640	-0.640	Cluster 6
INS2_61-72	1.121	-0.560	-0.560	Cluster 6
INS2_61-77	1.252	-0.626	-0.626	Cluster 6
INS2_61-78	1.272	-0.636	-0.636	Cluster 6
INS2_61-79	1.266	-0.637	-0.628	Cluster 6
INS2_61-80	1.288	-0.651	-0.636	Cluster 6
INS2_61-81	1.300	-0.655	-0.646	Cluster 6
INS2_61-82	1.309	-0.659	-0.650	Cluster 6
INS2_61-87	1.264	-0.632	-0.632	Cluster 6
INS2_62-72	1.181	-0.590	-0.590	Cluster 6

Peptide	Beta (Z score)	Alpha (Z score)	Delta (Z score)	Cluster
INS2_62-77	1.260	-0.630	-0.630	Cluster 6
INS2_62-79	1.128	-0.564	-0.564	Cluster 6
INS2_62-79.1	1.076	-0.538	-0.538	Cluster 6
INS2_62-80	1.127	-0.564	-0.564	Cluster 6
INS2_62-81	1.145	-0.573	-0.573	Cluster 6
INS2_62-82	1.185	-0.593	-0.593	Cluster 6
INS2_62-82.1	1.216	-0.608	-0.608	Cluster 6
INS2_63-72	1.164	-0.582	-0.582	Cluster 6
INS2_63-79	1.215	-0.608	-0.608	Cluster 6
INS2_63-80	1.101	-0.550	-0.550	Cluster 6
INS2_63-82	1.252	-0.626	-0.626	Cluster 6
INS2_64-79	1.233	-0.616	-0.616	Cluster 6
INS2_65-79	1.234	-0.617	-0.617	Cluster 6
INS2_65-80	1.182	-0.591	-0.591	Cluster 6
INS2_65-82	1.202	-0.601	-0.601	Cluster 6
INS2_66-78	1.213	-0.607	-0.607	Cluster 6
INS2_66-79	1.185	-0.596	-0.589	Cluster 6
INS2_66-82	1.254	-0.627	-0.627	Cluster 6
INS2_66-87	1.116	-0.558	-0.558	Cluster 6
INS2_67-77	1.263	-0.631	-0.631	Cluster 6
INS2_67-78	1.269	-0.634	-0.634	Cluster 6
INS2_67-79	1.199	-0.599	-0.599	Cluster 6
INS2_67-80	1.206	-0.610	-0.596	Cluster 6
INS2_67-81	1.225	-0.617	-0.608	Cluster 6
INS2_67-82	1.281	-0.652	-0.629	Cluster 6
INS2_67-87	1.059	-0.530	-0.530	Cluster 6
INS2_68-79	1.207	-0.604	-0.604	Cluster 6
INS2_68-80	1.167	-0.583	-0.583	Cluster 6
INS2_68-81	1.207	-0.603	-0.603	Cluster 6
INS2_69-80	1.200	-0.600	-0.600	Cluster 6
INS2_69-81	1.221	-0.619	-0.601	Cluster 6
INS2_69-82	1.206	-0.603	-0.603	Cluster 6
INS2_70-80	1.173	-0.586	-0.586	Cluster 6
INS2_70-81	1.194	-0.597	-0.597	Cluster 6
INS2_70-82	1.172	-0.586	-0.586	Cluster 6
INS2_71-80	1.203	-0.602	-0.602	Cluster 6
INS2_71-82	1.179	-0.589	-0.589	Cluster 6
INS2_73-81	1.080	-0.540	-0.540	Cluster 6
INS2_73-87	1.034	-0.517	-0.517	Cluster 6
INS2_80-87	1.232	-0.616	-0.616	Cluster 6
INS2_90-100	1.260	-0.630	-0.630	Cluster 6

Peptide	Beta (Z score)	Alpha (Z score)	Delta (Z score)	Cluster
INS2_90-102	1.240	-0.620	-0.620	Cluster 6
INS2_90-103	1.200	-0.600	-0.600	Cluster 6
INS2_90-107	1.195	-0.597	-0.597	Cluster 6
INS2_90-108	1.223	-0.612	-0.612	Cluster 6
INS2_90-110	1.129	-0.568	-0.561	Cluster 6
INS2_91-110	1.324	-0.662	-0.662	Cluster 6
INS2_95-110	1.205	-0.603	-0.603	Cluster 6
INS2_96-110	1.208	-0.604	-0.604	Cluster 6
NEC1_90-108	1.218	-0.682	-0.535	Cluster 6
NEC1_91-108	1.204	-0.602	-0.602	Cluster 6
NEC2_419-428	0.283	0.767	-1.050	Cluster 3
NEC2_616-634	-0.892	1.231	-0.339	Cluster 1
NEC2_616-637	-0.820	1.225	-0.405	Cluster 1
NEC2_616-637.1	-1.010	0.897	0.114	Cluster 2
NEC2_629-637	1.226	-0.613	-0.613	Cluster 6
NEC2_87-104	-0.174	-0.945	1.119	Cluster 4
NEC2_87-104.1	-0.625	-0.625	1.250	Cluster 4
NEC2_87-98	1.307	-0.653	-0.653	Cluster 6
NEC2_94-104	-1.025	1.158	-0.132	Cluster 1
NEC2_94-104.1	-0.965	1.189	-0.223	Cluster 1
PAHO_30-65	-0.802	0.764	0.038	Cluster 1
PAHO_30-65.1	-1.305	0.557	0.748	Cluster 2
PAHO_30-65.2	-1.186	0.788	0.398	Cluster 2
PAHO_30-65.3	-1.199	0.575	0.625	Cluster 2
PAHO_32-64	-0.877	0.825	0.052	Cluster 2
PAHO_32-65	-1.303	0.635	0.668	Cluster 2
PAHO_32-65.1	-1.313	0.563	0.750	Cluster 2
PAHO_32-65.2	-1.118	0.478	0.640	Cluster 2
PAHO_56-65	-1.195	0.099	1.096	Cluster 2
PAHO_69-100	-1.024	1.235	-0.210	Cluster 1
PCSK1_219-237	-0.658	1.316	-0.658	Cluster 1
PCSK1_219-238	-1.166	0.661	0.505	Cluster 2
PCSK1_219-240	-1.081	0.202	0.879	Cluster 4
PCSK1_243-258	-1.074	1.216	-0.142	Cluster 1
PCSK1_244-258	-0.309	-0.828	1.137	Cluster 4
PCSK1_42-57	-0.646	-0.646	1.292	Cluster 4
PCSK1_42-59	-0.995	-0.145	1.140	Cluster 4
PCSK1_62-76	1.246	-0.623	-0.623	Cluster 6
PCSK1_62-89	0.230	-1.051	0.820	Cluster 5
PDYN_166-175	1.060	-0.673	-0.388	Cluster 6
PDYN_177-199	1.079	-0.672	-0.407	Cluster 6

Peptide	Beta (Z score)	Alpha (Z score)	Delta (Z score)	Cluster
PDYN_221-233	0.871	-0.435	-0.435	Cluster 6
PYY_29-58	-0.636	-0.636	1.273	Cluster 4
PYY_29-62	-0.659	-0.659	1.318	Cluster 4
PYY_29-64	-0.645	-0.608	1.254	Cluster 4
PYY_31-64	-0.527	-0.527	1.054	Cluster 4
PYY_68-77	-0.823	1.174	-0.351	Cluster 1
PYY_68-78	-1.010	1.094	-0.084	Cluster 1
PYY_68-79	-0.810	-0.489	1.299	Cluster 4
PYY_68-93	-0.716	-0.597	1.313	Cluster 4
PYY_68-96	-0.684	-0.619	1.303	Cluster 4
PYY_68-97	-0.689	-0.627	1.316	Cluster 4
PYY_68-98	-0.844	-0.440	1.284	Cluster 4
PYY_78-98	-0.899	1.278	-0.378	Cluster 1
PYY_79-93	-0.658	-0.658	1.316	Cluster 4
PYY_79-96	-0.946	-0.175	1.122	Cluster 4
PYY_79-97	-0.594	-0.594	1.189	Cluster 4
PYY_79-98	-1.207	0.864	0.343	Cluster 2
PYY_81-98	-0.755	-0.418	1.173	Cluster 4
PYY_82-98	-0.656	-0.656	1.311	Cluster 4
PYY_85-98	-0.610	-0.610	1.220	Cluster 4
SCG1_21-61	0.203	-0.800	0.597	Cluster 5
SCG1_386-406	0.239	-0.989	0.749	Cluster 5
SCG1_386-417	-0.524	-0.783	1.308	Cluster 4
SCG1_386-435	-0.582	-0.582	1.165	Cluster 4
SCG1_438-446	-0.335	-0.919	1.254	Cluster 4
SCG1_438-453	-0.731	-0.578	1.309	Cluster 4
SCG1_438-454	-0.729	-0.590	1.318	Cluster 4
SCG1_440-454	0.824	-1.105	0.280	Cluster 5
SCG1_499-511	-0.658	-0.658	1.316	Cluster 4
SCG1_516-535	-0.493	-0.776	1.269	Cluster 4
SCG1_517-535	0.830	-0.943	0.113	Cluster 5
SCG1_588-597	-0.437	-0.810	1.247	Cluster 4
SCG1_600-613	-0.469	-0.482	0.952	Cluster 4
SCG1_600-613.1	-0.643	-0.643	1.285	Cluster 4
SCG1_602-613	1.122	-0.857	-0.265	Cluster 6
SCG1_603-613	1.229	-0.614	-0.614	Cluster 6
SCG1_64-86	-0.054	-0.768	0.821	Cluster 4
SCG1_655-675	-1.292	0.467	0.825	Cluster 2
SCG1_655-676	-0.652	-0.652	1.305	Cluster 4
SCG2_184-204	1.271	-0.635	-0.635	Cluster 6
SCG2_184-216	0.850	-1.188	0.337	Cluster 5

Peptide	Beta (Z score)	Alpha (Z score)	Delta (Z score)	Cluster
SCG2_202-216	1.300	-0.650	-0.650	Cluster 6
SCG2_205-216	1.192	-0.889	-0.303	Cluster 6
SCG2_287-297	1.238	-0.725	-0.514	Cluster 6
SCG2_287-301	1.247	-0.624	-0.624	Cluster 6
SCG2_287-314	1.186	-0.593	-0.593	Cluster 6
SCG2_287-316	1.252	-0.676	-0.577	Cluster 6
SCG2_300-316	1.238	-0.644	-0.594	Cluster 6
SCG2_301-316	1.228	-0.614	-0.614	Cluster 6
SCG2_359-389	1.154	-0.577	-0.577	Cluster 6
SCG2_493-524	1.195	-0.813	-0.383	Cluster 6
SCG2_527-566	-0.630	-0.630	1.260	Cluster 4
SCG2_569-609	0.897	-1.149	0.253	Cluster 5
SCG2_569-610	0.413	-1.059	0.646	Cluster 5
SCG2_569-610.1	1.105	-1.041	-0.063	Cluster 5
SCG3_23-36	1.319	-0.659	-0.659	Cluster 6
SCG3_38-53	1.119	-0.923	-0.196	Cluster 6
SCG3_38-55	1.219	-0.801	-0.418	Cluster 6
SCG3_38-57	1.280	-0.640	-0.640	Cluster 6
SCG3_83-97	1.254	-0.627	-0.627	Cluster 6
SMS_103-110	-0.665	-0.665	1.331	Cluster 4
SMS_103-112	-0.657	-0.657	1.314	Cluster 4
SMS_103-113	-0.652	-0.652	1.304	Cluster 4
SMS_103-114	-0.651	-0.651	1.301	Cluster 4
SMS_103-115	-0.661	-0.661	1.323	Cluster 4
SMS_103-116	-0.679	-0.643	1.322	Cluster 4
SMS_104-116	-0.660	-0.660	1.320	Cluster 4
SMS_105-116	-0.663	-0.663	1.325	Cluster 4
SMS_108-116	-0.660	-0.660	1.319	Cluster 4
SMS_109-116	-0.666	-0.666	1.332	Cluster 4
SMS_25-36	-0.666	-0.666	1.331	Cluster 4
SMS_25-47	-0.662	-0.662	1.324	Cluster 4
SMS_25-49	-0.666	-0.666	1.331	Cluster 4
SMS_25-51	-0.642	-0.642	1.285	Cluster 4
SMS_25-52	-0.562	-0.562	1.124	Cluster 4
SMS_25-55	-0.657	-0.657	1.314	Cluster 4
SMS_25-84	-0.654	-0.654	1.307	Cluster 4
SMS_25-85	-0.664	-0.664	1.327	Cluster 4
SMS_25-87	-0.658	-0.658	1.317	Cluster 4
SMS_25-87.1	-0.646	-0.646	1.292	Cluster 4
SMS_38-87	-0.527	-0.527	1.055	Cluster 4
SMS_52-100	-0.521	-0.521	1.042	Cluster 4

Peptide	Beta (Z score)	Alpha (Z score)	Delta (Z score)	Cluster
SMS_52-87	-0.656	-0.656	1.311	Cluster 4
SMS_54-87	-0.664	-0.664	1.329	Cluster 4
SMS_56-87	-0.685	-0.640	1.325	Cluster 4
SMS_57-100	-0.662	-0.662	1.325	Cluster 4
SMS_57-100.1	-0.610	-0.610	1.220	Cluster 4
SMS_57-81	-0.631	-0.631	1.263	Cluster 4
SMS_57-82	-0.666	-0.666	1.333	Cluster 4
SMS_57-84	-0.656	-0.656	1.312	Cluster 4
SMS_57-85	-0.703	-0.622	1.325	Cluster 4
SMS_57-85.1	-0.606	-0.606	1.212	Cluster 4
SMS_57-86	-0.667	-0.667	1.333	Cluster 4
SMS_57-87	-0.710	-0.619	1.329	Cluster 4
SMS_62-87	-0.619	-0.619	1.238	Cluster 4
SMS_66-87	-0.631	-0.631	1.261	Cluster 4
SMS_67-85	-0.649	-0.649	1.299	Cluster 4
SMS_67-87	-0.665	-0.665	1.330	Cluster 4
SMS_67-87.1	-0.607	-0.607	1.214	Cluster 4
SMS_73-100	-0.655	-0.655	1.311	Cluster 4
SMS_73-85	-0.665	-0.665	1.331	Cluster 4
SMS_73-87	-0.658	-0.658	1.315	Cluster 4
SMS_73-87.1	-0.641	-0.641	1.281	Cluster 4
SMS_78-87	-0.645	-0.645	1.289	Cluster 4
SMS_85-100	-0.664	-0.664	1.329	Cluster 4
SMS_89-100	-0.560	-0.560	1.120	Cluster 4
SMS_103-116.1	-0.621	-0.621	1.243	Cluster 4
TYB4_8-50	-0.534	1.301	-0.767	Cluster 1
UCN3_138-160	1.216	-0.608	-0.608	Cluster 6
UCN3_24-38	1.259	-0.358	-0.901	Cluster 6
UCN3_46-54	1.313	-0.656	-0.656	Cluster 6
UCN3_46-55	1.270	-0.635	-0.635	Cluster 6
UCN3_58-79	1.207	-0.604	-0.604	Cluster 6

Appendix 2: Peptides matched in peptidomic analysis of FACS purified α, β and δ cells from mouse islets with cluster assigned by hieracical clustering.